2018

Studies towards the syntheses of rocaglate natural products and synthetic analogues via ESIPT photocycloaddition

BOSTON UNIVERSITY

GRADUATE SCHOOL OF ARTS AND SCIENCES

Dissertation

STUDIES TOWARDS THE SYNTHESES OF ROCAGLATE NATURAL PRODUCTS AND SYNTHETIC ANALOGUES VIA ESIPT PHOTOCYCLOADDITION

by

WENYU WANG

B.A., Wuhan University, 2011

Submitted in partial fulfillment of the

requirements for the degree of

Doctor of Philosophy

2018

Approved by

First Reader

John A. Porco, Jr., Ph.D.
Professor of Chemistry

Second Reader

Aaron B. Beeler, Ph.D.
Professor of Chemistry

ACKNOWLEDGMENTS

Investing a five-year journey of PhD study in organic chemistry is certainly exciting but challenging, hard but fruitful for me. Before my PhD training, I cannot even properly show an aldol reaction mechanism. But I was fortunate to have John being my organic chemistry mechanism CH642 class professor who really demonstrated me what is total synthesis and how synthesis, methodology, and mechanistic understanding are interacting each other. Luckily, I was able to stand out from that class and impressed John a little bit to take me as a graduate student in his laboratory. The fresh memory of my first day in Porco lab still come to me sometimes that I set up my first reaction in the morning of Sandy Hurricane arriving Boston, but surprisingly in that morning the lab was still full of people working. Because the Green Line would shut down at 12:30 pm due to the hurricane, we all left around 11:30 to have a half-day off (that was a Monday). This really remind me a lot the intensity of lab work at Porco lab and well explained where the success of this group in the field come from.

First, I would like to thank Prof. Aaron Beeler, Prof. Scott Schaus, Prof. James Panek, and Prof. Lauren Brown for serving my thesis defense committee and providing helpful suggestion and insightful discussion of my research projects and PhD thesis. I would like to thank all the collaborators in my research projects. Prof. David Coker, Dr. Juanma Ortiz Sánchez, and Mr. Thomas Heavey helped us a lot for understanding the TADDOL-mediated enantioselective ESIPT photocycloaddition using metadynamics calculation. The collaboration with Prof. Sivaguru Jayaraman, Dr. Retheesh Krishnan, Anthony Clay (BGSU) not only educated us on photochemistry knowledge, but also helped us to

understand the mechanism of the ESIPT photocycloaddition reaction. I would also like to thank Prof. Jerry Pelletier (McGill University), Dr. Luke Whitesell (MIT), Prof. Tony Wang (SRI), Prof. John Connor (BU Medical School) for testing the biological activities of our compounds.

I was very fortunate to work with a lot of smart and talented chemists in my PhD study. Tian and Chao taught me tremendously on how to run experiments and establish the sense of beauty for appreciating and judging all the works appeared on journal articles. I really missed the "golden time" that we three together enjoy tasty food, play computer games, watching movies, and talking about chemistries. I want to thank Dr. Neil Lajkiewicz for being my mentor. Neil is certainly one of the kindest person I have ever met. He was always willing to help me and being optimistic to encourage me. I want to thank dear "grandma" Dr. Gina Kim. She was always very nice to me and help the whole group to be well-organized. Every time, when I met some obstacle or setback she would be the person to share with. I would like to thank Dr. Martin Himmelbauer, Dr. Diane Hamann, Dr. Robert Ziegler, Dr. Yuan Xiong, Dr. Anaïs Gervais, Dr. Andrew J. Little, Dr. Kiel Lazarski, Dr. Pieter Bos, Prof. Dr. Alex Grenning, Dr. Adam Scharf, Dr. Takayuki Iwata, Dr. Vincent Eschenbrenner-Lux, Dr. Davinia Fernández-Gonzalez, Dr. Munmun Mukerjee, Dr. Dana Winter, Sarah Spiegel; Zach Ariki, Steve Stone, Nicholas Intermaggio, Kalina Doytchinova, Kelley Danahy. You guys are awesome colleagues, and as a foreigner, you guys really made Boston like my second hometown and provide me a very precious experience in the past five years. I would like to thank Dr. Kyle Reichl for helping me reading and editing my thesis. He is such a smart and reliable chemist, never complain, and

always very chilled to run reactions and get work done beautifully. I would like to thank Mr. Adam Zahara for being my undergraduate research in the past 2 years. It's been great to with you and thank you for tolerating my impatience. Also I would like to thank all the current member and wish you all the best in the rest of your time in the group, Dr. Wenhan Zhang (Thank you for all the great launch time), Xiaowei Wu, Thomas Purgett (It's been great to sharing all chemistry with you.), Michael Smith, Zach Powers, Chun Chen, Saishuai Wen (I really enjoyed all the fun we had together with you two.), Madison Powers, Tyler Rauwolf, Mackenzie Marrs, Matthew Dyer, Andrew Cyr.

I would like to give me biggest thank you to Prof. John A. Porco, Jr. John really set up a model for being a chemist. His passion, strictness, toughness, and responsibility total reshaped me in the past five year from a "college boy" to a "chemist". Additionally, he has always been very supportive for my future career development and giving me helpful suggestions. I would like to say that choosing this group to do a PhD study is certainly well-spent and one of my rightest decisions I have ever made.

I would like to thank my dear girlfriend, my soulmate Shuran Huang. I could not imagine how hard this journey will be if it is without you. Thank you for your kind company in the past four years although very often that I need to stay at the lab until very late. Thank you for sharing so much beautiful memories with me, travelling, singing, skiing, swimming… If there would be a person I want to spend the rest of my life with, that has to be you. I would like to thank my parents Chongyi Wang and Shaojun Li. Thank you for creating such a wonderful, lovely family for me and supporting me whenever I need. From high school to college, from college to graduate school, if there was not this much support, I

would not even have a chance to reach this far. All I can do is to try my best to be a son that you two can be proud of. I would like to thank my grandparents for their love and support in the past 28 years of my life as well. You all brought so much beautiful memories that I would never forgot during my childhood and I wish I could spend more time to visit you in the future.

Lastly, the most important thing I learn during my PhD is organic synthesis as well as the passion towards chemistry in general, so I would like express my gratitude again to all the people that helped my along this pathway.

STUDIES TOWARDS THE SYNTHESES OF ROCAGLATE NATURAL PRODUCTS AND SYNTHETIC ANALOGUES VIA ESIPT PHOTOCYCLOADDITION

WENYU WANG

Boston University Graduate School of Arts and Sciences, 2018

Major Professor: John A. Porco, Jr., Professor of Chemistry

ABSTRACT

The total syntheses of isomeric aglain natural products (±)-foveoglin A and (±)-perviridisin B have been achieved *via* ESIPT (excited states intramolecular proton transfer)-mediated selective (3+2) photocycloaddition of 3-hydroxyflavone with *trans,trans*-1,4-diphenyl-1,3-butadiene (DPBD). Using TADDOLs or Pirkle's alcohol as chiral hydrogen-bonding additives, enantioselective ESIPT photocycloaddition was performed providing access to (+)-foveoglin A which also enabled confirmation of its absolute configuration. Photophysical studies have been conducted for ESIPT photocycloadditions revealing the possibility for exergonic electron transfer from the excited triplet state of 3-hydroxyflavones to dipolarophiles with appropriate redox potentials, which also provided a rationale for the observed selectivity.

Further application of ESIPT photocycloaddition using 1-alkyl-2-aryl-3-hydroxyquinolinones (3-HQ's) to synthesize nitrogen-containing analogues of flavaglines, *aza*-rocaglates, will be described. Differential photoreactivity between 2-aryl-3-hydroxyquinolinones (*N*-H-3-HQ's) and 1-alkyl-2-aryl-3-hydroxyquinolinones (*N*-alkyl-

3-HQ's) was observed. A rationale for this observation was also provided based on photophysical measurements. A novel method to synthesize *N*-alkyl-3-hydroxyquinolinones using sodium hydride as base was discovered to overcome limited access to photoreaction substrates. A recirculating photoflow reactor was applied to the ESIPT photocycloaddition to increase the efficiency of the reaction. Initial biological testing indicates that *aza*-rocaglates do not possess activity in comparison to related rocaglates which also provides further information on the SAR of the natural product scaffold.

Computational studies were conducted in collaboration with Prof. David Coker's group using Metadynamics simulation to study *tetrakis*-9-phenanthrenyl TADDOL-mediated asymmetric ESIPT photocycloadditions. With a choice of collective variables based on hydrogen-bonding interactions between TADDOL and 3-hydroxyflavone, the free energy surfaces associated with formation of the hydrogen-bonding complexes between TADDOL and the 3-hydroxyflavone/methyl cinnamate or 3-hydroxyflavone/stilebene pairs were obtained. The representative three-component model from the obtained free energy minimum indicate that in addition to hydrogen-bonding interactions, π-π stacking between the phenanthren-9-yl groups of TADDOL and the 3-hydroxyflavone substrate also facilitate the asymmetric photocycloaddition which has provided information for future asymmetric catalyst designs.

TABLE OF CONTENTS

LIST OF TABLES

LIST OF FIGURES

LIST OF SCHEMES

LIST OF JOURNAL ABBREVIATIONS

ACS Appl. Mater. Interfaces .....ACS Applied Materials & Interfaces

ACS Cent. Sci. .....ACS Central Science

Angew. Chem. Int. Ed.....Angewandte Chemie International Edition

Bioorganic Med. Chem. Lett. .....Bioorganic & Medicinal Chemistry Letters

Chem. - A Eur. J. .....Chemistry: A European Journal

Chem. Rev.....Chemical Review

Eur. J. Pharmacol. .....European Journal of Pharmacology

J. Am. Chem. Soc. ..... Journal of the American Chemical Society

J. Chem. Soc. Chem. Commun. .....Journal of the Chemical Society, Chemical Communications

J. Comput. Chem.....Journal of Computational Chemistry

J. Fluor. Chem. .....Journal of Fluorine Chemistry

J. Med. Chem. .....Journal of Medicinal Chemistry

J. Nat. Prod. ..... Journal of Natural Products

J. Org. Chem. .....Journal of Organic Chemistry

J. Phys. Chem. A. ..... Journal of Physical Chemistry A

Org. Biomol. Chem. ..... Organic and Biomolecular Chemistry

Org. Lett. .....Organic Letters

Proc. Natl. Acad. Sci. ..... Proceedings of the National Academy of Sciences of the United States of America

Tetrahedron Lett. ..... Tetrahedron Letter

LIST OF ABBREVIATIONS

[α] ..... specific rotation

Abs ..... absorbance

Ac ..... acetyl

Ac2O ..... acetic anhydride

AcOH ..... acetic acid

ACS ..... American Chemical Society

AIF ..... apoptosis-inducing factor

API ..... atmospheric pressure ionization

ATP ..... adenosine triphosphate

B3LYP ..... Becke, three-parameter, Lee-Yang-Parr

$BF_3 \bullet Et_2O$ ..... boron trifluoride diethyl ether complex

Bn ..... benzyl

br ..... broad

B.R.S.M. ..... based on recovered starting material

Bu ..... butyl

*n*BuLi ..... *n*-butyllithium

Bu_4NBH_4 ..... *n*-tetrabutylammonium borohydride

c ..... concentration

cat. ..... catalytic

CD ..... circular dichroism

$CDCl_3$ ..... deuterated chloroform

CH_2Cl_2 ..... methylene chloride

CH3CN ..... acetonitrile

$CHCl_3$ ..... chloroform

CI ..... chemical ionization

COSY ..... correlation spectroscopy

conc. ..... concentrated

conv. ..... conversion

Cp* ..... pentamethylcyclopentadiene

m-CPBA ..... *meta*-chloroperbenzoic acid

CuBr ..... copper(I) bromide

d ..... doublet

δ ..... chemical shift

DDQ 2,3-Dichloro-5,6-dicyano-1,4-benzoquinone

DMAP ..... 4-(dimethylamino)pyridine

DMF ..... *N*,*N*-dimethylformamide

DMQ 1,2-dimethyl-3-hydroxyquinolinone

DMSO ..... dimethyl sulfoxide

DMSO-d_6 ..... deuterated DMSO

DNA ..... deoxyribose nucleic acid

DPEN ..... diphenylethylenediamine

dr ..... diastereomeric ratio

ε ..... coefficient of absorptivity

EC_{50} ..... effective concentration 50%

EDCI ..... 1-Ethyl-3-(3-dimethylaminopropyl) carbodiimide

ee ..... enantiomeric excess

EI ..... electronic ionization

eIF4A ..... eukaryotic initiation factor-4A

ELSD ..... evaporative light scattering detector

equiv ..... equivalent

ESIPT ..... excited state intramolecular proton transfer

Et ..... ethyl

ET ..... electron transfer

Et_3N ..... triethylamine

EtOAc ..... ethyl acetate

EtOH ..... ethanol

FT-IR ..... Fourier transform-infrared spectroscopy

g ..... gram

h ..... hour

H_2 ..... hydrogen gas

HCl ..... hydrochloric acid

3-HF 3-hydroxyflavone

3-HQ 3-hydroxyquinolinones

HFIP 1,1,1,3,3,3-hexafluoroisopropanol

HMBC ..... heteronuclear multiple bond correlation

HMDS ..... hexamethyldisilazide

HMQC ..... heteronuclear multiple quantum coherence

HOBt ..... hydroxybenzotriazole

HOMO ..... highest occupied molecular orbita

HPLC ..... high performance liquid chromatography

HRMS ..... high resolution mass spectroscopy

HSF1 ..... heat shock factor 1

Hz ..... Hertz

hv ..... irradiation

IC_{50} ..... inhibitory concentration 50%

ISC ..... intersystem crossing

IR ..... infrared

IR ..... infrared

IR ..... infrared

IR ..... infrared

K_2CO_3 ..... potassium carbonate

KOH ..... potassium hydroxide

LiHMDS ..... lithium *bis*(trimethylsilyl)amide

LiOH ..... lithium hydroxide

LRMS ..... low resolution mass spectroscopy

LUMO ..... lowest occupied molecular orbital

M ..... molar

m ..... multiplet

MCL1 ..... myeloid cell leukemia 1

Me ..... methyl

$Me_4NBH(OAc)_3$ ..... tetramethylammonium triacetoxyborohydride

MeOH ..... methanol

MeONa ..... sodium methoxide

mg ..... milligram

$MgSO_4$ ..... magnesium sulfate

MHz ..... megaHertz

min ..... minutes

mmol ..... millimole

mol ..... mole

MOM ..... methoxymethyl

M.p. ..... melting point

mRNA ..... messenger ribo nucleic acid

MS ..... mass spectroscopy

nm ..... nanometer

µL ..... microliter

Na_2SO_4 ..... sodium sulfate

$NaBH_4$ ..... sodium borohydride

$NaBH(OAc)_3$ ..... sodium triacetoxyborohydride

NADH ..... nicotinamide adenine dinucleotide hydrogen

NADP ..... nicotinamide adenine dinucleotide phosphate

NaH ..... sodium hydride

$NaHCO_3$ ..... sodium bicarbonate

NaHMDS ..... sodium *bis*(trimethylsilyl)amide

NaOH ..... sodium hydroxide

NF-κB ..... nucleus factor kappa-light-chain-enhancer of activated B cells

NH_4Cl ..... ammonium chloride

nM ..... nanomolar

NMR ..... nuclear magnetic resonance

nOe ..... nuclear Overhauser effect

NOESY ..... nuclear Overhauser effect spectroscopy

ovrlp ..... overlapping

$Pb(OAc)_4$ ..... lead tetraacetate

PET ..... photoinduced electron transfer

Ph ..... phenyl

PHB ..... prohibitin

$PhCF_3$ ..... trifluorotoluene

PhH ..... benzene

PhMe ..... toluene

PKR ..... parallel kinetic resolution

PMB ..... *para*-methoxybenzyl

PMP..... *para*-methoxyphenyl

ppm ..... parts per million

PPTS ..... pyridinium *p*-toluenesulfonate

q..... quartet

Q-TOF.....quadrupole-time of flight mass analyzer

QM .....quinone methide

$[RhCl_2(Cp^*)]_2$ .....*Bis*[(pentamethylcyclopentadienyl)dichloro-rhodium]

rt .....room temperature

Rt..... retention time

s .....singlet

S_0 ..... singlet ground state

S'_0..... singlet ground state, tautomer form

S'_1.....singlet 1st excited state, tautomer form

S_1 .....singlet 1st excited state

SAR.....structure activity relationship

$Sc(OTf)_3$.....scandium triflate

SDR.....singlet diradical

$SOCl_2$ .....thionyl chloride

t .....triplet

T'_1 ..... triplet 1st excited state, tautomer

TADDOL .....α, α, α*'*, α*'*-tetraaryl-1,3-dioxolane-4,5-dimethanol

TBAF ..... *n*-tetrabutylammonium fluoride

TBS ..... *tert*-butyldimethylsilyl

TBSOTf..... *tert*-butyldimethylsilyl triflate

TDR..... triplet diradical

TFA ..... trifluoroacetic acid

TFE 2,2,2-trifluoroethanol

THF ..... tetrahdyrofuran

TIPSCl..... triisopropylsilyl chloride

TLC ..... thin layer chromatography

TMSOTf..... trimethylsilyl triflate

p-TsOH ..... *para*-tosic acid

UPLC ..... ultra performance liquid chromatography

UV ..... ultraviolet

µW ..... microwave

CHAPTER ONE

Flavagline Natural Products, Previous Synthetic Studies, and ESIPT Reactions

1.1 Isolation of Flavagline Natural Products and their Biological Activities

Aglaia is the largest genus of the family Meliaceae, containing more than 120 species, and is distributed throughout the tropical rainforest areas of southeast Asia and the Pacific region.[1] More than thirty of these plant species are found to be a rich source of the cyclopenta[*b*]benzofuran or "flavagline" class of compounds, many of which have been shown to possess insecticidal and anticancer activities (**Figure 1.1**). Since the isolation of rocaglamide (**1**), the first member of the flavaglines, by King and coworkers in 1982 from *A. elliptifolia*,[2] over 100 naturally occurring derivatives of rocaglamide have been isolated and characterized,[1] including (–)-methyl rocaglate (**2**),[3,4] (–)-rocagloic acid (**3**),[5] (–)-rocaglaol (**4**),[4] (+)-aglaiastatin (**5**),[6] and the complex rocaglate, (–)-silvestrol (**6**).[7] The cyclopenta[*b*]benzofuran natural products have been tested to show potential anticancer activity; in particular, rocaglamide (**1**) and silvestrol (**2**) have been found to exhibit antiproliferative activity against various human cancer cell lines at nanomolar concentrations. The absolute configuration for silvestrol (**2**) was determined by X-ray crystallography and the absolute stereochemical assignment of (–)-rocaglamide (**1**) was determined *via* total synthesis by Trost and coworkers.[8] The absolute configurations of (–)-methyl rocaglate (**2**), (–)-rocagloic acid (**3**), and (–)-rocaglaol (**4**) were confirmed through

asymmetric synthesis by Porco and coworkers.[9] The absolute stereochemistry of (+)-aglaiastatin (**5**) was confirmed *via* total synthesis by the Porco laboratory.[10]

Figure 1.1 Rocaglates, Aglains, and Forbaglins from Genus Aglaia.

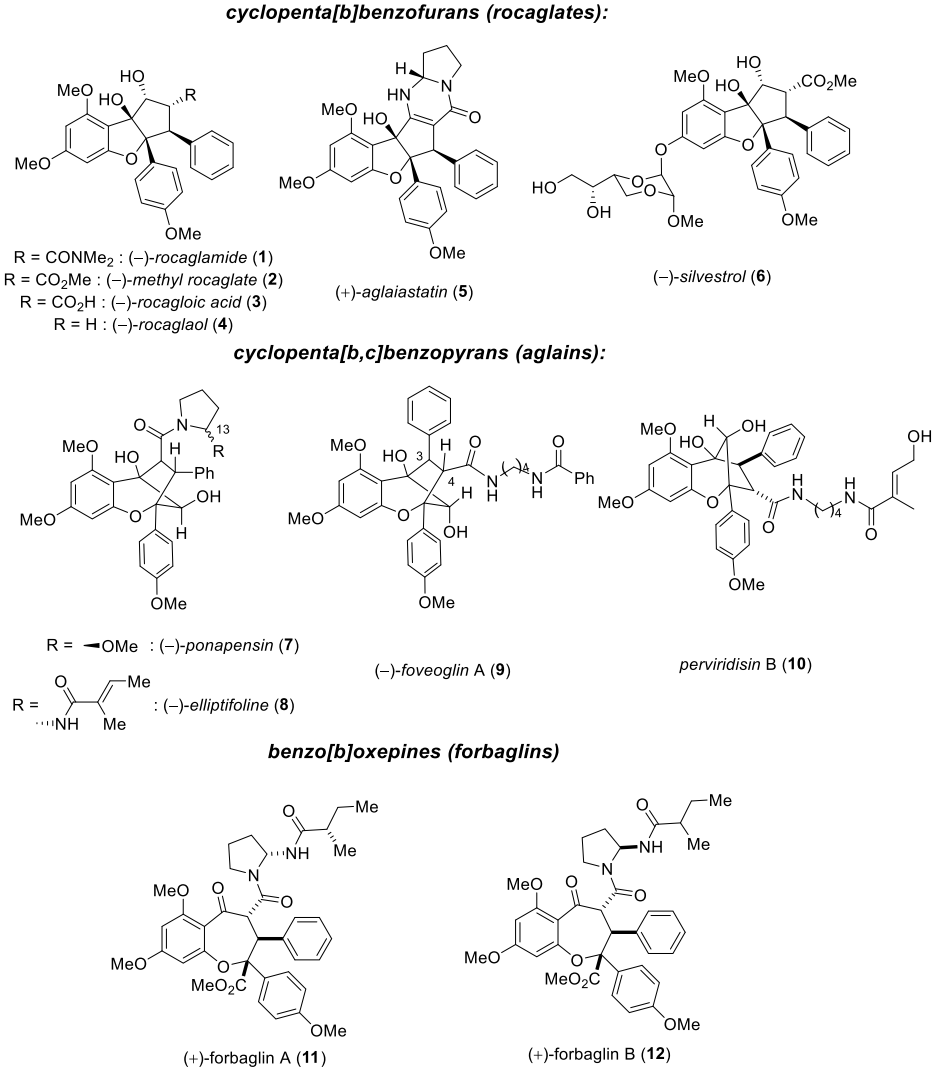

The other two classes of flavaglines, cyclopenta[*bc*]benzopyrans (aglains) and benzo[*b*]oxepines (forbaglins), are also presented in **Figure 1.1**. The absolute configuration of the hemiaminal-containing (–)-ponapensin (**7**)[11] and the aminal-containing (–)-elliptifoline (**8**)[5] was assigned *via* total synthesis by the Porco laboratory,[12]

which suggests that the biosynthetic precursor of aglain and rocaglate natural products possess the opposite absolute configuration. Additionally, the C13 position of (–)-elliptifoline (**8**) was reassigned to have the opposite configuration than that was reported in the isolation report. (–)-foveoglin A (**9**)[13] and (+)-perviridisin B (**10**)[14] are isomers of (–)-ponapensin (**7**) with the respect of phenyl and amide substituents at C3 and C4 position. (–)-foveoglin A (**9**) was found to have NF-*κ*B inhibitory activity (IC_{50} = 0.37 μM) and cytotoxicity towards three different cancer cell lines (ED_{50} = 1.4 to 1.8 μM).[13] (+)-Perviridisin B (**10**) also showed NF-*κ*B inhibitory activity (ED_{50} = 2.4 μM) and cytotoxicity towards HT-29 cancer cell lines (ED_{50} = 0.46 μM).[14]

(+)-Forbaglins A (**11**) and B (**12**)[15] have opposite stereochemistry at C13 in comparison to (–)-ponapensin (**7**) and (–)-elliptifoline (**8**) and their relative configurations were assigned through nOe experiments and X-ray crystallographic analysis. Thus far, no synthetic efforts towards determining the absolute configuration and biological activity of the forbaglins have been reported.

1.2 Proposed Biosynthesis of Aglains, Rocaglamides and Forbaglins

As previously mentioned, rocaglates, aglains, and forbaglins have all been isolated from genus *Aglaia*, and have the collective name "flavaglines" as these natural products are all proposed to share the same biosynthetic precursors, 3-hydroxyflavone (3-HF) **13** and cinnamic amides **14**. Proksch and coworkers[16] have proposed that a formal (3+2) cycloaddition between **13** and **14** *via* a Michael addition/aldol reaction sequence should afford a common precursor, aglain ketone **15**, for all the flavagline biosyntheses (**Figure 1.2**). Upon skeletal rearrangement/reduction, rocaglates (**16**) can be obtained. Direct

reduction of aglain ketone **15** provides access to aglains (**17**) which may be followed by oxidative cleavage of the C5-C10 bond to provide forbaglins (**18**).

Figure 1.2 Proksch's Biosynthetic Proposal of Flavaglines.

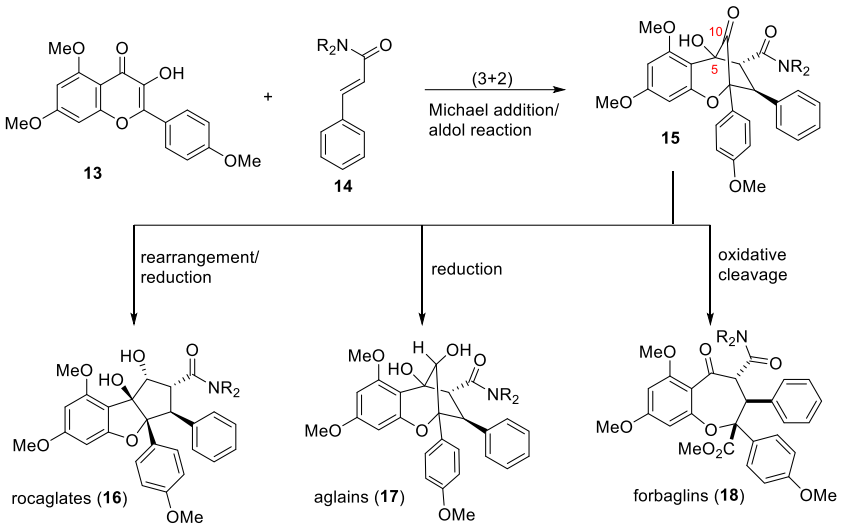

An alternative biosynthetic proposal has been suggested by Staunton and coworkers. In their proposal, photochemical [2+2] cycloaddition between 5,7,4'-trimethylapigenin (**19**) and dimethyl cinnamic amide **20** leads to **21**. Further rearrangement to intermediate **22** followed by hydration would afford rocaglamide (**1**) (**Figure 1.3**).[17]

Figure 1.3 Staunton and Coworkers' Proposed Biosynthesis.

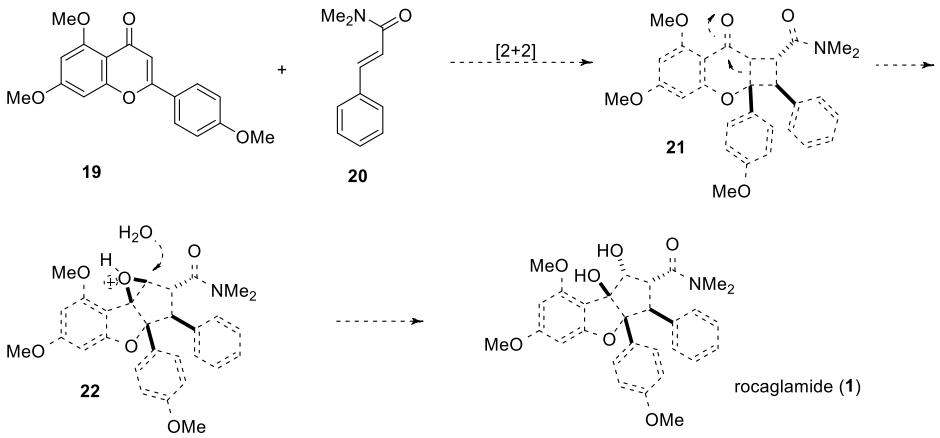

1.3 Previous Synthetic Approaches to Rocaglates

Due to their unique chemical structures (*i.e.* multiple functionalities and highly substituted skeletons) and fascinating biological activities, the total syntheses of rocaglates have been pursued by multiple synthetic organic groups. Additionally, the chemical synthesis of rocaglate analogues from a medicinal chemistry point of view has also been well documented in the past decades. This section will summarize the major advancements achieved in these areas in chronological order, including different approaches towards the rocaglate scaffold, development of asymmetric photochemistry, and biomimetic kinetic resolution.

1.3.1 The First Total Synthesis of Rocaglamide and Absolute Configuration Assignment

Scheme 1.1 Trost's Total Synthesis of (–)-Rocaglamide.

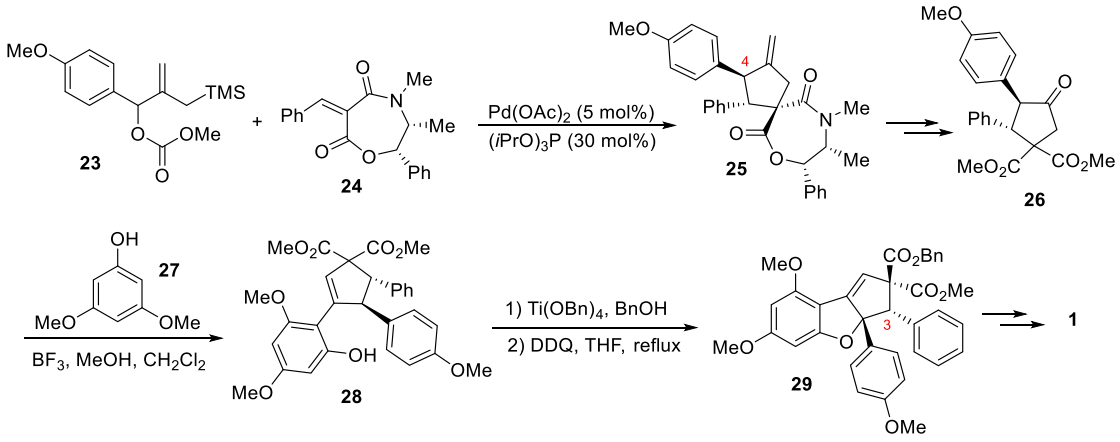

While several synthetic attempts have been reported,[18,19] the first total synthesis of a natural flavagline (rocaglate) was accomplished by Trost and coworkers (**Scheme 1.1**).[8] Asymmetric conjunctive allylic annulation of compound **23** with chiral, enantiopure oxazepinedione **24** afforded cyclopentene **25** which established the absolute configuration at C4. After removal of the chiral auxiliary and double bond cleavage by ozonolysis (*not*

shown), Friedel-Crafts alkylation of dimethylphloroglucinol **27** with compound **26** followed by dehydration afforded cyclopentene **28**. Selective transesterification with benzyl alcohol was then performed to facilitate subsequent decarboxylation. Oxidative cyclization with DDQ produced dihydrobenzofuran **29**. Several reactions were next performed to progress **29** to target structure **1** including dihydroxylation, decarboxylation, and stereochemical inversion at C3. The total synthesis was completed in 16 steps and fully established the absolute configuration of (–)-rocaglamide.

1.3.2 The Biomimetic Approach towards Rocaglate Natural Products

Scheme 1.2 Porco's Biomimetic Approach Towards Flavaglines and the Total Synthesis of Methyl Rocaglate (2).

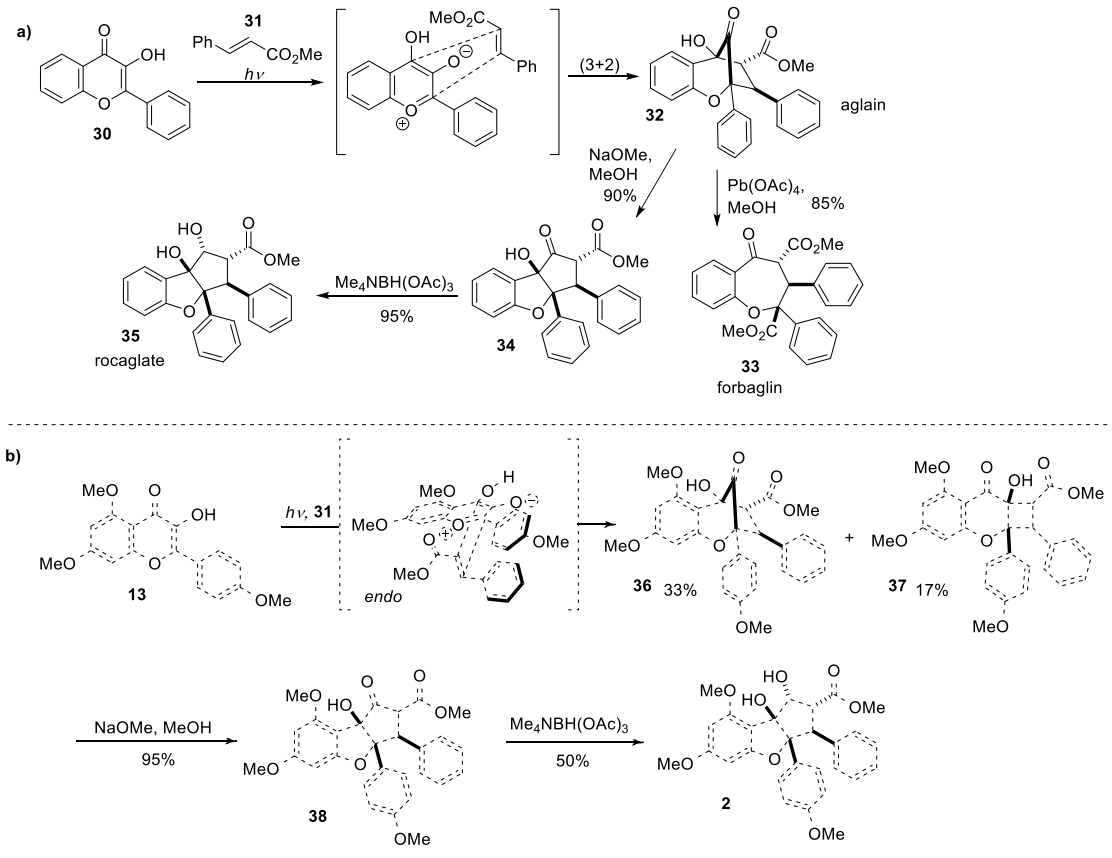

Figure 1.4 Excited State Intramolecular Proton Transfer of 3-Hydroxyflavone 30.

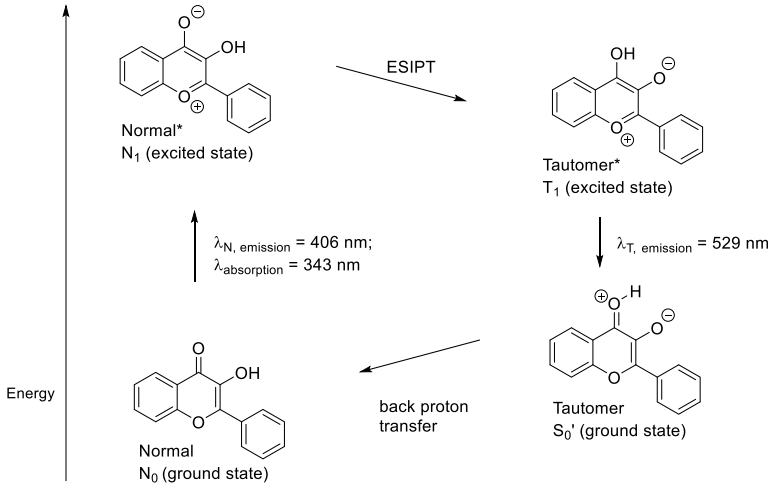

Based on Proksch and coworkers' proposal, accessing the aglain ketone intermediates derived from 3-hydroxyflavones (3-HFs) and cinnamic derivatives should offer access to rocaglates through bridgehead ketone reduction or skeletal rearrangement (*cf.* **Figure 1.2**).[16] In 2004, Porco and coworkers reported a unified biomimetic approach to rocaglamide, aglain, and forbaglin cores employing a biomimetic (3+2) photocycloaddition of 3-hydroxyflavones with methyl cinnamate (**Scheme 1.2a**).[20] Upon photo-irradiation of 3-HF **30** ($\lambda \sim 350$ nm) excited state intramolecular proton transfer (ESIPT)[21] may occur to generate an oxidopyrylium intermediate (T_1 excited state) (**Figure 1.4**) which could be trapped with a dipolarophile (*e.g. trans*-methyl cinnamate **31**) to afford the key aglain scaffold **32**. Forbaglin core **33** was then synthesized by treatment of **32** with $Pb(OAc)_4$ leading to oxidative fragmentation. Rocaglate core **35** may be obtained through base-mediated α-ketol shift, followed by hydroxyl-directed Evans–Saksena reduction of keto-rocaglate **34**.

The total synthesis of (±)-methyl rocaglate (**2**) was then achieved using this methodology (**Scheme 1.2b**). Upon photo-irradiation of 3-hydroxyflavone **13** in presence of methyl cinnamate **31**, aglain **36** and benzo[*b*]cyclobutapyran-8-one **37** were obtained. Conversion of both **36** and **37** to α-ketol rearrangement product **38** using sodium methoxide followed by hydroxyl-directed reduction efficiently yielded (±)-methyl rocaglate (**2**). This approach proved a significant advance towards the synthesis of flavagline natural products, as rocaglamide, aglain, and forbaglin natural products could all be accessed through this method.

Subsequently, Porco and coworkers developed an enantioselective variant of the (3+2) photocycloaddition and applied this methodology to the syntheses of (–)-methyl rocaglate (**2**), (–)-rocaglamide (**1**), (–)-rocagloic acid (**3**), and (–)-rocaglaol (**4**) (**Scheme 1.3**). Using *tetrakis*-1-pyrenyl TADDOL **39**[22] as a chiral hydrogen-bonding template, enantioselective ESIPT photocycloaddition was achieved in 86% ee (measured from rocaglate **2**). After recrystallization, the enantiomeric excess was enhanced to 94% with 86% recovery of (–)-methyl rocaglate (**2**) from the mother liquor.

Scheme 1.3 Enantioselective Syntheses of (–)-Rocaglamide and Congeners

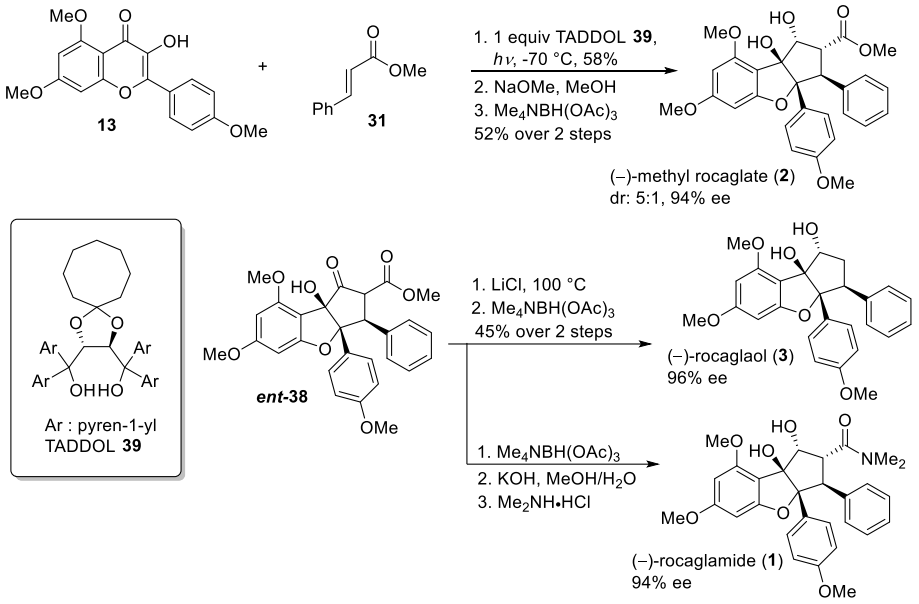

Krapcho decarboxylation of β-ketoester *ent*-**38** using lithium chloride, followed by hydroxyl-directed reduction, produced (–)-rocaglaol (**4**) in 96% ee after recrystallization. (–)-Rocaglamide (**1**) was obtained from (–)-methyl rocaglate (**2**) through saponification to (–)-rocagloic acid (**3**), and subsequent amide coupling with dimethylamine. Using this method, the absolute configurations of (–)-methyl rocaglate (**2**), (–)-rocagloic acid (**3**), and (–)-rocaglaol (**4**) were confirmed. Furthermore, this methodology by Porco and coworkers has been recognized as a major advancement in the field of enantioselective photochemistry.[23] Porco and coworkers subsequently applied this methodology to the total synthesis of the complex rocaglate natural product (**–**)-silvestrol (**6**).[24] Rizzacasa and coworkers also synthesized (–)-silvestrol (**6**) employing this ESIPT photocycloaddition methodology.[25]

Scheme 1.4 Porco's Enantioselective Total Syntheses of (+)-Ponapensin (7) and (+)-Elliptifoline (8), Enantiomers of the Natural Metabolites

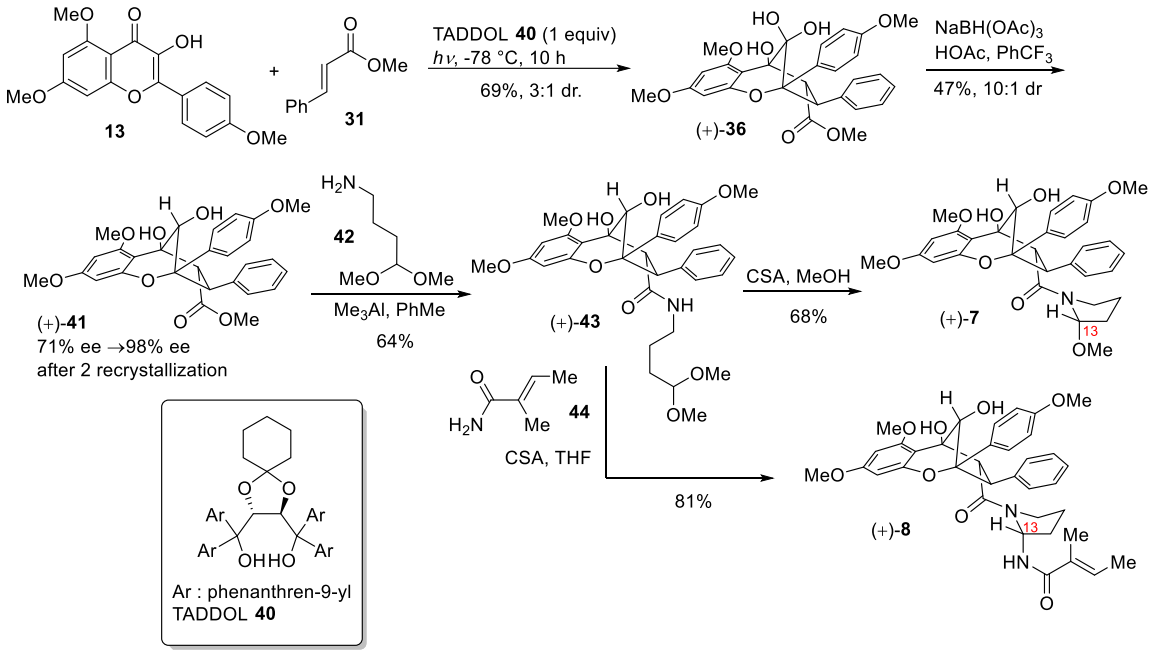

With this biomimetic asymmetric approach towards rocaglates in hand, Porco and coworkers also studied the enantioselective total syntheses of two aglain natural products, (+)-ponapensin (**7**) and (+)-elliptifoline (**8**) (**Scheme 1.4**).[12] Enantioselective ESIPT photocycloaddition of 3-hydroxyflavone **13** and methyl cinnamate **31** was performed in the presence of a stoichiometric amount of TADDOL **40** as a chiral hydrogen-bonding additive to yield aglain ketone in 69% yield and 3:1 dr. After recrystallization in acetonitrile, ketone hydrate (+)-**36** was obtained as a single compound. Reduction of hydrate (+)-**36** with sodium triacetoxyborohydride afforded aglain (+)-**41** in 10:1 dr. The enantiomeric excess of (+)-**41** was then enhanced to 98% *via* two recrystallizations and absolute stereochemistries were confirmed by X-ray analysis. Subsequent ester-amide exchange using trimethylaluminum afforded amide-acetal (+)-**43**, which was subjected to a CSA-promoted *N*-acyliminium cyclization in methanol to afford (+)-ponapensin (**7**). Using

tiglic amide **44** as nucleophile instead of methanol, (+)-elliptifoline (**8**) was obtained, which resulted in stereochemical reassignment of the C13 position. More interestingly, after optical rotation measurement, Porco and coworkers concluded that the synthetic aglain natural products were the enantiomers of the natural samples. Since ketone hydrate (+)-**36** was confirmed to be the synthetic precursor toward (–)-methyl rocaglate (**2**), they proposed that in nature an enzymatic, kinetic resolution may occur on the racemic aglain ketone core structure. In this resolution, (+)-aglains selectively undergo ketol rearrangement/reduction, and (–)-aglains are reduced leading to enantiopure (–)-rocaglates and (–)-aglain scaffolds, respectively.

Scheme 1.5 Porco's Asymmetric Total Synthesis of (+)-Aglaiastatin and (–)-Aglaroxin C

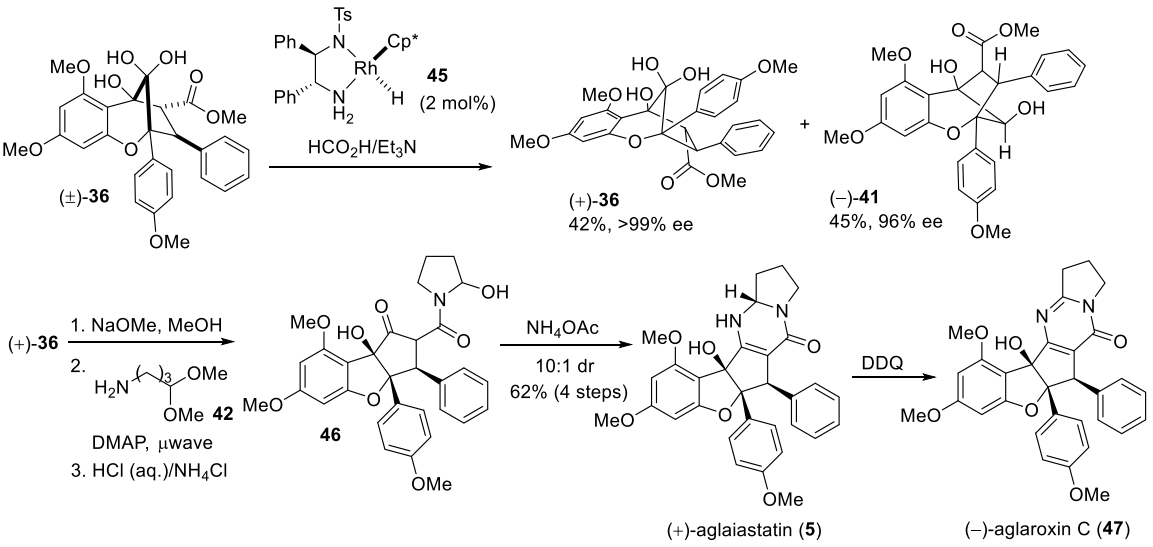

This biosynthetic proposal also led to the development of a biomimetic kinetic resolution using chiral, racemic aglain ketone hydrate (±)-**36** to produce enantiopure rocaglates by Porco and coworkers (**Scheme 1.5**).[10] A highly enantio- and diastereoselective transfer hydrogenation of racemic aglain ketones was developed using rhodium(III) chloride-Cp* dimer with (*R*,*R*)-diphenylethylenediamine[26] as the optimal

catalyst. Using this protocol, (–)-**41** was obtained in 45% yield and in 96% ee with recovery of enantiopure starting material in 42% yield. Ketol rearrangement of (+)-**36**, followed by ester-amide exchange and subsequent hemiaminal formation, led to the formation of **46**. Heating **46** with ammonium acetate produced (+)-aglaiastatin (**5**) which was then transformed to (–)-aglaroxin C (**47**) by DDQ-mediated dehydrogenation.

1.3.3 Frontier's and Tius' Approaches to Rocaglamide via Nazarov Cyclization

Scheme 1.6 Frontier's Synthesis of (±)-Rocaglamide (1)

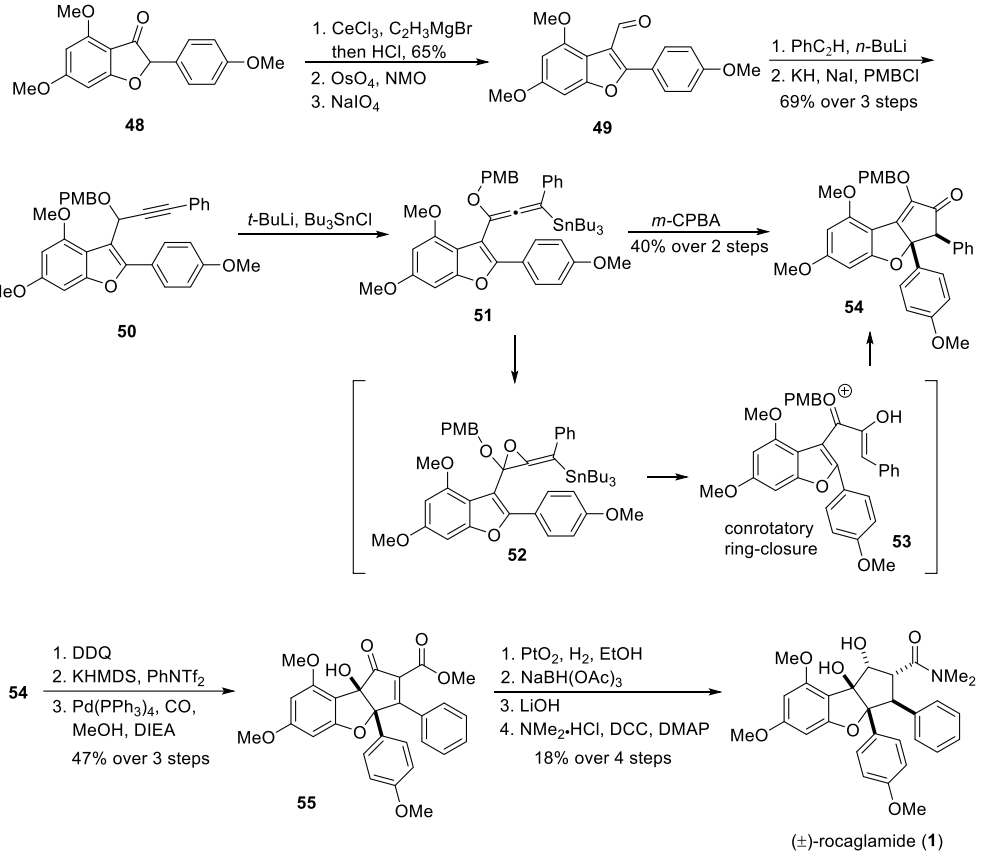

Frontier and coworkers also reported a synthesis of (±)-rocaglamide (**1**) which utilized the Nazarov cyclization as a key step.[27] Vinyl magnesium bromide addition to benzofuranone **48**, followed by acid-mediated dehydration and subsequent oxidative

double bond cleavage, furnished aldehyde **49**. Lithium phenylacetylide addition to **49**, followed by protection of the derived propargyl alcohol, afforded propargyl ether **50**, which was then transformed to stannyl alkoxyallene **51** by trapping the allenyl anion (generated by *tert*-butylithium deprotonation) with tri-*n*-butyltin chloride. Epoxidation of **51** using *m*-CPBA afforded epoxide intermediate **52** which underwent rearrangement to pentadienyl cation **53** and subsequent Nazarov cyclization afforded the tricyclic core structure **54**. Removal of the *para*-methoxybenzyl (PMB) protecting group by DDQ followed by triflation and palladium(0)-catalyzed carbonylation furnished the α,β-unsaturated ketone **55**. Diastereoselective hydrogenolysis of **55** provided a keto-rocaglate intermediate, which was subjected to hydroxyl-directed reduction with sodium triacetoxyborohydride, saponification, and amide coupling yielded (±)-rocaglamide (**1**). A similar Nazarov cyclization strategy was also utilized by Magnus and coworkers to synthesize intermediate **55** in a shorter step-count to achieve a formal synthesis of (±)-methyl rocaglate (**2**).[28]

More recently, Tius and coworkers reported an enantioselective synthesis of both enantiomers of rocaglamide (**1**) as shown in **Scheme 1.7**.[29] Diketo-ester **56** was treated with palladium(0) and a TADDOL-derived phosphoramidite ligand **57** to afford cyclopentenone **58** in 89:11 e.r., which set the stereochemistry at the C3 (rocaglamide numbering) position that will control all the subsequently introduced stereocenters. Treatment of **58** with PIFA in presence of allyl alcohol installed an allyloxy group at the C3a position stereoselectively. Exposure of the product to Meerwein's salt ($[Me_3O^+][BF_4^-]$) followed by ester hydrolysis and amide coupling led to production of enol ether **59**. With compound **59** in hand, commercially available 3,5-dimethoxyfluorobenzene **60** was

lithiated and transmetallated with $LaCl_3 \cdot 2LiCl$ prior to exposure to **59**, thereby producing tertiary alcohol **61** as a single isomer. After recrystallization of **61** leading to the recovery of highly optically enriched **61** (98.5:1.5 e.r.) in 75% yield from the mother liquor, selenium dioxide-mediated removal of the allyl protecting group followed by treatment with potassium *tert*-butoxide afforded dihydrobenzofuran intermediate **62**. Methyl enol ether cleavage using magnesium iodide (MgI_2) produced a keto-rocaglamide derivative which was afforded (–)-rocaglamide (**1**) after hydroxyl-directed reduction using sodium triacetoxyborohydride.

Scheme 1.8 Tius' Asymmetric Synthesis of (–)-Rocaglamide (1).

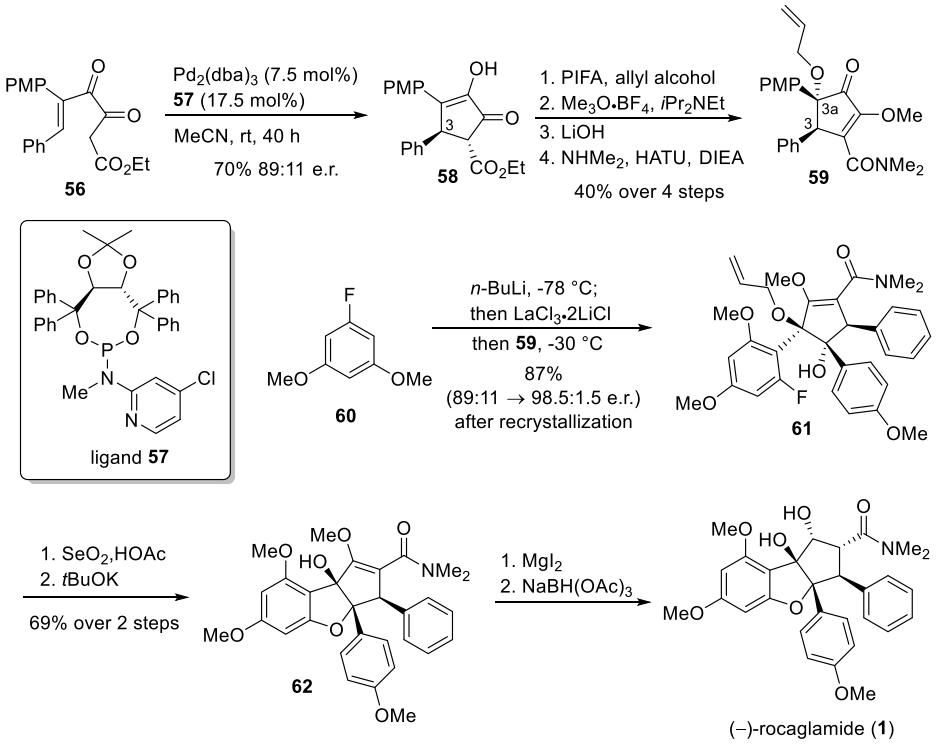

1.4 Development of ESIPT Photoreaction Methodologies

As shown in the previous section, ESIPT photocycloaddition has been proven to be an efficient approach toward flavagline natural products. Being a simple and fundamentally

important photochemical process, ESIPT-mediated photoreaction/photocycloaddition has drawn attention from other groups. In 1965, Weller and coworkers first reported ESIPT of salicylic ester substrate **63** and upon photoirradiation, the photoexcited tautomer T* was observed by fluorescence measurements (**Figure 1.5**).[30] For aromatic organic compounds, ESIPT generally arises upon electronic excitation when both acidic and basic functionalities on the molecule experience simultaneous enhancement of acidity and basicity. Although this phenomenon has been widely utilized in some modern designs for photostabilizers,[31] fluorescent chemosensors,[32] scintillators,[33] and solar collectors,[34] use of ESIPT photoexcited tautomeric intermediates to synthesize novel molecular scaffolds have not been extensively reported until recently. This section will serve to summarize the major advancements in ESIPT photoreaction/cycloaddition methodology.

Figure 1.5 First Reported Excited State Intramolecular Proton Transfer of Salicylic Ester 63.

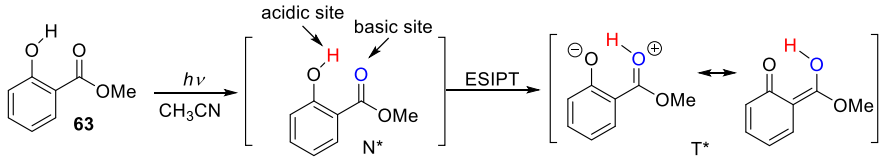

1.4.1 Yate's and Wan's ESIPT Reaction Discovery

The first ESIPT reaction reported by Yates and coworkers was based on photohydration of (*o*-hydroxyphenyl)acetylene **64** (**Scheme 1.9a**).[35] Upon photoexcitation, (*o*-hydroxyphenyl)acetylene **64** was transformed into a *o*-hydroxyacetophenone **66** under mild aqueous acidic conditions. More recently, Freccero and coworkers reported that (*o*-hydroxyphenyl)acetylenes can react with propylamine to afford compound **67** *via* an ESIPT mechanism in the aprotic solvent acetonitrile or CH_2Cl_2.[36] Additionally, ESIPT-

generated vinylidene quinone methides **65b** were characterized using transient spectroscopic measurements. Although ESIPT processes have been reported before, this report represented the first irreversible ESIPT photochemical process. Subsequently, Wan and coworkers reported the first example of ESIPT from phenol to a phenyl group.[37] 2-Phenylphenol **68** was irradiated in a mixture of D_2O/CH_3CN and deuterium-incorporated products **70** and **72** were observed (**Scheme 1.9b**), indicating that upon photoexcitation, ESIPT may occur from the phenol moiety to the 2-phenyl group to afford quinone methide intermediates **69a** or **69b** which may undergo reverse proton transfer to yield **70**. Alternatively, ESIPT through the protic solvent D_2O would allow formation of quinone methide intermediate **71** which led to formation of **72** by reverse proton transfer.

Since this deuterium incorporation experiments unambiguously demonstrated the formation of the ESIPT intermediate, Wan and coworkers subsequently reported an ESIPT cyclization utilizing *o*-hydroxybiaryl substrate **73** (**Scheme 1.9c**).[38] Water-mediated ESIPT occurred from the phenol moiety to the 7′-carbon atom of the accepting naphthyl ring to bring about a novel ring closure to form dihydrobenzoxanthene **74** in high yield. Compound **74** was readily oxidized to 1,9-benzoxanthene **75** by refluxing in toluene in the presence of catalytic amounts of Pd/C. A similar deuterium incorporation experiment was also performed to probe the mechanism of the reaction. Photoexcitation of substrate **73** in the presence of D_2O/CH_3CN led to formation of deuterium-incorporated product **77** *via* intermediate **76a** or **76b**. In addition, ESIPT to the 2'-carbon atom of the naphthyl ring also occurred to afford deuterium exchange at this position to provide compound **79**.

Wan and coworkers also reported that by extending aromatic ring system of a *o*-hydroxybiaryl compound from a naphthyl to an anthracenyl group, a different type of ESIPT occurred (**Scheme 1.9d**).[38] Following deuterium-labelling experiments, compound **80** was proposed to undergo a long range ESIPT process assisted by deuterium oxide to produce the quinone methide intermediate **82**. Subsequently, addition of H_2O (or D_2O) may form compound **83** and enolization of **82** would generate deuterated product **84**.

Scheme 1.9 Yate's and Wan's ESIPT Reaction Discovery

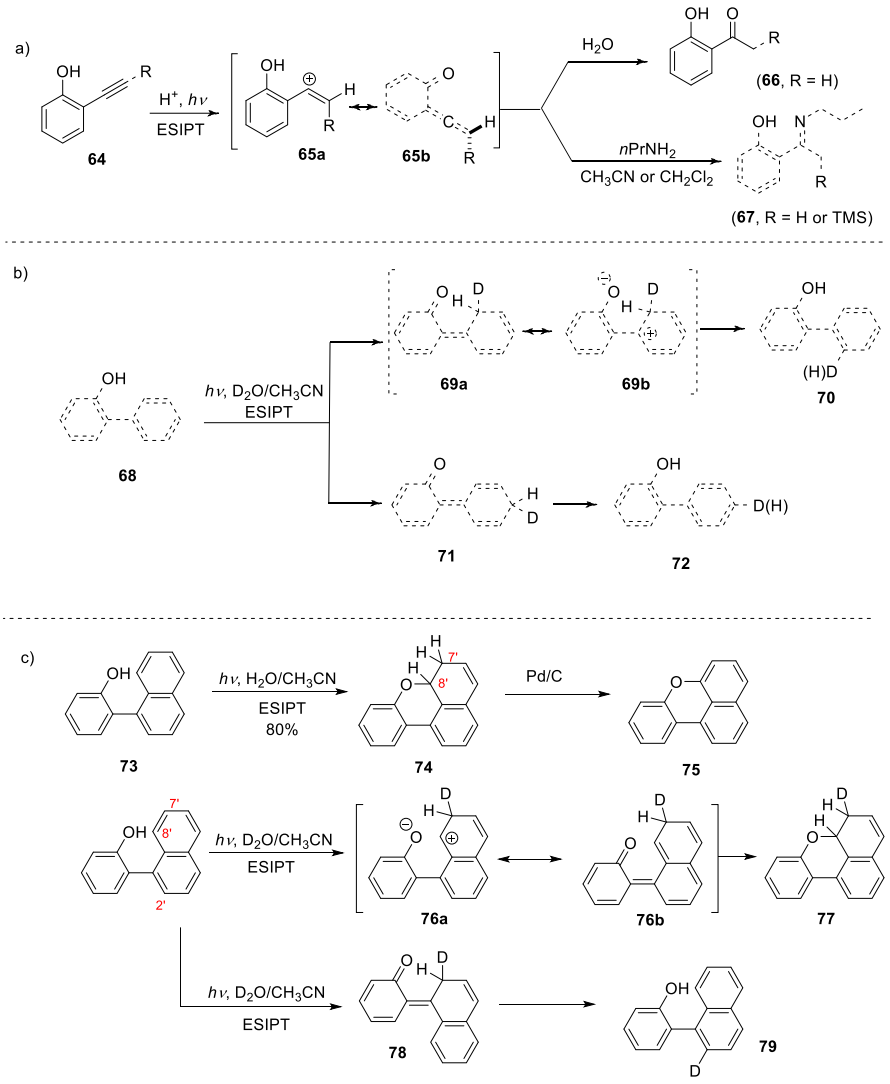

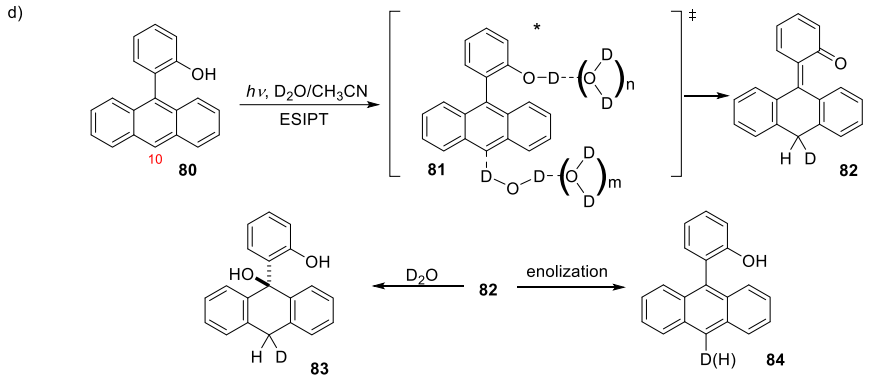

1.4.2 Kutateladze's ESIPT Photocycloaddition Methodology

As demonstrated in the previous section, irreversible ESIPT processes will lead to the formation of new products through a unique mechanism. More recently, Kutateladze and coworkers have reported highly interesting ESIPT-mediated reactions to access novel scaffolds that traditional chemical reactions were not able to. Using an *o*-azaxylylene as a photoexcited intermediate, Kutateladze and coworkers reported a number of novel, intramolecular ESIPT photocycloaddition reactions.

Scheme 1.10 Kutateladze's Photoassisted Access to Polyheterocycles

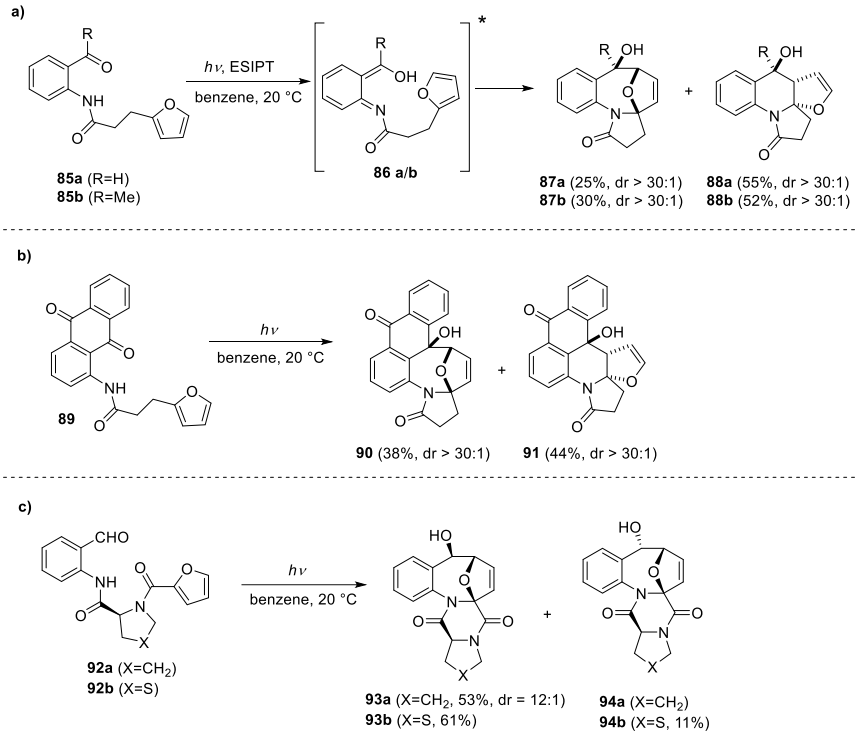

For example, Kutateladze and coworkers discovered that photo irradiation of 2-aminobenzaldehyde **85a** or 2-aminoacetophenone **85b** led to the formation of *o*-azaxylylenes **86a**/**86b** as ESIPT intermediates which may be trapped by the pendant furan in an intramolecular fashion to afford photocycloadducts (**Scheme 1.10**).[39] Both [4+2] and [4+4] photocycloadducts were obtained in high diastereoselectivity. This reaction represented the first example of [4+2] and [4+4] cycloaddition reactions of photogenerated *aza*-xylylenes with unsaturated pendant groups. More interestingly, compound **89** with an anthraquinone moiety was also able to undergo ESIPT photocycloaddition to provide products **90** and **91**. ESIPT photocycloaddition of enantiomerically pure precursors containing a cyclic amino acid such as **92a** and **92b** was also studied. Photocyclization of **92a** occurred exclusively *via* the [4 + 4] pathway to afford adduct **93a** (major) and its

hydroxy epimer with a d.r. of 12.5:1 for the proline derivative and 4:1 for the thiaproline analogue. The polyheterocyclic core of **93** and **94** was formed stereospecifically, thus indicating full stereochemical control of the folding of the tether in the transition state by the (thia)proline moiety and 100% chirality transfer.

Subsequently, Kutateladze and coworkers demonstrated that the aforementioned photo-excited *aza*-xylylene intermediates could also be generated from *o*-amido imines *via* ESIPT to undergo intramolecular cycloadditions.[40] Quinoxalinones **95** and **99** bearing a carbonyl group conjugated to the imine were designed to not only help to generate a more electron-deficient photogenerated azaxylylene but also allow for utilization of an oxophilic Lewis acid, such as $Ti(OiPr)_4$, to further polarize and activate the *aza*-xylylenes. Irradiation of **95** was carried out with Nichia 365 nm UV LEDs to give [4+4] cycloaddition product **96** and [4+2] cycloaddition products **97** and **98** (**Scheme 1.11a**). The quinoxalinone core was also found to be photoreactive toward pyrrole-based unsaturated pendants, as observed with compound **99**. Upon photo irradiation of **99**, stereoselective [4+2] photocycloaddition occurred to produce hexacyclic compound **100**. The enantiopure photocycloadduct **100** was further modified by post-photochemical transformations into diazacanes containing a spiro-quinoxalinone moiety and a total of five stereogenic centers.

Scheme 1.11 Kutateladze's Intramolecular ESIPT Photocycloaddition of *o*-Amido Imines and Development of an Asymmetric ESIPT Photocycloaddition Using Imine-Containing Chiral Auxiliaries.

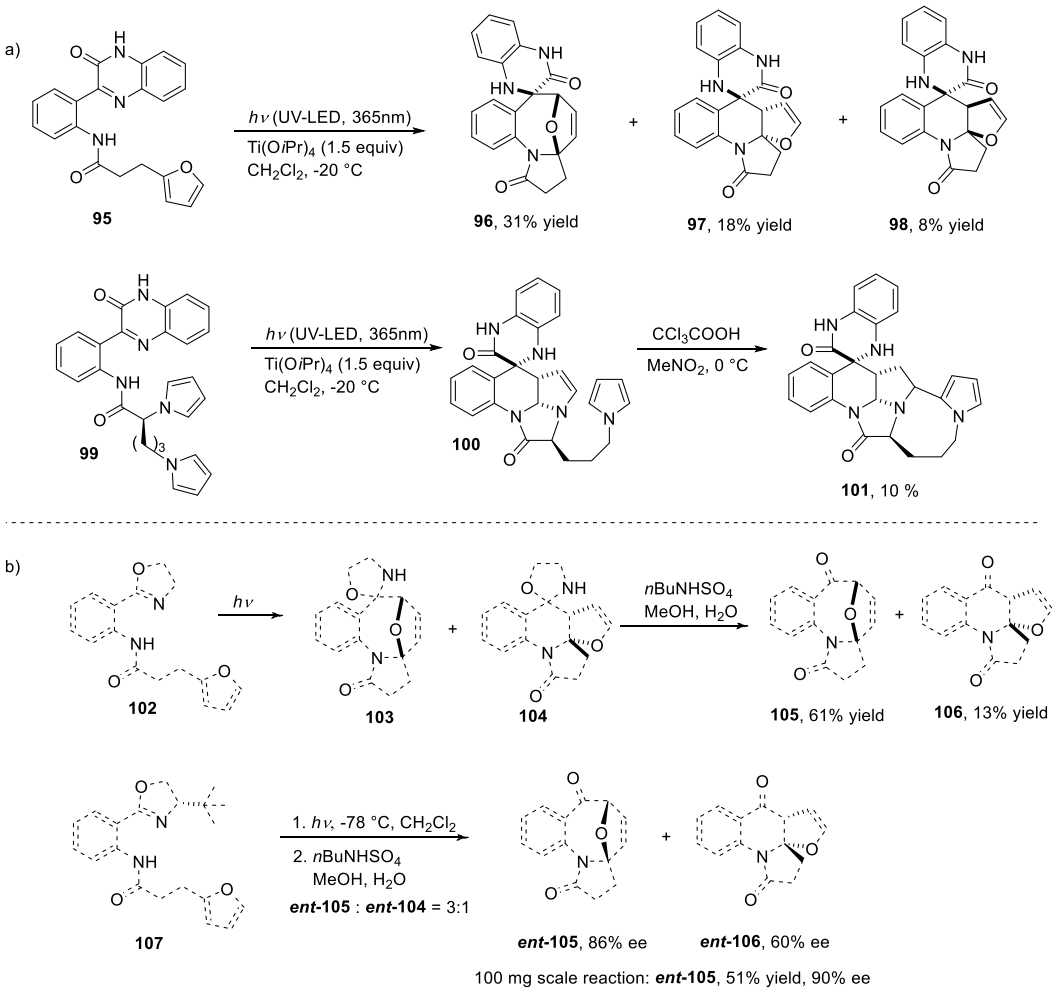

Since imine-containing compounds were found to be photoactive to produce ESIPT photocycloadducts, Kutateladze and coworkers also demonstrated that chiral oxazoline containing photoprecursors could also be utilized a chiral auxiliairies to undergo enantioselective intramolecular ESIPT photocycloadditions (**Scheme 1.11b**).[41] Photocycloaddition of achiral model compound **102** resulted in the clean formation of both [4+2] and [4+4] photoproducts **103** and **104**. Hydrolysis of the hemiaminal moiety on the spiro-oxazolidine photocycloadducts **103** and **104** led to the formation of ketones **105** and

106 thus demonstrating the feasibility to utilize chiral oxazoline auxiliaries in diastereoselective ESIPT photocycloadditions. A number of photoprecursors bearing chiral oxazoline auxiliaries were subsequently synthesized and evaluated in the photocycloaddition. Two diastereomers, distinguishable by NMR, were formed during the photocycloaddition which enabled calculation of diastereomeric excess prior to the workup of the reaction. Compound **107** bearing a chiral *t*-butyl group on the oxazoline moiety proved to be the optimal auxiliary, providing ***ent*-105** in 86% enantiomeric excess following hydrolysis of the [4+4] photocycloaddition product, and 60% ee for the [4+2] photocycloadduct ***ent*-106**. A preparative scale (100 mg) of this reaction was also conducted to yield ***ent*-105** in 90% ee and 51% isolated yield.

Scheme 1.12 Kutateladze's Dearomatization of Arenes with *Aza*-*o*-xylylenes *via* Intramolecular ESIPT Photocycloaddition

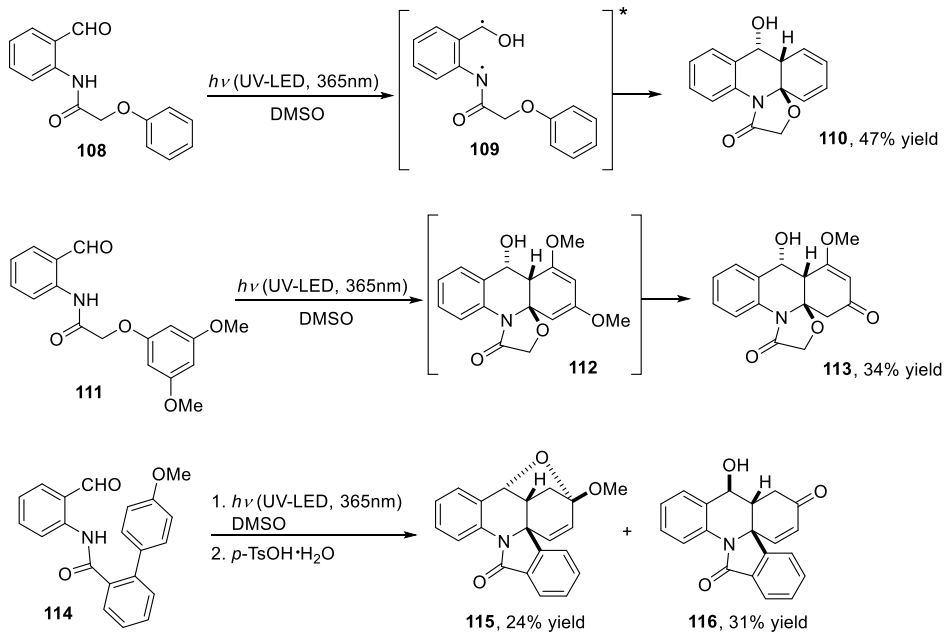

Kutateladze and coworkers also reported that photo-generated *aza*-*o*-xylylene intermediates could be used to directly dearomatize electron-rich arenes *via* intramolecular

ESIPT photocycloadditions (**Scheme 1.12**).[42] Upon photo excitation of **108**, an ESIPT intermediate was generated which would further lead to excited triplet intermediate **109** *via* intersystem crossing (ISC). The electrophilic *N*-centered radical on **109** could first initiate the dearomatization reaction,[43] with the overall process resembling a formal inverse-electron-demand Diels–Alder cycloaddition to produce photocycloadduct **110** in 47% yield. Compound **111** with a dimethoxyphenol moiety was also found to undergo cycloaddition, resulting in the formation of methoxycyclohexadiene product **112** which spontaneously hydrolyzed to cyclohexenone product **113**. Aromatic amides, such as photoprecursor **114** also underwent photocycloaddition to provide two diastereomers. Upon treatment with *p*-TsOH, intramolecular acid-catalyzed nucleophilic capture of the benzylic hydroxy group of the *anti*-diastereomer produced a stable ketal product **115**, while the *syn*-diastereomer hydrolyzed directly to enone compound **116**.

1.4.3 Porco's ESIPT Photocycloaddition to Access Rocaglate Scaffolds

Porco and coworkers, using optimized reaction conditions and sequences, demonstrated the broad substrate scope of their ESIPT photocycloaddition methodology in the syntheses of rocaglate analogs **117** to **131** (**Scheme 1.13**).[44] In this study, the use of a $CHCl_3$/TFE(trifluoroethanol) (7:3) solvent mixture was found to be the optimal condition for the cycloadduct production as well as diastereoselectivity. Conversion of the resulting aglain photocycloadduct to cyclopenta[*b*]benzofurans was achieved using two methods. Methyl ester-containing aglain scaffolds could be converted to keto-rocaglates using sodium methoxide to induce α-ketol shift. However, in some cases TMSOTf-mediated ketol rearrangement was found to be necessary due to the sensitivity of certain moieties,

such as thioesters, to nucleophilic methoxide. Novel rocaglates were obtained using this methodology including thioester **117**, Weinreb amide **118**, amide **119**, and nitrile **121**. Variation of the aromatic ring of the cinnamate reaction partner also showed broad substrate scope, including electron withdrawing groups as found in **126**, heterocycle **127**, and diene **122**. The favored *endo* diastereoselectivity of the ESIPT photocycloaddition is presumably due to a π-π stacking interactions between the aromatic group on cinnamate and the *para*-methoxyphenyl moiety on 3-hydroxyflavone **13**.

An *in vitro* protein translation inhibition assay of the synthetic rocaglates performed by Prof. Jerry Pelletier at McGill University showed that compounds **119** and **120** were the most potent derivatives, with IC_{50} values of 300-400 nM demonstrating excellent potency when compared with the positive control, (–)-silvestrol (**6**), which showed an IC_{50} of 100 nM in the same assay. *In vivo* studies demonstrated that Weinreb amide **118** was identified to be a highly potent translation inhibitor, inhibiting 85% of protein synthesis over the course of an hour, similar to (-)-silvestrol (**6**). Subsequently, Weinreb amide **118** was also identified as a potent inhibitor of heat shock factor 1 (HSF1), a transcriptional regulator of tumorigenesis and other cellular processes.[45] Tumor masses in mouse xenograft models (5e7 M0-91 cells) were significantly reduced by low doses of Weinreb amide **118**.

Scheme 1.13 Porco's ESIPT Photocycloaddition Methodology to Access Rocaglate Analogs

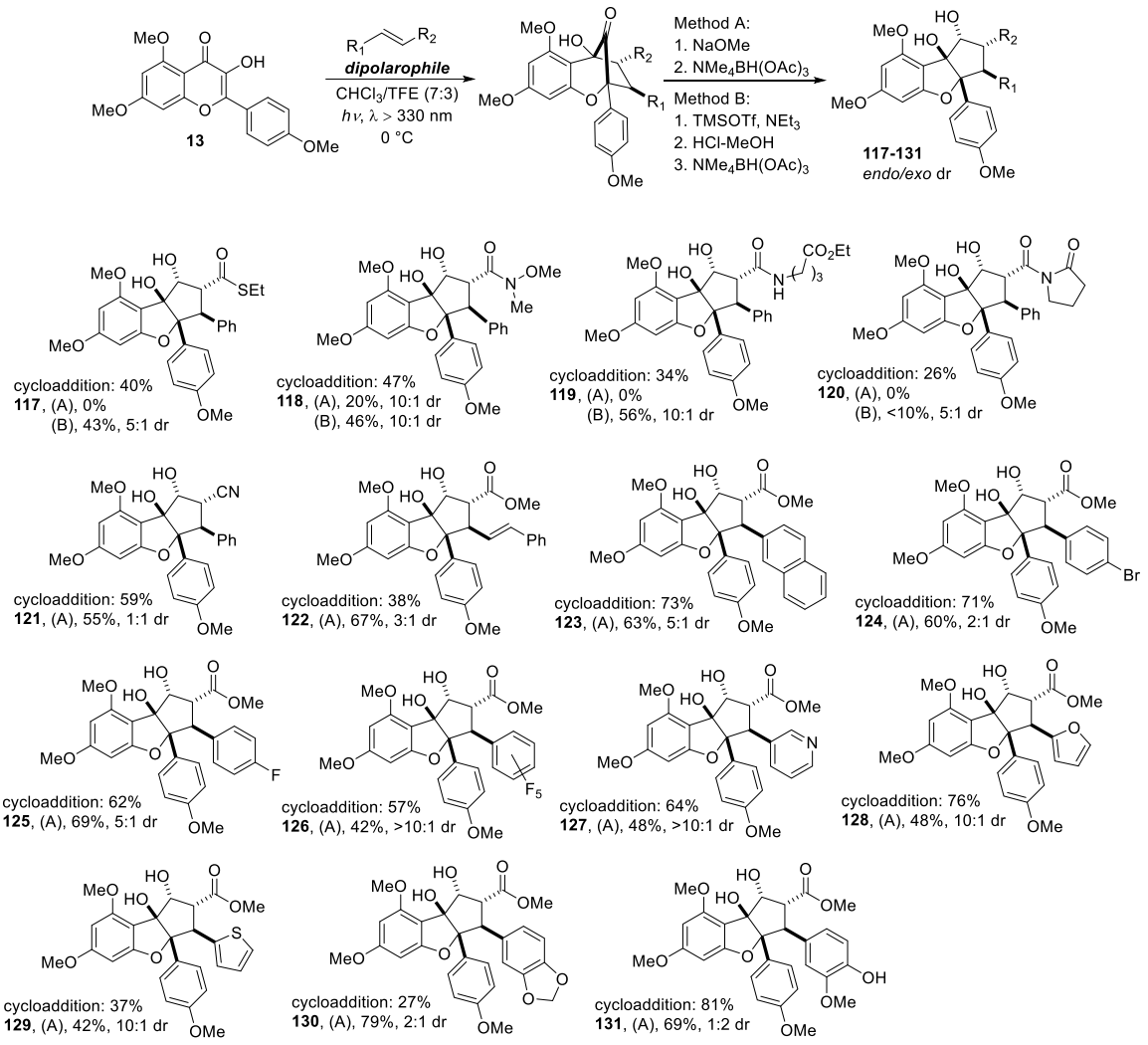

1.5 Conclusion

In summary, this chapter described flavagline natural products, bioactive species biosynthetically generated from 3-hydroxyflavones and cinnamic derivatives. Many synthetic approaches towards rocaglamides have been achieved, including the first asymmetric synthesis by the Trost group, as well as the biomimetic approach by the Porco group. Asymmetric syntheses of aglain natural products were also reported by the Porco

group using biomimetic, ESIPT-mediated (3+2) photocycloadditions. Although syntheses of rocaglates and aglain natural products have been achieved, no efforts towards isomeric aglain natural products, such as foveoglin A (**9**), have been reported. In addition to the ESIPT photocycloadditions reported by the Porco laboratory, other literature-reported ESIPT reactions and photocycloadditions were also discussed. Even though only limited synthetic methodologies involving ESIPT-generated intermediates can be found in the literature, this type of photoreaction demonstrated unique reactivity patterns, and that further methodology development will undoubtedly lead to new reactivity.

In the following chapter, we will describe our efforts towards the isomeric aglain natural products (±)-foveoglin A (**9**) and (±)-perviridisin B (**10**), as well as the asymmetric synthesis of (+)-foveoglin A (**9**) and its absolute stereochemistry determination. These studies also involved a collaboration with Prof. Jayaraman Sivaguru and coworkers at North Dakota State University to conduct photophysical and mechanism experiments. We next will disclose studies involving ESIPT photocycloadditions of 3-hydroxyquinolinones with methyl cinnamate to access nitrogen-containing analogs, called *aza*-rocaglates. In collaboration with Professor David Coker and coworkers at Boston University, we additionally have studied the mechanism of the asymmetric ESIPT photocycloaddition of 3-hydroxyflavone with cinnamates using TADDOL as a chiral additive using computational approaches. These studies have also served to guide our design of photocatalysts for catalytic asymmetric ESIPT photocycloaddition.

CHAPTER TWO

Total Syntheses of Isomeric Aglain Natural Products Foveoglin A and Perviridisin B: The Mechanistic Studies of ESIPT Photocycloadditions

2.1 ESIPT Photocycloaddition of 3-Hydroxyflavone with Diphenylbutadiene

Although the asymmetric syntheses of (+)-ponapensin and (+)-elliptifoline were achieved using ESIPT photocycloaddition reactions (*cf.* Chapter 1.3.2),[12] the isolation of isomeric aglain natural products such as foveoglin A[13] provides new challenges for the application of ESIPT photocycloaddition reactions in total synthesis. Based on previous work carried out in the Porco laboratory demonstrating that ESIPT photocycloaddition of 3-hydroxyflavone (3-HF, **1**) with *trans*-stilbene **2** was able to provide photocycloadduct **3** in 5:1 d.r. (**Scheme 2.1a**),[44] we planned to perform an ESIPT photocycloaddition of 3-hydroxyflavone **1** with *trans*,*trans*-1,4-diphenyl-1,3-butadiene (DPBD, **4**). In theory, if the photocycloaddition occurred, photocycloadducts **5**-**8** can potentially be generated. In particular, selective synthesis of diastereomers **7** and **8** could be utilized for the total synthesis of the congeners foveoglin A (**9**) and perviridisin B (**10**) (**Scheme 2.1b**). Retrosynthetically, we proposed that foveoglin A (**9**) and perviridisin B (**10**) could be formed through oxidative amidation of aldehydes **11** and **12** with the corresponding amines. Aldehydes **11** and **12** in turn could arise from oxidative cleavage of the styrenyl moiety on the aglain core structures resulting from diastereoselective reduction of photocycloadducts **7** and **8** (**Scheme 2.1c**).

Scheme 2.1 (3+2)-Photocycloaddition Involving 3-Hydroxyflavones with Dipolarophiles 2 and 4 and Retrosynthetic Analysis of the Isomeric Aglain Natural Products

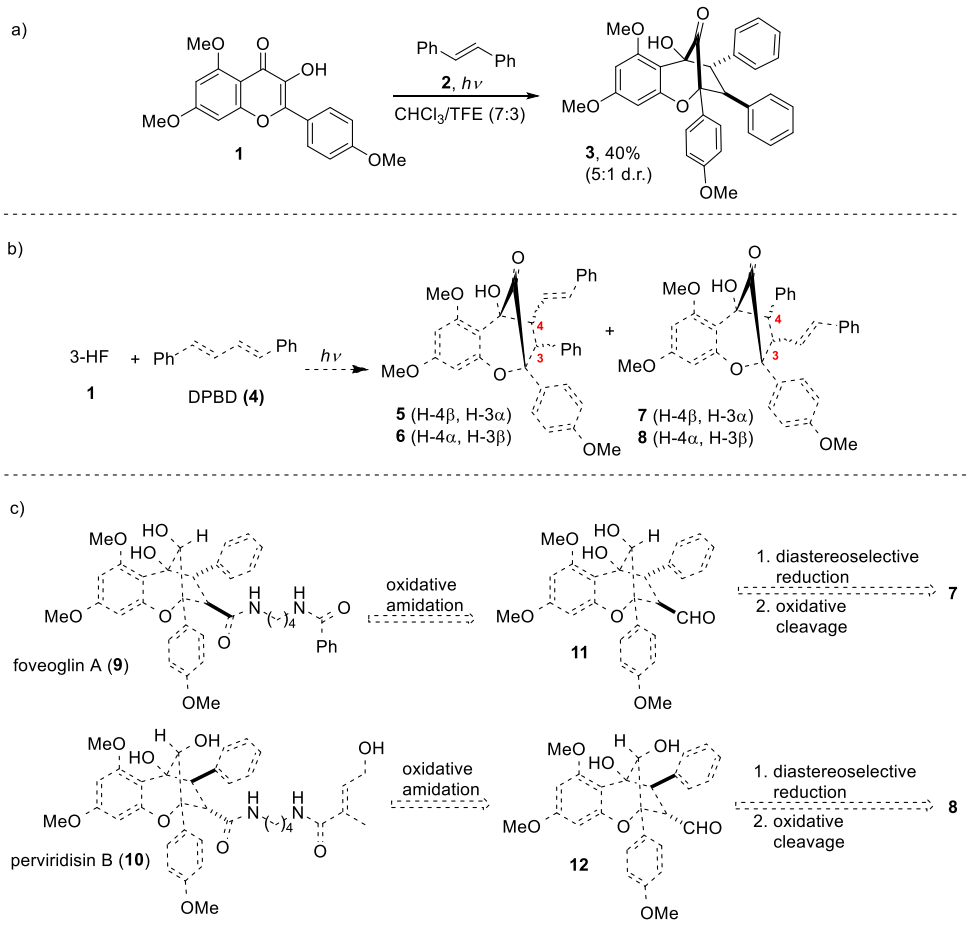

To begin our synthetic studies, ESIPT photocycloaddition of 3-hydroxyflavone **1** with DPBD **4** was first conducted using standard reaction conditions (**Scheme 2.2a**). Gratifyingly, upon photoirradiation of 3-hydroxyflavone **1** and DPBD **4** in a $CHCl_3$/TFE = 7:3 solvent mixture at 0 °C for 12 h, substantial formation of diastereomers **7** and **8** was observed as an inseparable mixture in 49% yield and in 4:1 ratio of diastereomers. Although there was potential that extending the conjugation of the dipolarophile into a diene would erode selectivity of the ESIPT photocycloaddition, we observed good regio and diastereoselectivity, which further encouraged us to apply this methodology to the total

syntheses of **9** and **10**. The inseparable mixture of diastereomers was treated with $NaBH_4$ in THF to afford the corresponding secondary alcohols in 5:1 d.r., which ultimately enabled isolation of the desired major diastereomer **13** in 32% yield. The relative stereochemistry of **13** was also unambiguously established by X-ray crystallographic analysis of the corresponding *para*-bromobenzoate derivative **14** (**Scheme 2.2b**). To further test the stability of **14** towards oxidative conditions, aglain derivative **13** was treated with the mild oxidant MnO_2 which led to C-C bond oxidative fragmentation providing benzo[*b*]oxepine **15**, demonstrating the fragility of the C5-C10 bond.

Scheme 2.2 ESIPT Photocycloaddition of 3-Hydroxyflavone with DPBD 4

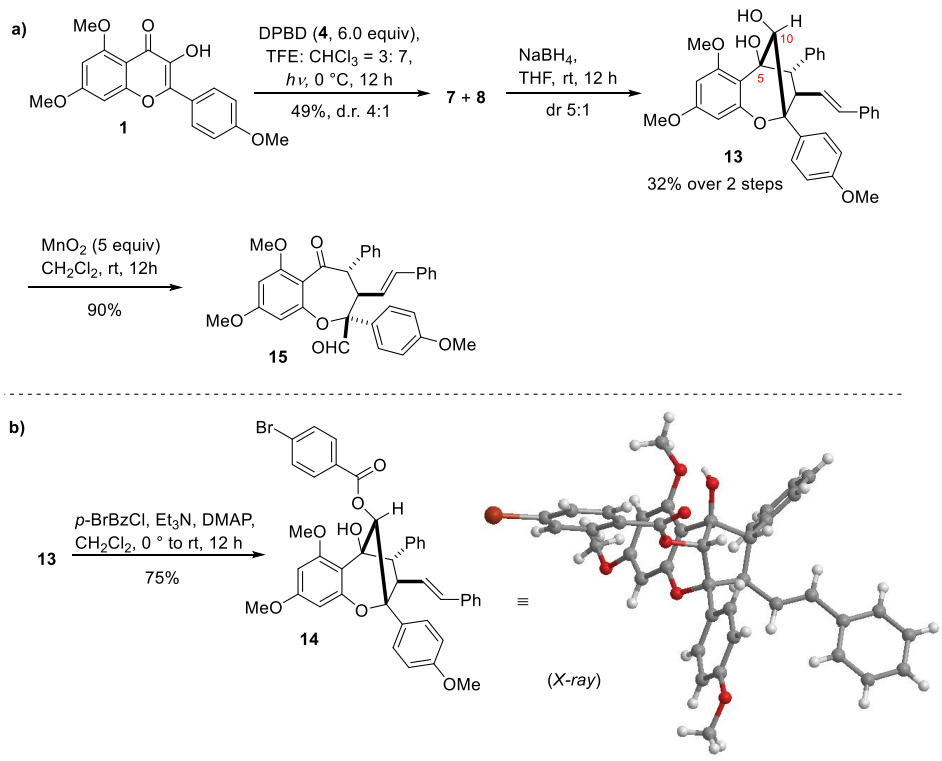

2.2 Design of a Recirculating Photoflow Reactor for the ESIPT Photocycloadditions

We next considered conducting the ESIPT photocycloaddition of 3-HF **1** and DPBD **8** in a recirculating photoflow reactor to make this reaction more scalable. As

previous photoreactions were all conducted in a Pyrex glass tube, several limitations were found during these studies: 1) limited amounts of starting material can be applied, thus limiting our reactions to milligram scale; 2) more than 10 hours irradiation was required for most of the substrates to afford useful yields and conversion; 3) low temperature (0 °C) was needed for the photoreaction to minimize photodegradation of 3-HF **1**,[46] which was complicated by the significant amount of heat release by the UV-lamp. The use of photoflow chemistry would not only alleviate these issues, but may additionally facilitate our reaction when compared to traditional photochemical setups/methods.[47]

Figure 2.1 Design of the Rayonet Continuous Photoflow Reactor

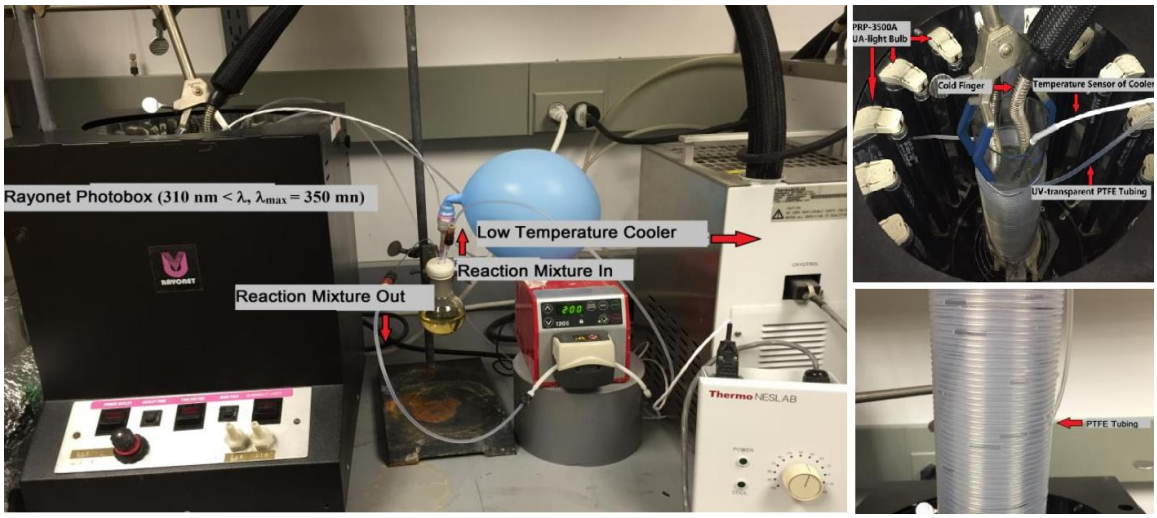

For our continuous photoflow reactor design, a Rayonet® recirculating photoflow reactor was constructed using PTFE Tubing (1/32"ID x 1/16"OD) (Cole-Parmer® Instrument Company) wrapped around a 500 mL Pyrex graduated cylinder (**Figure 2.1**). The reactor (tubing) volume was measured to be 56 mL. The reactor was placed into Rayonet RPR-100 photobox equipped with RPR-3500Å irradiation lamps (λ_{max} = 350 nm). The tubing was connected to a peristaltic pump (Benchtop pump with 114DV flip top

single channel pumphead, model: 120S, Waston Marlow Fluid Technology Group) using 2 conical adapter assemblies (IDEX Health & Science, P-798). Two needle adapters (IDEX Health & Science, Flangeless Ferrule Tefzel®, P-300X; Flangeless Short Nut, P-335X; Luer Adapters, P-655) were also installed to connect the reaction flask to the peristaltic pump and reaction tubing. A Thermo Scientific™ Neslab CC65 Immersion Cooler was used as a cooling system for the photoflow reactor, which was found to maintain reaction temperatures below 0 °C for 8 h.

Table 2.1 Diastereoselectivity of ESIPT Photocycloaddition.

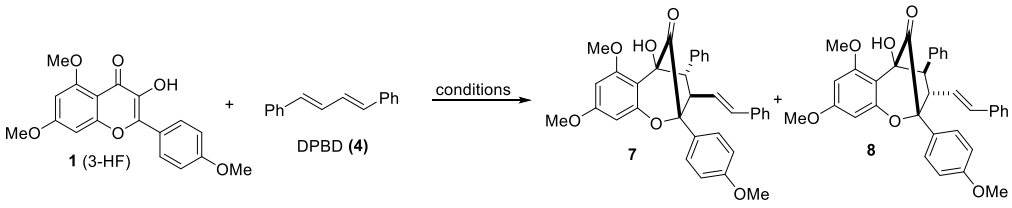

Entry	Solvent	Temp. Time	Additive	Outcome (**7**:**8**) [a,b]
1	CH_2Cl_2	0 °C, 6 h	N.A.	48%, 2:1 d.r.
2	CH_2Cl_2/MeOH (3:1)	0 °C, 6 h	N.A.	43%, 3:1 d.r.
3	CH_2Cl_2	0 °C, 6 h	*p*-TsOH	37%, 3:1 d.r.
4	CH_2Cl_2/*i*-PrOH (2:1)	0 °C, 6 h	N.A.	51%, 1:1 d.r.
5	CH_2Cl_2	0 °C, 6 h	benzophenone	50%, 2:1 d.r.
6	CH_3CN/MeOH (1:1)	0 °C, 6 h	N.A.	47%, 2:1 d.r.
7	THF	0 °C, 6 h	N.A.	47%, 3:1 d.r.
8	$CHCl_3$/TFE (7:3)	0°C, 6 h	N.A.	67%, 5:1 d.r.

[a]Isolated yield of mixture of **7** and **8**. [b]Diastereoselectivity was determined by ^{1}H NMR integration.

With the reciculating photoflow reactor in hand, we next studied the ESIPT photocycloaddition under recirculating flow conditions (**Table 2.1**). In comparison with batch photoreactions, higher yields were obtained in a shorter reaction time period and less photodegradation byproducts were observed. ESIPT photocycloadditions of 3-HF **1** with DPBD **4** using various solvents was also conducted using the Rayonet recirculating photoflow reactor to examine effects on diastereoselectivity. From these experiments, we found that although the mildly acidic alcohol trifluoroethanol (pKa = 12) was able to facilitate the photocycloaddition reaction and highest d.r. for production of *endo*-diastereomer **7** (**entry 8**), use of the more acidic additive, *para*-toluenesulfonic acid (pKa = 8.5) resulted in higher photodecomposition and lowered isolated yields (**entry 3**). Triplet sensitizers such as benzophenone led to a slight increase in yield but no significant improvement was found (**entry 5**). Isopropanol in combination with dichloromethane provided the best solvent for production of the *exo*-diastereomer **8** which paved the way for the synthesis of perviridisin B (**10**).

2.3 Total Syntheses of (±)-Foveoglin A and (±)-Perviridisin B

With increased amounts of **7**/**8**, and in turn aglain **13**, in hand, the synthesis of (±)-foveoglin A was next undertaken. Treatment of **13** with TBSOTf yielded the mono-silylated compound **16**; the silylation step was considered in order to prevent undesired oxidative fragmentation. However, **16** could not be desilylated under numerous acidic or fluoride-based deprotection conditions (**Scheme 2.3a**). Presumably, this lack of reactivity is due to further stabilization of the silyl group from the phloroglucinol moiety. Accordingly, a trimethylsilyl ether protecting group was examined as a more labile

protecting group and upon treatment of **13** with TMSOTf, double silylation was achieved to afford compound **17**. The crude product was directly subjected to osmium tetroxide-catalyzed dihydroxylation and lead (IV) acetate-mediated diol cleavage to produce aldehyde **18** in 71% yield. The aldehyde **18** was further reacted with amine **19** *in-situ* generate a corresponding imine intermediate which was subsequently oxidized under Pinnick-type oxidation conditions[48] using sodium chlorite to access amidation product **20** in 75% yield. Treatment of **20** with tetrabutylammonium fluoride then yielded (±)-foveoglin A (**9**) in 6 steps and 22% over-all yield (**Scheme 2.3b**).

Scheme 2.3 Total Synthesis of (±)-Foveoglin A

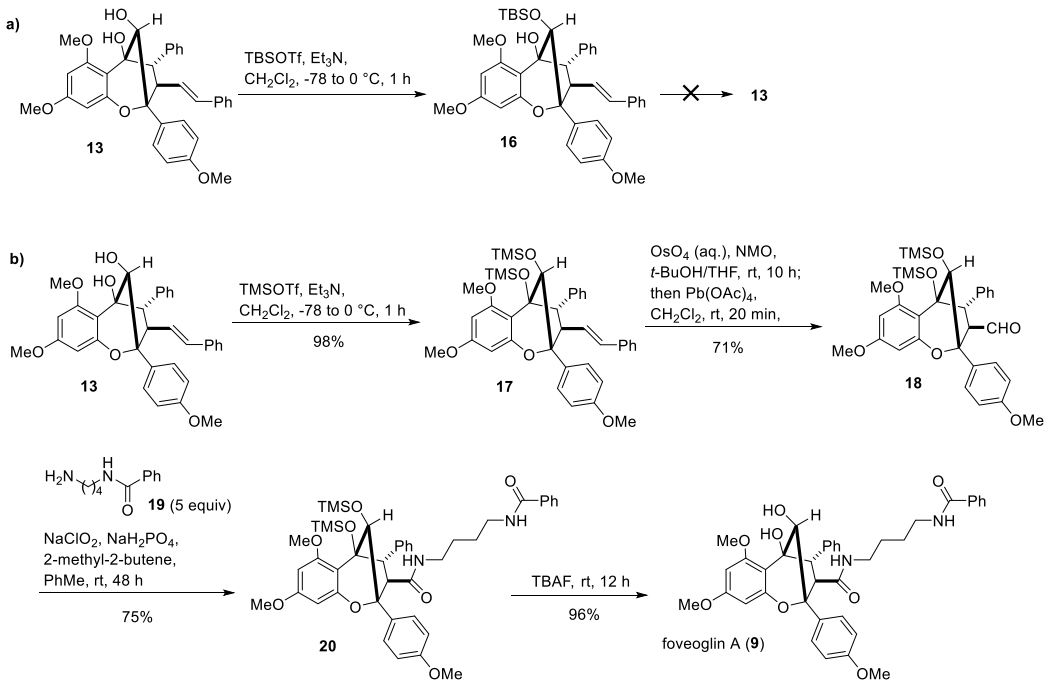

In order to achieve the synthesis of the congener perviridisin B (**10**), practical access to the *exo*-diastereomer **8** was required. Therefore, the photocycloaddition of **1** with **4** was conducted using 2:1 CH_2Cl_2 /*i*PrOH which provided the highest selectivity for **8** (*cf.* **Table 2.1**). With the 1:1 mixture of **7** and **8** in hand, diastereoselective reduction of the

mixture using sodium triacetoxyborohydride followed by silylation with TMSOTf afforded 10*S*-*exo*-aglain scaffold **22** (**Scheme 2.4**). Using the previously demonstrated double bond oxidative cleavage conditions with foveoglin A (**9**), 10*S*-*exo*-aldehyde compound **23** was obtained. To prepare amine **27**, tiglic ester **24** was saponified and coupled with mono-Boc-protected 1,4-diaminobutane to furnish amide **25**. The allylic alcohol moiety was further protected with an acetate group to prevent undesired decomposition in the following deprotection step. Removal of the Boc protecting group using trifluoroacetic acid afforded amine **27** which was directly subjected to Pinnick-type oxidative amidation conditions with aldehyde **23** to obtain amide **28**. After treatment of tetrabutylammonium fluoride for silyl deprotection and *in situ* hydrolysis of the allylic acetate with aqueous sodium bicarbonate, (±)-perviridisin B (**10**) was cleanly obtained.[49]

Scheme 2.4 Total Synthesis of (±)-Perviridisin B (10)

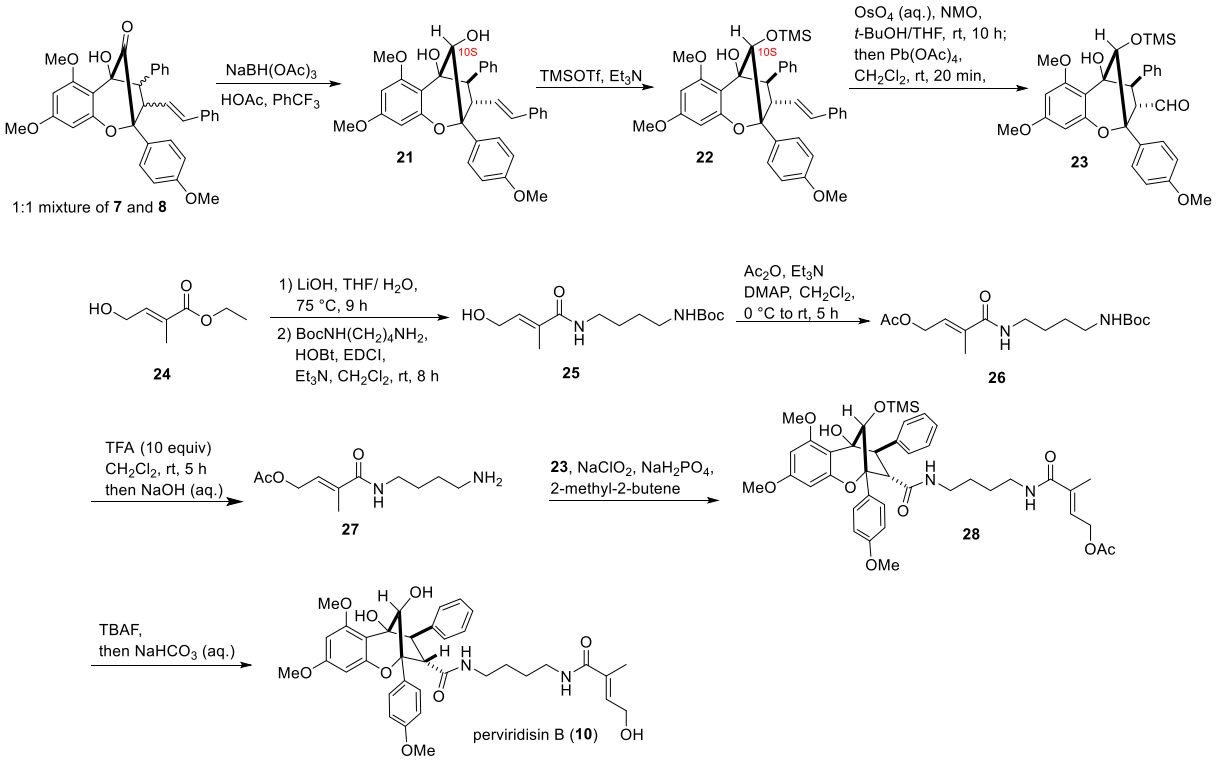

2.4 Enantioselective Synthesis of (+)-Foveoglin A and Assignment of its Absolute Configuration

Having established an efficient route towards isomeric aglain natural products **9** and **10**, asymmetric syntheses of these natural products *via* an enantioselective ESIPT photocycloaddition was studied. Although we have previously reported the enantioselective ESIPT photocycloaddition of 3-hydroxyflavone with methyl cinnamate using TADDOLs as chiral hydrogen bonding additives (*cf.* **Section 1.3.2**), the reported dipolarophile scope was limited to cinnamate derivatives. The use of a dipolarophile such as DPBD **4** which lacks the ester moiety as a potential hydrogen-bonding acceptor should provide further information on the previous mechanistic proposal that a host-guest complexation of 3-HF **1** by hydrogen-bonding additives controls enantioselectivity in ESIPT photocycloadditions.

Table 2.2 Enantioselective ESIPT Photocycloaddition Using Chiral Hydrogen Bonding Additives

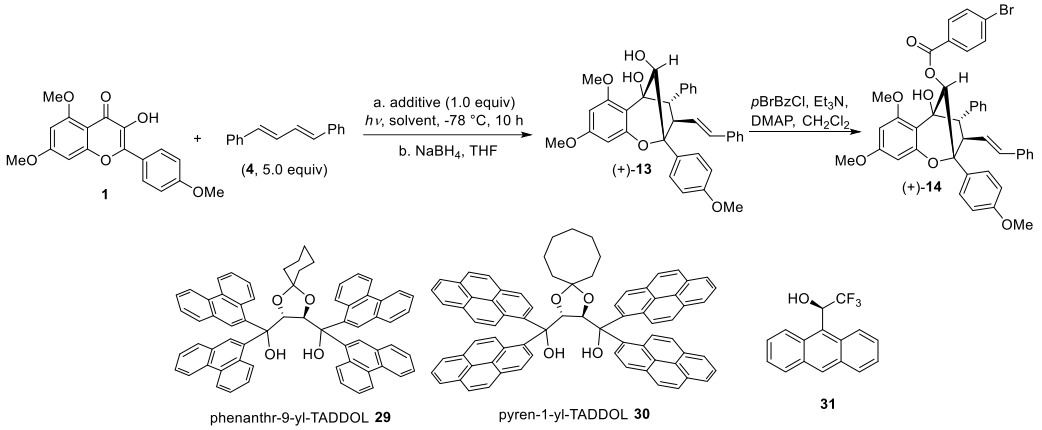

Entry	Time, Temperature	Light Source	Solvent	Chiral Additive	Yield (%)[a], Enantiomeric excess[b]
1	12 h, -75 °C	Rayonet (310 - 400 nm)	PhMe/CH_2Cl_2 (1:2)	**29**	40%, 52% ee
2	12 h, -75 °C	Rayonet	PhMe/CH_2Cl_2 (1:2)	**30**	39%, 45% ee
3	12 h, -75 °C	Rayonet	CH_2Cl_2	**29**	41%, 69% ee
4	12 h, -75 °C	Rayonet	CH_2Cl_2	**31**	30%, 49% ee
5	5 h, -30 °C	Rayonet Photoflow	CH_2Cl_2	**29**	67%, 31% ee
6	10 h, -78 °C	UV-LED (365 - 370 nm)	CH_2Cl_2	**30**	65%, 49% ee
7	10 h, -78 °C	UV-LED	PhMe/CH_2Cl_2 (1:2)	**29**	31%, 71% ee
8	10 h, -78 °C	UV-LED	CH_2Cl_2	**29**	67%, 83% ee
9	10 h, -78 °C	UV-LED	CH_2Cl_2	**31**	41%, 71% ee

[a]Isolated yield of mixture of (+)-**13**. [b]Enantiomeric excess of (+)-**13**.

Figure 2.2 Pirkle's Alcohol 31 as an NMR Additive to Determine Enantiomeric Ratios of γ-Lactones.

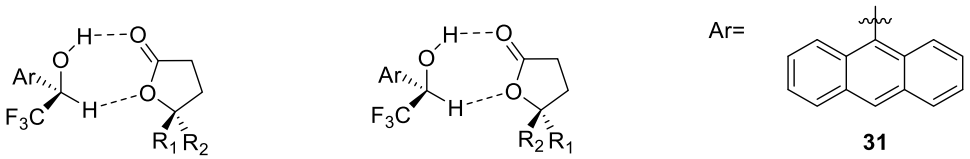

In the presence of a stoichiometric amount of a hydrogen-bonding additive, 3-HF **1** and DPBD **4** were irradiated for 12 h at -75 °C using a Rayonet photobox and low temperature was maintained by a dry ice / isopropanol mixture (dry ice bath was refilled every hour). Limited solubility of DPBD **4** at low temperatures was observed which prompted us to dilute the reaction mixture (0.005 M for 3-HF **1**) to achieve homogeneity. The resulting crude mixture of diastereomers was directly reduced to afford aglain **13** for enantiomeric excess determination *via* chiral HPLC analysis. phenanthr-9-yl-TADDOL **29** was found to provide the best enantioselectivity in dichloromethane (**Table 2.2**) while use of a toluene/dichloromethane solvent mixture or pyren-1-yl-TADDOL **30** did not result in improved enantioselectivity. Presumably, this may be due to the reduced solubility of DPBD **4** and pyren-1-yl-TADDOL **30** in toluene solvent. The previously mentioned recirculating photoflow reactor was also employed for this reaction; however, in this case only 31% ee was observed. More interestingly, we are able to demonstrate that a chiral trifluoroethanol derivative, Pirkle's alcohol **31** can also mediate this reaction to provide **13** in 49% ee. Pirkle's alcohol **31** has been previously used as an additive in NMR analysis to determine enantiomeric ratios of γ-lactones through formation of diastereomeric complexes (**Figure 2.2**),[50] and this result demonstrates the first example of using Pirkle's alcohol as a chiral hydrogen bonding additive for enantioselective photocycloaddition.

In order to achieve more optimal temperature control for the enantioselective photocycloaddition and also simplify the operation of the photoreaction, a novel UV-LED low temperature setup was developed (**Figure 2.3**). A UV-LED (365 nm) light source provides narrow band UV emission which well covers the absorption wavelength of 3-hydroxyflavone **1**, but generates very little heat in comparison to the Rayonet photobox. Using a dry ice dewar with an optic window, the temperature of reaction mixture could be maintained at -78 °C for 10 h with only one addition of dry ice, thereby enhancing operational simplicity.

Figure 2.3 Graphic Description of UV-LED Low Temperature Photoreaction Setup.

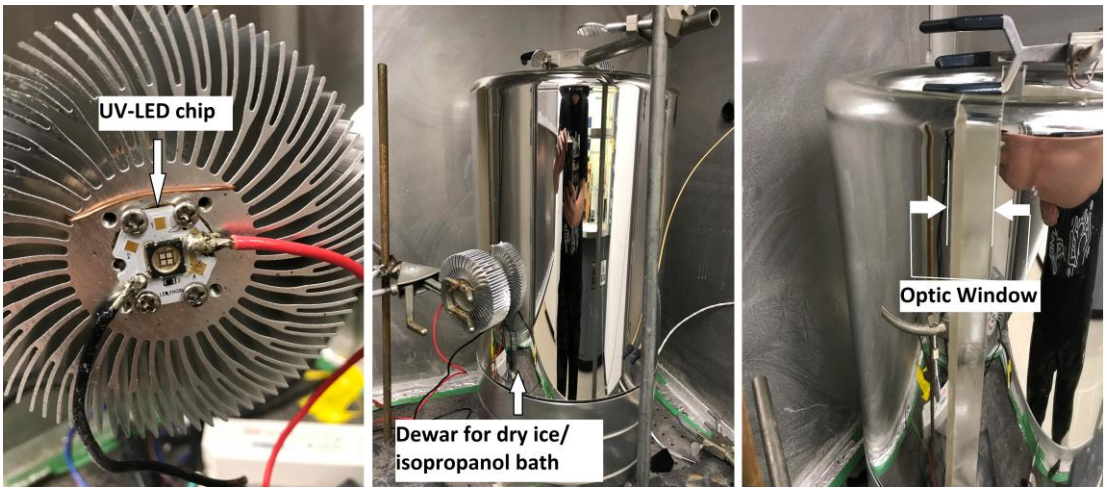

Enantioselective ESIPT photocycloadditions using this new UV-LED photo reaction setup were then conducted. To our delight, a general improvement was observed. Using phenanthr-9-yl-TADDOL **29**, an 83% ee was achieved after reduction of the inseparable mixture of diastereomers (d.r. = 6:1) by sodium borohydride to product (+)-**13** (**entry 8**), whereas use of pyren-1-yl-TADDOL **30** only delivered 49% ee of the product (**entry 6**). Pirkle's alcohol **31** was able to mediate this reaction to provide 71% ee of the

product. We subsequently attempted recrystallization of the product (+)-**13** to obtain enantiopure material. However, crystals of centrosymmetric racemate (±)-**13** were obtained with enantiomeric enrichment of the mother liquor to 93% ee. The corresponding *p*-bromobenzoate (+)-**14** was next prepared but also failed to provide an enantiopure crystal. The absolute configuration of (+)-**13** was ultimately determined by comparison of a calculated VCD (vibrational circular dichroism) spectrum of (+)-**14** with the experimental VCD spectrum of (+)-**14**.[50] The latter studies were conducted in collaboration with Dr. Lauren Brown in the BU-CMD.

Scheme 2.5 Asymmetric Synthesis of (+)-Foveoglin A

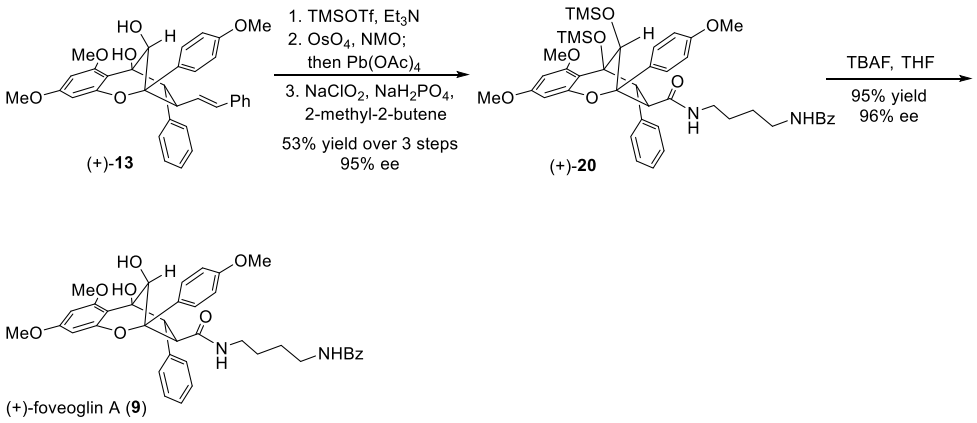

With aglain scaffold (+)-**13** in hand, we next turned our attention to synthesize (+)-foveoglin A (**9**). Using the previously described synthetic sequence, (+)-**13** was subjected to silylation, oxidative double cleavage, Pinnick-type oxidative amidation sequence to afford the core structure of the natural product (+)-**20** in 95% ee followed by deprotection using TBAF to furnish (+)-foveoglin A (**9**) in 96% ee ($[\alpha]_D^{20}$ -30.0 natural (c 0.16, $CHCl_3$), $[\alpha]_D^{23}$ +25.3 synthetic (c 0.16, $CHCl_3$)). As the absolute configuration of (+)-**13** was determined by VCD spectrum, we were able to assign the absolute configuration of natural

foveoglin A (**Figure 2.4**) as levorotatory which showed good agreement with our previous observation for aglain natural products such as ponapensin (*cf.* **Section 1.3.2**).

Figure 2.4 Absolute Configuration of Natural (–)-Ponapensin in Comparison with (–)-Foveoglin A.

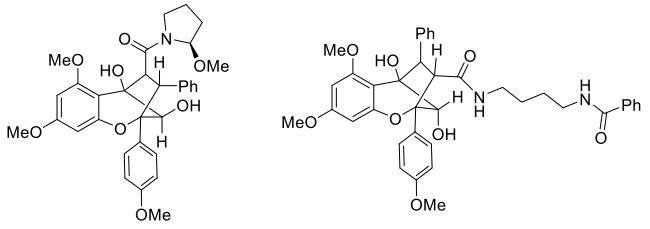

2.5 Mechanistic Studies of ESIPT Photocycloadditions

Photophysical investigations were next conducted to elucidate a mechanistic rationale for the observed diastereoselectivity for photocycloadducts **7** and **8** as well as understand the comparative excited state reactivity of 3-HF **1** with various dipolarophiles such as methyl cinnamate **30** and *trans*-stilbene **2**. Extensive photophysical measurements were first conducted to understand the ESIPT process of 3-HF **1**. These studies were done in collaboration with Professor Jayaraman Sivaguru and Anthony Clay at North Dakota State University (NDSU) (now at Bowling Green State University). A dual fluorescence emission (fluorescence of the normal state N centered at 439 nm and the tautomer state T centered at 527 nm) was observed for **1** at both room temperature and 77 K (**Figure 2.5 A**). The phosphorescence spectrum of **1** recorded in freezed TFE at – 78 °C (**Figure 2.5 B**) shows a λ_{max} for phosphorescence emission (528 nm) indicating a triplet energy (E_T) of 54.2 kcal/mol. As the photocycloaddition occurs with various dipolarophiles, fluorescence quenching of 3-HF **1** in the presence of methyl cinnamate **32** and *trans*-stilbene **2** was investigated in the solvent $CHCl_3$. Upon addition of various equivalents of either methyl

cinnamate **32** or *trans*-stilbene **2**, no noticeable quenching of the excited tautomer fluorescence signal of 3-HF **1** was observed (**Figure 2.5 C-D**) which indicated that the singlet excited state of 3-HF **1** did not play a role in the initiation of ESIPT photocycloadditions.

Figure 2.5 Photophysical Studies to Probe Excited State Reactivity of 3-HF 1.

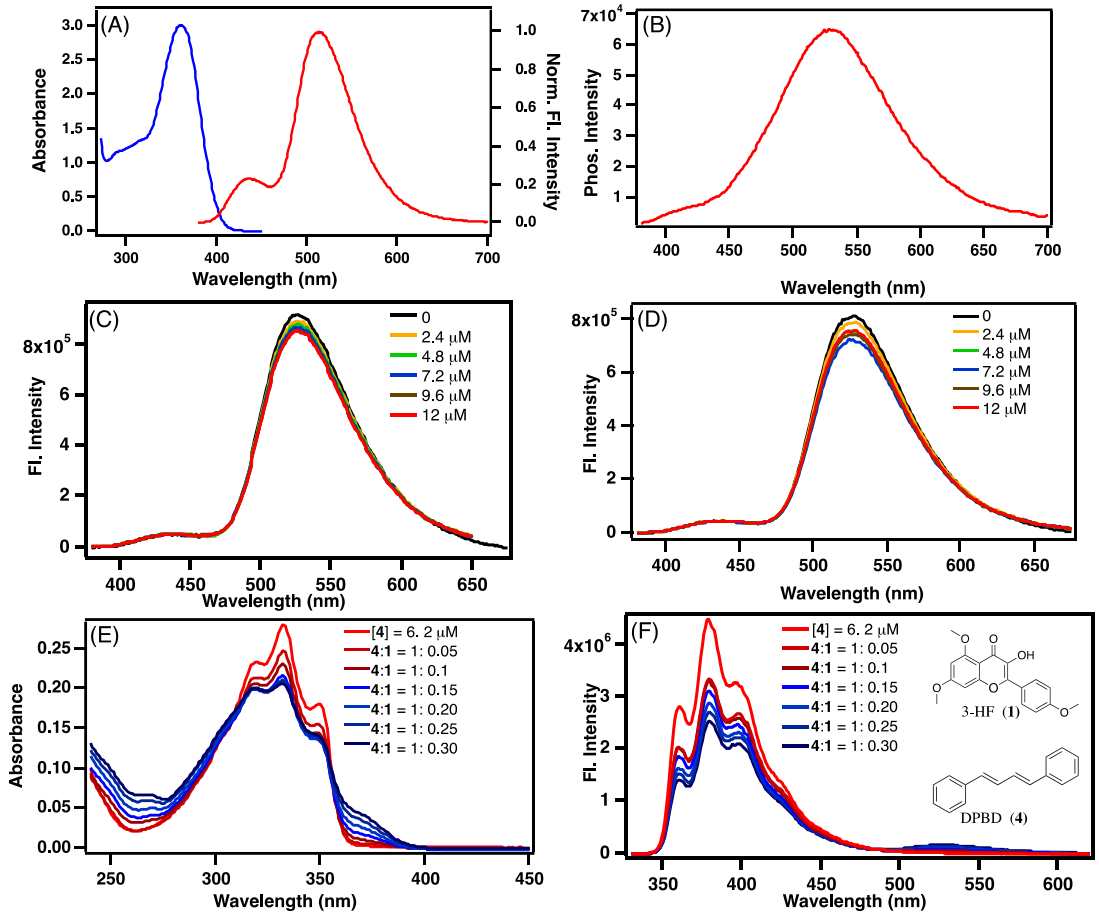

A) Absorbance (*blue*) of **1** in TFE [**1**] =2.35 μM. Fluorescence (*red*) of **1** in TFE with λ_{exc}=360 nm. **B**) Phosphorescence of **1** recorded in TFE glass, λ_{exc}=360 nm. **C**) Quenching of the fluorescence of **1** with varying concentrations (2.35 to 12 μM) of **32** $CHCl_3$:TFE (7:3 v/v). **D**) Quenching of the fluorescence of **1** with varying concentrations (2.35 to 12 μM) of **2** in $CHCl_3$:TFE (7:3 v/v). **E**) Absorbance of **4** (6.2 M) with addition of **1** at increasing equivalents (0 to 1.9 μM) recorded in a mixture of $CHCl_3$:EtOH (7:3) **F**) Fluorescence of **4** with addition of **1** at various equivalents (0 to 1.9 M) recorded in a mixture of $CHCl_3$:EtOH (7:3); λ_{exc}=320 nm; λ_{emiss}=330-620 nm.)

From the quenching experiments, we were able to identify that no significant quenching of fluorescence signal was observed by addition of methyl cinnamate **32** or *trans*-stilbene **2**. Therefore, a singlet energy transfer mechanism can likely be ruled out. This result is also consistent with the fact that the singlet energy of DPBD (80 kcal/mol) is higher than the singlet energy of 3-HF **1** (71 kcal/mol) in which singlet energy transfer is forbidden. Based on a previous literature report, the triplet energy of DPBD is 42 kcal/mol, which supports the possibility of a triplet energy transfer mechanism when considering that the triplet energy of 3-HF **1** is 55 kcal/mol based on the λ_{max} = 520 nm observed in the phosphorescence spectrum of **1**.

To further study this process, our NDSU collaborators subsequently attempted to record the transient absorption of 3-hydroxyflavones both in the presence and absence of various dipolarophiles. Previous literature has already suggested that the transient absorption of the parent 3-hydroxyflavone **33** is complicated by overlapping absorptions from both the singlet and triplet excited states of the normal and the photo-tautomerized species.[51] Unfortunately, attempts to record transient absorptions of both **1** and **33** met with similar complications as previously investigated 3-hydroxyflavones, namely the aforementioned overlapping absorptions of differential excited states, as well as low stability of the 3-hydroxflavones under laser irradiation. These complications ruled out the use of transient absorption studies to gain useful information regarding the quenching of the presumed triplet excited states of **1** and **33** with various dipolarophiles.

Alternatively, as 3-hydroxyflavones are known to be antioxidants,[52] a low oxidation potential could be expected for these compounds which allows us to also consider a

photoinduced electron transfer (PET) mechanism. In order to elucidate and characterize excited state reactivity through a possible PET pathway, we determined the oxidation and reduction potentials of 3-HF **1** and various dipolarophiles using cyclic voltammetry and differential pulse voltammetry (**Table 2.3**). Based on the reduction and oxidation potentials as well as the excited state energy of 3-HF **1** (E_T =54.6 kcal/mol), the feasibility of electron transfer was ascertained using the Rehm-Weller equation (**Table 2.3**). Inspection of **Table 2.3** reveals that exergonic electron transfer from the excited triplet state of **1** to *trans*,*trans*-1,4-diphenyl-1,3-butadienes **1** as well as methyl cinnamate **32** is feasible. Due to lack of fluorescence quenching of **1** (**Figure 2.5 D**), electron transfer or energy transfer from the singlet excited state of **1** is likely not operative, so the phototautomer triplet state (^{3}T) of 3-HF **1** can feasibly initiate ESIPT photocycloaddition.

Table 2.3 Photophysical and Electrochemical Parameters for Photocycloaddition of 3-HF with Dipolarophiles.[a]

Entry	Parameter	**1**	**32**	**2**	**4**
1	E_T (kcal/mol)	54.2	49	55	42
2	E_{red} (V)	-	-2.34	-1.08	-0.96
3	ΔG (eV)	-	1.15	-0.11	-0.23
4	ΔG (kcal/mol)	-	26.5	-2.54	-5.3

[a]All redox values were taken in MeCN as solvent. Glassy carbon was used as the working electrode for *trans-trans*-1,4-diphenyl-1,3-butadiene **4** and 3-hydroxyflavone **1**. A platinum (Pt) electrode was used for **1**. The reference electrode employed was Ag/AgCl and Ag wire pseudo-electrode, respectively. Tertbutylammonium-hexafluorophosphate (TBAHFP) was used as the supporting electrolyte. In all cases, ferrocene was used as internal standard. The singlet (3.08 eV) and triplet (2.35 eV) state energies of energy of **1** were computed from the fluorescence and phosphorescence spectra, respectively.

Based on the computed free energies from Rehm-Weller equation for **1** and **4** and the absorptivity of the reactants under the concentrations employed for photoreactions,

deciphering the nature of the excited reactant initiating the (3+2) photocycloaddition became vital. To address this point, absorption and emission studies were performed with **1** and **4** at varying concentrations (**Figure 2.5 E-F**). Examination of **Figure 2.5 E** shows that the absorption of **4** centered at 332 nm undergoes a hypochromic shift upon addition of **1** indicating that there is likely a distortion of diene geometry in the presence of **1**. Similarly, the fluorescence intensity of **4** centered at 379 nm was lowered upon addition of **1**. This is likely due to the reduction in the absorptivity (hypochromic effect) of **4** by addition of **1**. Additionally, the rise of an emission band centered at 530 nm was observed which matched the emission of the phototautomer of **1**. These observations indicate that upon excitation of the reaction mixture at 320 nm, both DPBD **4** and the 3-hydroxyflavone **1** are excited. Due to the overlap of the absorption spectra for reaction partners **1** and **4**, control experiments were conducted to achieve selective excitation of **1** (1 equiv.) *vs*. **4** (5 equiv.) (*cf.* **Figure 2.5A** and **2.5E**) for ESIPT photocycloaddition. Using a purple LED as light source (395 nm < λ < 405 nm), photocycloadducts were produced indicating that selective photoexcitation of 3-HF **1** can mediate ESIPT photocycloaddition with reaction partners such as DPDB **4**. As a result, this adds credibility to the hypothesis that ^{3}T of 3-HF **1** most likely initiates the ESIPT photocycloaddition.

Scheme 2.6 Mechanism of ESIPT Photocycloaddition Involving Excited 3-HF 1 with Dipolarophiles

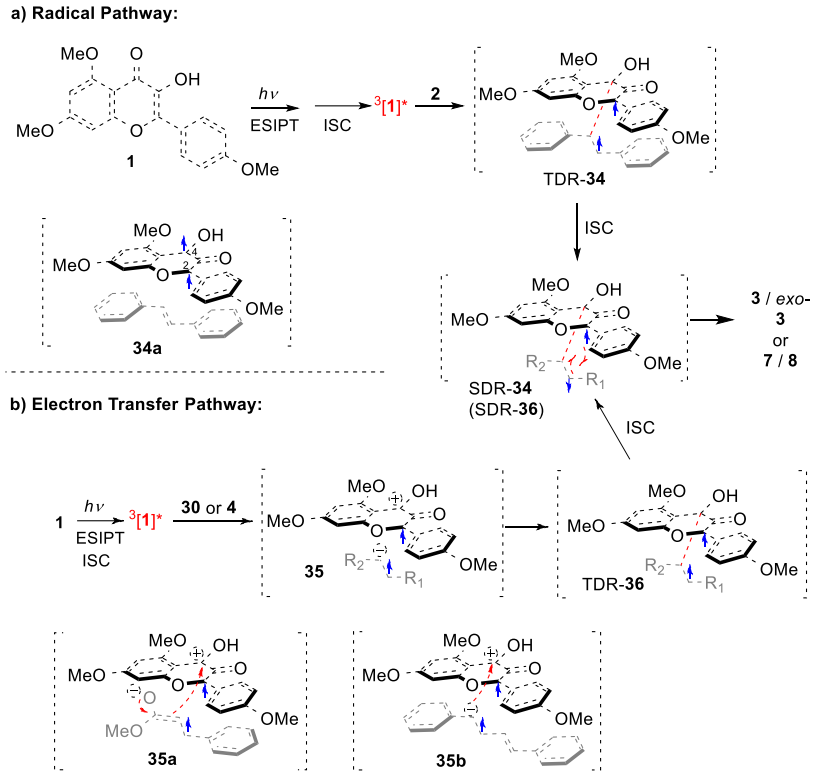

According to our photochemical and photophysical studies, depending on the excitation wavelength of the photoreaction and type of reactants employed, photocycloadditions can occur through different pathways leading to (3+2) photocycloaddition (**Scheme 5**). Based on the triplet energy and redox potential of **1** and the nature of the dipolarophile (**Table 2.3**), we hypothesize that either triplet diradical or electron transfer pathways are available for (3+2) photocycloaddition. Irradiation of **1** where the incident wavelength is greater than 390 nm (due to overlapping chromophores, competitive absorbance occurs with respect to DPBD **4** and **1** in the deep UV region spectrum when broad band irradiation is employed) results in the normal singlet excited state (^{1}N) that undergoes ESIPT affording the phototautomer singlet (^{1}T). This

phototautomer (^{1}T) subsequently undergoes intersystem crossing (ISC) to the corresponding triplet excited state (^{3}T). The phototautomer triplet (^{3}T) undergoes coupling with a dipolarophile (*e.g.* stilbene **2**) *via* a radical pathway (**Scheme 2.6**) resulting in production of the triplet diradical TDR-**34** (initial bond formation at the C2 position is also possible). Finally, the triplet diradical TDR-**34** may undergo intersystem crossing to the singlet diradical SDR-**34** which may be followed by ring closure to the observed photocycloadduct **3**. With dipolarophiles such as DPBD **4** and methyl cinnamate **32** which possess favorable redox potentials (*cf.* **Table 2.3**), an electron transfer pathway is also feasible resulting in the radical ion pair **35** (*cf.* **35a** and **35b** for cinnamate **32** and DPBD **4**, respectively) which undergoes subsequent addition resulting in the triplet diradical TDR-**36**. The latter species undergo intersystem crossing to the singlet diradical SDR-**36** which subsequently forms the observed photocycloadducts. We believe that the approach and the electronics of the donor-acceptor pair control the selectivity for the photocycloaddition. In addition, although an electron donor-acceptor (EDA) complex formation after photoinduced electron transfer was not observed from spectroscopic measurement, formation of an EDA complex between the excited triplet state of **1** and **4** then followed by subsequent bond formation cannot be excluded.

2.6 ESIPT Photocycloadditions of 3-Hydroxyflavone with Unsymmetrical DPBDs

Scheme 2.7 ESIPT Photocycloaddition of 3-HF 1 with Substituted Unsymmetrical Dipolarophiles

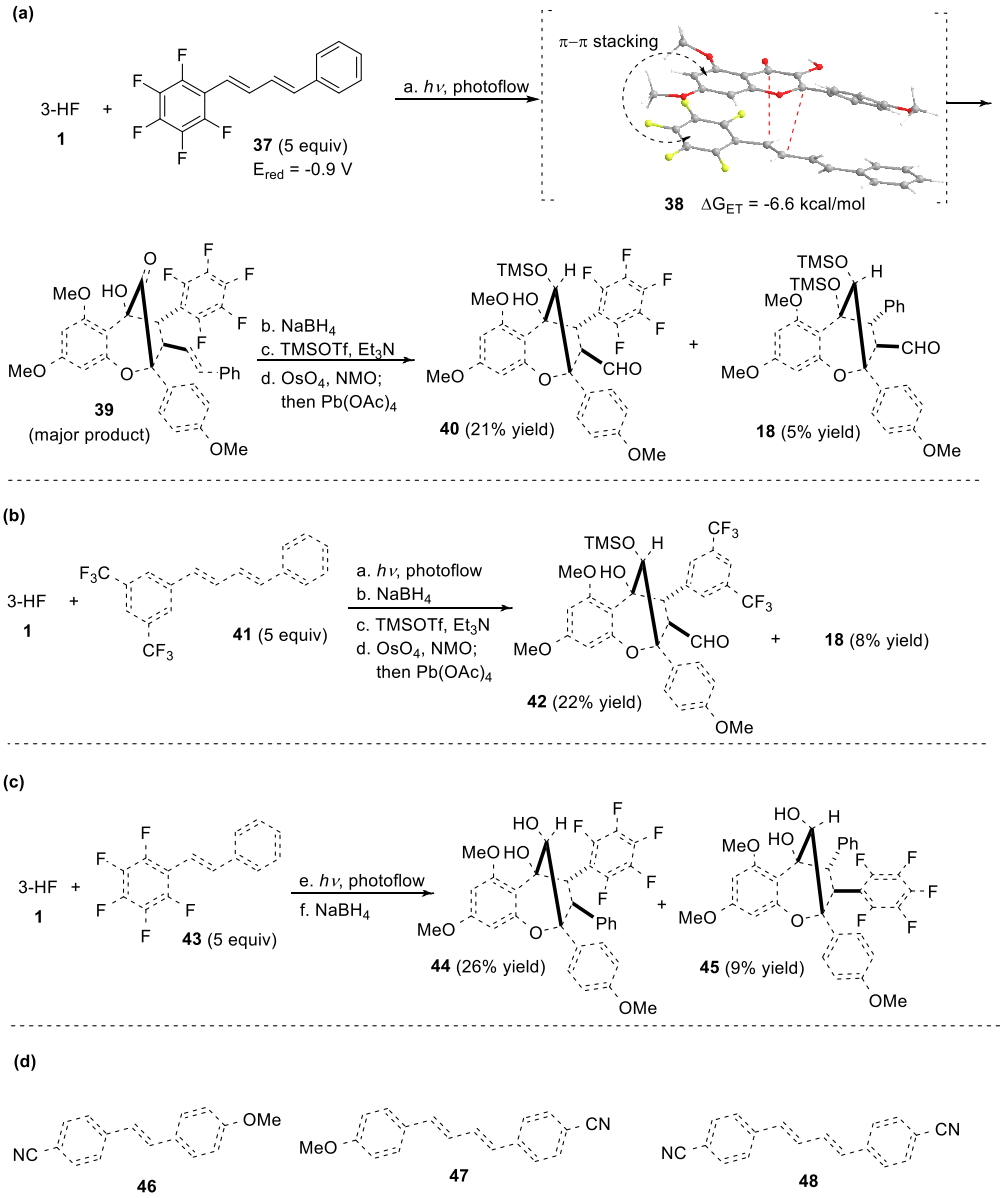

Based on our mechanistic hypothesis, we also evaluated ESIPT photocycloadditions of 3-HF **1** with a number of DPBD and stilbene derivatives bearing various substitution patterns (**Scheme 2.7**). As shown in **section 2.5**, photoinduced electron

transfer (PET) from the triplet excited state of 3-HF **1** to dipolarophile may occur. Therefore, installation of electron withdrawing groups on the dipolarophile may improve reactivity and result in enhanced yields. With this hypothesis as a guide, a number of diphenylbutadienes or stilbenes were then synthesized *via* Horner-Wadsworth-Emmons methodology which exclusively provided the *E*-olefin for the ESIPT photocycloaddition studies.

For example, pentafluorophenyl DPBD **37**[53] was found to readily undergo ESIPT photocycloaddition with 3-HF **1** (**Scheme 2.7a**). In order to determine the regioselectivity for the photocycloaddition, the inseparable mixture of photocycloadducts was reduced using sodium borohydride followed by silylation and oxidative double cleavage to afford two isolable products (ratio = 4:1) in which the major product was found to be aldehyde **40** and the minor product was a previously synthesized compound **18**. This result indicated that upon photoirradiation, the electron-deficient pentafluorophenyl moiety of **37** may further stabilize negative charge after formation of a radical ion pair which appears to dominate the selectivity for the photocycloaddition. Additionally, a π-π stacking (donor-acceptor) interaction (*cf.* **38**, **Scheme 2.7**)[53] between the phloroglucinol moiety of **1** and the pentafluorophenyl substituent on **37** also appears to effect the regioselectivity during the photocycloaddition. The free energy for ESIPT photocycloaddition of 3-HF **5** with pentafluorophenyl DPBD **37** was calculated to be ΔG = -6.6 kcal/mol from Relm-Weller equation[54], thus indicating an exergonic PET pathway. Other dipolarophiles such as *bis*-trifluoromethylphenyl DPBD **41**[55] underwent site-selective photocycloaddition. Pentafluorophenyl stilbene **43**[56] was also found to participate in site-selective

photocycloaddition with 3-HF **5** to yield **44** and **45** in 3:1 ratio after reduction. Installation of cyano substitution appears to attenuate photoreactivity and only decomposition of 3-HF **1** was observed. In the case of dipolarophiles such as **46** and **47**, the presence of push-pull substituents may lead to TICT (Twisted Intramolecular Charge Transfer)[57] excited state of dipolarophiles which may attenuate photoreactivity *via* unproductive relaxations. Additionally, the generally low solubility of all the cyano-containing DPBDs examined may contribute to the lack of ESIPT photocycloaddition reactivity.

2.7 Summary and Outlook

In summary, selective ESIPT photocycloaddition of 3-HF **1** with *trans*,*trans*,-1,4-diphenyl-1,3-butadiene **4** has been achieved, which has served as a key reaction step to accomplish syntheses of the isomeric aglain natural products (±)-foveoglin A (**9**) and (±)-perviridisin B (**10**). Additionally, a Rayonet-based continuous photoflow reactor was designed for the ESIPT photocycloadditions to increase photoreaction efficiency and minimize byproduct formation. By choosing various solvent mixtures for these ESIPT photocycloadditions, the diastereomeric ratio of **7**/**8** could be controlled from 5:1 (by using $CHCl_3$/TFE = 7:3) to 1:1 (by using CH_2Cl_2/isopropanol = 2:1). Diastereoselective reduction using borohydride reagents followed by silylation, oxidative double cleavage, and oxidative amidation afforded foveoglin A (**9**) and perviridisin B (**10**). An enantioselective variant of this ESIPT photocycloaddition was further developed by using a stoichiometric amount of chiral hydrogen bonding additives. Using a UV-LED as light source in combination with TADDOL **27** at -78 °C provided 83% enantiomeric excess of the photocycloadduct **13** which enabled the asymmetric synthesis of (+)-foveoglin A in 96%

ee and as well as absolute configuration assignment. Photophysical and mechanistic studies have been conducted for the ESIPT-photocycloadditions revealing the possibility for exergonic electron transfer from the excited triplet state of 3-hydroxyflavone **1** to dipolarophiles with appropriate redox potentials including methyl cinnamate **32** and DPBD's including **4** (and **37**). ESIPT photocycloaddition of 3-HF **1** with substituted, unsymmetrical *trans*,*trans*-1,4-diphenyl-1,3-butadienes and stilbenes has also been conducted leading to site-selective photocycloadditions in some cases based on presumed π-π stacking (donor-acceptor) interactions.

While we have been able to demonstrate enantioselective ESIPT photocycloaddition of 3-HF **1** with DPBD **4** in the synthesis of (+)-foveoglin A, enantioselective synthesis of related *exo*-aglain natural products, such as perviridisin B is still challenging due to the high *endo*-diastereoselectivity of the photocycloaddition. In order to achieve asymmetric *exo*-aglain natural product synthesis, an achiral ESIPT photocycloaddition followed by kinetic resolution using asymmetric transfer hydrogenation (*cf.* **Section 1.3.2**) on chiral racemic aglain ketone compound may provide a solution to this problem (**Scheme 2.8**).

Scheme 2.8 Proposed Asymmetric Synthesis of Perviridisin B

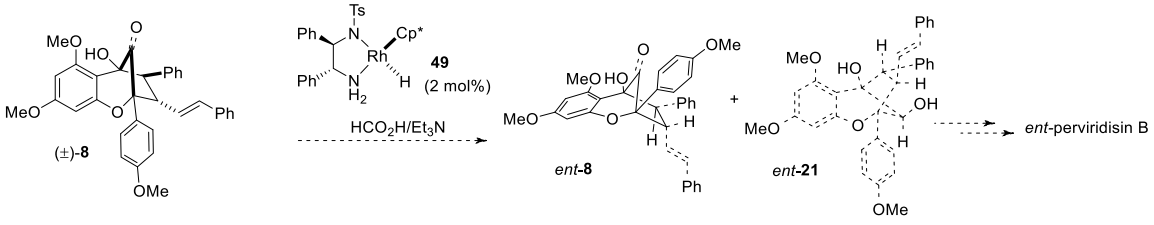

2.8 Experimental Section

General Information: ^{1}H NMR spectra were recorded at 400 or 500 MHz at ambient temperature with $CDCl_3$ (Cambridge Isotope Laboratories, Inc.) as the solvent unless otherwise stated. ^{13}C NMR spectra were recorded at 100 or 125 MHz at ambient temperature with $CDCl_3$ as the solvent unless otherwise stated. Chemical shifts are reported in parts per million relative to $CDCl_3$ (^{1}H, δ 7.26; ^{13}C, δ 77.16). Data for ^{1}H NMR are reported as follows: chemical shift, integration, multiplicity (br = broad, ovrlp = overlapping, s = singlet, d = doublet, t = triplet, q = quartet, m = multiplet) and coupling constants. All ^{13}C NMR spectra were recorded with complete proton decoupling. Infrared spectra were recorded on a Nicolet Nexus 670 FT-IR spectrophotometer. High-resolution mass spectra were obtained at the Boston University Chemical Instrumentation Center using a Waters Q-TOF mass spectrometer. Melting points were recorded on a Mel-temp apparatus (Laboratory Devices). Analytical LCMS was performed on a Waters Acquity UPLC (Ultra Performance Liquid Chromatography (Waters MassLynx Version 4.1) with a Binary solvent manager, SQ mass spectrometer, Water 2996 PDA (PhotoDiode Array) detector, and ELSD (Evaporative Light Scattering Detector). An Acquity UPLC BEH C18 1.7μm column was used for analytical UPLC-MS. Preparative HPLC was performed on a Gilson PLC2020 using a Waters SunFire™ Prep C18 OBD™ 5μm 19×50 mm column. Analytical thin layer chromatography (TLC) was performed using 0.25 mm silica gel 60-F plates (Silicycle, Inc.). Flash chromatography was performed using 200-400 mesh silica gel (Sorbent Technologies, Inc.). Preparative TLC was conducted with glass backed 250

μm or 1000 μm silica gel 60-F plates (Silicycle, Inc.). Preparative HPLC was conducted using a PLC 2020 Personal Purification System (Gilson, Inc.). Yields refer to chromatographically and spectroscopically pure compounds, unless otherwise stated. Photochemistry experiments were performed using a Rayonet RPR-100 photochemical reactor equipped with RPR-3500Å irradiation lamps ($\lambda > 330$ nm, $\lambda_{max} = 350$ nm). For the Rayonet photoflow reactor, a Rayonet RPR-100 photobox was used as light source and a Thermo Scientific™ Neslab CC65 Immersion Cooler was using as a cooling system. The PTFE Tubing (1/32"ID x 1/16"OD) (Cole-Parmer Instrument Company) twined around a 500 mL Pyrex graduated cylinder and connected to a peristaltic pump (Benchtop pump with 114DV flip top single channel pumphead, model: 120S, Waston Marlow Fluid Technology Group) using 2 conical adapter assemblies (IDEX Health & Science, P-798). Two needle adapters (IDEX Health & Science, Flangeless Ferrule Tefzel®, P-300X; Flangeless Short Nut, P-335X; Luer Adapters, P-655) were also installed to connect the reaction flask with the peristaltic pump and reaction tubing. For the purple-LED reactor, the LED strip was purchased from Amazon (Lumcrissy 12V Flexible LED Strip Lights Waterproof 3528 SMD 5M 300LED 300 Units LEDs Light Strip (Purple)). All other reactions were carried out in oven-dried glassware under an argon/nitrogen atmosphere unless otherwise noted. The Scilligence ELN Reaction Planner (Scilligence Corp.) was used for experimental procedure planning. Spectrophotometric solvents (Sigma-Aldrich®) were used whenever necessary unless or otherwise mentioned. UV quality fluorimeter cells (with range until 190 nm) were purchased from Luzchem®. Absorbance measurements were performed using a Carey 300 UV-Vis spectrophotometer. Emission spectra were

recorded on a Horiba Scientific® Fluorolog 3 spectrometer (FL3-22) equipped with double-grating monochromators, dual lamp housing containing a 450-watt CW xenon lamp and a UV xenon flash lamp (FL-1040), Fluorohub/MCA/MCS electronics and R928 PMT detector. Emission and excitation spectra were corrected in all the cases for source intensity (lamp and grating) and emission spectral response (detector and grating) by standard instrument correction provided in the instrument software. Fluorescence emission spectra were processed by FluorEssence® software. Fluorescence lifetimes were determined by time correlated single photon counting using a pulsed diode (NanoLED) emitting at 263 nm and processed using DAS6® V6.4 software. The goodness-of-fit was assessed by minimizing the reduced chi squared function and was further judged by the symmetrical distribution of the residuals. Cyclic voltammetry was performed using HPLC grade acetonitrile as the solvent on a CH instrument. HPLC grade tetrahydrofuran, methylene chloride, diethyl ether, toluene, acetonitrile, and benzene were purchased from Fisher and VWR and were purified and dried by passing through a PURE SOLV® solvent purification system (Innovative Technology, Inc.). Reagents were purchased from Sigma Aldrich, Oakwood, and Alfa Aesar and were used as received.

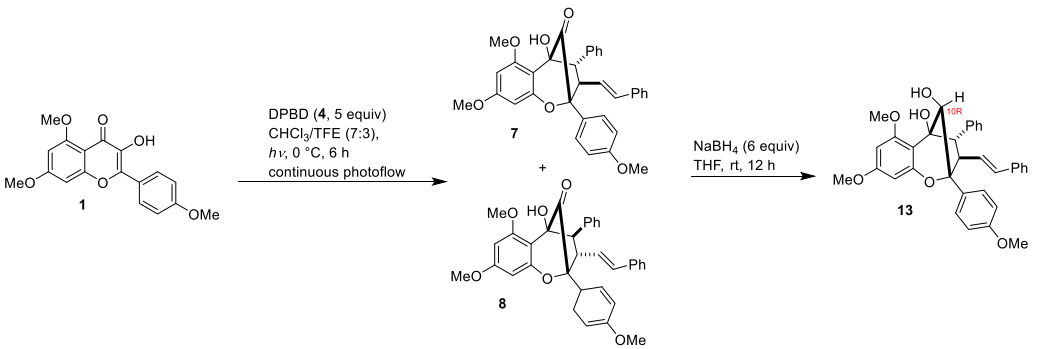

***Endo-10R*-aglain 13:** A 100 mL round bottom flask was charged with 3-hydroxyflavone **5** (500 mg, 1.52 mmol, 1 equiv), DPBD **8** (1.57 g, 7.61 mmol, 5 equiv), and 75 mL of a $CHCl_3$/TFE(7:3) mixture (0.02 M for 3-HF **5**). The flask was connected with the continuous photoflow reactor and placed into a sonicator with an ice-bath. Subsequently, the peristaltic pump was turned on to circulate the reaction mixture and argon bubbling with sonication was continued for another 20 min before the UV-lamp (Rayonet, λ_{max} = 350 nm) was turned on. After 6 h, the reaction mixture was collected back to the flask and concentrated *in vacuo*. Purification *via* flash chromatography using a gradient of hexanes/EtOAc (10:1 to 3:1) afforded cyclopenta[*bc*]benzopyrans **11-12** as mixture of isomers which were used in next step without further purification. The isomeric ratio (**11** : **12**) was determined by ^{1}H NMR analysis to be 5:1 (545 mg, 67% yield, 1.02 mmol).

A flame-dried 100 mL flask was charged with a mixture of **11** and **12** (545 mg, 1.02 mmol, 1 equiv) and THF (6.8 mL, 0.15 M). Subsequently, $NaBH_4$ (232 mg, 6.12 mmol, 6 equiv) was added to the reaction at rt in one portion. The resulting mixture was then stirred for 12 h and was quenched with ice-cooled saturated ammonium chloride. The mixture was extracted with CH_2Cl_2 (10 mL × 3), washed with saturated sodium bicarbonate, and dried over sodium sulfate. The filtrate was concentrated *in vacuo* and ^{1}H NMR analysis of the crude extract was obtained. NMR analysis indicated that the reduction was diastereoselective to favor the *10R*-isomer (d.r.=5:1). Column chromatography purification using hexanes/EtOAc (5:1 to 3:1) afforded the aglain derivative **13** (360 mg, 44% over 2 steps) as a white solid. After recrystallization from EtOAc, trace amounts of impurities were removed and 276 mg of **13** (33%) was obtained.

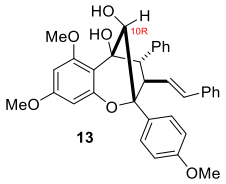

13: R_f: 0.41 (hexanes: EtOAc = 1:1). m.p. = 223 °C (CH_2Cl_2). ^{1}H NMR (500 MHz, $CDCl_3$)□δ 7.57 (d, J = 8.9 Hz, 2H), 7.18 (m, 3H), 7.10 (m, 3H), 6.97 (m, 2H), 6.94 (d, J = 8.9 Hz, 2H), 6.90 (m, 2H), 6.28 (d, J = 2.3 Hz, 1H), 5.98 (d, J = 15.6 Hz, 1H), 5.87 (d, J = 2.3 Hz, 1H), 5.49 (dd, J_1 = 15.6 Hz, J_2 = 8.7 Hz, 1H), 5.42 (s, 1H, OH), 4.75 (d, J = 4.8 Hz, 1H), 3.796 (s, 3H), 3.793 (s, 3H), 3.48 (dd, J_1 = 9.4 Hz, J_2 = 8.7 Hz, 1H), 3.28 (d, J =9.4 Hz, 1H), 2.36 (d, J = 4.8 Hz, 1H, OH); ^{13}C NMR (125 MHz, CDCl3) δ 160.8, 160.3, 159.2, 153.4, 137.0, 136.7, 130.1, 129.6, 129.6, 128.7, 128.2, 128.2, 127.7, 127.0, 126.9, 126.1, 113.8, 104.0, 94.0, 92.9, 86.8, 82.0, 73.3, 61.6, 55.5, 55.4, 55.3, 53.7; IR υ_{max} (film): 3498, 2968, 1618, 1456, 1254, 1148, 1101, 831 cm^{-1}. HRMS-ESI (m/z) calculated $[M+Na]^+$ $C_{34}H_{32}O_6Na$, 559.2097, found 559.2091.

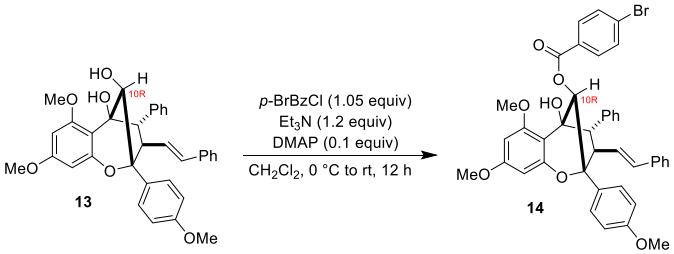

***Para*-bromobenzoate 14:** To a flame dried test tube were added aglain **13** (120 mg, 0.22 mmol, 1 equiv), Et_3N (37 μL, 0.27 mmol, 1.2 equiv), DMAP (2.7 mg, 0.02 mmol, 0.1 equiv), and dry CH_2Cl_2 (7.5 mL, 0.1 M) at 0 °C. Subsequently, 4-bromobenzoyl chloride (51.5 mg, 0.23 mmol, 1.05 equiv) was added in one portion. The resulting mixture was allowed to warm to room temperature and was stirred for 12 h before being quenching with 10 mL of saturated $NaHCO_3$ (aq.). The mixture was extracted with CH_2Cl_2 (5 mL × 3), washed with saturated NaCl (aq.), and dried over sodium sulfate. Column chromatography

purification using hexanes/EtOAc (7:1 to 4:1) afforded the *para*-bromobenzoate **14** (121 mg, 75% yield) as a white solid.

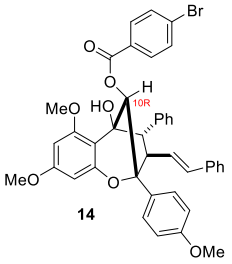

14

14: R_f: 0.61 (hexanes: EtOAc = 3:1). m.p. = 244 °C (CH_2Cl_2). ^{1}H NMR (500 MHz, $CDCl_3$) δ 7.70 (d, J = 8.7 Hz, 2H), 7.54 (d, J = 9.0 Hz, 2H), 7.42 (d, J = 8.7 Hz, 2H), 7.20 (m, 3H), 7.10 (m, 3H), 7.01 (m, 2H), 6.91 (m, 2H), 6.88 (d, J = 9.0 Hz, 2H), 6.50 (s, 1H), 6.36 (d, J = 2.4 Hz, 1H), 6.51 (d, J = 15.6 Hz, 1H), 5.86 (d, J = 2.4 Hz, 1H), 5.53 (dd, J_1 = 8.4 Hz, J_2 = 15.6 Hz, 1H), 5.32 (s, 1H, OH), 3.86 (s, 3H), 3.74 (s, 3H), 3.54 (dd, J_1 = 9.4 Hz, J_2 = 8.4 Hz, 1H), 3.49 (d, J = 9.4 Hz, 1H), 3.06 (s, 1H); ^{13}C NMR (125 MHz, CDCl3) δ 165.2, 160.7, 159.7, 159.2, 153.6, 136.9, 136.3, 131.5, 131.5, 130.5, 129.2, 129.0, 128.7, 128.7, 128.2, 128.1, 127.7, 127.5, 127.1, 127.0, 126.1, 113.8, 104.6, 93.9, 92.5, 86.5, 81.4, 72.6, 61.6, 55.5, 55.4, 55.2, 54.5; IR υ_{max} (film): 3499, 2918, 1726, 1617, 1589, 1266, 1148, 1099, 1012, 753 cm^{-1}. HRMS-ESI (m/z) calculated $[M+Na]^+$ $C_{41}H_{36}O_7Br$ 719.1644, found 719.1643.

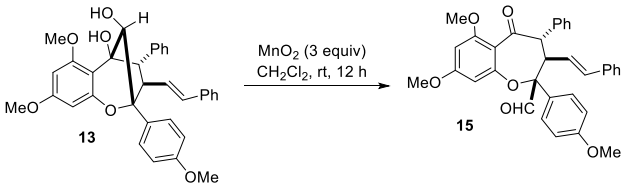

Forbaglin aldehyde 15: To a flame dried test tube were added aglain **13** (50 mg, 0.093 mmol, 1 equiv), MnO_2 (24 mg, 0.28 mmol, 3 equiv), and dry CH_2Cl_2 (1 mL, 0.1 M) at rt. The mixture was stirred at rt for 12 h before the insoluble oxidant was removed by filtration. The solution obtained was subjected to column chromatography purification

using hexanes/EtOAc (4:1 to 2:1) to afford forbaglin aldehyde **15** (45 mg, 90% yield) as a colorless oil.

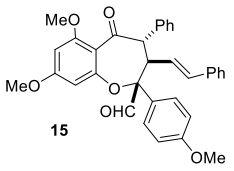

15

15: R_f: 0.21 (hexanes: EtOAc = 7:3). ^{1}H NMR (500 MHz, $CDCl_3$) δ 9.29 (s, 1H), 7.35 (m, 2H), 7.31 (s, 2H), 7.29 (d, J = 8.9 Hz, 2H), 7.21 (m, 4H), 7.12 (m, 2H), 6.82 (d, J = 8.9 Hz, 2H), 6.44 (d, J = 2.3 Hz, 1H), 6.15 (dd, J_1 = 15.8 Hz, J_2 = 9.5 Hz, 1H), 6.06 (d, J = 15.8 Hz, 1H), 6.08 (d, J = 2.3 Hz, 1H), 4.22 (d, J = 9.5 Hz, 1H), 4.11 (dd, J_1 = J_2 = 9.5 Hz, 1H), 3.85 (s, 3H), 3.76 (s, 3H), 3.60 (s, 3H); ^{13}C NMR (125 MHz, $CDCl_3$) δ 165.2, 160.7, 159.7, 159.2, 153.6, 136.9, 136.3, 131.5, 131.5, 130.5, 129.2, 129.0, 128.7, 128.7, 128.2, 128.1, 127.7, 127.5, 127.1, 127.0, 126.1, 113.8, 104.6, 93.9, 92.5, 86.5, 81.4, 72.6, 61.6, 55.5, 55.4, 55.2, 54.5; IR υ_{max} (film): 3499, 2918, 1726, 1617, 1589, 1266, 1148, 1099, 1012, 753 cm^{-1}. HRMS-ESI (m/z) calculated $[M+Na]^+$ $C_{41}H_{36}O_7Br$ 719.1644, found 719.1643.

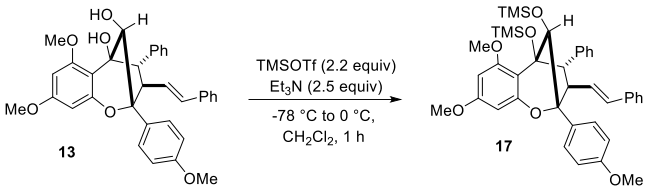

13 **17**

TMS-aglain 17: A flame dried test tube was charged with aglain **13** (200 mg, 0.37 mmol, 1 equiv) and dry CH_2Cl_2 (2.5 mL, 0.15 M). The solution was cooled to -78 °C before Et_3N (130 μL, 0.93 mmol, 2.5 equiv) and TMSOTf (148 μL, 0.82 mmol, 2.2 equiv) were added. The resulting mixture was stirred at -78 °C for another 10 min before warming up to 0 °C. After 1 h, the reaction was quenched with 5 mL of saturated $NaHCO_3$ (aq.). The mixture was extracted with CH_2Cl_2 (3 mL × 3), washed with saturated NaCl (aq.), and dried over sodium sulfate. Column chromatography purification using

hexanes/EtOAc (20:1 to 15:1) afforded TMS-aglain **17** (249 mg, 98% yield) as a colorless oil.

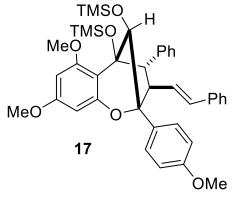

17: R_f: 0.67 (hexanes: EtOAc = 4:1). ^{1}H NMR (500 MHz, $CDCl_3$) δ 7.53 (d, J = 8.9 Hz, 2H), 7.11 (m, 5H), 7.05 (m, 1H), 7.00 (m, 2H), 6.93 (d, J = 8.9 Hz, 2H), 6.19 (d, J = 2.4 Hz, 1H), 5.92 (d, J = 15.9 Hz, 1H), 5.73 (d, J = 2.4 Hz, 1H), 5.50 (dd, J_1 = 15.9 Hz, J_2 = 7.4 Hz, 1H), 4.60 (s, 1H, OH), 3.82 (s, 3H), 3.80 (s, 3H), 3.39 (d, J = 10.7 Hz, 1H), 3.33 (dd, J_1 = 10.7 Hz, J_2 = 7.4 Hz, 1H), 2.94 (s, 3H), 0.04 (s, 9H), -0.22 (s, 9H); ^{13}C NMR (125 MHz, CDCl3) δ 194.8, 192.7, 163.2, 160.1, 159.4, 159.0, 136.5, 136.2, 135.3, 130.4, 129.7, 128.4, 128.2, 127.8, 127.3, 126.4, 125.5, 123.9, 115.0, 114.5, 98.0, 94.4, 91.7, 62.1, 56.1, 55.7, 55.2, 52.0; IR υ_{max} (film): 2937, 2848, 1696, 1607, 1512, 1456, 1403, 1260, 1155, 1104, 830, 751, 698 cm^{-1}. HRMS-ESI (m/z) calculated $[M+H]^+$ $C_{40}H_{49}O_6Si_2$, 681.3068, found 681.3069.

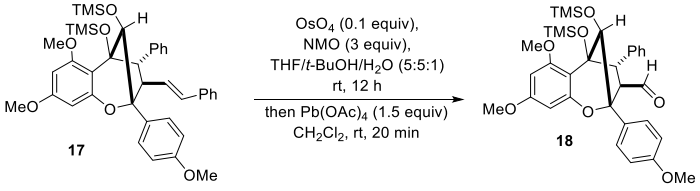

***Endo*-10*R*-TMS-aldehyde 18:** A test tube was charged with TMS-aglain **17** (249 mg, 0.37 mmol, 1 equiv), THF (4.7 mL) and *t*-BuOH (4.7 mL). Subsequently, 0.93 mL OsO_4 (aq., 10 mg/mL) (9.3 mg, 0.036 mmol, 0.1 equiv) was added to the solution followed by addition of N-methylmorpholine oxide (NMO) (128.5 mg, 1.1 mmol, 3 equiv). The resulting mixture was stirred at room temperature for 12 h before 10 mL of saturated NaCl (aq.) was added. The mixture was extracted with Et_2O (5 mL × 3), washed with saturated NaCl (aq.),

and dried over sodium sulfate. The filtrate was concentrated *in vacuo* to afford the diol compound as a brown oil which was subjected to next step without further purification. The brown oil was dissolved in a test tube with 10 mL of CH_2Cl_2. Subsequently, $Pb(OAc)_4$ (243 mg, 0.55 mmol, 1.5 equiv) was added. The resulting solution was stirred at room temperature for 20 min before 20 mL saturated $Na_2S_2O_3$ was added to quench the reaction. The mixture was extracted with CH_2Cl_2 (10 mL × 3), washed with saturated NaCl (aq.), and dried over sodium sulfate. Column chromatography purification using hexanes/EtOAc (15:1 to 10:1) afforded *endo*-TMS-aldehyde **18** (158 mg, 71% yield) as a colorless oil.

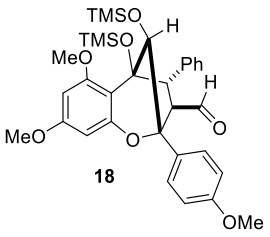

18: R_f: 0.35 (hexanes:EtOAc = 3:17). ^{1}H NMR (500 MHz, $CDCl_3$) δ 8.94 (d, J = 2.8 Hz, 1H), 7.54 (d, J = 8.8 Hz, 2H), 7.11 (m, 3H), 6.98 (d, J = 8.8 Hz, 2H), 6.92 (m, 2H), 6.21 (d, J = 1.2 Hz, 1H), 5.76 (d, J = 1.2 Hz, 1H), (d, J = 1.2 Hz, 1H), 4.53 (s, 1H, OH), 3.88 (d, J = 10.6 Hz, 1H), 3.84 (s, 3H), 3.82 (s, 3H), 3.52 (dd, J_1 = 10.6 Hz, J_2 = 2.8 Hz, 1H), 2.94 (s, 3H), 0.04 (s, 9H), -0.22 (s, 9H); ^{13}C NMR (125 MHz, $CDCl_3$) δ 160.7, 160.0, 158.9, 154.1, 137.6, 137.3, 130.8, 130.1, 130.0, 128.9, 128.1, 127.7, 126.84, 126.77, 126.2, 126.0, 113.1, 106.7, 92.7, 91.4, 86.2, 83.4, 78.7, 59.7, 55.3, 55.1, 53.9, 52.4, 2.1, 1.3; IR υ_{max} (film): 2957, 1721, 1613, 1587, 1516, 1465, 1250, 1195, 1151, 1110, 1035, 899, 839, 743, 696 cm^{-1}. HRMS-ESI (m/z) calculated $[M+H]^+$ $C_{33}H_{43}O_7Si_2$, 607.2547, found 607.2556.

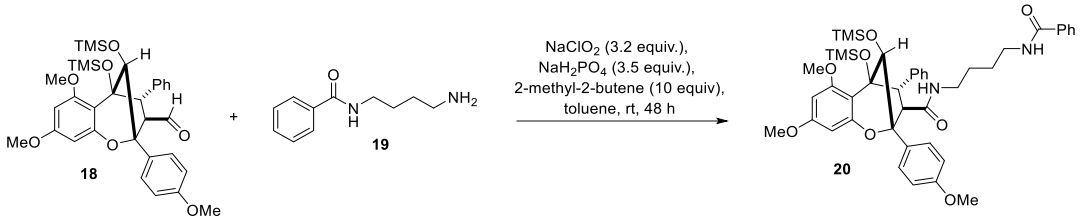

TMS-foveoglin A 20: A flame-dried test tube was charged with *endo*-TMS-aldehyde **18** (150 mg, 0.25 mmol, 1 equiv), amine **19**[58] (238 mg, 1.24 mmol, 5 equiv) and dry toluene (2.5 mL, 0.1 M) under argon. The mixture was stirred at room temperature for 5 min before NaH_2PO_4 (104 mg, 0.87 mmol, 3.5 equiv), 2-methyl-2-butene (0.26 mL, 2.5 mmol, 10 equiv) and $NaClO_2$ (72 mg, 0.79 mmol, 3.2 equiv) were consecutively added. The resulting heterogeneous mixture was stirred for 48 h at room temperature. The reaction mixture was then filtered to remove insoluble inorganic salts. And the filtrate was concentrated *in vacuo.* Column chromatography purification using hexanes/EtOAc (6:1 to 3:1) afforded TMS-foveoglin A **20** (147 mg, 71% yield) as a colorless oil.

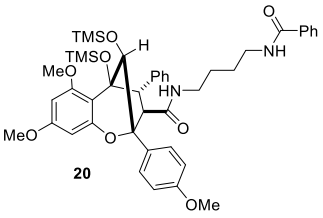

20: R_f: 0.37 (hexanes: EtOAc = 1:1). ^{1}H NMR (500 MHz, $CDCl_3$) δ 7.82 (m, 2H), 7.58 (d, J = 8.8 Hz, 2H), 7.50 (m, 1H), 7.44 (m, 2H), 7.08 (m, 3H), 6.92 (m, 2H), 6.85 (d, J = 8.8 Hz, 2H), 6.64 (t, J = 5.8 Hz, 1H, NH), 6.15 (d, J = 2.5 Hz, 1H), 5.73 (d, J = 2.5 Hz, 1H), 5.23 (t, J = 5.7 Hz, 1H, NH), 4.65 (s, 1H, OH), 4.02 (d, J = 10.2 Hz, 1H), 3.79 (s, 3H), 3.77 (s, 3H), 3.25 (m, 1H), 3.12 (m, 1H), 3.07 (d, J = 10.2 Hz, 2H), 2.93 (s, 3H), 2.74 (m, 1H), 2.49 (m, 1H), 1.07 (m, 2H), 0.84 (m, 2H), 0.03 (s, 9H), -0.27 (s, 9H); ^{13}C NMR (125 MHz, CDCl3) δ 169.8, 167.4, 160.8, 160.0, 159.3, 153.5, 137.6, 134.6, 131.3, 130.2, 128.9, 128.4, 128.0, 127.0, 126.9, 126.3, 113.0, 107.0, 92.8, 91.8, 84.7, 83.1, 78.5, 58.8, 55.4, 55.1, 53.9, 39.4, 38.9, 26.23, 26.21, 2.1, 1.2; IR υ_{max} (film): 3308, 2958, 2904, 1642, 1614, 1615, 1520, 1151, 1112, 1040, 905, 839, 696 cm^{-1}. HRMS-ESI (m/z) calculated $[M+H]^+$ $C_{44}H_{57}N_2O_8Si_2$, 797.3653, found 797.3659.

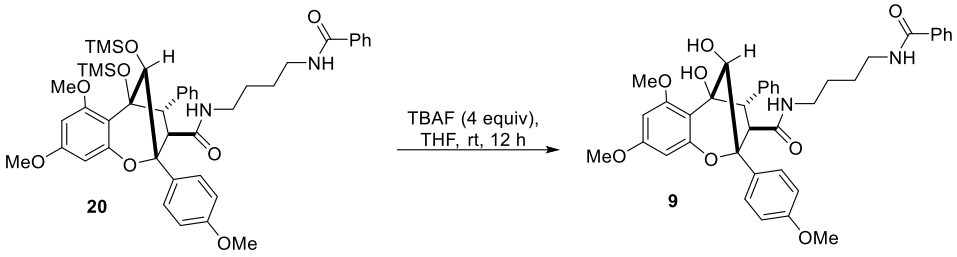

Foveoglin A 9: A flame dried test tube was charged with TMS-foveoglin A **20** (120 mg, 0.15 mmol, 1 equiv) and dry THF (2 mL). Subsequently, TBAF (1 M THF solution, 0.36 mL, 0.36 mmol, 2.4 equiv) was added dropwise. The resulting mixture was stirred for 12 h before 5 mL of saturated NaCl (aq.) was added to quench the reaction. The mixture was extracted with EtOAc (5 mL × 3), washed with saturated NaCl (aq.), and dried over sodium sulfate. The filtrate was concentrated *in vacuo.* Column chromatography purification using hexanes/EtOAc (2:1 to 1:2) afforded foveoglin A **9** (94 mg, 96% yield) as an amorphous solid.

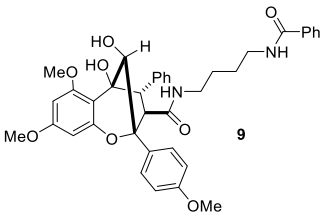

9: R_f: 0.51 (EtOAc). m.p. = 153 °C (CH_2Cl_2). ^{1}H NMR (500 MHz, $CDCl_3$) δ 7.81 (d, J = 7.5 Hz, 2H), 7.61 (d, J = 8.9 Hz, 2H), 7.52 (t, J = 7.3 Hz, 1H), 7.47 (t, J = 7.8 Hz, 2H), 7.16 (m, 3H), 6.93 (m, 2H), 6.89 (d, J = 8.9 Hz, 2H), 6.47 (brt, J = 5.7 Hz, 1H, NH), 6.25 (d, J = 2.3 Hz, 1H), 5.85 (d, J = 2.3 Hz, 1H), 5.54 (brt, J = 5.9 Hz, 1H, NH), 5.43 (s, 1H, OH), 4.91 (d, J = 5.5 Hz, 1H), 4.00 (d, J = 9.0 Hz, 1H), 3.78 (s, 3H), 3.77 (s, 3H), 3.29 (m, 1H), 3.23 (d, J = 9.0 Hz, 1H), 3.15 (m, 1H), 3.10 (s, 3H), 2.92 (m, 1H), 2.60 (m, 1H), 2.31 (d, J = 5.5 Hz, 1H, OH), 1.14 (m, 2H), 0.96 (m, 2H); ^{13}C NMR (125 MHz, CDCl3) δ 169.9, 167.4, 160.8, 160.3, 159.3, 152.9, 136.9, 134.6, 131.4, 129.2, 128.6, 128.5, 128.0, 127.7, 127.0, 126.9, 113.5, 104.3, 94.0, 93.0, 85.6, 81.8, 73.5, 59.0,

57.1, 55.5, 55.4, 39.4, 39.0, 26.3, 26.2; IR υ_{max} (film): 3375, 2955, 1641, 1618, 1517, 1492, 1458, 1305, 1254, 1148, 1105, 1037, 833 cm^{-1}. HRMS-ESI (m/z) calculated $[M+H]^+$ $C_{38}H_{41}N_2O_8$, 653.2863, found 653.2858.

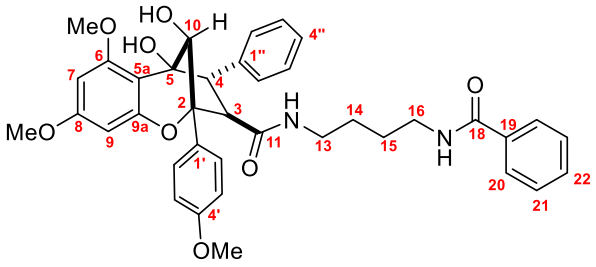

(±)-foveoglin A (3)

^{1}H NMR

	natural (–)-**3**	synthetic (±)-**3** (this work)
Positions	δ lit ($CDCl_3$) ($J_{H\text{-}H}$ in Hz)	δ (500 MHz, $CDCl_3$) ($J_{H\text{-}H}$ in Hz)
2		
3	3.22, d (9.0)	3.23, d (9.0)
4	4.00, d (9.0)	4.00, d (9.0)
5		
5-OH	5.44, s	5.43, s
5a		
6		
7	5.86, d (2.2)	5.85, d (2.3)
8		
9	6.26, d (2.2)	6.25, d (2.3)
9a		
10	4.91, s	4.91, d (5.5)
10-OH		2.31, d (5.5)
11		
NH-12	5.49, brt (5.5)	5.54, brt (5.7)
13	2.93, m 2.61, m	2.92, m 2.60, m
14	0.98, m	0.96, m
15	1.16, m	1.14, m

16	3.29, m	3.29, m
	3.16, m	3.15, m
NH-17	6.46, brt (5.5)	6.47, brt (5.7)
18		
19		
20, 24	7.82, d (8.0)	7.81, d (7.5)
21, 23	7.47, t (7.7)	7.47, t (7.8)
22	7.53, t (7.2)	7.52, t (7.3)
1’		
2’, 6’	7.62, d (8.9)	7.61, d (8.9)
3’, 5’	6.89, d (8.7)	6.89, d (8.9)
4’		
1’’		
2’’, 6’’	6.93, m	6.93 m
3’’, 5’’	7.16, m	7.16, m
4’’	7.16, m	7.16, m
OCH_3-6	3.11, s	3.10, s
OCH_3-8	3.79, s	3.78, s
OCH_3-4’	3.77, s	3.77, s

^{13}C NMR

	natural (–)-**3**	synthetic (±)-**3** (this work)
Positions	δ lit. ($CDCl_3$)	δ (125 MHz, $CDCl_3$)
2	85.6	85.6
3	59.0	59.0
4	57.1	57.1
5	81.8	81.8
5-OH		
5a	104.2	104.3
6	160.3	160.3
7	93.0	93.0
8	160.8	160.8
9	93.9	94.0
9a	152.8	152.9
10	73.5	73.5
10-OH		
11	170.0	170.0
NH-12		
13	39.0	39.0

14	26.2	26.2
15	26.3	26.3
16	39.4	39.4
NH-17		
18	167.5	167.4
19	134.5	134.6
20, 24	127.0	127.0
21, 23	128.6	128.6
22	131.5	131.4
1’	129.2	129.2
2’, 6’	128.0	128.0
3’, 5’	113.6	113.5
4’	159.3	159.3
1’’	136.8	140.7
2’’, 6’’	128.6	128.5
3’’, 5’’	127.7	127.7
4’’	127.0	127.0
OCH_3-6	55.5	55.5
OCH_3-8	55.4	55.4
OCH_3-4’	55.4	55.4

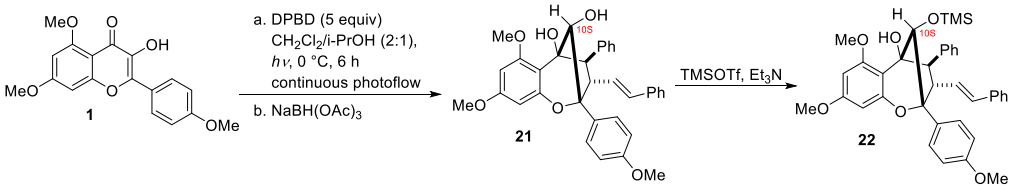

***Exo-10S*-TMS-aglain 22:** A 100 mL round bottom flask was charged with 3-hydroxyflavone **1** (500 mg, 1.52 mmol, 1 equiv) and DPBD **4** (1.57 g, 7.61 mmol, 5 equiv) in 75 mL of CH_2Cl_2/*i*-PrOH (2:1) (0.02 M for 3-HF **5**). The flask was connected with the continuous photoflow reactor followed by degassing with argon gas for 10 min. Subsequently, the peristaltic pump was turned on to circulate the reaction mixture and the argon gas was kept for another 10 min before the UV-lamp (Rayonet, $\lambda > 315$ nm) was turned on. After 6 h, the reaction mixture was collected back into the flask and concentrated

under vacuum. Purification *via* flash chromatography using a gradient of hexanes/EtOAc (10:1 to 3:1) afforded cyclopenta[*bc*]benzopyrans **7** and **8** as mixture of isomers which were used in next step without further purification. The isomeric ratio was determined using ^{1}H NMR analysis to be 1:1 (426 mg, 52% yield, 0.8 mmol). A flame-dried 100 mL flask was charged with $NaBH(OAc)_3$ (1.01 g, 4,78 mmol, 6 equiv) and HOAc (0.27 mL, 4.78 mmol) in $PhCF_3$ (20 mL) at rt under argon. The mixture was then sonicated briefly and stirred at rt for 10 min. A mixture of **7** and **8** (426 mg, 0.8 mmol, 1 equiv) in 20 mL of $PhCF_3$ (0.02 M) was then added at rt at one portion under argon. The resulting mixture was then stirred for 14 h and was quenched with saturated ammonium chloride. The mixture was extracted with CH_2Cl_2, washed with saturated sodium bicarbonate, dried over sodium sulfate, and the filtrate concentrated *in vacuo.* ^{1}H NMR analysis of the crude extract indicated that the reduction was diastereoselective in favor of the *10S*-isomer (d.r.= 10:1). Column chromatography purification using hexanes/EtOAc (5:1) afforded an inseparable mixture of isomeric aglains (4 isomers combined, 406 mg, 95% yield) which was used in the next step without further purification. Preparative thin layer chromatography purification of 20 mg mixture material using hexanes/EtOAc (9:1) afforded pure **21** (15 mg, 0.028 mmol).

To a flame dried test tube were added the mixture of isomeric aglains (406 mg, 0.76 mmol, 1 equiv), Et_3N (0.33 mL, 2.39 mmol, 3 equiv) and CH_2Cl_2 (7.5 mL, 0.1 M). After the resulting mixture was cooled to -78 °C, TMSOTf (290 μL, 1.6 mmol, 2 equiv) was added dropwise before the temperature was raised to 0 °C for 1 h. Ice-cooled saturated sodium bicarbonate was added to quench the reaction and CH_2Cl_2 (5 mL × 2) was employed for

extraction. The combined organic layer was washed with saturated sodium chloride and dried over sodium sulfate. The filtrate was concentrated *in vacuo* and purified by column chromatography using a gradient of hexanes/Et_2O (30:1 to 20:1). *Exo-10S*-TMS-aglain **22** (186 mg, 0.35 mmol) was obtained in 23% yield from the 3-HF **1** as a colorless oil.

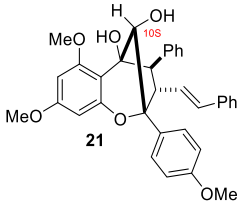

21

21: R_f: 0.30 (hexanes: EtOAc = 7:3). ^{1}H NMR (500 MHz, $CDCl_3$) δ 7.74 (d, J = 9.0 Hz, 2H), 7.49 (d, J = 7.3 Hz, 2H), 7.36 (t, J = 7.3 Hz, 2H), 7.28 (d, J = 7.3 Hz, 1H), 7.20 (m, 4H), 7.12 (m, 1H), 6.96 (d, J = 9.0 Hz, 2H), 6.83 (dd, J_1 = 16 Hz, J_2 = 8.3 Hz, 1H), 6.28 (d, J = 2.3 Hz, 1H), 6.25 (d, J = 16 Hz, 1H), 6.14 (d, J = 2.3 Hz, 1H), 5.18 (s, 1H, OH), 4.40 (s, 1H, OH), 4.37 (dd, J_1 = 8.3 Hz, J_2 = 7.7 Hz, 1H), 3.88 (s, 3H), 3.82 (s, 3H), 3.81 (s, 3H), 3.65 (d, J = 7.7 Hz, 1H), 2.90 (s, 1H, OH); ^{13}C NMR (125 MHz, CDCl3) δ 160.5, 159.3, 155.9, 153.9, 140.4, 137.2, 132.1, 130.2, 130.1, 128.8, 128.2, 128.1, 127.8, 127.1, 126.7, 126.2, 113.6, 113.3, 94.2, 92.3, 88.3, 81.6, 79.7, 64.9, 57.2, 56.1, 55.5, 55.2; IR υ_{max} (film): 3497, 3027, 2939, 1615, 1589, 1515, 1456, 1253, 1150, 1097, 1050, 830, 749, 698 cm^{-1}. HRMS-ESI (m/z) calculated $[M+Na]^+$ $C_{34}H_{32}O_6Na$, 559.2097, found 559.2095.

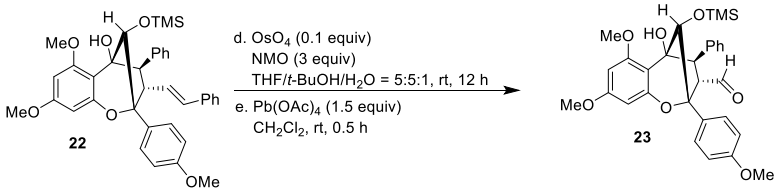

22 **23**

***Exo-10S*-TMS-aglain aldehyde 23:** A flame dried test tube was charged with **22** (150 mg, 0.25 mmol, 1 equiv), *N*-methylmorpholine-*N*-oxide (86.6 mg, 0.74 mmol, 3 equiv) and mixture of THF/*t*-BuOH (1:1) (6.4 mL, 0.04 M). After formation of a homogeneous solution, 0.64 mL OsO_4 (10 wt.% aq., 6.4 mg, 0.025 mmol, 0.1 equiv) aqueous solution

was added. The solution immediately turned brown and was stirred for 12 h before 5 mL of saturated sodium chloride was added to quench the reaction. The reaction mixture was extracted with Et_2O (5 mL × 3), the combined organic layer was washed with 10 mL of saturated sodium chloride, and dried over sodium sulfate. The filtrate was concentrated *in vacuo*. The crude diol product was used in the next step without further purification. Subsequently, the crude diol product was dissolved in 5 mL of CH_2Cl_2. $Pb(OAc)_4$ (164 mg, 0.37 mmol, 1.5 equiv) was added. The resulting mixture was stirred for 0.5 h before 5 mL of saturated $Na_2S_2O_3$ was added to quench the reaction. The combined organic layer from extraction with CH_2Cl_2 (3 mL × 3) was washed with 10 mL of saturated sodium chloride and dried over sodium sulfate. The filtrate was concentrated *in vacuo* and purified by column chromatography using a gradient of hexanes/CH_2Cl_2/EtOAc (20:1:1 to 15:1:1) to afford the *exo-10S*-TMS-aglain aldehyde **23** (95.4 mg, 0.18 mmol, 73% yield) as a colorless oil.

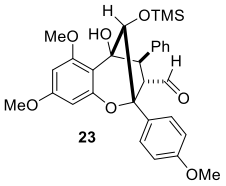

23

23: R_f: 0.19 (EtOAc). ^{1}H NMR (500 MHz, $CDCl_3$) δ 9.69 (d, J = 0.8 Hz, 1H), 7.71 (d, J = 8.8 Hz, 2H), 7.54 (d, J = 7.5 Hz, 2H), 7.32 (t, J = 7.5 Hz, 2H), 7.23 (t, J = 7.5 Hz, 1H), 7.00 (d, J = 8.8 Hz, 2H), 6.14 (d, J = 2.3 Hz, 1H), 6.13 (d, J = 2.3 Hz, 1H), 5.04 (s, 1H, OH), 4.34 (d, J = 6.2, 1H), 4.24 (dd, J_1 = 6.2 Hz, J_2 = 0.8 Hz, 1H), 4.19 (s, 1H), 3.87 (s, 3H), 3.85 (s, 3H), 3.77 (s, 3H), -0.16 (s, 9H); ^{13}C NMR (125 MHz, CDCl3) δ 200.1, 160.4, 159.6, 156.4, 153.1, 140.9, 130.6, 129.6, 128.7, 127.8, 126.5, 113.5, 113.2, 93.8, 93.0, 88.7, 82.99, 92.96, 80.5, 66.2, 56.1, 55.5, 55.3, -0.26; IR υ_{max} (film): 3502, 2927, 2856, 1728,

1617, 1515, 1459, 1253, 1152, 1089, 840 cm^{-1}. HRMS-ESI (m/z) calculated $[M+H]^+$ $C_{30}H_{35}O_7Si$, 535.2152, found 535.2144.

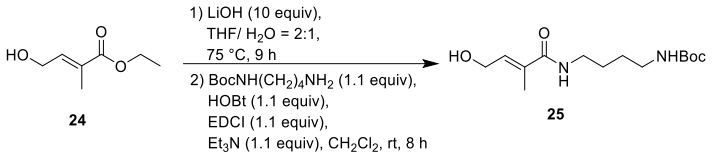

Boc-protected hydroxytiglic amide 25: Compound **24** was prepared using a reported procedure.[59] Subsequently, a 100 mL round bottom flask was charged with compound **24** (2.0 g, 13.9 mmol, 1 equiv), LiOH (3.32g, 139 mmol, 10 equiv), and 50 mL of THF/H_2O (2:1) as solvent. The mixture was stirred for 9 h at 75 °C. After the reaction was cooled to room temperature, 1M HCl (aq.) was added to acidify the pH of the solution to 4. The mixture was then extracted with EtOAc (20 mL × 3). The combined organic layers were washed with saturated sodium chloride and dried over sodium sulfate. After concentration *in vacuo*, the crude material was purified by column chromatography using a gradient of hexanes/EtOAc (1:1 to 1:4). The hydroxytiglic acid (1.6 g, quantitative) was obtained as a white solid. Next, a 50 mL flame-dried flask was charged with hydroxytiglic acid (1.6, 8.5 mmol, 1 equiv), HOBt (1.26 g, 9.35 mmol, 1.1 equiv), EDCI (1.79 g, 9.35 mmol, 1.1 equiv), *mono*-Boc-protected diaminobutane (1.09 g, 9.35 mmol, 1.1 equiv), Et_3N (1.3 mL, 9.35 mmol, 1.1 equiv), and CH_2Cl_2 (57 mL, 0.15 M). The resulting mixture was stirred at room temperature for 8 h. Then, 50 mL of saturated ammonium chloride was added to quench the reaction. The reaction mixture was extracted with CH_2Cl_2 (50 mL × 3). The combined organic layer was washed with saturated sodium chloride and dried over sodium sulfate. After concentration *in vacuo*, purification by column chromatography using a

gradient of hexanes/EtOAc (1:2 to 1:5) afforded compound **25** (2.25 g, 7.86 mmol) in 92% yield as a white solid.

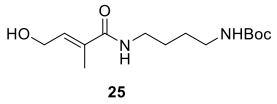

25

25: R_f: 0.19 (EtOAc). m.p. = 80 °C (CH_2Cl_2). ^{1}H NMR (500 MHz, $CDCl_3$) δ 6.35 (td, J_1 = 6.1 Hz, J_2 = 1.1 Hz, 1H), 6.22 (brs, 1H, NH), 4.73 (brs, 1H, NH), 4.29 (d, J = 6.1 Hz, 2H), 3.31 (m, 2H), 3.11 (m, 2H), 1.84 (d, J = 1.1 Hz, 3H), 1.53 (m, 4H), 1.42 (s, 9H); ^{13}C NMR (125 MHz, CDCl3) δ 169.4, 156.2, 133.9, 132.4, 79.3, 59.3, 40.1, 39.4, 28.4, 27.6, 26.6, 13.0; IR υ_{max} (film): 3338, 2934, 1690, 1621, 1533, 1366, 1281, 1169, 1017 cm^{-1}. HRMS-ESI (m/z) calculated $[M+Na]^+$ $C_{14}H_{26}O_4N_2Na$, 309.1790, found 309.1799.

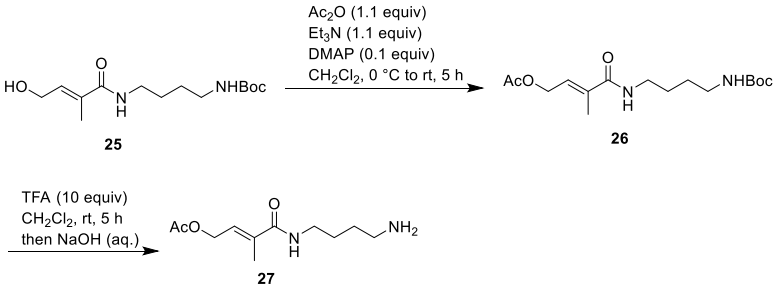

25 **26** **27**

Tiglic amide acetate 27: A 50 mL flame-dried round bottom flask was charged with compound **25** (2.0 g, 7.0 mmol, 1 equiv), Et_3N (1.1 mL, 7.7 mmol, 1.1 equiv), DMAP (85 mg, 0.7 mmol, 0.1 equiv), and CH_2Cl_2 (47 mL, 0.15 M). After the mixture was cooled to 0 °C by ice bath, Ac_2O (0.75 mL, 7.7 mmol, 1.1 equiv) was added dropwise. The reaction was warmed to rt and stirred for 5 h before 20 mL of saturated sodium bicarbonate was added. The mixture was extracted with CH_2Cl_2 (50 mL × 3), washed with saturated sodium chloride (50 mL), and dried over anhydrous sodium sulfate. Purification by column chromatography using a gradient of hexanes/EtOAc (1:1 to 1:3) afforded compound **26**

(2.1 g, 6.4 mmol) as a white solid (92% yield). Subsequently, compound **26** (2.1 g, 6.4 mmol, 1 equiv) was redissolved by CH_2Cl_2 (43 mL, 0.15 M) in a 25 mL flame-dried round bottom flask. Trifluoroacetic acid (4.9 mL, 64 mmol, 10 equiv) was then added dropwise to the solution and the reaction was stirred for 5 h. The reaction mixture was concentrated *in vacuo*. The remaining TFA was removed by azeotrope with benzene (15 mL × 3). The material was reconstituted with 50 mL of EtOAc and washed with sat. sodium chloride and aqueous 1M NaOH . After the aqueous layer was discarded, the organic layer was washed with saturated sodium chloride (50 mL) and dried over sodium sulfate to afford tiglic amide acetate **27** (1.05 g, 4.6 mmol, 72% yield) as a colorless oil. Compound **27** was found to undergo acyl transfer to afford byproduct. Accordingly, compound **27** was used in the next step without further purification after preparation.

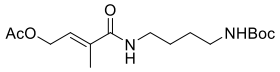

26

26: R_f: 0.19 (EtOAc/hexanes = 1:1). m.p. = 64 °C (CH_2Cl_2). ^{1}H NMR (500 MHz, $CDCl_3$) δ 6.30 (brs, 1H, NH), 6.23 (td, J_1 = 6.3 Hz, J_2 = 1.3 Hz, 1H), 4.80 (brs, 1H, NH), 4.63 (d, J = 6.3 Hz, 2H), 3.26 (m, 2H), 3.05 (m, 2H), 1.99 (s, 3H), 1.83 (d, J = 1.3 Hz, 3H), 1.47 (m, 4H), 1.35 (s, 9H); ^{13}C NMR (125 MHz, $CDCl_3$) δ 169.4, 156.2, 133.9, 132.4, 79.3, 59.3, 40.1, 39.4, 28.4, 27.6, 26.6, 13.0; IR υ_{max} (film): 3338, 2933, 1694, 1627, 1529, 1365, 1228, 1168, 1028 cm^{-1}. HRMS-ESI (m/z) calculated $[M+Na]^+$ $C_{16}H_{28}O_5N_2Na$, 351.1896, found 351.1901.

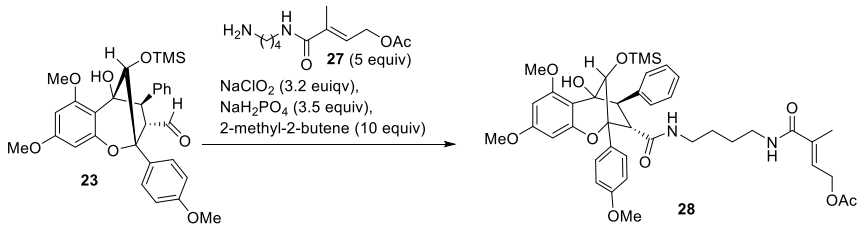

Protected perviridisin B 28: A flame-dried test tube was charged with aldehyde **23** (95.4 mg, 0.18 mmol, 1 equiv) and amine **27** (259 mg, 0.9 mmol, 5 equiv), and 2 mL of dry toluene (0.09 M). After stirring for 5 min, $NaClO_2$ (52 mg, 0.57 mmol, 3.2 equiv), NaH_2PO_4 (75 mg, 0.62 mmol, 3.5 equiv) and 2-methyl-2-butene (0.19 mL, 1.78 mmol, 10 equiv) were added. The resulting mixture was stirred for 48 h at room temperature before filtration to remove solids. The filtrate was concentrated *in vacuo* and purified by column chromatography using a gradient of hexanes/EtOAc (2:1 to 1:2) to afford silyl-protected perviridisin B **28** (111 mg, 0.15 mmol, 82%) as a colorless oil.

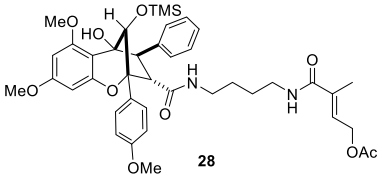

28: R_f: 0.2 (EtOAc/hexanes = 2:1). ^{1}H NMR (500 MHz, $CDCl_3$) δ 7.71 (d, J = 8.7 Hz, 2H), 7.57 (d, J = 7.8 Hz, 2H), 7.31 (m, 2H), 7.22 (m, 1H), 6.98 (d, J = 8.7 Hz, 2H), 6.28 (td, J_1 = 6.5 Hz, J_2 = 1.3 Hz, 1H), 6.15 (d, J = 2.6 Hz, 1H), 6.12 (d, J = 2.6 Hz, 1H), 5.94 (brs, 1H, NH), 5.22 (brt, J = 5.8 Hz, 1H, NH), 4.99 (s, 1H, OH), 4.70 (d, J = 6.5 Hz, 2H), 4.34 (d, J = 6.8 Hz, 1H), 4.14 (s, 1H), 4.12 (d, J = 6.8 Hz, 1H), 3.86 (s, 3H), 3.83 (s, 3H), 3.77 (s, 3H), 3.19 (m, 3H), 2.87 (m, 1H), 2.08 (s, 3H), 1.86 (d, J = 1.3 Hz, 3H), -0.14 (s, 9H); ^{13}C NMR (125 MHz, $CDCl_3$) δ 170.8, 169.8, 168.4, 160.2, 159.5, 156.4, 153.1, 141.5, 134.9, 130.6, 130.2, 128.6, 128.2, 128.1, 127.7, 126.4, 113.6, 113.5, 93.9, 92.7, 88.0, 83.3, 80.1, 60.8, 60.7, 58.5, 56.1, 55.4, 39.4, 38.5, 27.2, 25.9, 20.8, 13.1, -0.2; IR υ_{max} (film): 3506, 3416, 3346, 2957, 1742, 1619,

1516, 1458, 1253, 1152, 1091, 839 cm^{-1}. HRMS-ESI (m/z) calculated $[M+Na]^+$ $C_{41}H_{52}O_{10}N_2SiNa$, 783.3289, found 783.3279.

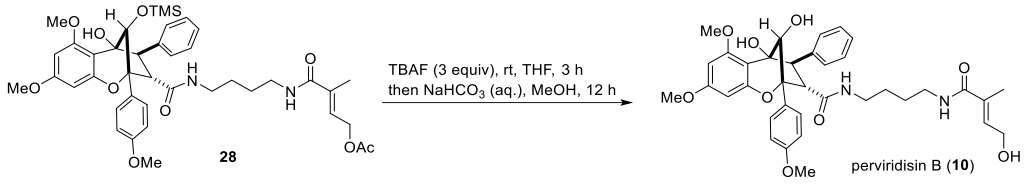

Perviridisin B 10: A flame dried test tube was charged with compound **28** (111 mg, 0.15 mmol, 1 equiv), 1 mL THF and tetra-*n*-butylammonium fluoride (1M solution in THF, 0.44 mL, 0.44 mmol, 3 equiv). The resulting solution was stirred for 3 h. 3 mL of saturated sodium chloride and 10 mL EtOAc then was added to form a bilayer mixture and the aqueous layer was discarded. The organic layer was washed with 5 mL saturated sodium chloride and dried over sodium sulfate. The filtrate was concentrated *in vacuo* and was redissolved in 2 mL of MeOH which was followed by addition of 0.2 mL of saturated sodium bicarbonate. The mixture was stirred for 12 h and concentrated *in vacuo*. Purification by preparative TLC using EtOAc as solvent afforded perviridisin B **10** (86 mg, 0.12 mmol, 82% yield) as a white solid.

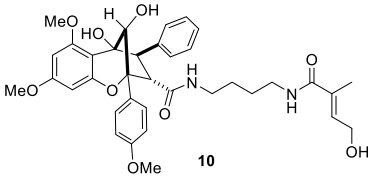

10: R_f: 0.11 (EtOAc). m.p. = 269 - 271 °C (CH_2Cl_2). ^1H NMR (500 MHz, $CDCl_3$) δ 7.84 (d, J = 8.5 Hz, 2H), 7.52 (d, J = 7.5 Hz, 2H), 7.35 (t, J = 7.5 Hz, 2H), 7.28 (m, 1H), 7.04 (d, J = 8.5 Hz, 2H), 6.26 (td, J_1 = 6.5 Hz, J_2 = 1.5 Hz, 1H), 6.16 (d, J = 2.5 Hz, 1H), 6.14 (d, J = 2.5 Hz, 1H), 6.09 (brs, 1H), 5.22 (s, 1H, OH), 5.22 (brt, d = 6.4 Hz, 1H, NH), 4.39 (d, J = 6.5 Hz, 1H), 4.28 (d, J = 6.5 Hz, 1H), 4.26 (d, J = 5.1 Hz, 2H), 4.19 (s, 1H), 3.89 (s, 3H), 3.87 (s, 3H), 3.77 (s, 3H), 3.26 (m, 2H), 3.16 (m, 1H), 2.85 (m,

1H), 2.61 (s, 1H, OH), 1.81 (d, J = 1.5 Hz, 3H), 1.64 (m, 2H), 1.31 (m, 2H); ^{13}C NMR (125 MHz, $CDCl_3$) δ 169.5, 169.1, 160.4, 150.6, 156.1, 153.0, 140.6, 133.1, 132.9, 129.9, 129.6, 128.2, 126.8, 114.0, 112.1, 94.0, 92.6, 87.1, 82.4, 79.8, 60.3, 59.4, 58.1, 55.4, 39.3, 38.6, 27.3, 25.7, 13.0; IR υ_{max} (film): 3408, 2937, 1669, 1619, 1591, 1516, 1459, 1440, 1255, 1252, 1201, 1152, 1098, 1034, 834, 755 cm^{-1}. HRMS-ESI (m/z) calculated $[M+H]^+$ $C_{36}H_{43}O_9N_2$, 647.2969, found 647.2970.

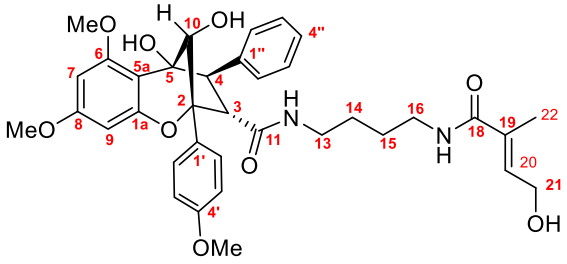

(±)-perviridisin B (10)

^{1}H NMR

	natural (+)-**10**	synthetic (±)-**10** (this work)
Positions	δ lit ($CDCl_3$) (J_{H-H} in Hz)	δ (500 MHz, $CDCl_3$) (J_{H-H} in Hz)
2		
3	4.28, d (6.7)	4.28, d (6.5)
4	4.40, d (6.5)	4.39, d (6.5)
5		
5-OH	5.23, s	5.22, s
5a		
6		
7	6.14, d (2.1)	6.14, d (2.5)
8		
9	6.16, d (2.2)	6.16, d (2.5)
9a		
10	4.20, s	4.19, s
10-OH	2.97, brs	2.98, brs
11		
NH-12	5.21, brt (6.4)	5.22, brt (6.4)
13	2.86, m 3.17, m	2.85, m 3.16, m

14	1.33, m	1.31, m
15	1.60, m	1.64, m
16	3.26, m	3.26, m
NH-17	6.10, brt (5.2)	6.09, brs
18		
19		
20	6.27, brt (6.0)	6.26, td (6.5, 1.5
21	4.27	4.26
22	1.82, s	1.81, d (1.5)
1’		
2’, 6’	7.84, d (8.9)	7.84, d (8.5)
3’, 5’	7.05, d (8.9)	7.04, d (8.5)
4’		
1’’		
2’’, 6’’	7.52, d (7.3)	7.52 d (7.5)
3’’, 5’’	7.36, t (7.4)	7.35, t (7.5)
4’’	7.29 (overlapped)	7.28 (overlapped)
OCH_3-6	3.89, s	3.89, s
OCH_3-8	3.77, s	3.77, s
OCH_3-4’	3.87, s	3.87, s

^{13}C NMR

	natural (+)-**10**	synthetic (±)-**10** (this work)
Positions	δ lit. ($CDCl_3$)	δ (125 MHz, $CDCl_3$)
2	87.1	87.1
3	60.3	60.3
4	58.1	58.1
5	79.9	79.8
5-OH		
5a	112.0	112.1
6	156.2	156.1
7	92.6	92.6
8	160.4	160.4
9	94.0	94.0
9a	153.0	153.0
10	82.4	82.4
10-OH		
11	169.5	169.5
NH-12		
13	38.5	38.6
14	27.3	27.3
15	25.6	25.7

16	39.4	39.3
NH-17		
18	169.1	169.1
19	133.0	133.0
20	133.1	133.1
21	59.4	59.4
22	13.0	13.0
1’	129.6	129.6
2’, 6’	128.3	128.2
3’, 5’	114.0	114.0
4’	159.6	159.6
1’’	140.7	140.7
2’’, 6’’	129.9	129.9
3’’, 5’’	128.3	128.3
4’’	126.8	126.8
OCH_3-6	56.2	56.2
OCH_3-8	55.4	55.4
OCH_3-4’	55.5	55.5

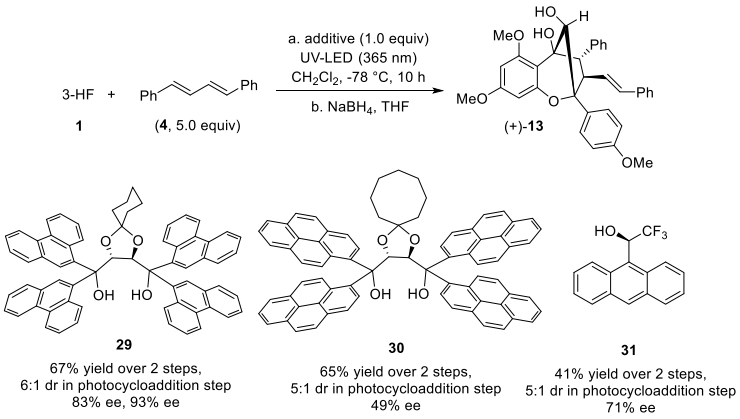

entry	time, temperature	light source	solvent	chiral additive	yield, enantiomeric excess
1	12 h, -70 °C	Rayonet	PhMe/CH_2Cl_2 (1:2)	**29**	49% yield 52% ee
2	12 h, -70 °C	Rayonet	PhMe/CH_2Cl_2 (1:2)	**30**	51% yield 45% ee

3	12 h, -70 °C	Rayonet	CH_2Cl_2	**29**	56% yield 69% ee
4	12 h, -70 °C	Rayonet	CH_2Cl_2	**31**	30% yield 49% ee
5	2 h, -30 °C	Rayonet Photoflow	CH_2Cl_2	**29**	67% yield 31% ee
6	10 h, -78 °C	UV-LED	CH_2Cl_2	**30**	65% yield 49% ee
7	10 h, -78 °C	UV-LED	PhMe/CH_2Cl_2 (1:2)	**29**	31% yield 71% ee
8	10 h, -78 °C	UV-LED	CH_2Cl_2	**29**	67% yield 83% ee
9	10 h, -78 °C	UV-LED	CH_2Cl_2	**31**	41% yield 71% ee

General procedure for asymmetric ESIPT photocycloaddition of 3-HF 1 with DPBD 4:

A flame-dried 100 mL photoreaction tube was charged with 3-hydroxyflavone **1** (50 mg, 0.15 mmol, 1 equiv), DPBD **4** (1.57 g, 7.61 mmol, 5 equiv) and 1.0 equivalent of hydrogen-bonding additive in 30 mL of dry CH_2Cl_2 (0.005 M for 3-HF **1**). Subsequently, the reaction mixture was degassed by argon gas bubbling combined with sonication for 10 min. During degassing, the reaction mixture should be put in an ice bath to prevent solvent evaporation. In order to conduct low temperature photochemistry experiments, a UV-LED (λ_{max} = 365 nm) was introduced as light source and a special dewar flask with a transparent window was used as temperature control.[41] The dewar was filled with dry ice and isopropanol to achieve -78 °C and then the reaction tube was inserted into the dry ice bath. Due to the low solubility of DPBD **4** at -78 °C, the reaction mixture was diluted to 0.005 M instead of the

previously described 0.03 M concentration. The reaction was then irradiated for 10 h. The solvent was concentrated *in vacuo* and redissolved in 10 mL dry THF. Subsequently, $NaBH_4$ (29 mg, 0.76 mmol, 5 eq) was then added to directly reduce the mixture. After 5 h, saturated NH_4Cl (aq.) was added to the reaction mixture to quench the reaction. The reaction was extracted with EtOAc (30 mL × 3), washed with saturated NaCl (aq.) and dried with anhydrous Na_2SO_4. The filtrate was then concentrated *in vacuo* and purified by column chromatography using a gradient of hexanes/EtOAc (20:1 to 10:1 to remove DPBD and hydrogen-bonding additive, then 8:1 to 3:1). Aglain derivative (+)-**13** was obtained as a white solid. The enantioselectivity was determine using analytical chiral HPLC. $[\alpha]_D^{20}$= + 71.4° (*c* = 1.0, $CHCl_3$). (+)-**13** was further converted to (+)-**14** using the previously described method. $[\alpha]_D^{20}$= + 92.3° (*c* = 1.0, $CHCl_3$).

Chiral HPLC Analysis of aglain **13**: *Chiralcel OD* column with an isocratic mobile phase of isopropanol/hexanes (10:90), with a flow rate of 1.0 mL/min for 40 min.

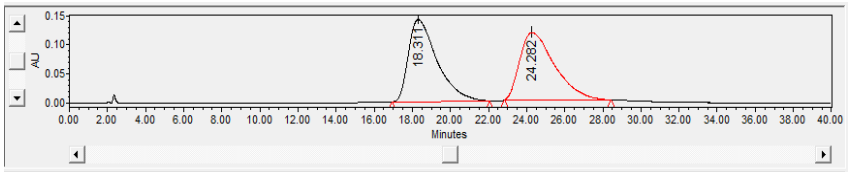

	Name	Retention Time (min)	Area (μV*sec)	% Area	Height (μV)	Int Type	Amount	Units	Peak Type	Peak Codes
1		18.311	14721323	50.03	141541	bb			Unknown	
2		24.282	14705746	49.97	115616	bb			Unknown	

3D Channels | 2D Channels | Peaks

Enantioselectivity using TADDOL **23**:

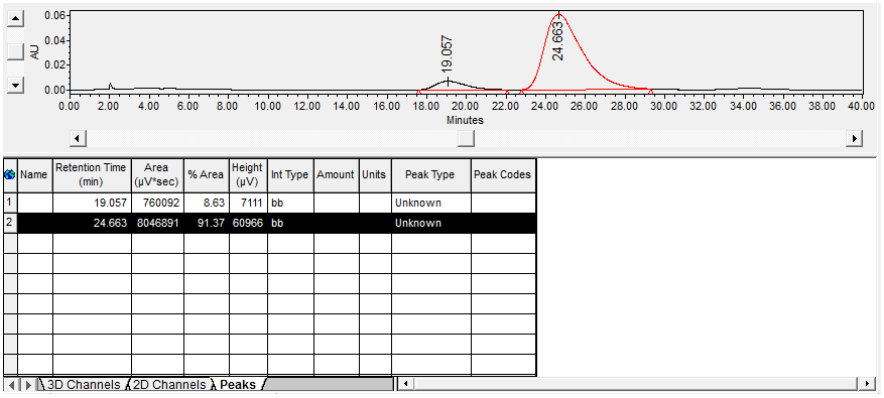

	Name	Retention Time (min)	Area (μV*sec)	% Area	Height (μV)	Int Type	Amount	Units	Peak Type	Peak Codes
1		19.057	760092	8.63	7111	bb			Unknown	
2		24.663	8046891	91.37	60966	bb			Unknown	

3D Channels | 2D Channels | Peaks

Enantiomeric excess after recrystallization of aglain (+)-**13** obtained from photoreaction with TADDOL **29**:

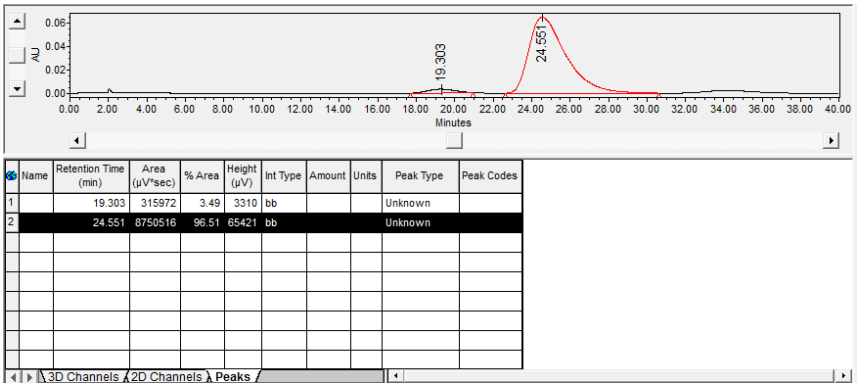

	Name	Retention Time (min)	Area (μV*sec)	% Area	Height (μV)	Int Type	Amount	Units	Peak Type	Peak Codes
1		19.303	315972	3.49	3310	bb			Unknown	
2		24.551	8750516	96.51	65421	bb			Unknown	

3D Channels | 2D Channels | Peaks

Enantioselectivity using TADDOL **30**:

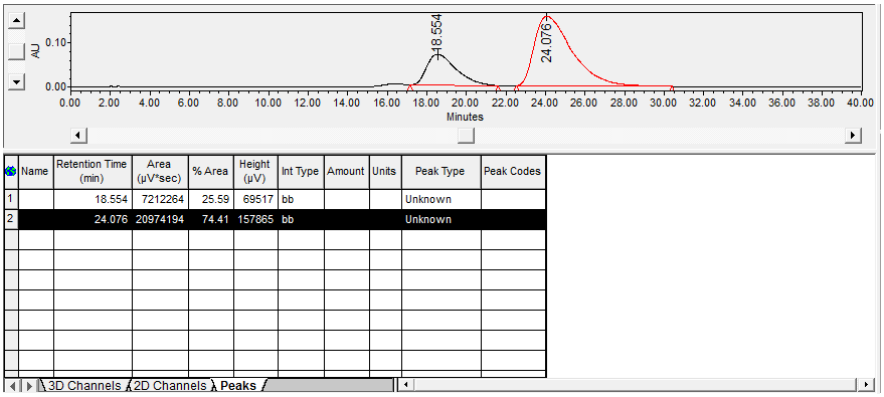

	Name	Retention Time (min)	Area (μV*sec)	% Area	Height (μV)	Int Type	Amount	Units	Peak Type	Peak Codes
1		18.554	7212264	25.59	69517	bb			Unknown	
2		24.076	20974194	74.41	157865	bb			Unknown	

3D Channels | 2D Channels | Peaks

Enantioselectivity using Pirkle's alcohol **31**:

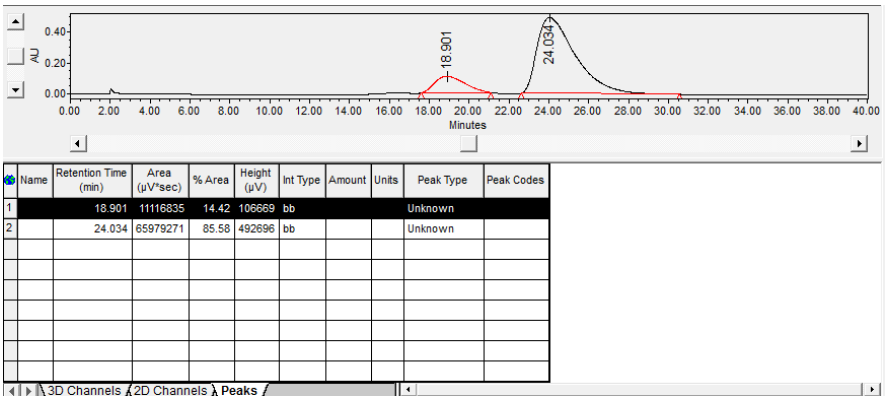

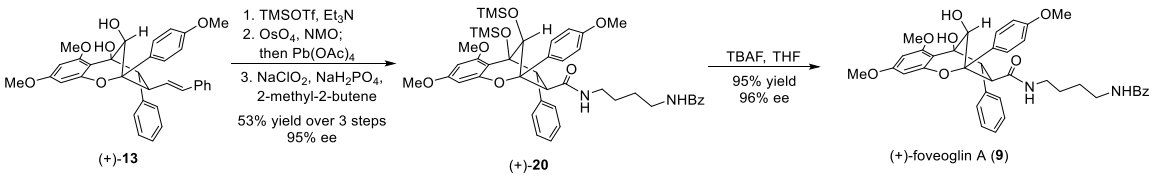

With (+)-**13** in hand, silylation, oxidative cleavage of the double bond followed by oxidative amidation was performed using previously described procedure to furnish the core of foveoglin A in 53% yield and 95% ee, $[\alpha]_D^{20}$ +43.1 (c 0.1, $CHCl_3$). Silyl group deprotection by TBAF provided us (+)-foveoglin A **9** in 95% yield and 96% ee, $[\alpha]_D^{23}$ +25.3 (c 0.16, $CHCl_3$).

Chiral HPLC Analysis of aglain **20**: *Chiralpak AD* column with an isocratic mobile phase of isopropanol/hexanes (5:95), with a flow rate of 1.0 mL/min for 40 min.

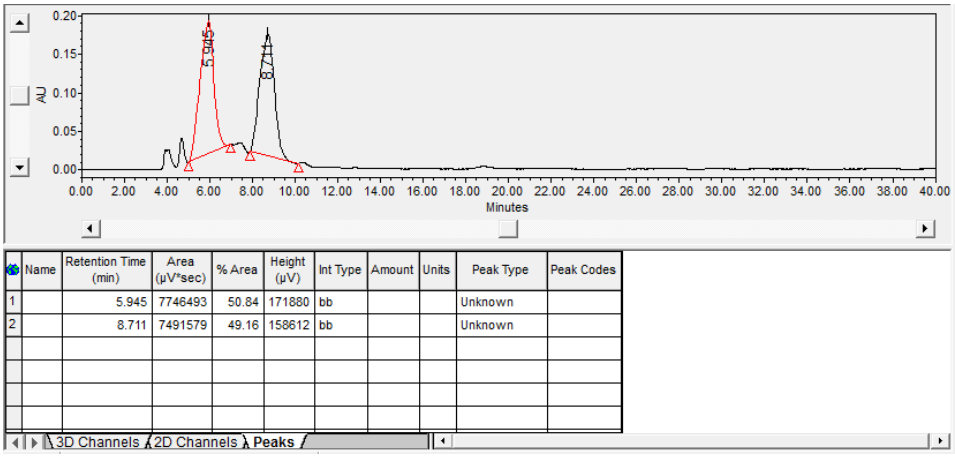

	Name	Retention Time (min)	Area (μV*sec)	% Area	Height (μV)	Int Type	Amount	Units	Peak Type	Peak Codes
1		5.945	7746493	50.84	171880	bb			Unknown	
2		8.711	7491579	49.16	158612	bb			Unknown	

3D Channels | 2D Channels | Peaks

Enantiomeric excess of (+)-**20**:

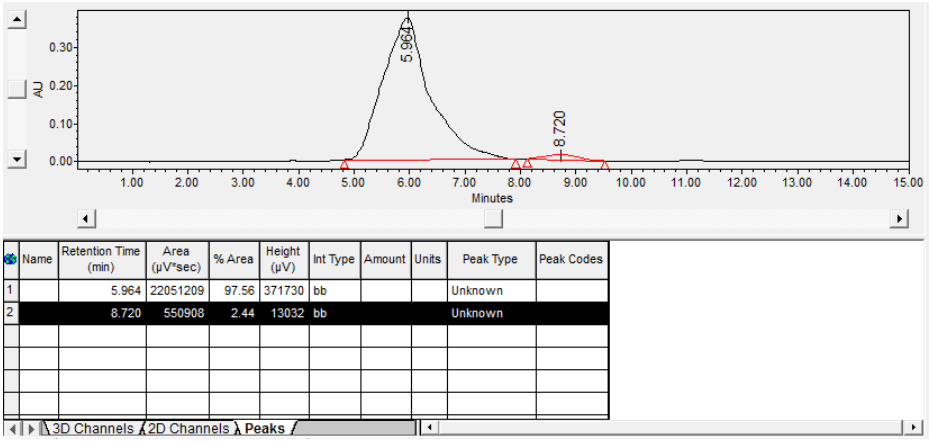

	Name	Retention Time (min)	Area (μV*sec)	% Area	Height (μV)	Int Type	Amount	Units	Peak Type	Peak Codes
1		5.964	22051209	97.56	371730	bb			Unknown	
2		8.720	550908	2.44	13032	bb			Unknown	

3D Channels | 2D Channels | Peaks

Chiral HPLC Analysis of (±)-foveoglin A **9**: *Chiralpak AD* column with an isocratic mobile phase of isopropanol/hexanes (20:80), with a flow rate of 1.0 mL/min for 40 min.

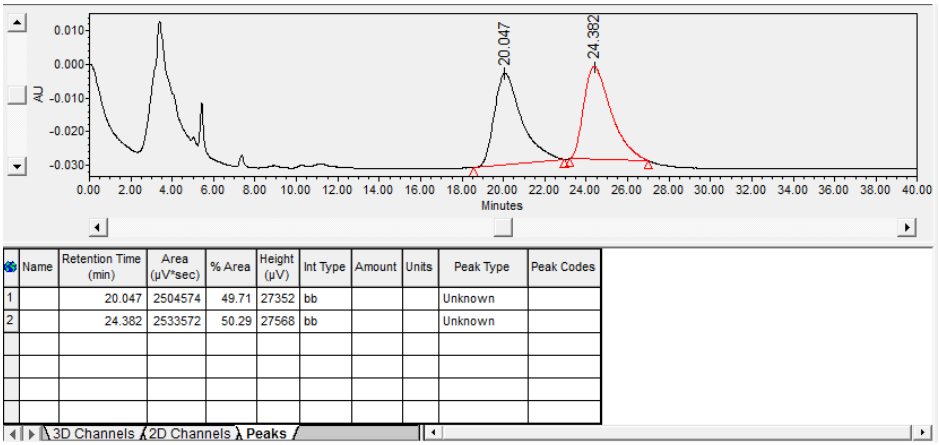

Enantiomeric excess of (+)-foveoglin A **9**:

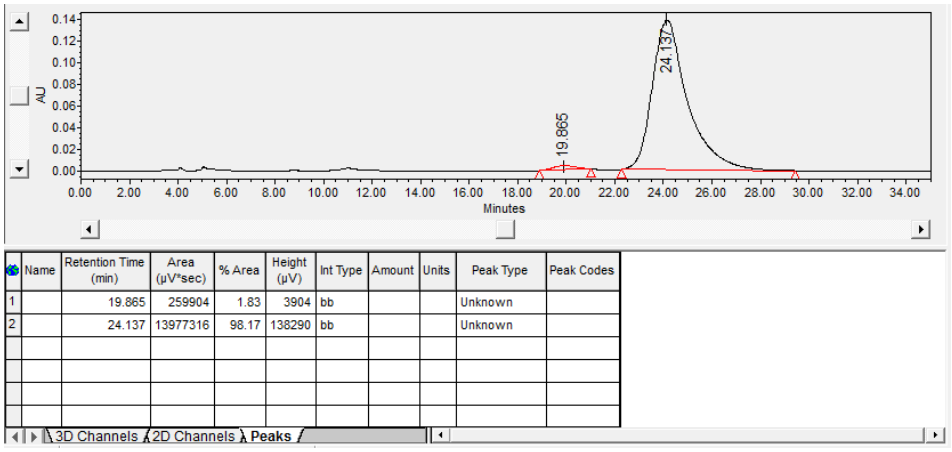

Determination of absolute configuration of *para*-bromo benzoate (+)-14 by VCD (vibrational circular dichroism):

Experimental VCD:

VCD and IR spectra for (+)-**14** were recorded using a KBr pellet on a Bruker FT-IR TENSOR II spectrometer with 8 cm^{-1} spectral resolution, polarization modulation efficiency set to 1300 cm^{-1}, and a 1900 cm^{-1} optical filter used to improve the signal-to-noise ratio. The VCD spectrum was collected from 1950 to 800 cm^{-1} at six different orientations of the tablet in the holder, with a 20 minutes acquisition time for each orientation. An averaged spectrum was calculated for the six orientations.

Predicted VCD:

Theoretical VCD calculations were performed using the "VCD Workflow" in Schrodinger, Inc.'s Maestro software.[60] Conformers were generated *via* a Macromodel conformational search (force field: OPLS 2005, mixed torsional/low-mode sampling, 5 kcal/mol MM

energy window) followed by quantum mechanical screening for conformer retention (0.5 Angstrom deviation, 5.0 kcal/mol QM energy window), followed by DFT geometry optimizations (B3LYP/LACVP**) and VCD/IR spectrum predictions on the retained conformers. DFT calculations were performed in the absence of solvent. From the VCD Workflow module, seven conformers were obtained with final gas phase energies within 2.7 kcal/mol of the lowest energy conformer. The conformers and their gas phase energies are depicted in **Figure 2.6**. Due to the highly rigid fused bicyclic structure of **14**, the differences in conformers mainly arose from bond rotations at the aryl methoxy groups and the styryl substituent. The VCD workflow was also repeated on the enantiomer of **14**, with seven similar enantiomeric conformers also obtained (*not shown*). Single-point energy calculations with vibrational frequencies and VCD prediction were then performed on the enantiomeric sets of seven conformers querying alternative functional and basis set combinations. It was determined that B3PW91/TZV** gave the best agreement with the experimental IR/VCD spectra with respect to signal location and intensities.

VCD Analysis:

Following the DFT calculations, average computed VCD and IR spectra for the seven output conformers (B3PW91/TZV*) were generated using Boltzmann weighting based on calculated gas phase energies, with a Lortentzian line shape at 8 cm^{-1} resolution. For the purpose of visual comparison, the experimental IR and VCD intensities have been scaled by 1,000-fold and 10,000-fold, respectively, and the predicted IR and VCD frequencies have been offset by -20.0 cm^{-1}, based on a direct comparison of the predicted and experimental IRs (**Figure 2.7A/B**).[61] A qualitative assessment of the measured vs. predicted VCD spectra for **14** (**Figure 2.7C/D**) and **ent-14** (**Figure 2.7E/F**) strongly supports the assignment of absolute stereochemistry for **14**.

Figure 2.6 Seven Conformers and Relative Gas Phase Energies (B3PW91/TZV) Obtained for Compound 14 Using Schrodinger's Jaguar VCD Workflow.**

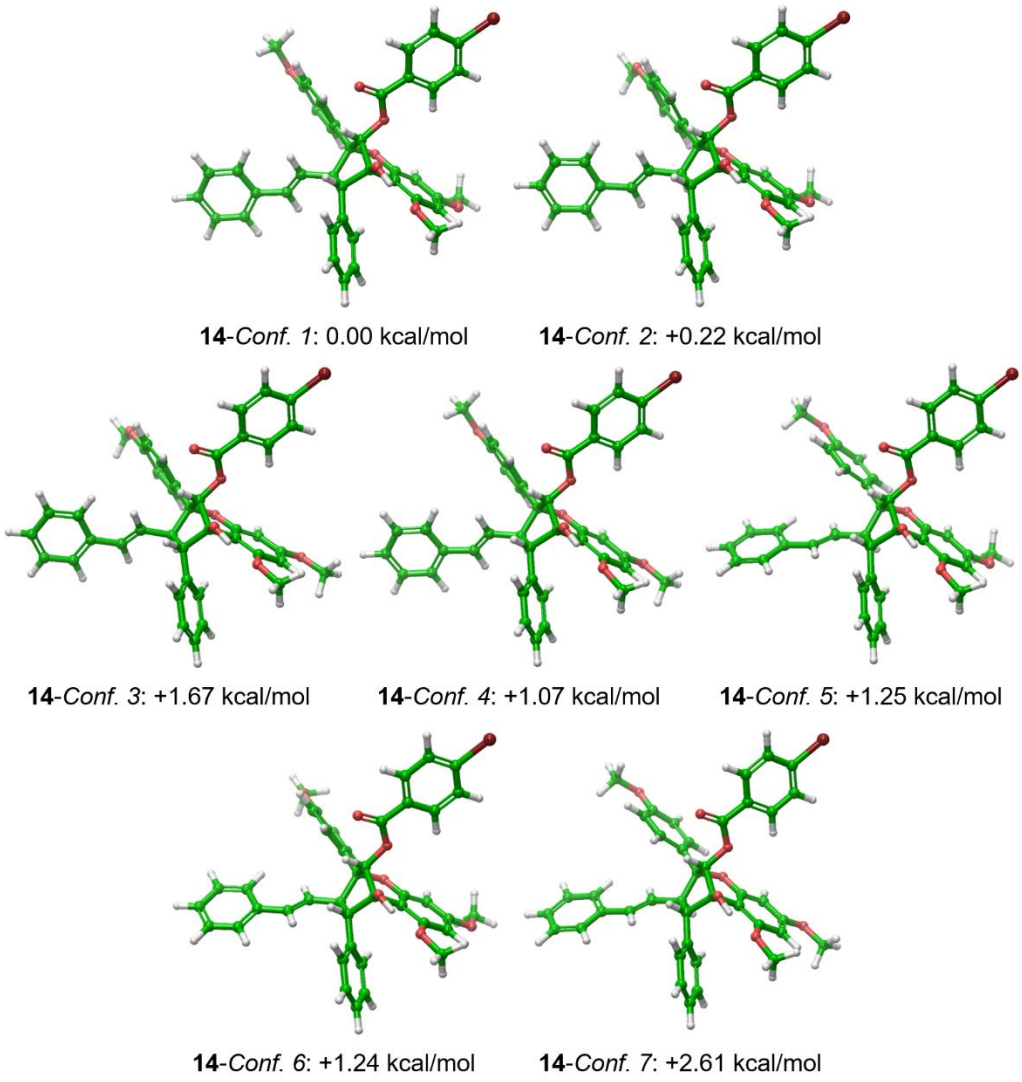

Figure 2.7 Predicted (red) and Measured (blue) IR and VCD Spectra Comparisons For 14 and *ent*-14. All Predicted Spectra Are Offset by 20 cm^{-1} Based on the IR Comparisons.

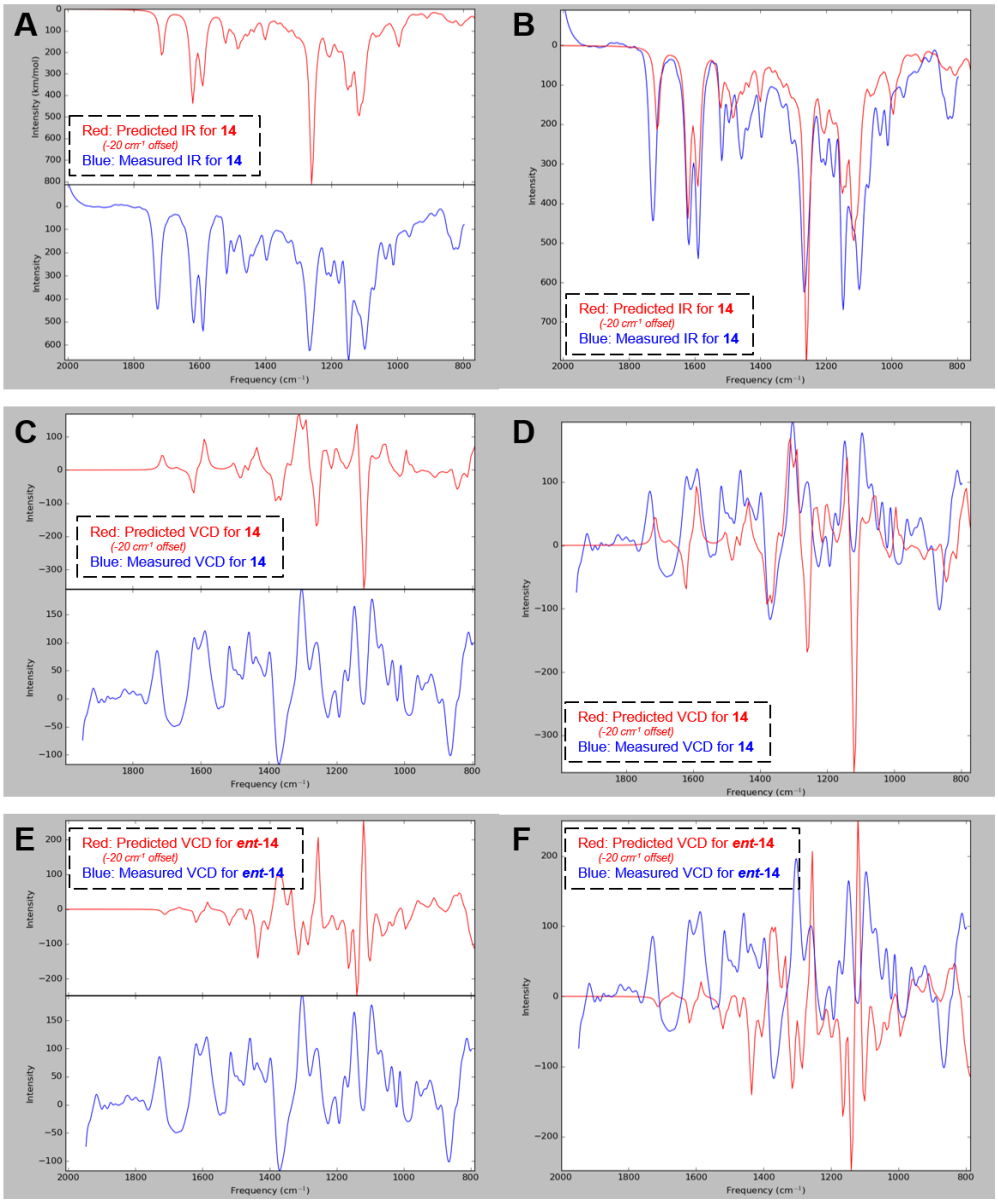

A) IR comparisons, stacked; **B**) IR comparisons, overlaid; **C**) VCD comparisons for **14**, stacked; **D**) VCD comparisons for **14**, overlaid; **E**) VCD comparisons for ***ent*-14**, stacked; **F**) VCD comparisons for ***ent*-14**, overlaid.

ESIPT Photocycloaddition of 3-HF 1 with Unsymmetrical DPBDs:

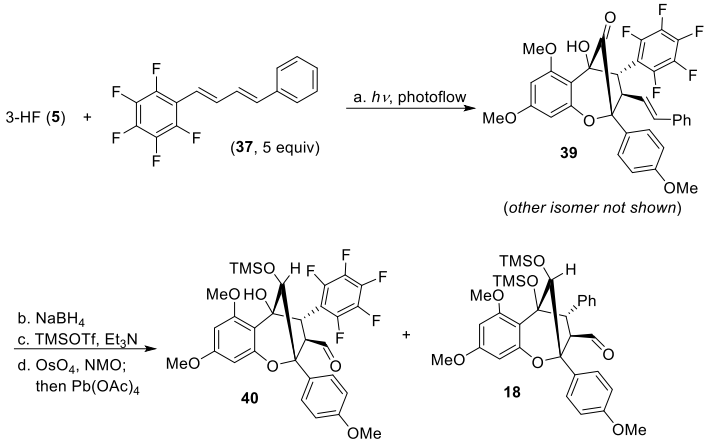

A 100 mL round bottom flask was charged with 3-hydroxyflavone **1** (300 mg, 0.91 mmol, 1 equiv), pentafluoro-DPBD **37**[62] (1.35 g, 4.6 mmol, 5 equiv), and 90 mL of CH_2Cl_2 (0.01 M for 3-HF **1**). The flask was connected with the continuous photoflow reactor followed by degassing of the reaction at 0 ^oC with argon bubbling for 5 min with sonication. Subsequently, the peristaltic pump was turned on to circulate the reaction mixture and argon bubbling with sonication was continued for an additional 15 min before the UV-lamp (Rayonet, λ_{max} = 350 nm) was turned on. After 6 h, the reaction mixture was collected back into the flask and was concentrated *in vacuo*. Purification *via* flash chromatography using a gradient of hexanes/EtOAc (10:1 to 3:1) afforded the cyclopenta[*bc*]benzopyran products as a mixture of isomers (photocycloadducts were identified based on a ^1H NMR spectrum of the crude product) which were used in the next step without further purification. A flame-dried 100 mL flask was charged with the mixture of compounds (338 mg, 0.54 mmol, 1 equiv) and THF (4 mL, 0.14 M) was added. Subsequently, $NaBH_4$ (123 mg, 3.25 mmol, 6 equiv) was added at rt in one portion. The resulting mixture was then stirred for 12 h and was quenched with ice-cooled saturated ammonium chloride. The

mixture was extracted with CH_2Cl_2 (10 mL × 3), washed with saturated sodium bicarbonate, and dried over sodium sulfate. The filtrate was concentrated *in vacuo*. Column chromatography purification using hexanes/EtOAc (5:1 to 3:1) afforded an inseparable mixture of aglain products (321.6 mg), which was redissolved in CH_2Cl_2 (5 mL) and cooled to -78 °C. Subsequently, Et_3N (188 μL, 1.35 mmol, 2.5 equiv) and TMSOTf (210 μL, 1.14 mmol, 2.1 equiv) were added. The resulting mixture was stirred at -78 °C for an additional 10 min and was then to warmed to 0 °C for another 20 min before 10 mL of saturated Na_2CO_3 (aq.) was added to quench the reaction. The reaction mixture was further extracted with CH_2Cl_2 (3 mL × 3). The combined organic layer was washed with 10 mL saturated NaCl (aq.), dried over anhydrous Na_2SO_4, and concentrated *in vacuo*. Subsequently, the crude compound mixture was redissolved in 13 mL of THF/*t*-BuOH (1:1). Subsequently, 1.3 mL OsO_4 (10 mg/mL, aq., 0.1 equiv) solution was added followed by addition of NMO (190 mg, 1.62 mmol, 3 equiv). The resulting mixture was stirred at room temperature for 12 h, before being extracted with Et_2O (5mL × 3). The combined organic layers were washed with saturated NaCl (aq.), dried over anhydrous Na_2SO_4, and concentrated *in vacuo*. The obtained brown oil was redissolved in CH_2Cl_2 (5 mL) and $Pb(OAc)_4$ (360 mg, 0.81 mmol, 1.5 equiv) was added. The reaction mixture was stirred at room temperature for 20 min before 10 mL of saturated $Na_2S_2O_3$ (aq.) was added to quench the reaction. The reaction mixture was extracted with CH_2Cl_2 (5 mL × 3), washed with 10 mL saturated NaCl (aq.), dried over anhydrous Na_2SO_4, and concentrated *in vacuo*. Purification *via* column chromatography purification using hexanes/EtOAc (20:1 to 6:1) afforded pentafluoro-

aglain aldehyde **40** (126 mg, 25% overall yield) as a colorless oil and compound **17** (45.3 mg, 8.2 % overall yield) (for characterization data for **17**, see page S10).

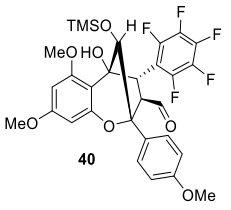

40: R_f: 0.37 (EtOAc/hexanes = 1:4). ^{1}H NMR (500 MHz, $CDCl_3$) δ 9.01 (d, J = 1.5 Hz, 1H), 7.50 (d, J = 8.9 Hz, 2H), 6.98 (d, J = 8.9 Hz, 2H), 6.30 (d, J = 1.1 Hz, 1H), 5.97 (d, J = 1.1 Hz, 1H), 5.54 (s, 1H, OH), 4.55 (s, 1H), 4.34 (d, J = 4.7 Hz, 1H), 4.01 (dd, J_1 = 4.7 Hz, J_2 = 1.5 Hz, 1H), 3.83 (s, 3H), 3.80 (s, 3H), 3.48 (s, 3H), 0.002 (s, 9H); ^{13}C NMR (125 MHz, $CDCl_3$) δ 198.0, 160.9, 159.6, 158.9, 154.3, 147.6, 145.2, 138.5, 136.0, 127.9, 127.4, 114.2, 111.0, 103.8, 94.3, 92.5, 84.4, 81.4, 73.6, 58.5, 55.8, 55.32, 55.30, 44.2, 0.6; IR υ_{max} (film): 3497, 2959, 1720, 1619, 1496, 1378, 1253, 1149, 1098, 1098, 1029, 875, 841 cm^{-1}. HRMS-ESI (m/z) calculated $[M+H]^+$ $C_{30}H_{29}F_5O_7Si$, 647.2969, found 647.2970.

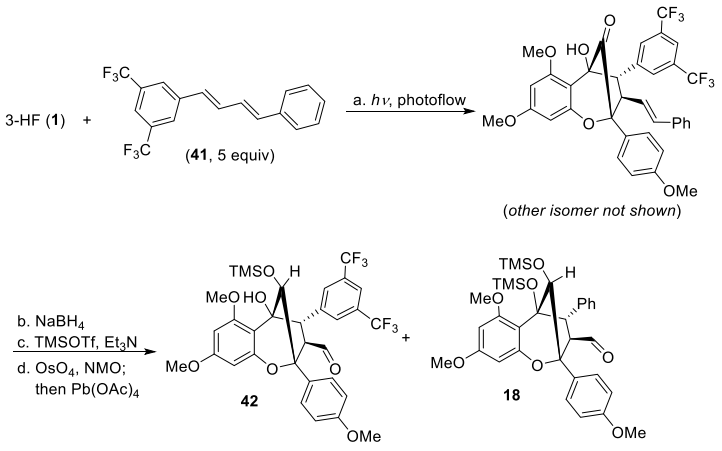

The previously mentioned general procedure for mechanistic validation reactions was employed using 3-HF **1** (300 mg, 0.91 mmol, 1 equiv.) and DPBD **41**[63] (1.56 g, 4.6 mmol, 5 equiv.). Aldehyde **42** (132 mg, 22 % overall yield) was isolated as a colorless oil and compound **18** (39 mg, 7.5 % overall yield) was isolated as a minor product.

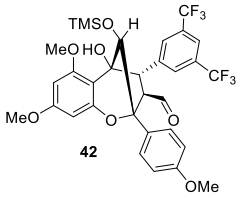

42: R_f: 0.43 (EtOAc/hexanes = 1:4). ^{1}H NMR (500 MHz, $CDCl_3$) δ 9.04 (d, J = 1.8 Hz, 1H), 7.69 (s, 1H), 7.52 (d, J = 8.8 Hz, 2H), 7.35 (s, 2H), 6.99 (d, J = 8.8 Hz, 2H), 6.33 (d, J = 2.2 Hz, 1H), 5.83 (d, J = 2.2 Hz, 1H), 5.42 (s, 1H, OH), 4.59 (s, 1H, OH), 3.97 (d, J = 9.0 Hz, 1H), 3.83 (s, 3H), 3.78 (s, 3H), 3.57 (dd, J_1 = 9 Hz, J_2 = 1.8 Hz, 1H), 3.14 (s, 3H), 0.01 (s, 9H); ^{13}C NMR (125 MHz, $CDCl_3$) δ 197.6, 161.0, 159.6, 159.1, 153.0, 140.0, 130.8, 128.6, 127.7, 127.4, 124.3, 122.2, 120.7, 114.2, 103.5, 94.6, 94.5, 92.3, 84.2, 82.0, 74.4, 61.2, 55.4, 55.3, 55.2, 52.7, 0.6; IR υ_{max} (film): 3498, 2960, 2843, 1722, 1619, 1589, 1518, 1383, 1378, 1174, 1134, 1100, 1027, 875, 844 cm^{-1}. HRMS-ESI (m/z) calculated $[M+H]^+$ $C_{32}H_{33}F_6O_7Si_2$, 671.1900, found 671.1906.

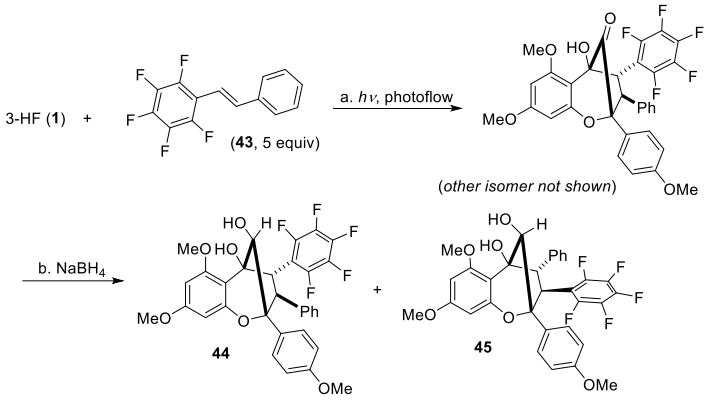

The previously mentioned general procedure for mechanistic validation reactions was employed using 3-HF **1** (300 mg, 0.91 mmol, 1 equiv.) and stilbene **43**[61] (1.23 g, 4.6 mmol, 5 equiv.). After photocycloaddition, the inseparable mixture was purified *via* flash column chromatography using a gradient of hexanes/EtOAc (10:1 to 3:1) to afford 252 mg of a white solid. The crude product was reduced with $NaBH_4$ (96 mg, 2.52 mmol, 6 equiv.) in THF. Purification *via* flash column chromatography using a gradient of hexanes/EtOAc

(9:1 to 4:1) afforded a mixture of compounds **44** and **45**. The mixture was further purified *via* preparative thin layer chromatography using hexanes/EtOAx/CH_2Cl_2 (7:1.5:1.5) afforded compound **44** (142 mg, 26 % overall yield) as a white solid and **45** (51 mg, 9.3 % overall yield) as a colorless oil.

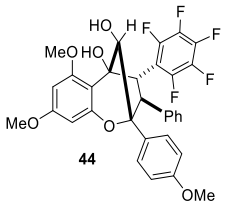

44

44: R_f: 0.13 (EtOAc/hexanes = 3:7). m.p. = 224 - 225 °C (CH_2Cl_2). ^{1}H NMR (500 MHz, $CDCl_3$) δ 7.31 (d, J = 8.7 Hz, 2H), 7.01 (t, J = 7.2 Hz, 2H), 6.95 (t, J = 7.2 Hz, 1H), 6.90 (d, J = 7.2 Hz, 2H), 6.68 (d, J = 8.7 Hz, 2H), 6.31 (d, J = 2.1 Hz, 1H), 6.04 (d, J = 2.1 Hz, 1H), 5.63 (s, 1H, OH), 4.92 (d, J = 3.3 Hz, 1H), 4.39 (d, J = 10.6 Hz, 1H), 4.10 (d, J = 10.6 Hz, 1H), 3.80 (s, 3H), 3.69 (s, 3H), 3.51 (s, 3H), 2.63 (brs, 1H, OH); ^{13}C NMR (125 MHz, $CDCl_3$) δ 161.3, 159.3, 158.8, 154.4, 147.5, 140.7, 139.3, 138.2, 136.2, 129.0, 128.9, 128.5, 128.2, 126.8, 113.2, 110.8, 102.8, 94.6, 92.8, 87.7, 81.5, 73.0, 55.7, 55.5, 55.1, 54.5, 54.3; IR υ_{max} (film): 3495, 2944, 1713, 1617, 1519, 1493, 1375, 1146, 1097, 998, 828, 701, 652 cm^{-1}. HRMS-ESI (m/z) calculated $[M+H]^+$ $C_{32}H_{26}F_5O_6$, 601.1650, found 601.1659.

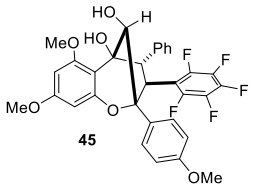

45

45: R_f: 0.13 (EtOAc/hexanes = 3:7). ^{1}H NMR (500 MHz, $CDCl_3$) δ 7.45 (d, J = 8.6 Hz, 2H), 7.19 (m, 3H), 7.00 (m, 2H), 6.80 (d, J = 8.6 Hz, 2H), 6.28 (d, J = 2.2 Hz, 1H), 5.89 (d, J = 2.2 Hz, 1H), 5.48 (s, 1H, OH), 5.17 (s, 1H), 4.45 (d, J = 10.9 Hz, 1H), 3.79 (s, 3H), 3.76 (s, 3H), 3.74 (d, J = 10.9 Hz, 1H), 3.10 (s, 3H); ^{13}C NMR (125 MHz, $CDCl_3$) δ 161.0, 160.3, 159.4, 153.2, 145.4, 143.4, 140.8, 138.3, 135.9, 135.4, 128.7, 128.1, 127.9, 127.5, 144.0, 113.5, 103.1, 94.3, 93.2, 86.6, 82.2, 72.1, 58.7, 55.43, 55.37, 55.21, 55.16, 45.7; IR υ_{max} (film): 3498, 2960, 2843, 1722, 1619, 1589, 1518, 1383, 1378, 1174, 1134,

1100, 1027, 875, 844 cm^{-1}. IR υ_{max} (film): 3495, 2944, 1713, 1617, 1519, 1493, 1375, 1146, 1097, 998, 828, 701, 652 cm^{-1}. HRMS-ESI (m/z) calculated $[M+H]^+$ $C_{32}H_{26}F_5O_6$, 601.1650, found 601.1655.

X-ray crystallographic data for compound 14:

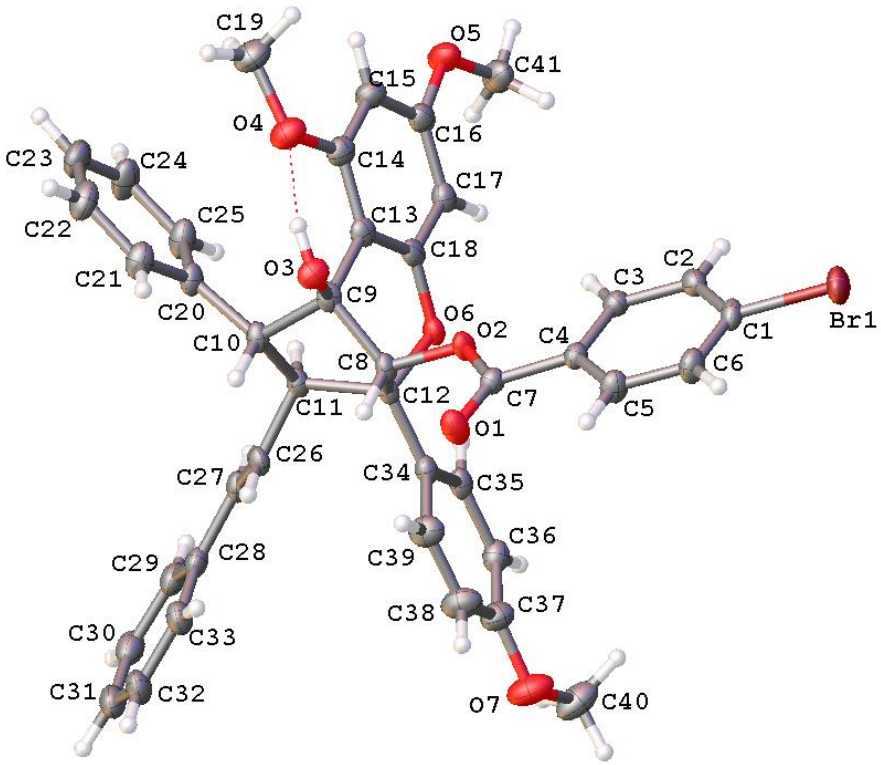

Crystals of compound **14** suitable for X-ray analysis were obtained by slow evaporation from dichloromethane/hexanes. Crystallographic data have been deposited with the Cambridge Cystallograhic Data Centre (CCDC#1523489). Copies of the data can be obtained free of charge on application to the CCDC, 12 Union Road, Cambridge CB21EZ, UK (fax: (+44)-1223-336-033; e-mail: deposit@ccdc.cam.ac.uk).

Computing details

Data collection: APEX2 (Bruker, 2006); cell refinement: SAINT (Bruker, 2006); data reduction: SAINT (Bruker, 2006); program(s) used to solve structure: SHELXS97 (Sheldrick, 1990); program(s) used to refine structure: SHELXL (Sheldrick, 2008); molecular graphics: Olex2 (Dolomanov et al., 2009); software used to prepare material for publication: Olex2 (Dolomanov et al., 2009).

References

Sheldrick, G. M. (1996). SADABS. University of Göttingen, Germany.

Sheldrick, G. M. (1997). SHELXL97. University of Göttingen, Germany.

Bruker (2006). SAINT. Bruker Analytical X-ray Instruments Inc., Madison, Wisconsin, USA.

Bruker (2006). APEX2. Bruker Analytical X-ray Instruments Inc., Madison, Wisconsin, USA.

Dolmanov, O. V., et al. (2009). OLEX2: A complete structure solution, refinement and analysis program. J. Appl. Cryst. 42, 339-341 (2009).

(**Compound 14**)

Crystal data

$C_{41}H_{35}BrO_7$	$F(000)$ = 2976
M_r = 719.60	D_x = 1.411 Mg m^{-3}
Monoclinic, $P2_1/c$	Cu $K\alpha$ radiation, λ = 1.54178 Å
a = 22.603 (2) Å	Cell parameters from 9408 reflections
b = 20.3183 (19) Å	θ = 3.9–66.7°
c = 14.8174 (13) Å	μ = 2.08 mm^{-1}
β = 95.493 (4)°	T = 100 K
V = 6773.6 (11) Å^3	Bar, colorless

$Z = 8$	0.22 × 0.09 × 0.08 mm

Data collection

Bruker Proteum-R diffractometer	11948 independent reflections
Radiation source: rotating anode	10807 reflections with $I > 2\sigma(I)$
Multilayer monochromator	$R_{int} = 0.055$
ϕ & ω scans	$\theta_{max} = 66.8°$, $\theta_{min} = 2.0°$
Absorption correction: multi-scan *SADABS* (Sheldrick, 1997)	$h = -26 \rightarrow 26$
$T_{min} = 0.646$, $T_{max} = 0.753$	$k = -24 \rightarrow 24$
133915 measured reflections	$l = -17 \rightarrow 17$

Refinement

Refinement on F^2	932 restraints
Least-squares matrix: full	Hydrogen site location: inferred from neighbouring sites
$R[F^2 > 2\sigma(F^2)] = 0.055$	H-atom parameters constrained
$wR(F^2) = 0.150$	$w = 1/[\sigma^2(F_o^2) + (0.0923P)^2 + 7.6376P]$ where $P = (F_o^2 + 2F_c^2)/3$
$S = 1.05$	$(\Delta/\sigma)_{max} = 0.002$
11948 reflections	$\Delta\rangle_{max} = 2.89$ e Å^{-3}
891 parameters	$\Delta\rangle_{min} = -0.70$ e Å^{-3}

Special details

Geometry. All esds (except the esd in the dihedral angle between two l.s. planes) are estimated using the full covariance matrix.The cell esds are taken into account individually in the estimation of esds in distances, angles and torsion angles; correlations between esds in cell parameters are only used when they are defined

by crystal symmetry. An approximate (isotropic) treatment of cell esds is used for estimating esds involving l.s. planes.

*Fractional atomic coordinates and isotropic or equivalent isotropic displacement parameters (Å^2) for (compound **14**)*

	x	*y*	*z*	U_{iso}*/U_{eq}
Br1A	0.97710 (2)	0.53306 (2)	-0.20398 (2)	0.04010 (12)
Br1	0.51754 (2)	0.44864 (2)	0.69611 (2)	0.03416 (11)
O2A	0.87551 (7)	0.55160 (9)	0.21092 (11)	0.0232 (4)
O6A	0.95160 (8)	0.55620 (10)	0.35916 (12)	0.0288 (4)
O3A	0.79380 (7)	0.65392 (9)	0.27061 (11)	0.0239 (4)
H3A	0.8002	0.6944	0.2659	0.036*
O4A	0.85823 (8)	0.76389 (10)	0.29108 (13)	0.0318 (4)
O5A	1.07190 (9)	0.74106 (13)	0.35515 (15)	0.0475 (6)
O7A	0.91566 (10)	0.25004 (11)	0.37981 (16)	0.0473 (6)
O1A	0.79113 (9)	0.51226 (13)	0.13760 (14)	0.0430 (5)
O2	0.63002 (7)	0.43773 (8)	0.28899 (11)	0.0214 (4)
O6	0.55489 (7)	0.43391 (8)	0.13652 (11)	0.0205 (3)
O3	0.71734 (8)	0.34668 (9)	0.22227 (12)	0.0259 (4)
H3	0.7165	0.3056	0.2154	0.039*
O4	0.66788 (8)	0.23558 (9)	0.15981 (14)	0.0332 (4)
O5	0.45908 (8)	0.22425 (9)	0.10366 (14)	0.0348 (4)
O7	0.55952 (10)	0.74087 (10)	0.16014 (16)	0.0455 (5)
O1	0.70742 (8)	0.49126 (10)	0.36401 (12)	0.0300 (4)
C1A	0.93542 (12)	0.53365 (14)	-0.09829 (17)	0.0292 (6)
C2A	0.88247 (14)	0.49994 (19)	-0.0993 (2)	0.0434 (8)
H2A	0.8670	0.4769	-0.1521	0.052*
C3A	0.85220 (13)	0.50006 (19)	-0.0225 (2)	0.0440 (8)
H3AA	0.8152	0.4777	-0.0232	0.053*
C4A	0.87541 (11)	0.53266 (13)	0.05584 (17)	0.0253 (5)
C7A	0.84201 (12)	0.53033 (13)	0.13736 (18)	0.0257 (5)

C8A	0.84965 (11)	0.55479 (13)	0.29565 (16)	0.0229 (5)
H8A	0.8115	0.5297	0.2924	0.027*
C12A	0.89412 (11)	0.52826 (14)	0.37171 (17)	0.0263 (6)
C11A	0.87237 (12)	0.56072 (14)	0.46042 (17)	0.0273 (6)
H11A	0.9064	0.5877	0.4882	0.033*
C26A	0.85717 (13)	0.51332 (15)	0.53201 (18)	0.0326 (6)
H26A	0.8827	0.4764	0.5417	0.039*
C27A	0.81306 (12)	0.51653 (14)	0.58286 (18)	0.0306 (6)
H27A	0.7859	0.5520	0.5721	0.037*
C28A	0.80180 (11)	0.46959 (14)	0.65585 (18)	0.0281 (6)
C29A	0.76281 (12)	0.48665 (14)	0.71995 (18)	0.0293 (6)
H29A	0.7436	0.5283	0.7162	0.035*
C30A	0.75187 (12)	0.44329 (15)	0.78920 (18)	0.0328 (6)
H30A	0.7246	0.4551	0.8314	0.039*
C31A	0.78042 (13)	0.38309 (16)	0.7969 (2)	0.0364 (6)
H31A	0.7734	0.3540	0.8449	0.044*
C5A	0.92904 (11)	0.56607 (13)	0.05532 (17)	0.0244 (5)
H5A	0.9452	0.5884	0.1084	0.029*
C6A	0.95912 (12)	0.56712 (14)	-0.02190 (18)	0.0297 (6)
H6A	0.9955	0.5905	-0.0224	0.036*
C18A	0.95274 (11)	0.62277 (15)	0.34670 (16)	0.0285 (6)
C13A	0.90073 (11)	0.66008 (14)	0.32741 (16)	0.0258 (5)
C9A	0.84085 (11)	0.62479 (13)	0.32637 (16)	0.0229 (5)
C10A	0.82361 (11)	0.61011 (13)	0.42431 (16)	0.0241 (5)
H10A	0.7850	0.5857	0.4178	0.029*
C32A	0.81955 (13)	0.36527 (16)	0.7339 (2)	0.0360 (6)
H32A	0.8397	0.3242	0.7393	0.043*
C33A	0.82910 (12)	0.40769 (15)	0.66296 (19)	0.0314 (6)
H33A	0.8545	0.3945	0.6188	0.038*
C20A	0.81465 (12)	0.67072 (14)	0.47981 (16)	0.0266 (5)
C21A	0.86134 (13)	0.71121 (16)	0.51519 (18)	0.0362 (6)

H21A	0.9012	0.6990	0.5080	0.043*
C22A	0.85007 (16)	0.76905 (16)	0.5607 (2)	0.0431 (7)
H22A	0.8821	0.7962	0.5841	0.052*
C23A	0.79223 (16)	0.78704 (16)	0.57198 (19)	0.0429 (8)
H23A	0.7846	0.8265	0.6032	0.051*
C24A	0.74603 (15)	0.74796 (16)	0.5382 (2)	0.0400 (7)
H24A	0.7063	0.7604	0.5461	0.048*
C25A	0.75686 (13)	0.69018 (15)	0.49239 (18)	0.0324 (6)
H25A	0.7244	0.6635	0.4693	0.039*
C14A	0.90889 (11)	0.72741 (15)	0.31388 (17)	0.0283 (6)
C19A	0.86490 (13)	0.82991 (15)	0.2582 (2)	0.0383 (7)
H19A	0.8787	0.8588	0.3089	0.057*
H19B	0.8265	0.8458	0.2300	0.057*
H19C	0.8940	0.8301	0.2133	0.057*
C15A	0.96509 (12)	0.75720 (16)	0.32294 (18)	0.0338 (6)
H15A	0.9692	0.8033	0.3152	0.041*
C16A	1.01493 (12)	0.71736 (17)	0.34367 (18)	0.0365 (7)
C41A	1.07965 (13)	0.8102 (2)	0.3543 (2)	0.0499 (9)
H41A	1.0622	0.8279	0.2963	0.075*
H41B	1.1222	0.8205	0.3623	0.075*
H41C	1.0599	0.8299	0.4038	0.075*
C17A	1.00901 (12)	0.65061 (17)	0.35386 (18)	0.0347 (6)
H17A	1.0432	0.6237	0.3657	0.042*
C34A	0.90172 (12)	0.45486 (15)	0.37292 (17)	0.0287 (6)
C39A	0.95644 (13)	0.42596 (16)	0.40050 (17)	0.0337 (6)
H39A	0.9899	0.4532	0.4170	0.040*
C38A	0.96302 (13)	0.35773 (16)	0.40435 (18)	0.0370 (7)
H38A	1.0006	0.3390	0.4236	0.044*
C37A	0.91483 (14)	0.31731 (16)	0.3802 (2)	0.0379 (7)
C40A	0.97115 (15)	0.21840 (18)	0.4014 (2)	0.0483 (8)
H40A	0.9994	0.2331	0.3594	0.072*

H40B	0.9659	0.1706	0.3962	0.072*
H40C	0.9865	0.2296	0.4636	0.072*
C36A	0.85988 (13)	0.34547 (16)	0.3525 (2)	0.0409 (7)
H36A	0.8266	0.3181	0.3357	0.049*
C35A	0.85365 (12)	0.41311 (16)	0.3494 (2)	0.0364 (7)
H35A	0.8158	0.4316	0.3309	0.044*
C1	0.56037 (12)	0.45366 (13)	0.59212 (18)	0.0254 (5)
C6	0.61621 (12)	0.48257 (14)	0.59970 (18)	0.0299 (6)
H6	0.6326	0.5001	0.6561	0.036*
C5	0.64780 (12)	0.48566 (14)	0.52427 (18)	0.0280 (6)
H5	0.6860	0.5056	0.5288	0.034*
C4	0.62389 (11)	0.45977 (12)	0.44203 (17)	0.0203 (5)
C7	0.65918 (11)	0.46523 (12)	0.36280 (17)	0.0205 (5)
C8	0.65590 (11)	0.44216 (12)	0.20495 (16)	0.0202 (5)
H8	0.6922	0.4705	0.2115	0.024*
C12	0.61051 (11)	0.46915 (12)	0.13144 (16)	0.0200 (5)
C11	0.63722 (11)	0.44790 (12)	0.04082 (16)	0.0206 (5)
H11	0.6057	0.4247	0.0009	0.025*
C26	0.66014 (11)	0.50423 (13)	-0.01067 (17)	0.0242 (5)
H26	0.6955	0.5251	0.0148	0.029*
C27	0.63548 (11)	0.52715 (13)	-0.08810 (17)	0.0251 (5)
H27	0.5995	0.5070	-0.1123	0.030*
C28	0.65858 (12)	0.58148 (13)	-0.14130 (17)	0.0270 (5)
C29	0.62960 (13)	0.59710 (13)	-0.22570 (18)	0.0302 (6)
H29	0.5942	0.5746	-0.2470	0.036*
C30	0.65237 (15)	0.64563 (14)	-0.2790 (2)	0.0375 (7)
H30	0.6330	0.6552	-0.3372	0.045*
C31	0.70264 (14)	0.67977 (15)	-0.2479 (2)	0.0381 (7)
H31	0.7183	0.7124	-0.2849	0.046*
C3	0.56806 (11)	0.43017 (12)	0.43620 (17)	0.0223 (5)
H3B	0.5518	0.4120	0.3802	0.027*

C2	0.53612 (11)	0.42692 (12)	0.51107 (18)	0.0254 (5)
H2	0.4981	0.4066	0.5069	0.030*
C18	0.55909 (11)	0.36621 (12)	0.13964 (15)	0.0217 (5)
C13	0.61362 (11)	0.33457 (13)	0.15492 (16)	0.0229 (5)
C9	0.67001 (11)	0.37548 (12)	0.16646 (16)	0.0215 (5)
C10	0.68705 (10)	0.39772 (13)	0.07198 (16)	0.0215 (5)
H10	0.7250	0.4230	0.0823	0.026*
C32	0.73053 (14)	0.66647 (15)	-0.1625 (2)	0.0374 (7)
H32	0.7645	0.6911	-0.1400	0.045*
C33	0.70884 (13)	0.61737 (14)	-0.11013 (19)	0.0336 (6)
H33	0.7285	0.6080	-0.0520	0.040*
C20	0.69847 (11)	0.34031 (13)	0.01135 (17)	0.0249 (5)
C25	0.65643 (12)	0.31261 (15)	-0.05128 (19)	0.0332 (6)
H25	0.6188	0.3332	-0.0637	0.040*
C24	0.66873 (13)	0.25466 (16)	-0.0964 (2)	0.0390 (7)
H24	0.6395	0.2364	-0.1395	0.047*
C23	0.72293 (14)	0.22360 (15)	-0.0789 (2)	0.0373 (7)
H23	0.7305	0.1832	-0.1080	0.045*
C22	0.76610 (14)	0.25189 (16)	-0.0187 (2)	0.0376 (7)
H22	0.8039	0.2315	-0.0073	0.045*
C21	0.75418 (12)	0.31008 (15)	0.02508 (19)	0.0312 (6)
H21	0.7844	0.3298	0.0652	0.037*
C14	0.61349 (12)	0.26527 (13)	0.15020 (17)	0.0269 (5)
C19	0.66994 (14)	0.16698 (14)	0.1368 (2)	0.0382 (7)
H19D	0.6513	0.1411	0.1821	0.057*
H19E	0.7114	0.1532	0.1358	0.057*
H19F	0.6486	0.1599	0.0769	0.057*
C15	0.56102 (12)	0.23043 (13)	0.13503 (18)	0.0292 (6)
H15	0.5616	0.1837	0.1338	0.035*
C16	0.50743 (12)	0.26422 (13)	0.12160 (17)	0.0277 (6)
C41	0.40269 (12)	0.25516 (15)	0.0917 (2)	0.0392 (7)

H41D	0.3967	0.2815	0.1454	0.059*
H41E	0.3716	0.2216	0.0830	0.059*
H41F	0.4008	0.2838	0.0383	0.059*
C17	0.50532 (11)	0.33243 (13)	0.12380 (16)	0.0238 (5)
H17	0.4686	0.3553	0.1148	0.029*
C34	0.59630 (11)	0.54114 (12)	0.13893 (17)	0.0221 (5)
C39	0.63764 (12)	0.58551 (14)	0.1799 (2)	0.0322 (6)
H39	0.6756	0.5701	0.2037	0.039*
C38	0.62410 (13)	0.65139 (14)	0.1862 (2)	0.0379 (7)
H38	0.6526	0.6809	0.2149	0.046*
C37	0.56861 (13)	0.67483 (13)	0.15044 (19)	0.0329 (6)
C40	0.50080 (15)	0.76470 (16)	0.1374 (2)	0.0454 (8)
H40D	0.4907	0.7611	0.0718	0.068*
H40E	0.4985	0.8109	0.1558	0.068*
H40F	0.4728	0.7385	0.1690	0.068*
C36	0.52761 (12)	0.63166 (13)	0.10826 (17)	0.0269 (5)
H36	0.4900	0.6472	0.0828	0.032*
C35	0.54172 (11)	0.56536 (13)	0.10331 (16)	0.0230 (5)
H35	0.5132	0.5358	0.0748	0.028*

Selected NMR Spectra

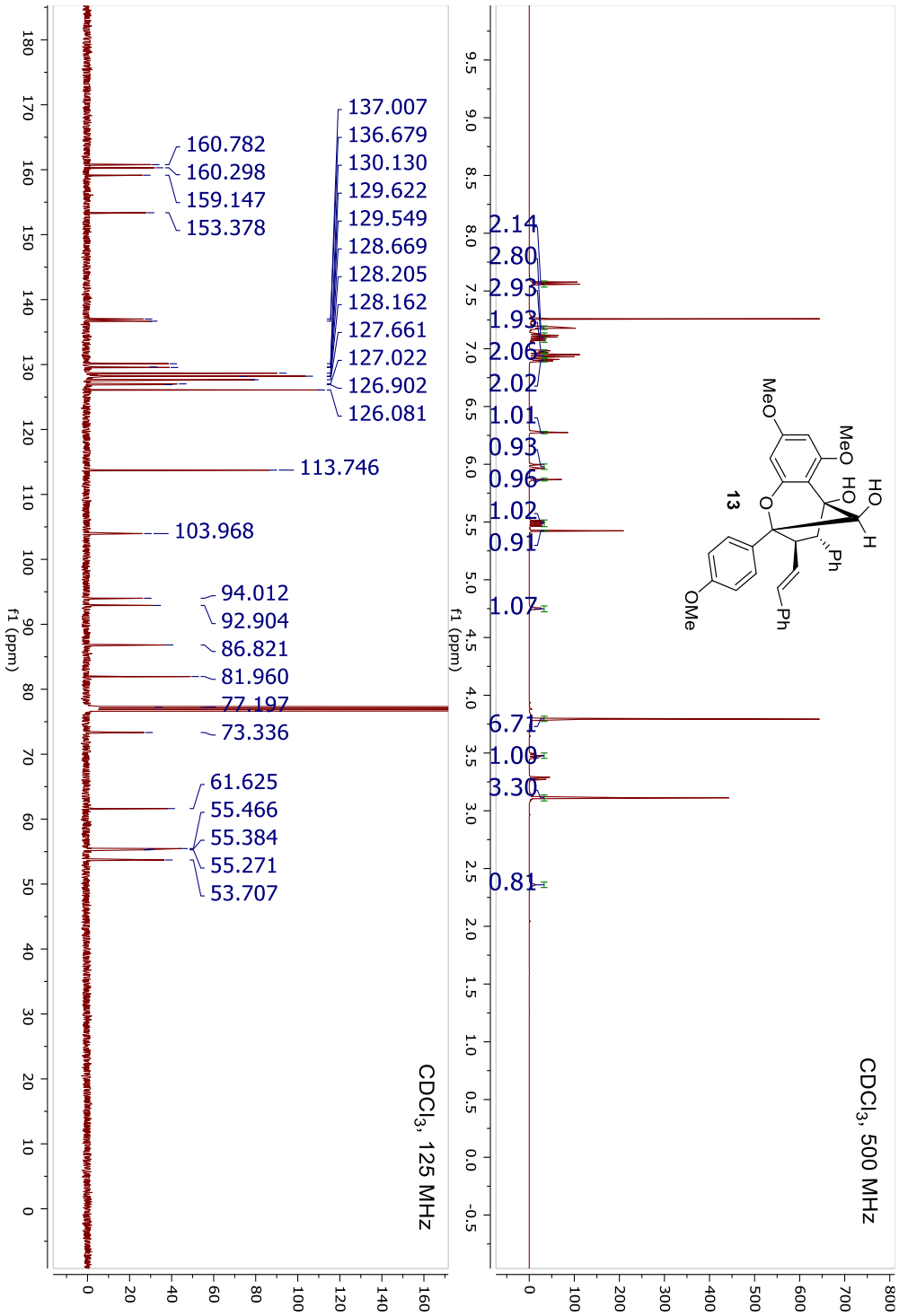

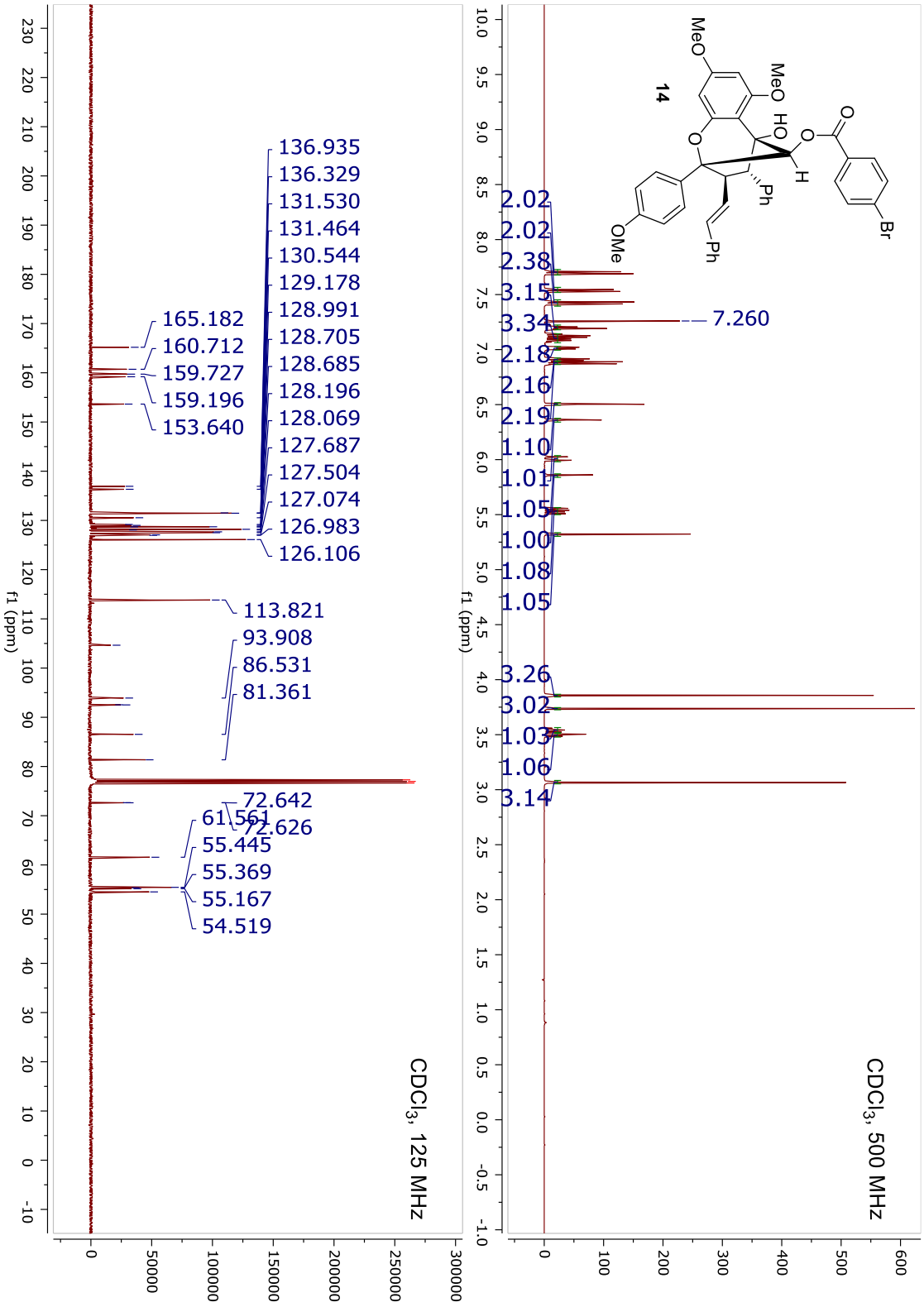
14
MeO
MeO
HO
O
O
H
Ph
Ph
OMe
Br
2.02
2.02
2.38
3.15
3.34
2.18
2.16
2.19
1.10
1.01
1.05
1.00
1.08
1.05
3.26
3.02
1.03
1.06
3.14
7.260
CDCl3, 500 MHz
f1 (ppm)
136.935
136.329
131.530
131.464
130.544
129.178
128.991
128.705
128.685
128.196
128.069
127.687
127.504
127.074
126.983
126.106
165.182
160.712
159.727
159.196
153.640
113.821
93.908
86.531
81.361
72.642
72.626
61.561
55.445
55.369
55.167
54.519
CDCl3, 125 MHz
f1 (ppm)

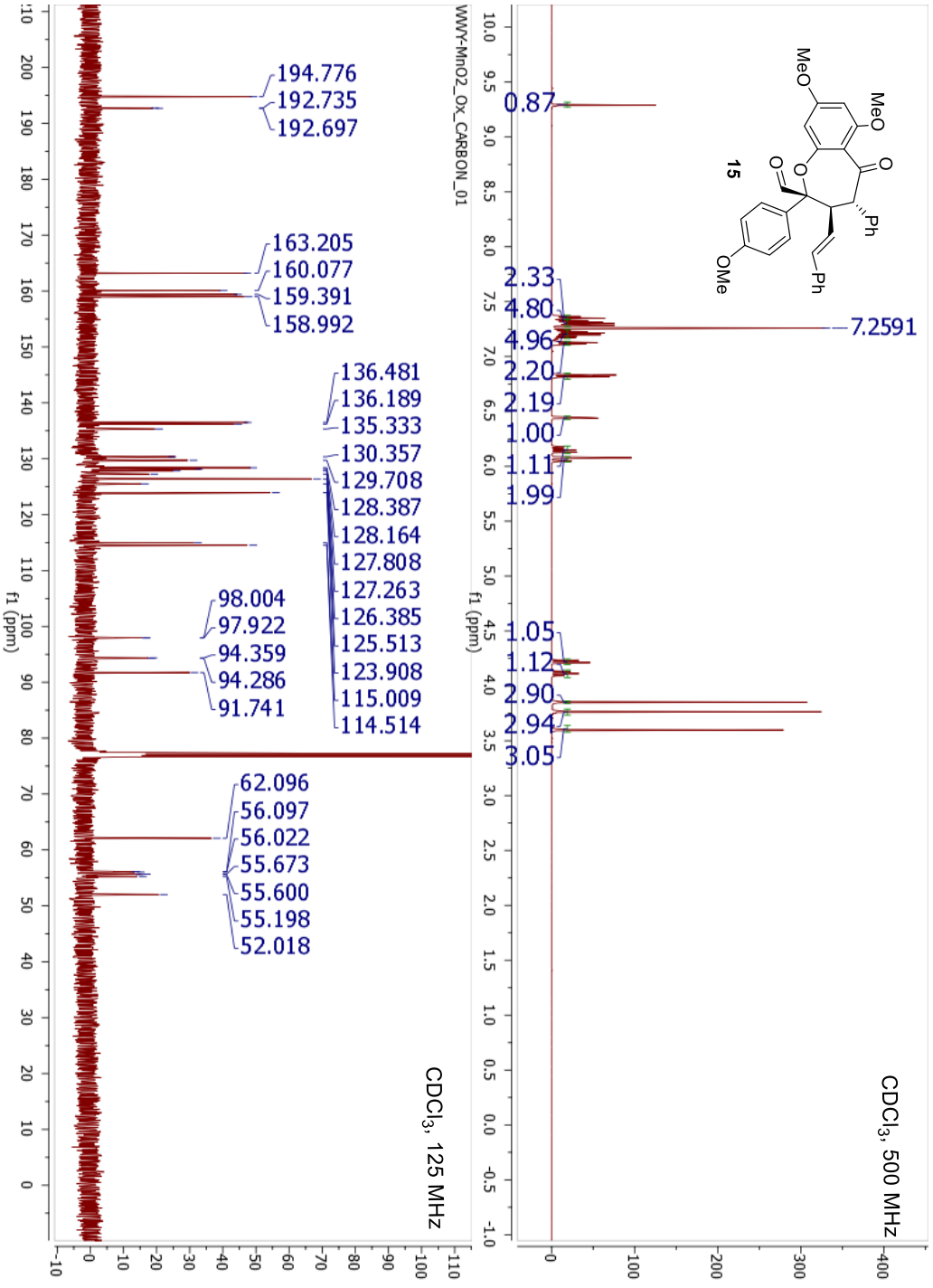
WWY-MnO2_Ox_CARBON_01
194.776
192.735
192.697
163.205
160.077
159.391
158.992
136.481
136.189
135.333
130.357
129.708
128.387
128.164
127.808
127.263
126.385
125.513
123.908
115.009
114.514
98.004
97.922
94.359
94.286
91.741
62.096
56.097
56.022
55.673
55.600
55.198
52.018
CDCl3, 125 MHz
f1 (ppm)
MeO
MeO
O
O
O
O
Ph
Ph
OMe
15
0.87
2.33
4.80
4.96
2.20
2.19
1.00
1.11
1.99
7.2591
1.05
1.12
2.90
2.94
3.05
CDCl3, 500 MHz
f1 (ppm)

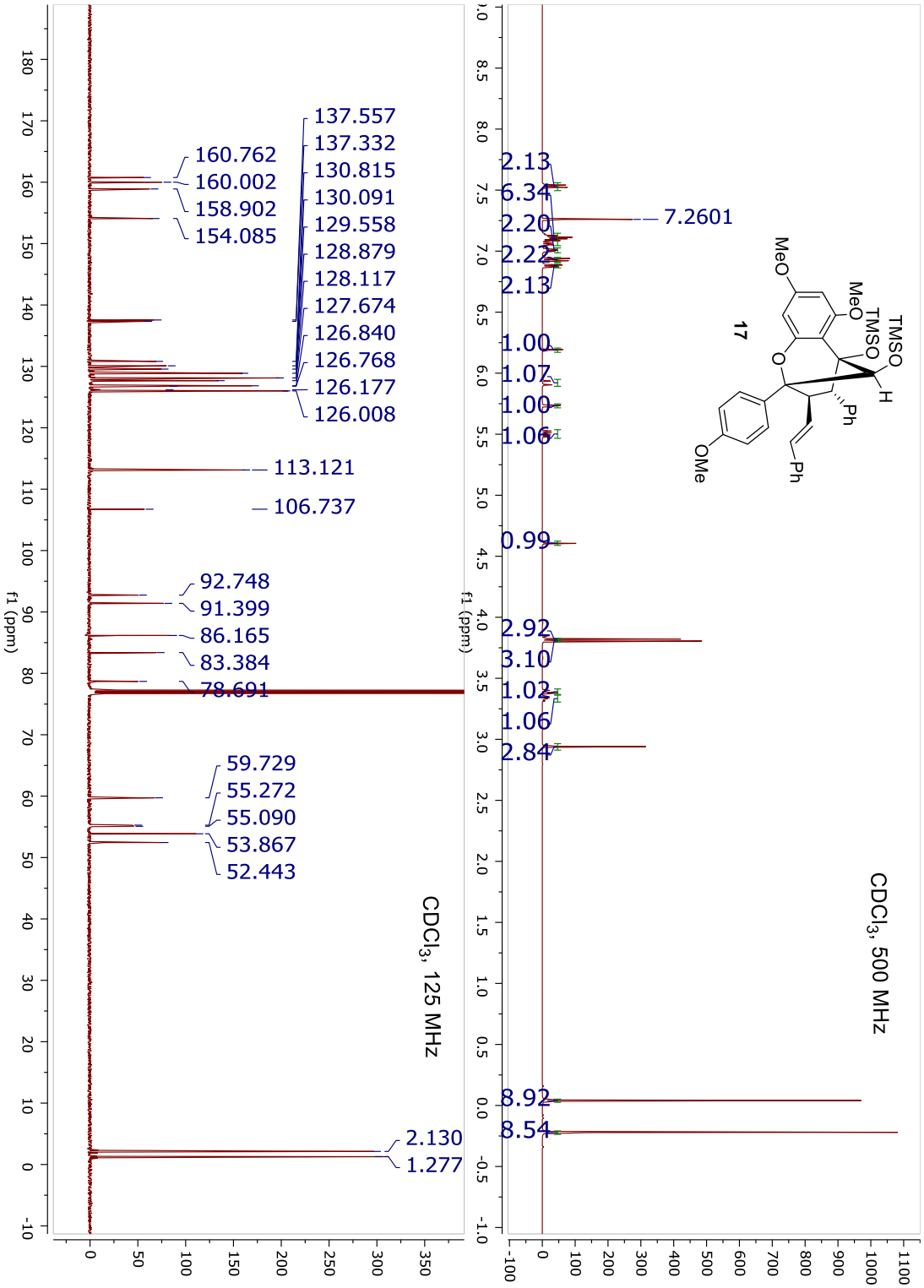
17
MeO
MeO
TMSO
H
O
Ph
Ph
OMe
CDCl3, 500 MHz
CDCl3, 125 MHz
f1 (ppm)
7.2601
2.13
6.34
2.20
2.22
2.13
1.00
1.07
1.00
1.06
0.99
2.92
3.10
1.02
1.06
2.84
8.92
8.54
137.557
137.332
130.815
130.091
129.558
128.879
128.117
127.674
126.840
126.768
126.177
126.008
160.762
160.002
158.902
154.085
113.121
106.737
92.748
91.399
86.165
83.384
78.691
59.729
55.272
55.090
53.867
52.443
2.130
1.277

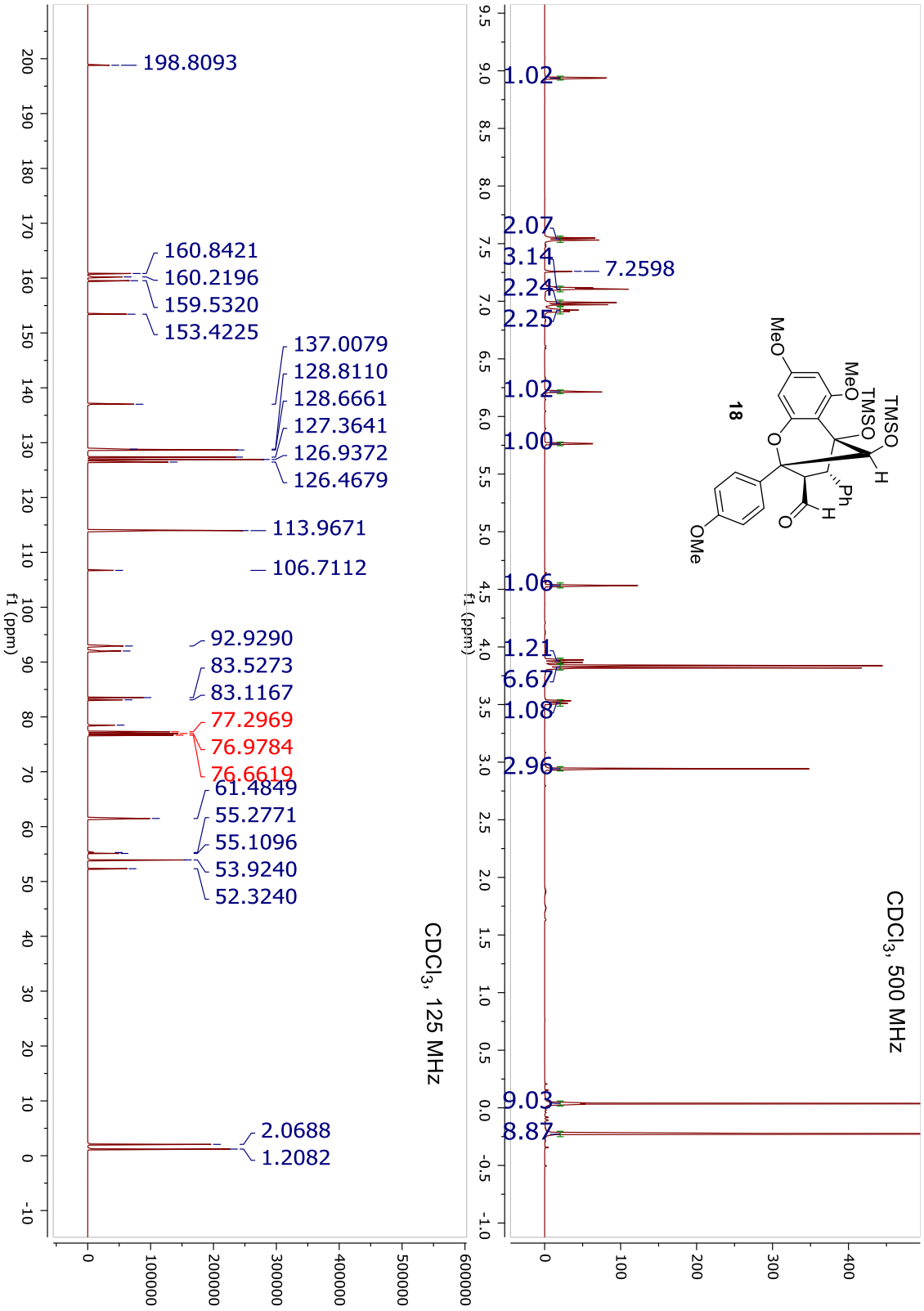
198.8093
160.8421
160.2196
159.5320
153.4225
137.0079
128.8110
128.6661
127.3641
126.9372
126.4679
113.9671
106.7112
92.9290
83.5273
83.1167
77.2969
76.9784
76.6619
61.4849
55.2771
55.1096
53.9240
52.3240
2.0688
1.2082
f1 (ppm)
CDCl3, 125 MHz
1.02
2.07
3.14
7.2598
2.24
2.25
1.02
1.00
1.06
1.21
6.67
1.08
2.96
9.03
8.87
f1 (ppm)
CDCl3, 500 MHz
18
MeO
MeO
TMSO
H
Ph
H
O
OMe

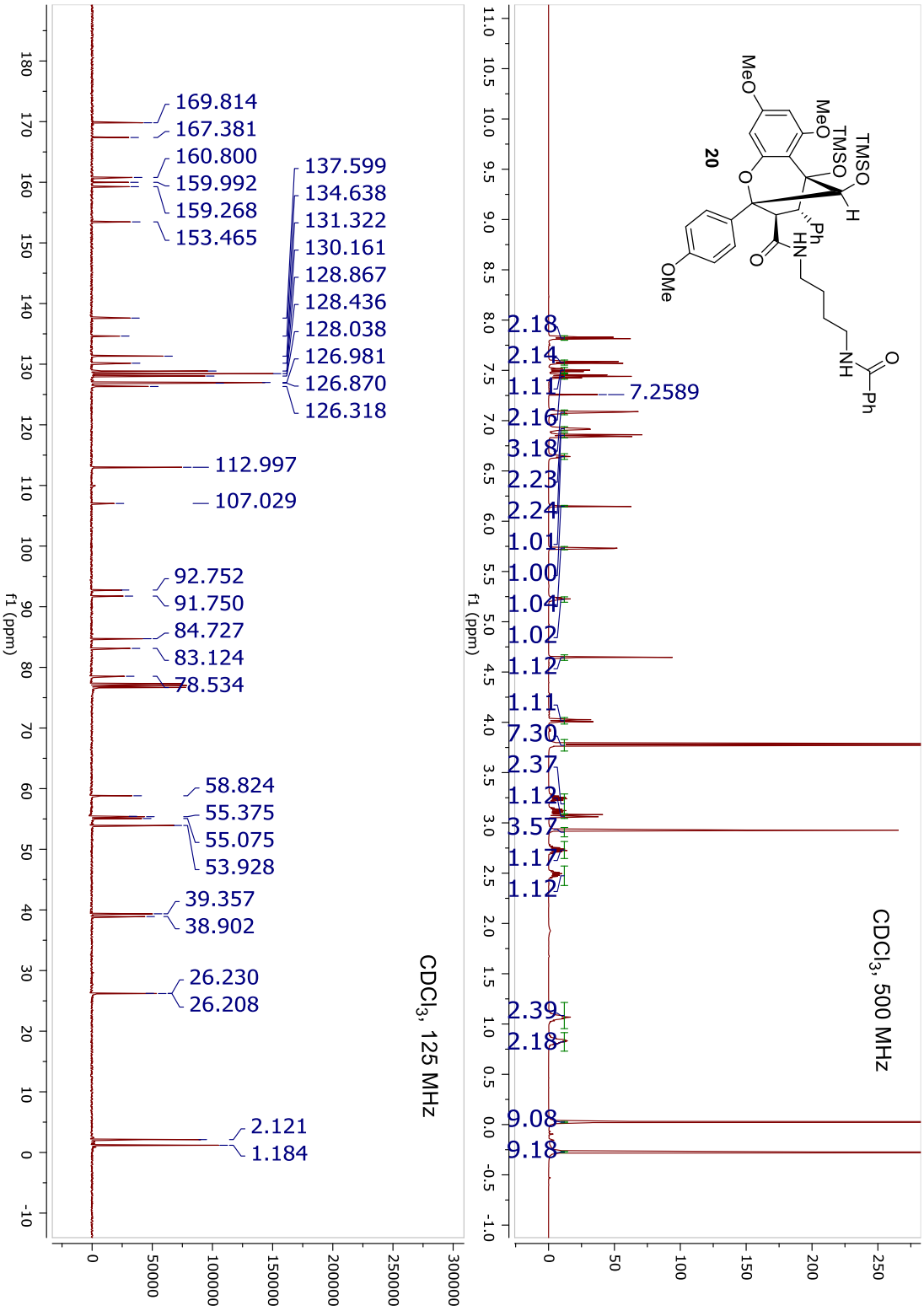
20
MeO
MeO
TMSO
TMSO
H
Ph
HN
O
OMe
NH
O
Ph
2.18
2.14
1.11
7.2589
2.16
3.18
2.23
2.24
1.01
1.00
1.04
1.02
1.12
1.11
7.30
2.37
1.12
3.57
1.17
1.12
2.39
2.18
9.08
9.18
CDCl3, 500 MHz
f1 (ppm)
169.814
167.381
160.800
159.992
159.268
153.465
137.599
134.638
131.322
130.161
128.867
128.436
128.038
126.981
126.870
126.318
112.997
107.029
92.752
91.750
84.727
83.124
78.534
58.824
55.375
55.075
53.928
39.357
38.902
26.230
26.208
2.121
1.184
CDCl3, 125 MHz
f1 (ppm)

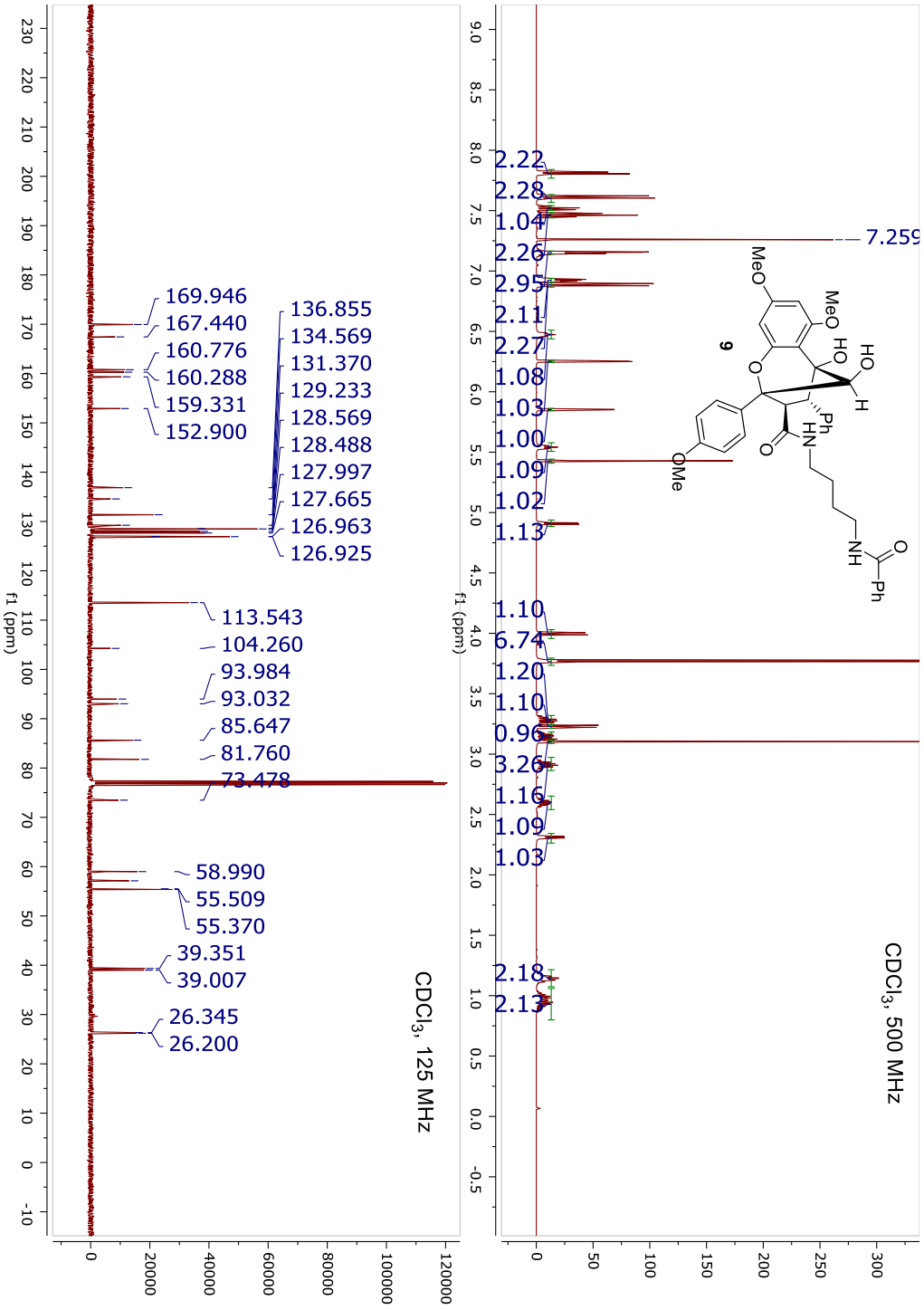
169.946
167.440
160.776
160.288
159.331
152.900
136.855
134.569
131.370
129.233
128.569
128.488
127.997
127.665
126.963
126.925
113.543
104.260
93.984
93.032
85.647
81.760
73.478
58.990
55.509
55.370
39.351
39.007
26.345
26.200
CDCl3, 125 MHz
f1 (ppm)
2.22
2.28
1.04
7.259
2.26
2.95
2.11
2.27
1.08
1.03
1.00
1.09
1.02
1.13
1.10
6.74
1.20
1.10
0.96
3.26
1.16
1.09
1.03
2.18
2.13
CDCl3, 500 MHz
f1 (ppm)
MeO
MeO
HO
HO
H
O
9
Ph
HN
O
OMe
NH
O
Ph

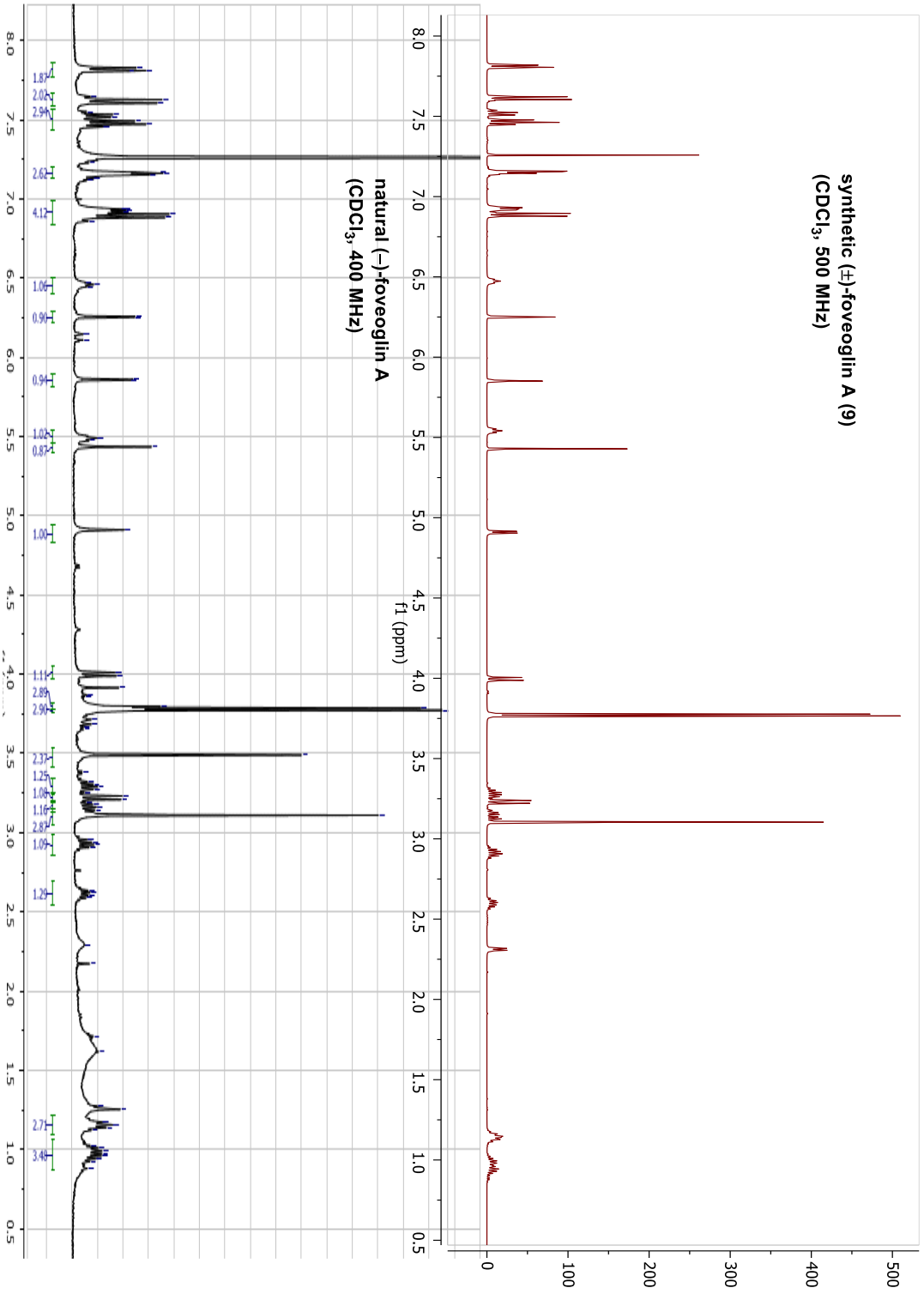
synthetic (±)-foveoglin A (9)
(CDCl3, 500 MHz)
natural (–)-foveoglin A
(CDCl3, 400 MHz)
f1 (ppm)

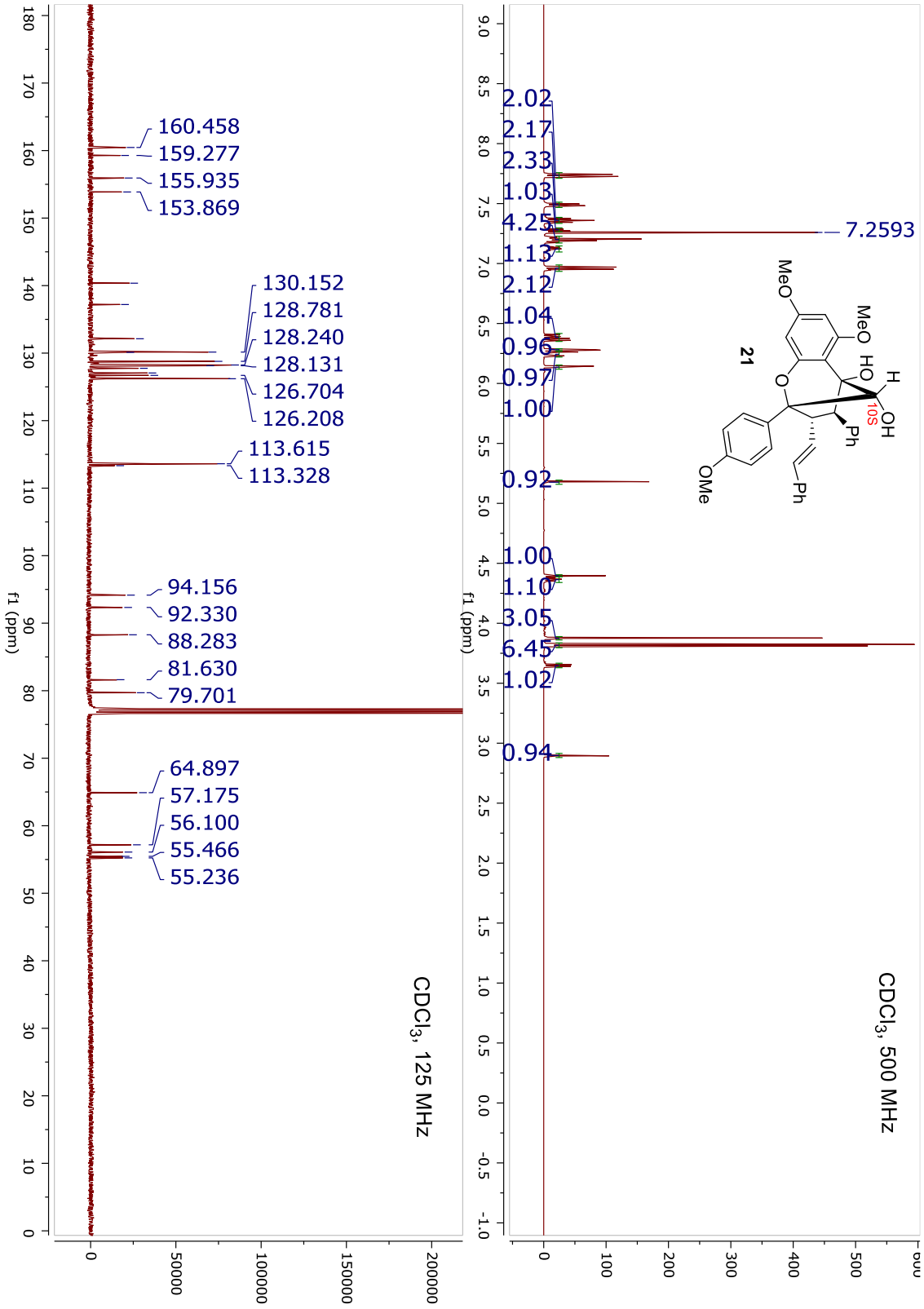
CDCl3, 500 MHz
CDCl3, 125 MHz
f1 (ppm)
7.2593
2.02
2.17
2.33
1.03
4.25
1.13
2.12
1.04
0.96
0.97
1.00
0.92
1.00
1.10
3.05
6.45
1.02
0.94
160.458
159.277
155.935
153.869
130.152
128.781
128.240
128.131
126.704
126.208
113.615
113.328
94.156
92.330
88.283
81.630
79.701
64.897
57.175
56.100
55.466
55.236
21
MeO
MeO
HO
H
OH
10S
Ph
Ph
OMe

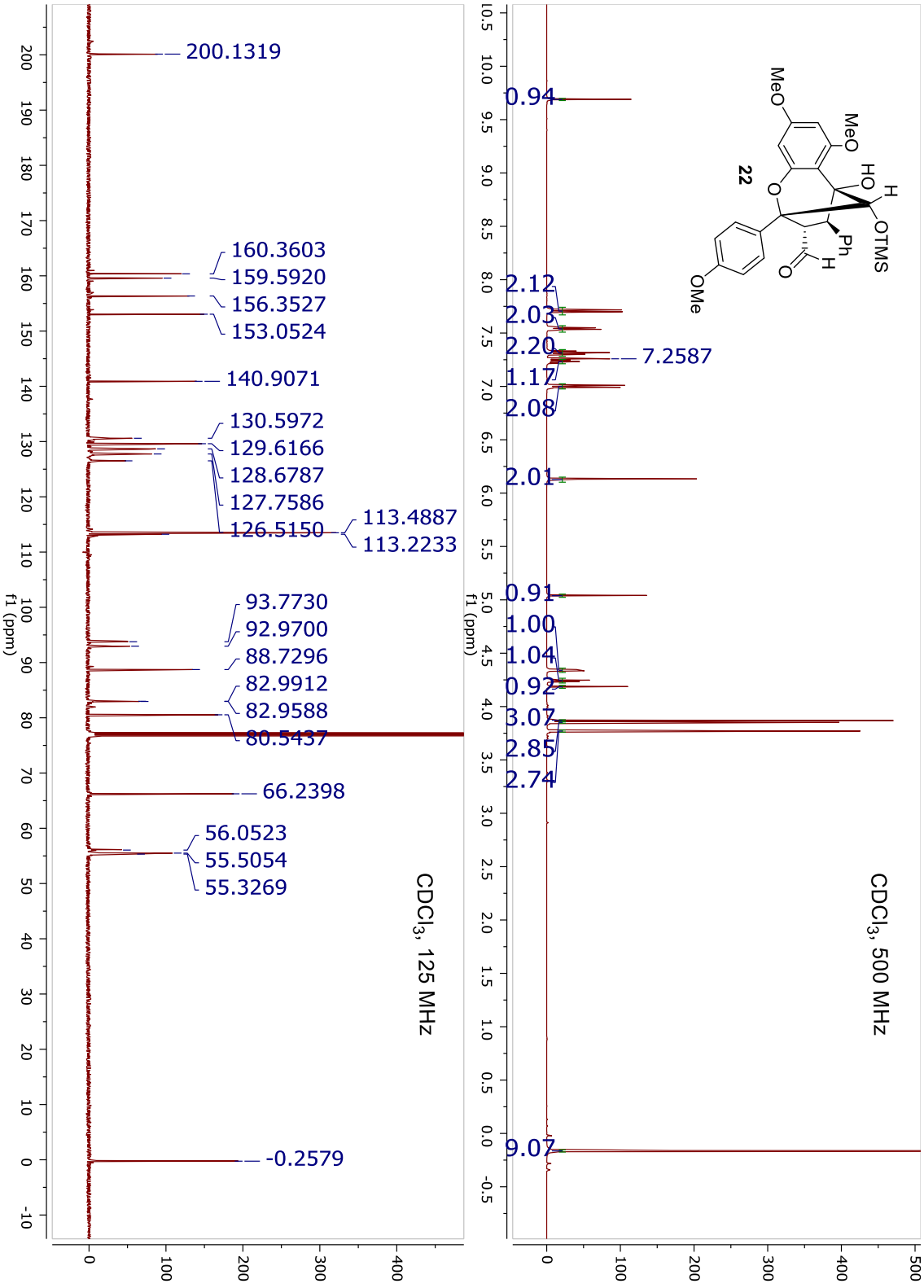
22
MeO
MeO
HO
H
OTMS
O
Ph
H
O
OMe
0.94
2.12
2.03
2.20
1.17
2.08
2.01
0.91
1.00
1.04
0.92
3.07
2.85
2.74
9.07
7.2587
CDCl3, 500 MHz
f1 (ppm)
200.1319
160.3603
159.5920
156.3527
153.0524
140.9071
130.5972
129.6166
128.6787
127.7586
126.5150
113.4887
113.2233
93.7730
92.9700
88.7296
82.9912
82.9588
80.5437
66.2398
56.0523
55.5054
55.3269
-0.2579
CDCl3, 125 MHz
f1 (ppm)

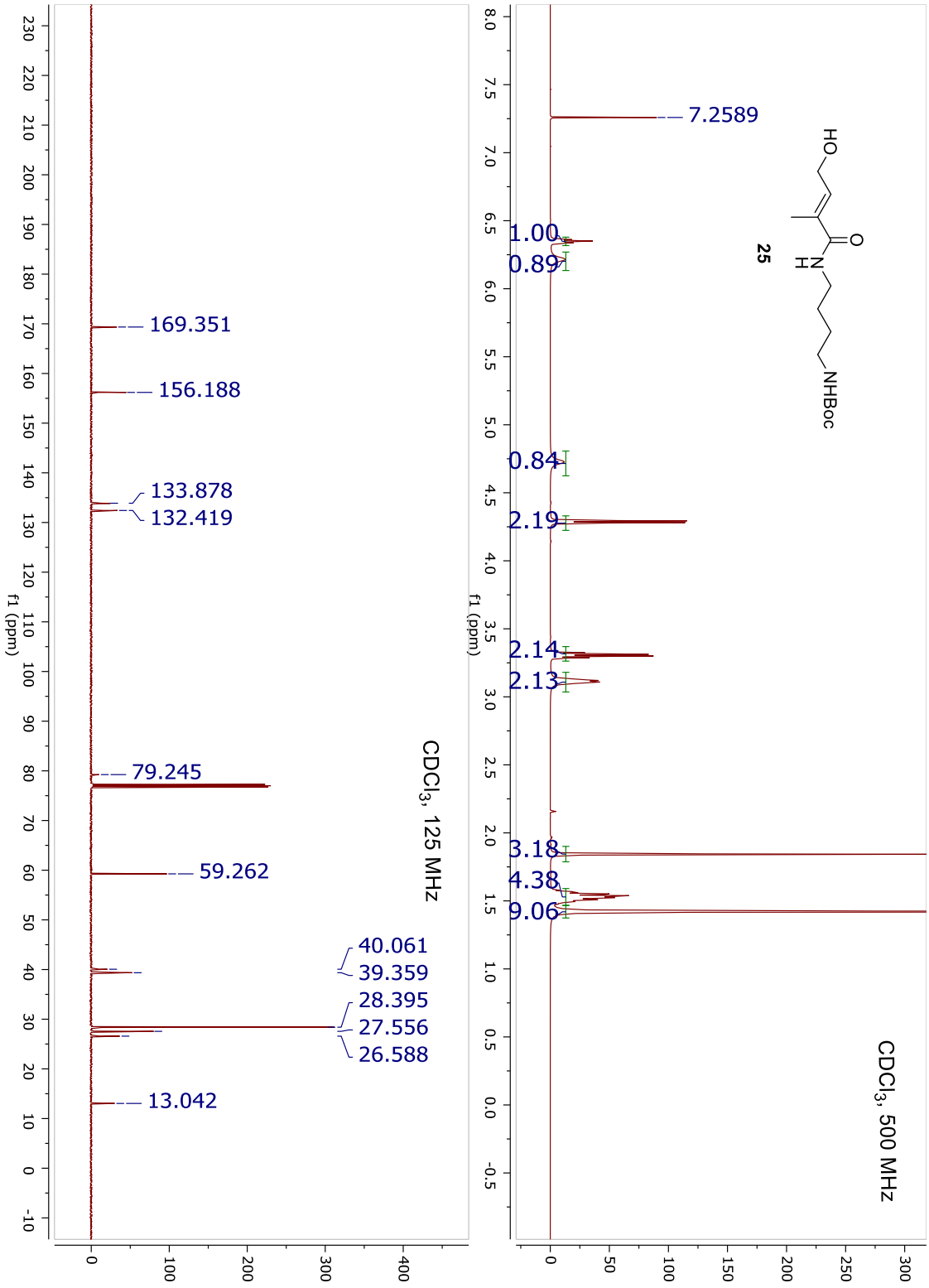
7.2589
1.00
0.89
0.84
2.19
2.14
2.13
3.18
4.38
9.06
HO
O
N
H
NHBoc
25
CDCl3, 500 MHz
f1 (ppm)
169.351
156.188
133.878
132.419
79.245
59.262
40.061
39.359
28.395
27.556
26.588
13.042
CDCl3, 125 MHz
f1 (ppm)

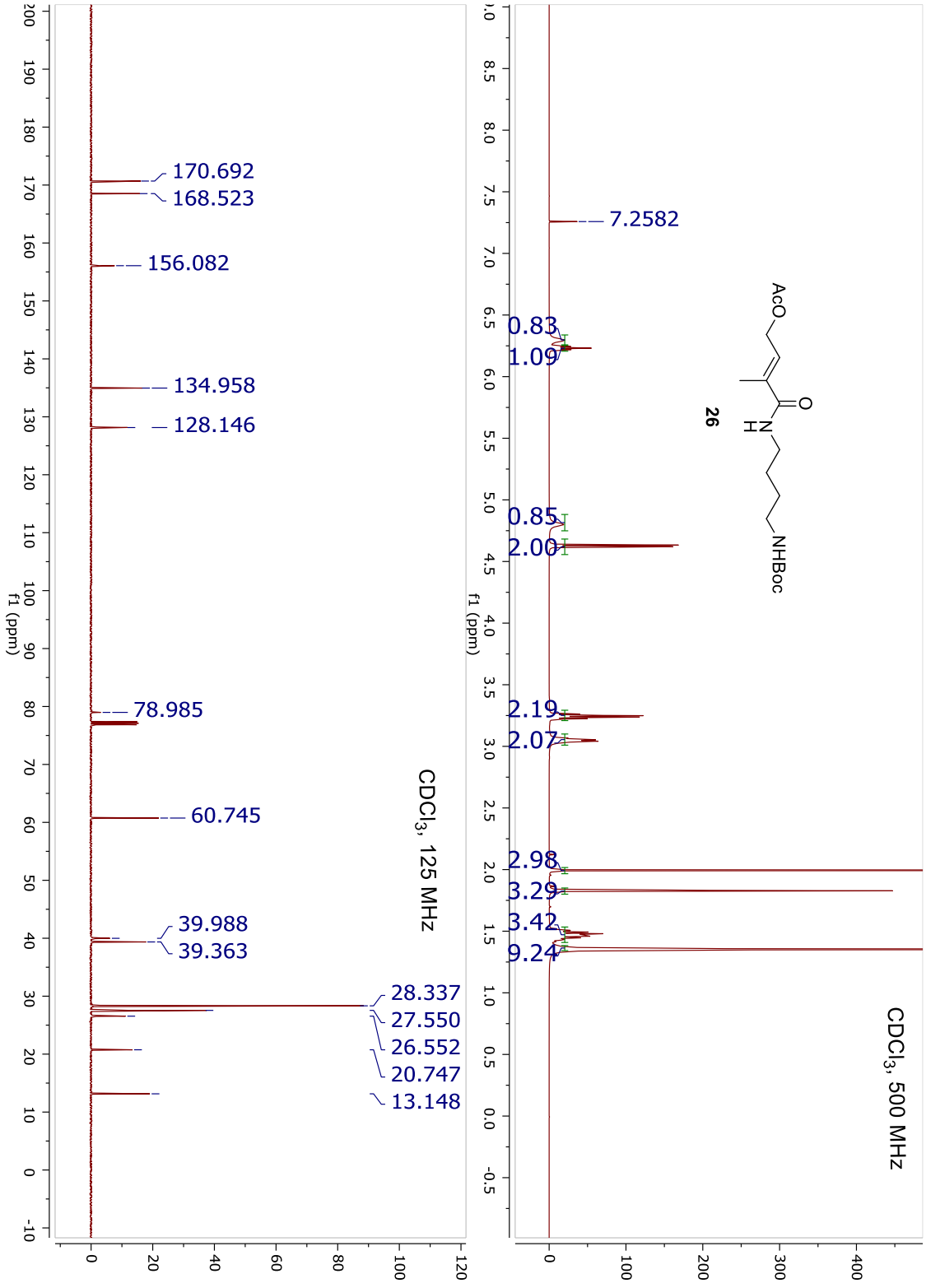
170.692
168.523
156.082
134.958
128.146
78.985
60.745
39.988
39.363
28.337
27.550
26.552
20.747
13.148
CDCl3, 125 MHz
f1 (ppm)
7.2582
0.83
1.09
0.85
2.00
2.19
2.07
2.98
3.29
3.42
9.24
CDCl3, 500 MHz
AcO
O
N
H
NHBoc
26

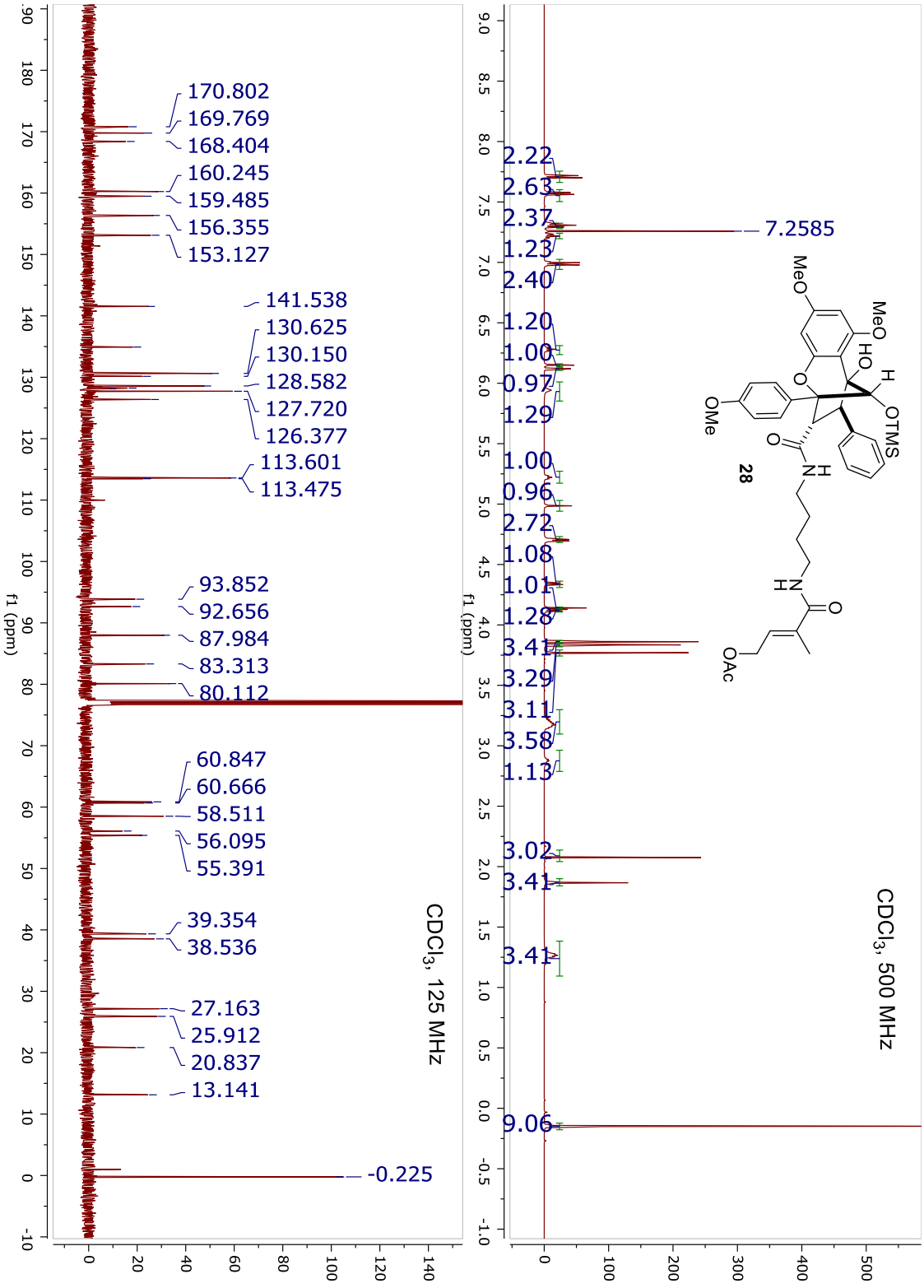
CDCl3, 500 MHz
7.2585
2.22
2.63
2.37
1.23
2.40
1.20
1.00
0.97
1.29
1.00
0.96
2.72
1.08
1.01
1.28
3.41
3.29
3.11
3.58
1.13
3.02
3.41
3.41
9.06
MeO
MeO
HO
H
OTMS
OMe
O
O
N
H
28
N
H
O
OAc
f1 (ppm)
CDCl3, 125 MHz
170.802
169.769
168.404
160.245
159.485
156.355
153.127
141.538
130.625
130.150
128.582
127.720
126.377
113.601
113.475
93.852
92.656
87.984
83.313
80.112
60.847
60.666
58.511
56.095
55.391
39.354
38.536
27.163
25.912
20.837
13.141
-0.225
f1 (ppm)

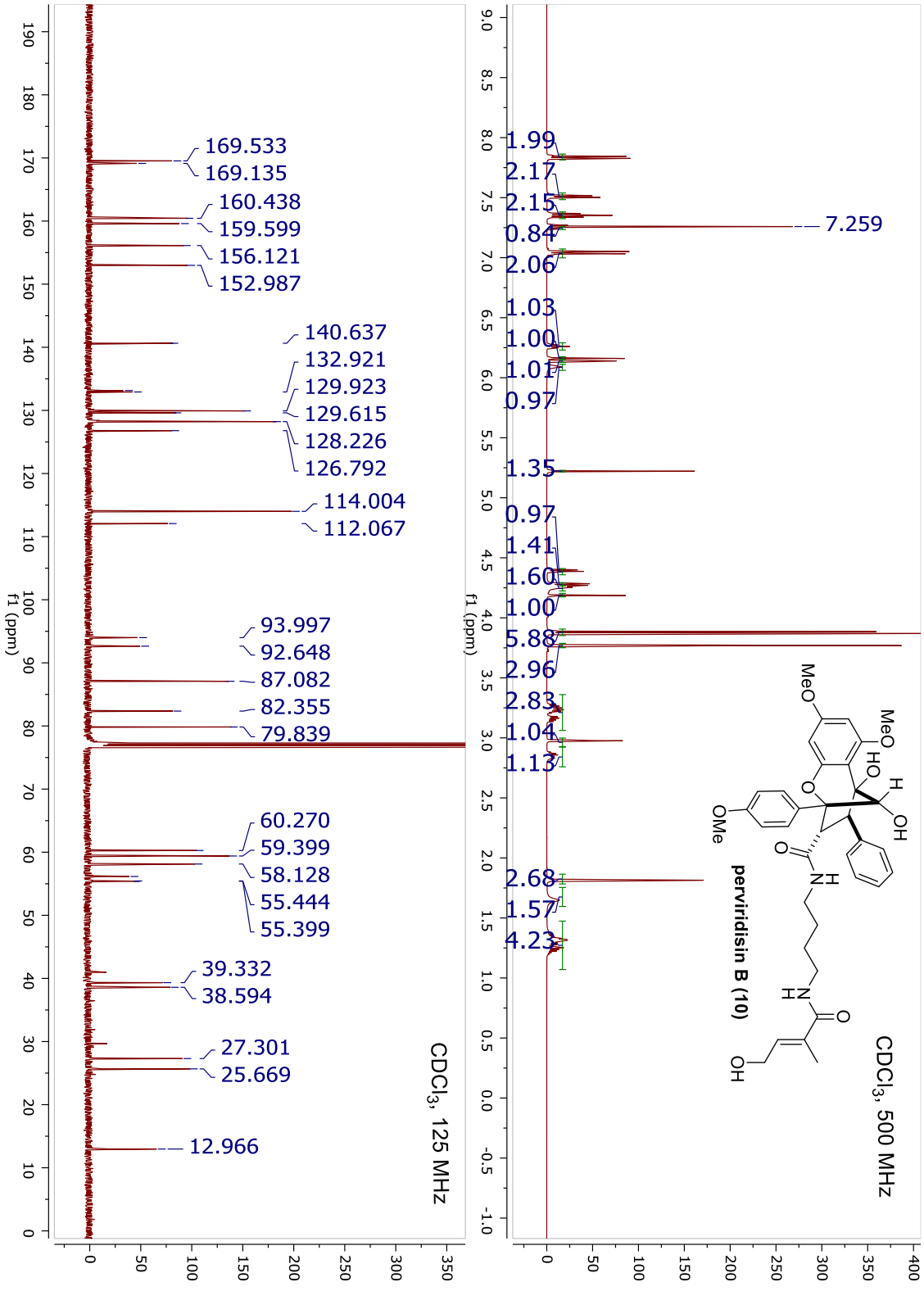
1.99
2.17
2.15
0.84
2.06
1.03
1.00
1.01
0.97
1.35
0.97
1.41
1.60
1.00
5.88
2.96
2.83
1.04
1.13
2.68
1.57
4.23
7.259
CDCl3, 500 MHz
f1 (ppm)
perviridisin B (10)
MeO
MeO
HO
H
OH
O
OMe
O
N
H
N
H
O
OH
169.533
169.135
160.438
159.599
156.121
152.987
140.637
132.921
129.923
129.615
128.226
126.792
114.004
112.067
93.997
92.648
87.082
82.355
79.839
60.270
59.399
58.128
55.444
55.399
39.332
38.594
27.301
25.669
12.966
CDCl3, 125 MHz
f1 (ppm)

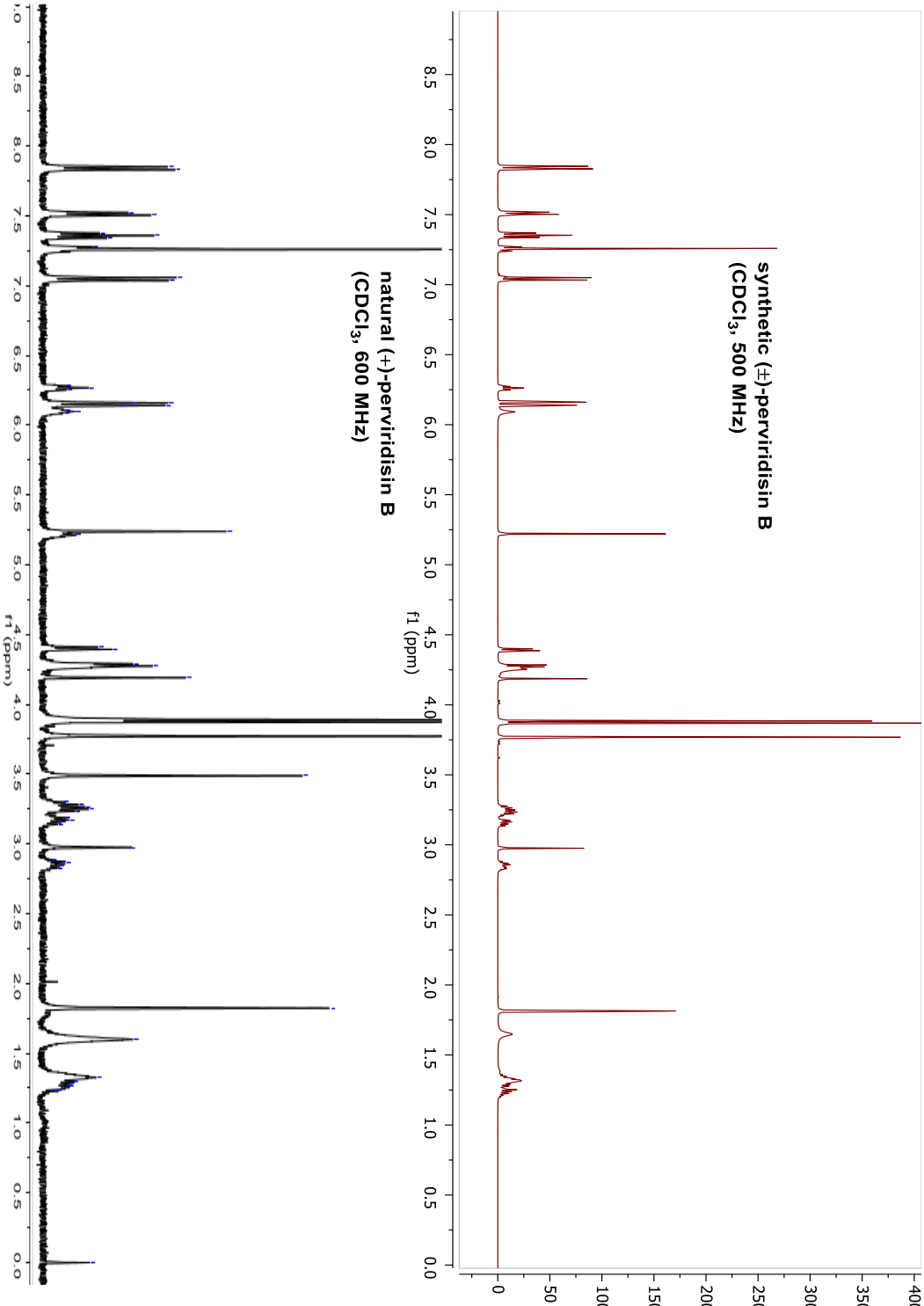
synthetic (±)-perviridisin B
(CDCl3, 500 MHz)
natural (+)-perviridisin B
(CDCl3, 600 MHz)
f1 (ppm)

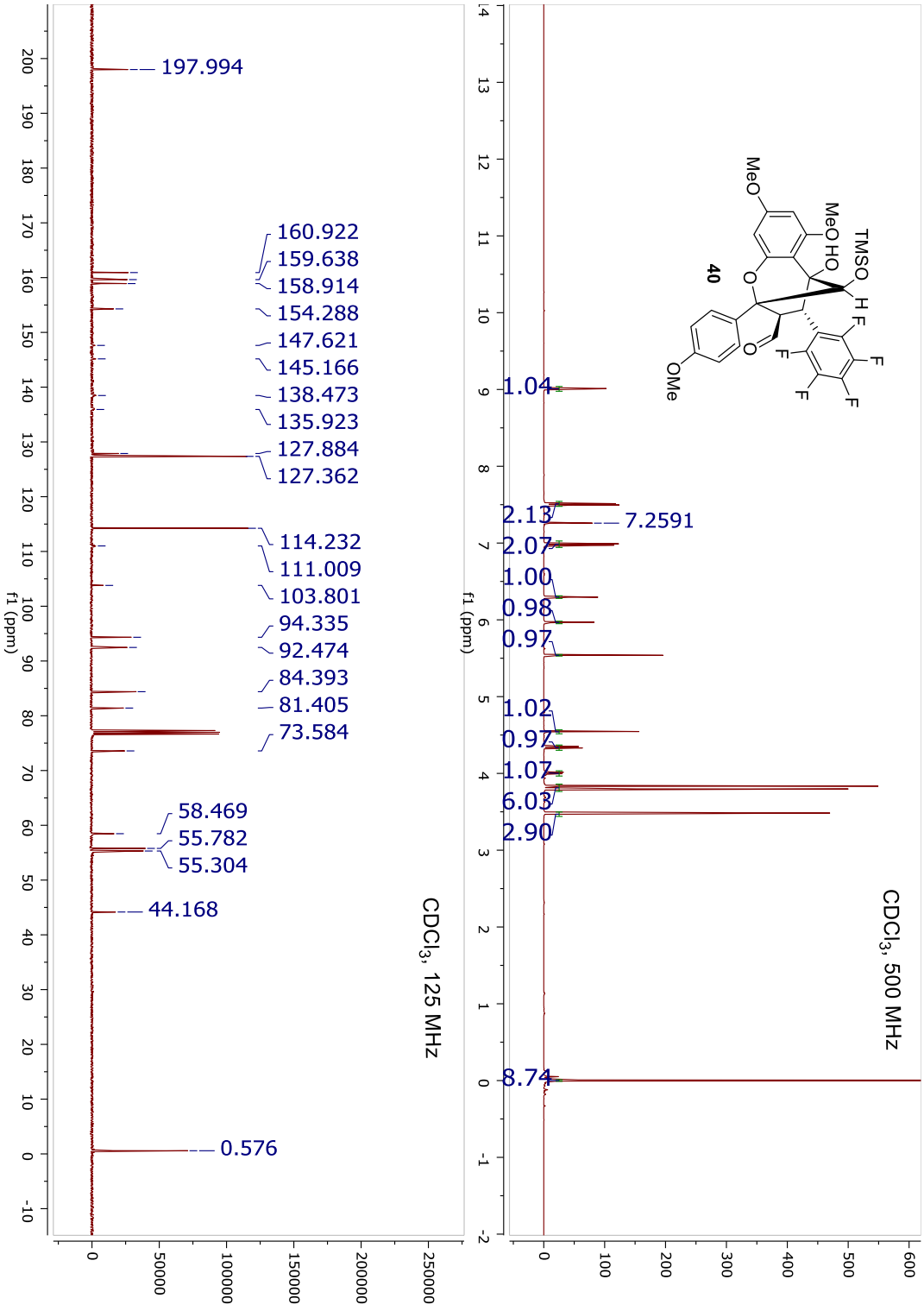
197.994
160.922
159.638
158.914
154.288
147.621
145.166
138.473
135.923
127.884
127.362
114.232
111.009
103.801
94.335
92.474
84.393
81.405
73.584
58.469
55.782
55.304
44.168
0.576
CDCl3, 125 MHz
f1 (ppm)
1.04
2.13
7.2591
2.07
1.00
0.98
0.97
1.02
0.97
1.07
6.03
2.90
8.74
CDCl3, 500 MHz
f1 (ppm)
MeO
MeO
HO
TMSO
H
F
F
F
F
F
O
O
OMe
40

^{19}F NMR of **40**, $CDCl_3$, 375 MHz.

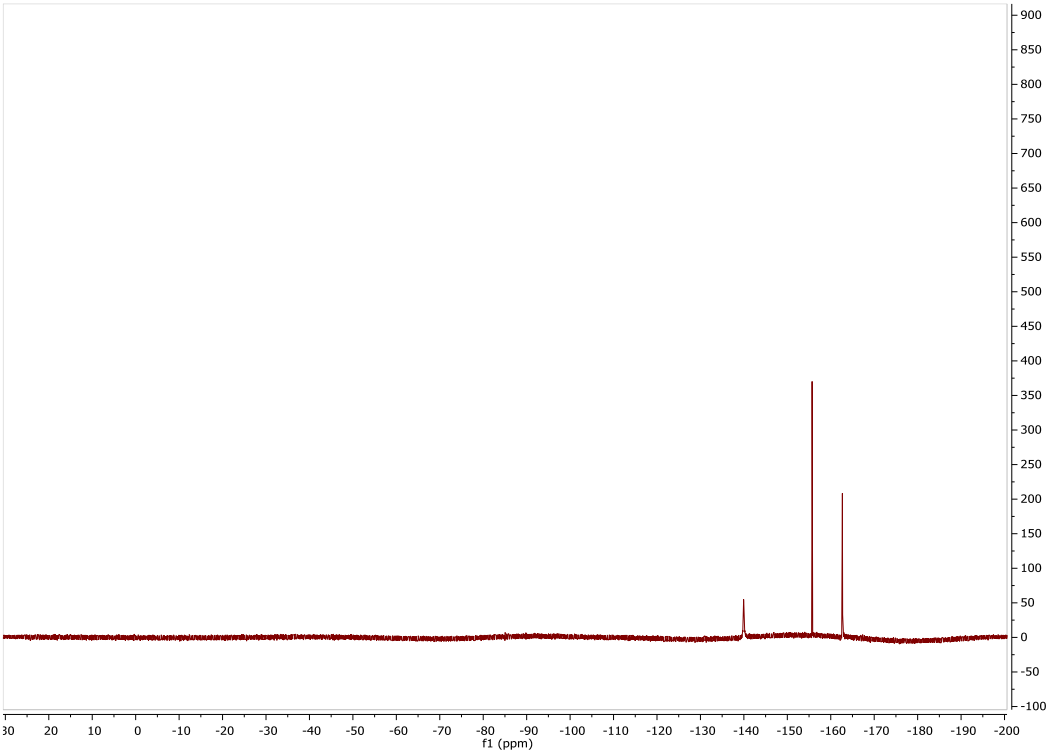

HSQC

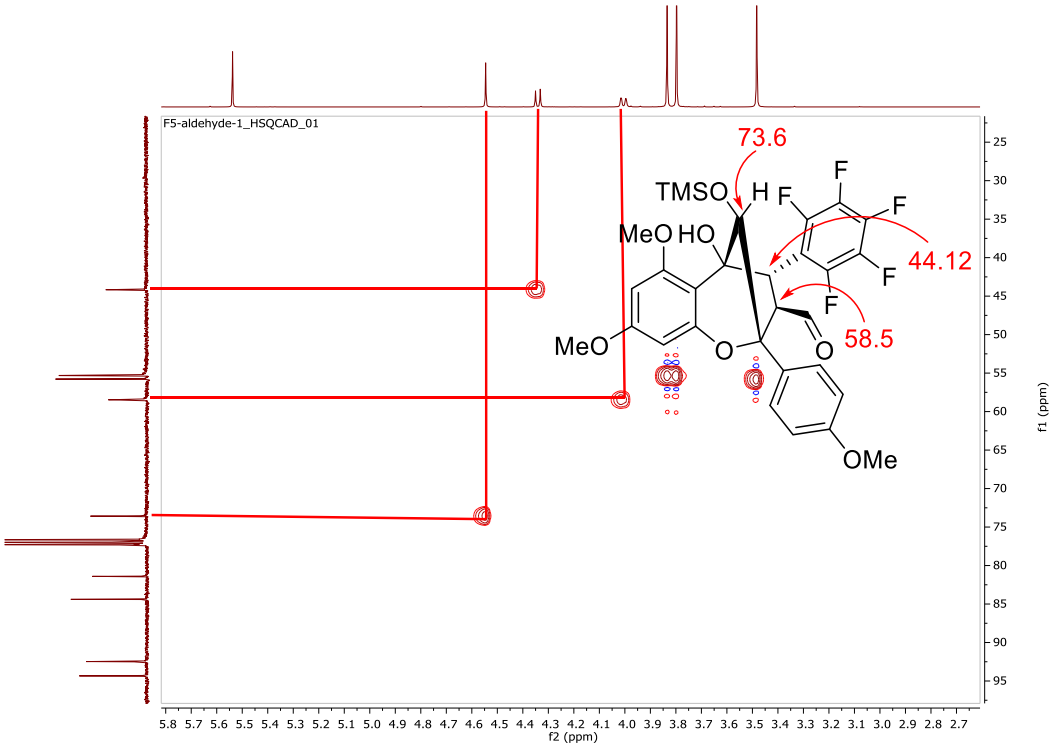

HMBC

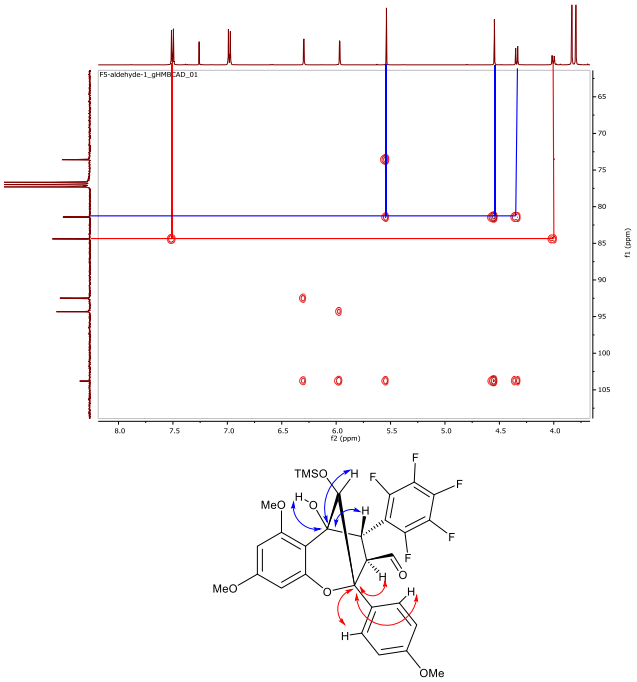
F5-aldehyde-1_gHMBCAD_01
f2 (ppm)
f1 (ppm)
TMSO
MeO
MeO
OMe
F
O
H

NOESY

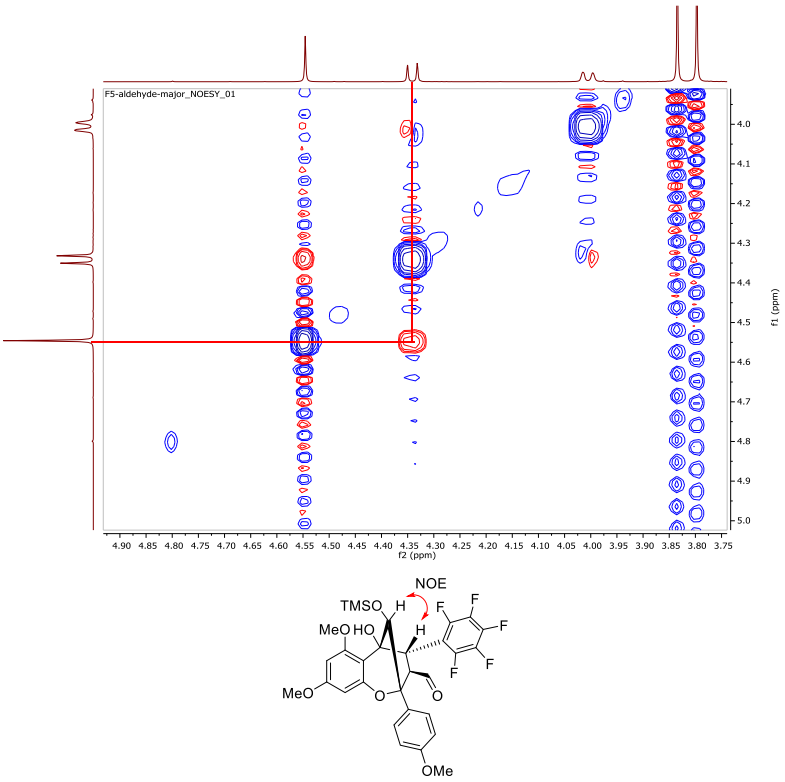
F5-aldehyde-major_NOESY_01
f2 (ppm)
f1 (ppm)
NOE
TMSO
MeO HO
MeO
OMe
F
O
H

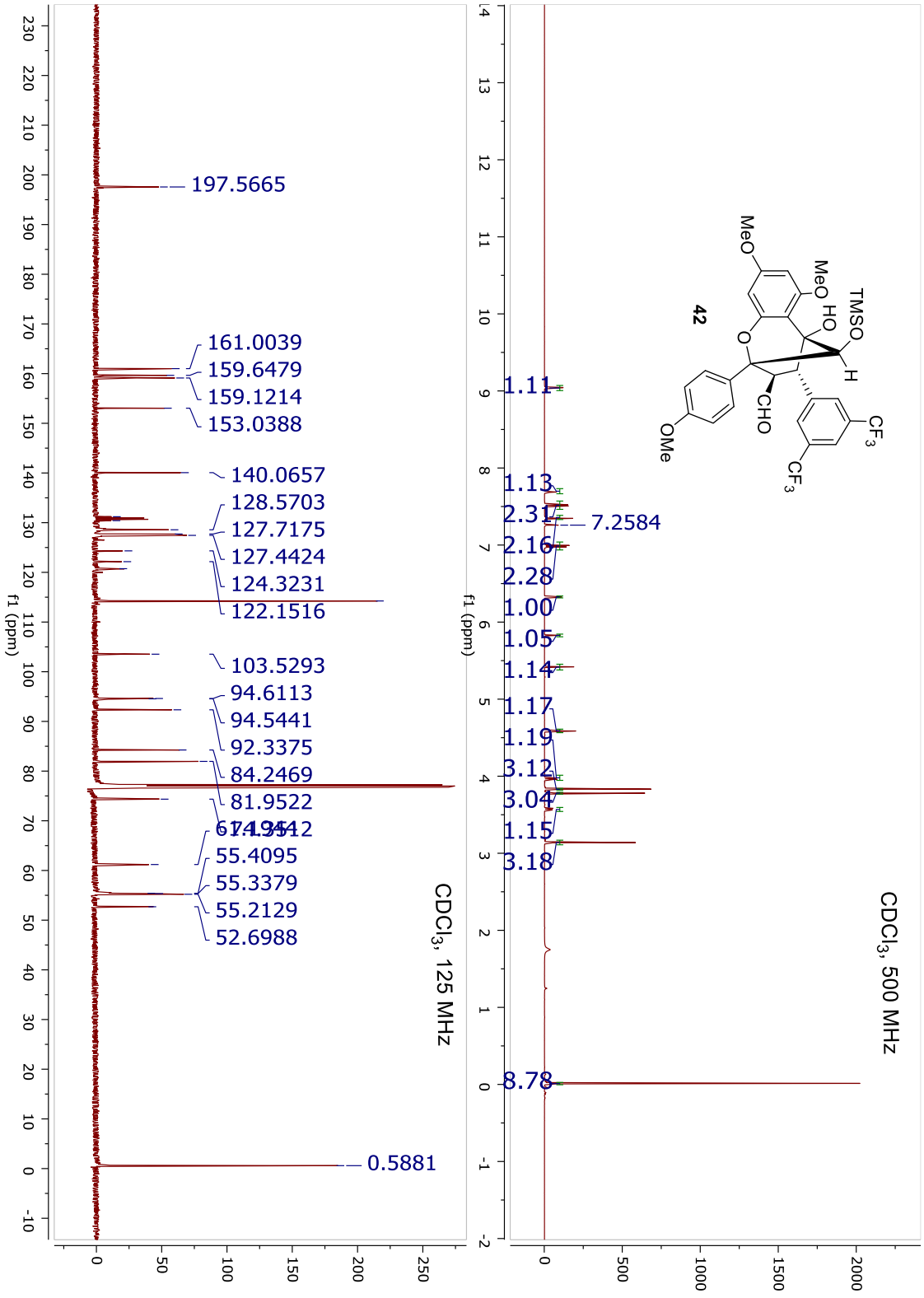
42
MeO
MeO
HO
TMSO
H
O
CHO
OMe
CF3
CF3
CDCl3, 500 MHz
1.11
1.13
2.31
7.2584
2.16
2.28
1.00
1.05
1.14
1.17
1.19
3.12
3.04
1.15
3.18
8.78
CDCl3, 125 MHz
197.5665
161.0039
159.6479
159.1214
153.0388
140.0657
128.5703
127.7175
127.4424
124.3231
122.1516
103.5293
94.6113
94.5441
92.3375
84.2469
81.9522
55.4095
55.3379
55.2129
52.6988
0.5881
f1 (ppm)

^{19}F NMR of **42**, $CDCl_3$, 375 MHz.

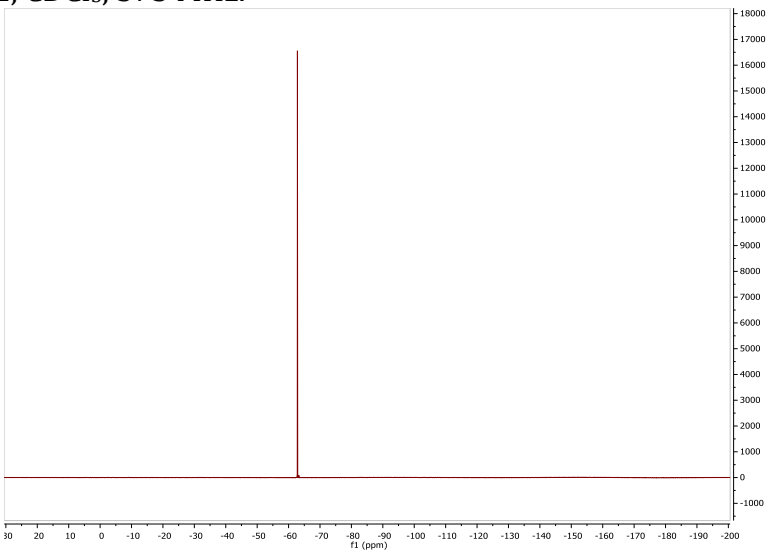

HSQC:

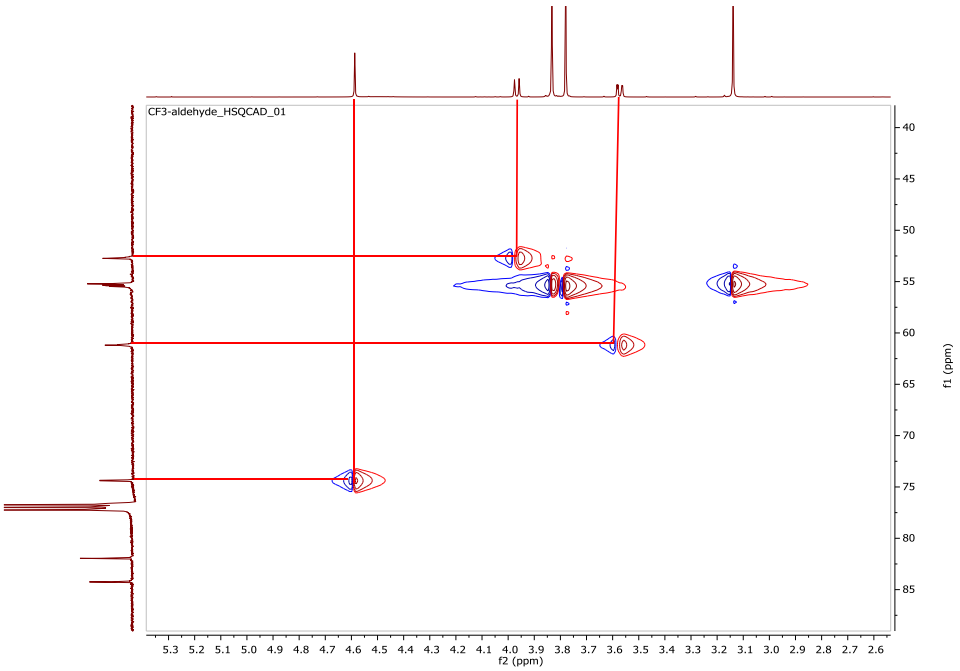

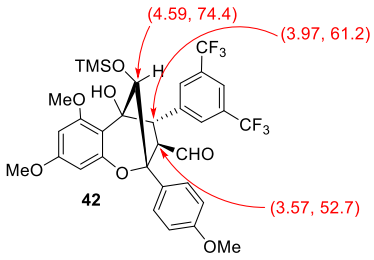

HMBC:

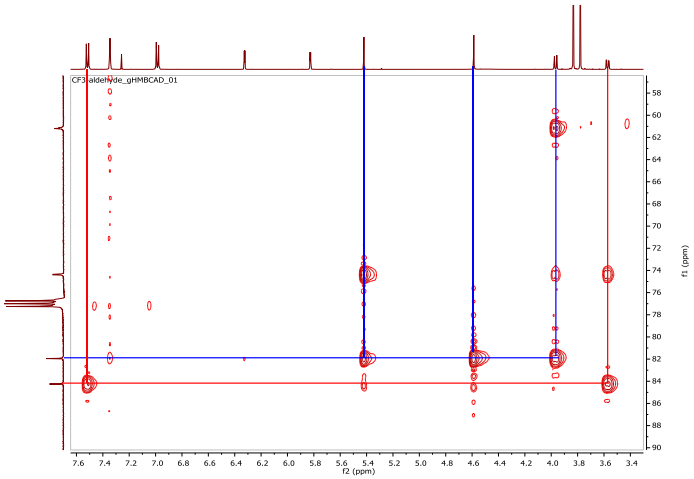
CF3-aldehyde_gHMBCAD_01
f2 (ppm)
f1 (ppm)
TMSO
H
HO
MeO
CF3
CF3
CHO
MeO
O
H
H
H
OMe
42

NOESY:

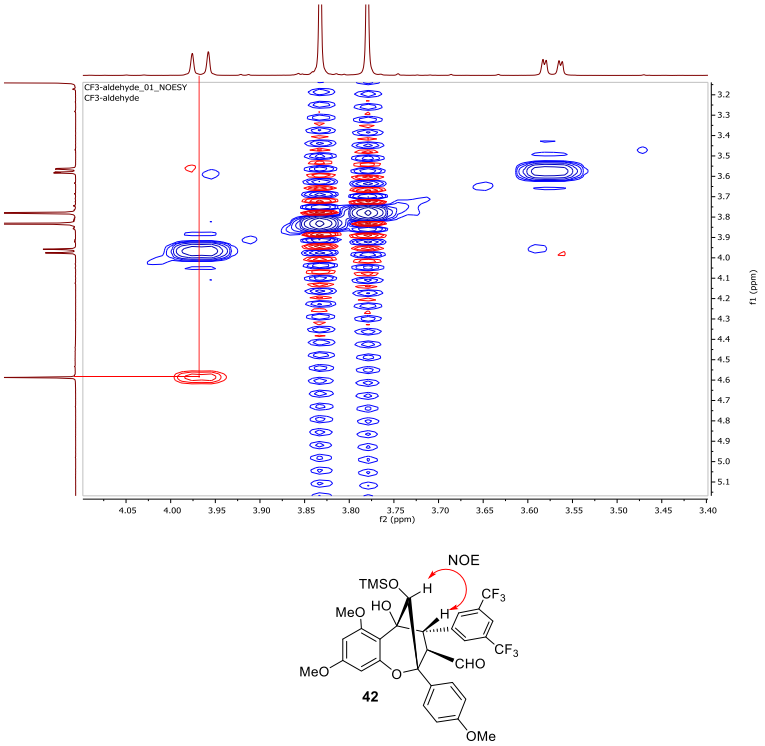
CF3-aldehyde_01_NOESY
CF3-aldehyde
f2 (ppm)
f1 (ppm)
NOE
TMSO
H
HO
MeO
H
CF3
CF3
CHO
MeO
O
42
OMe

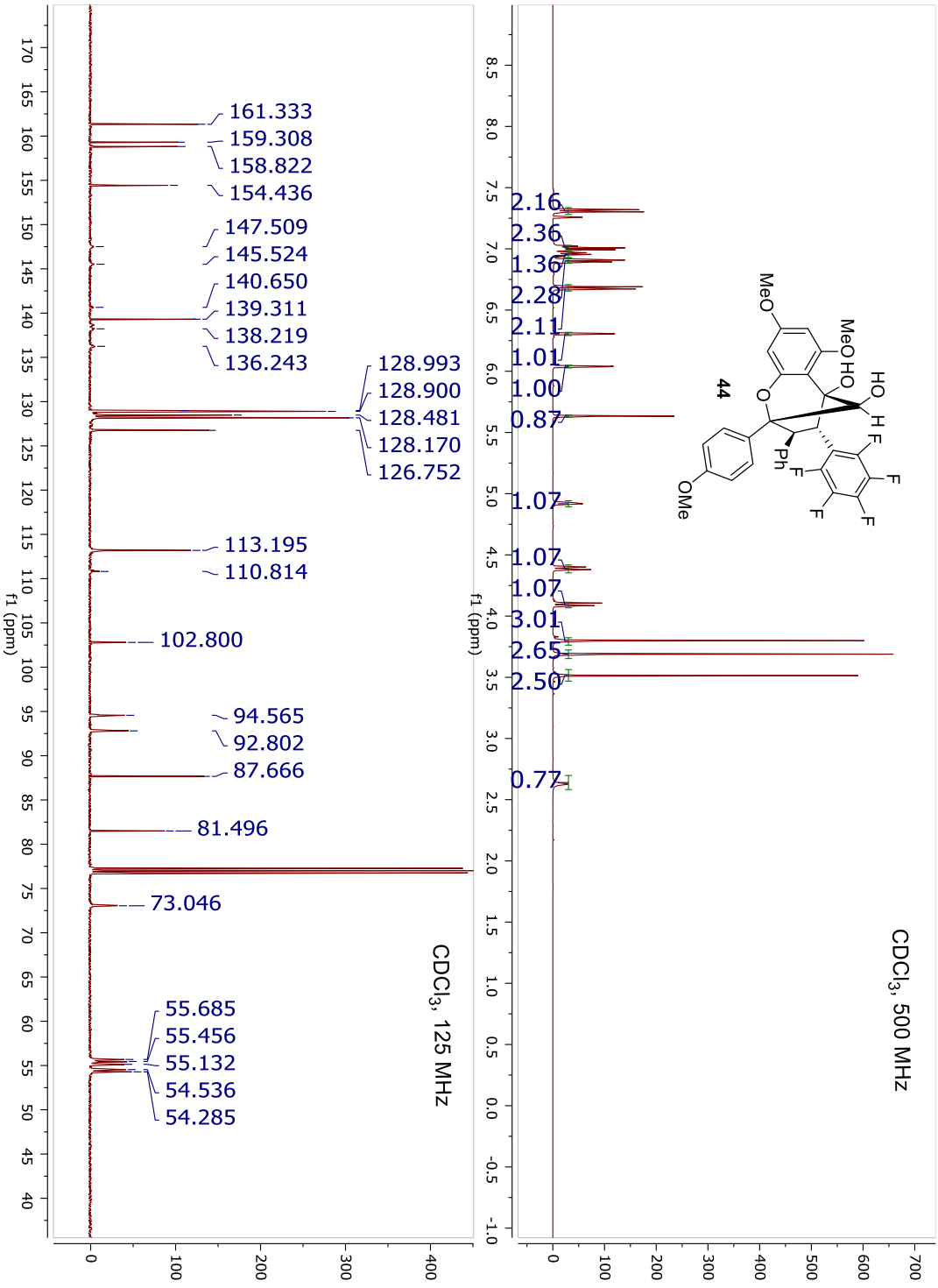
161.333
159.308
158.822
154.436
147.509
145.524
140.650
139.311
138.219
136.243
128.993
128.900
128.481
128.170
126.752
113.195
110.814
102.800
94.565
92.802
87.666
81.496
73.046
55.685
55.456
55.132
54.536
54.285
CDCl3, 125 MHz
f1 (ppm)
2.16
2.36
1.36
2.28
2.11
1.01
1.00
0.87
1.07
1.07
1.07
3.01
2.65
2.50
0.77
CDCl3, 500 MHz
f1 (ppm)
MeO
MeO
HO
HO
H
F
F
F
F
F
Ph
O
OMe
44

^{19}F NMR of **44**, $CDCl_3$, 375 MHz.

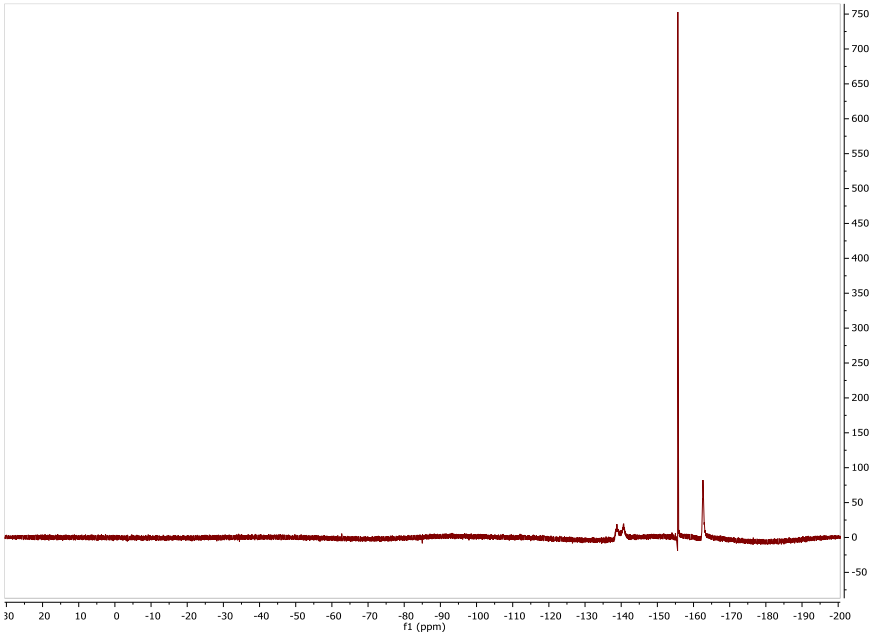

HSQC:

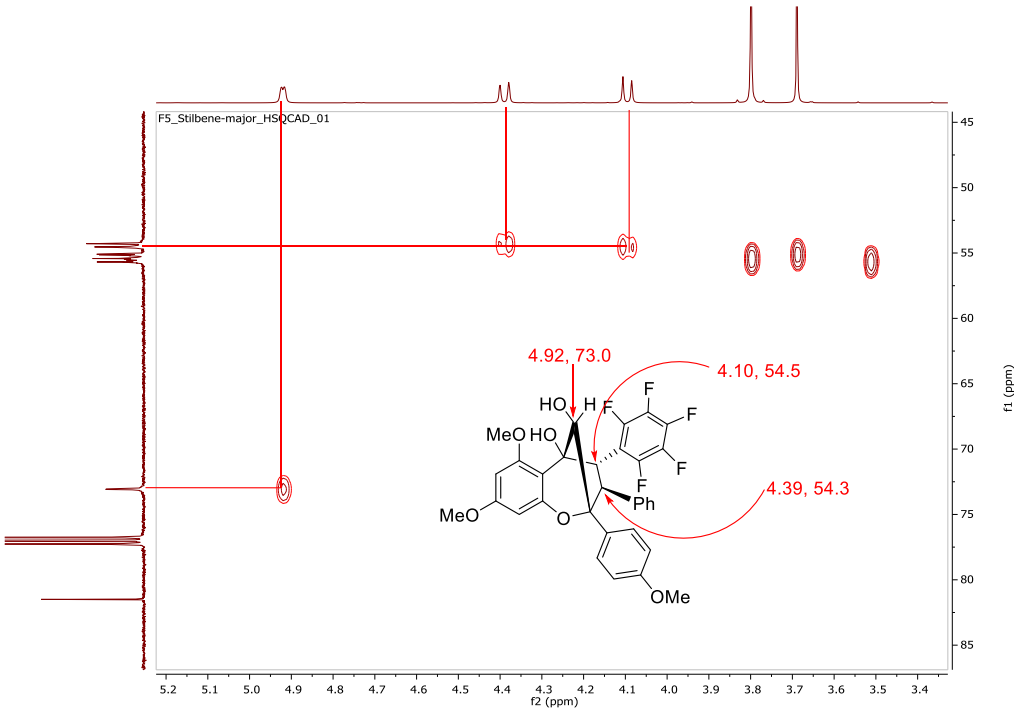

HMBC:

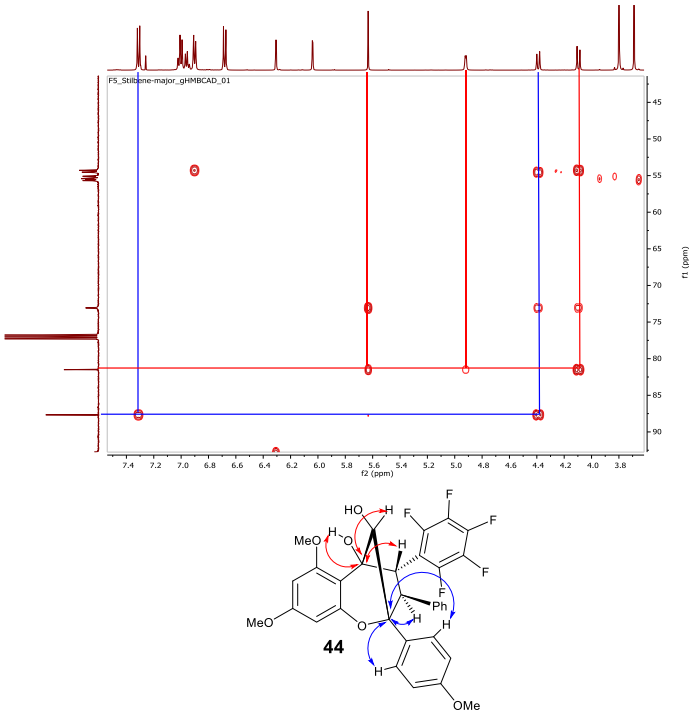
FS_Stilbene-major_gHMBCAD_01
f2 (ppm)
f1 (ppm)
HO
H
F
MeO
H
O
H
F
F
F
F
Ph
MeO
O
H
H
44
H
OMe

NOESY:

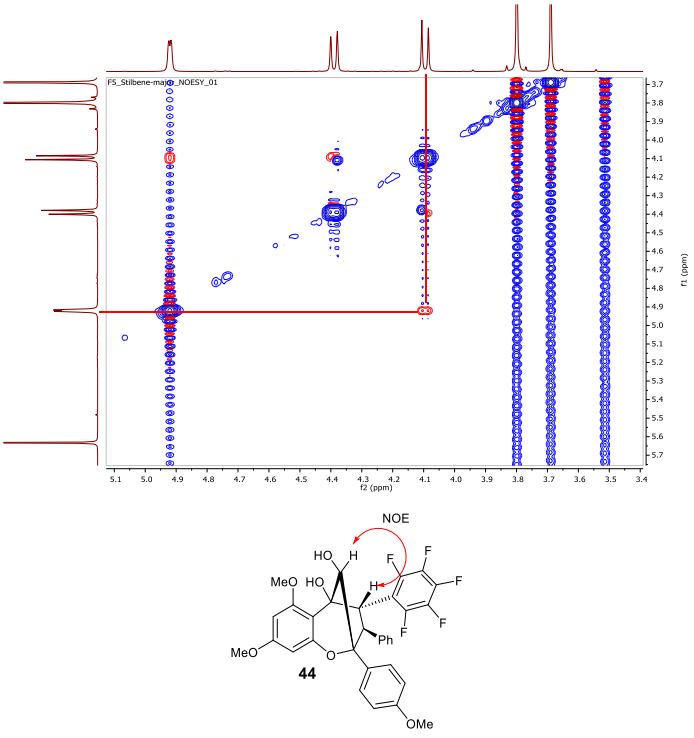
FS_Stilbene-major_NOESY_01
f2 (ppm)
f1 (ppm)
NOE
HO
H
F
F
MeO
HO
H
F
F
Ph
MeO
O
44
OMe

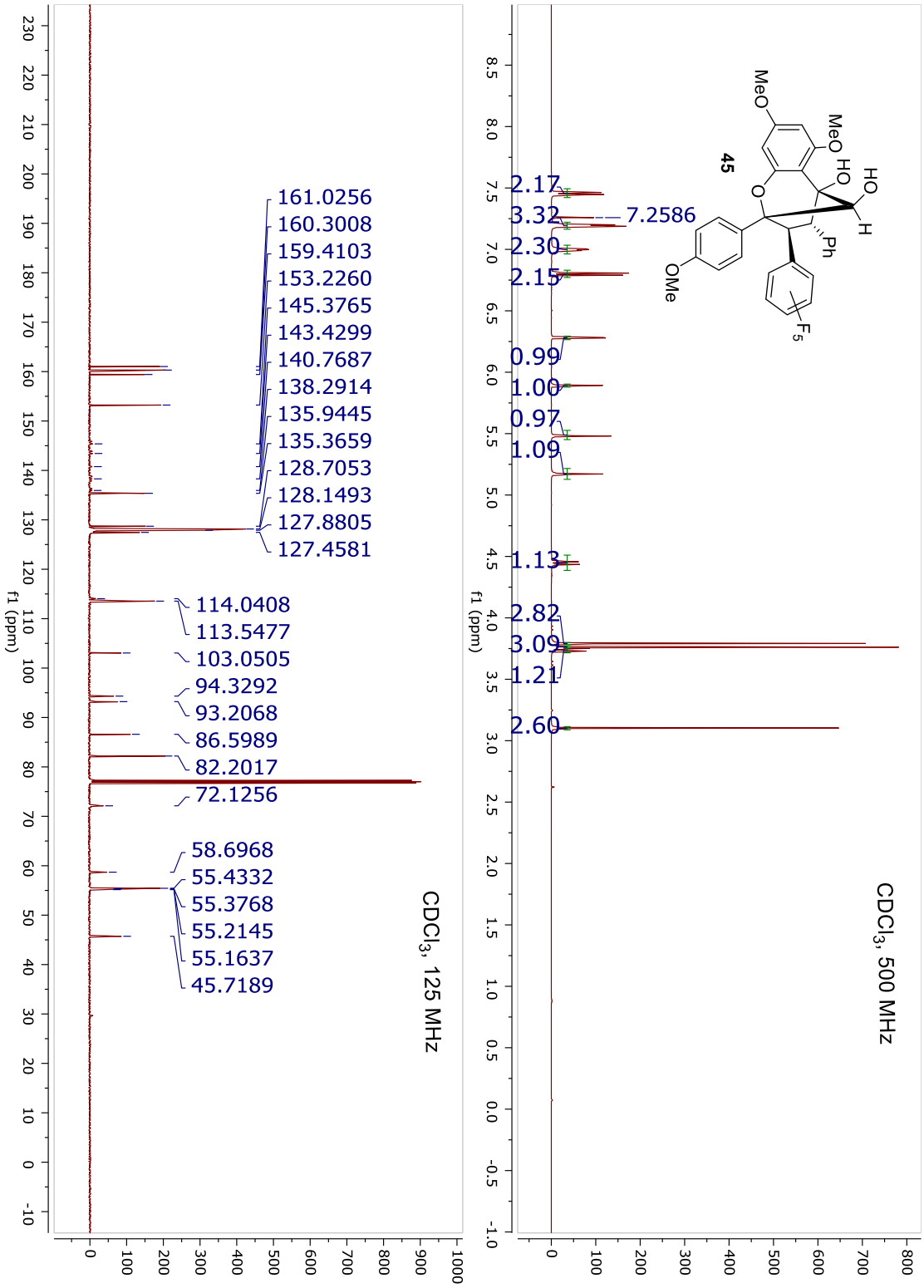
45
MeO
MeO
HO
HO
H
Ph
OMe
F5
2.17
3.32
7.2586
2.30
2.15
0.99
1.00
0.97
1.09
1.13
2.82
3.09
1.21
2.60
CDCl3, 500 MHz
f1 (ppm)
161.0256
160.3008
159.4103
153.2260
145.3765
143.4299
140.7687
138.2914
135.9445
135.3659
128.7053
128.1493
127.8805
127.4581
114.0408
113.5477
103.0505
94.3292
93.2068
86.5989
82.2017
72.1256
58.6968
55.4332
55.3768
55.2145
55.1637
45.7189
CDCl3, 125 MHz
f1 (ppm)

^{19}F NMR of **45**, $CDCl_3$, 375 MHz.

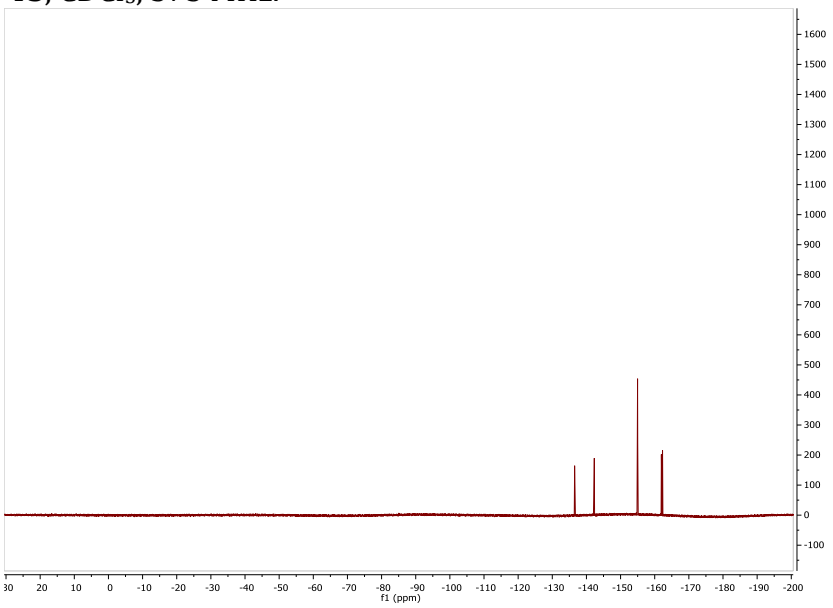

HSQC:

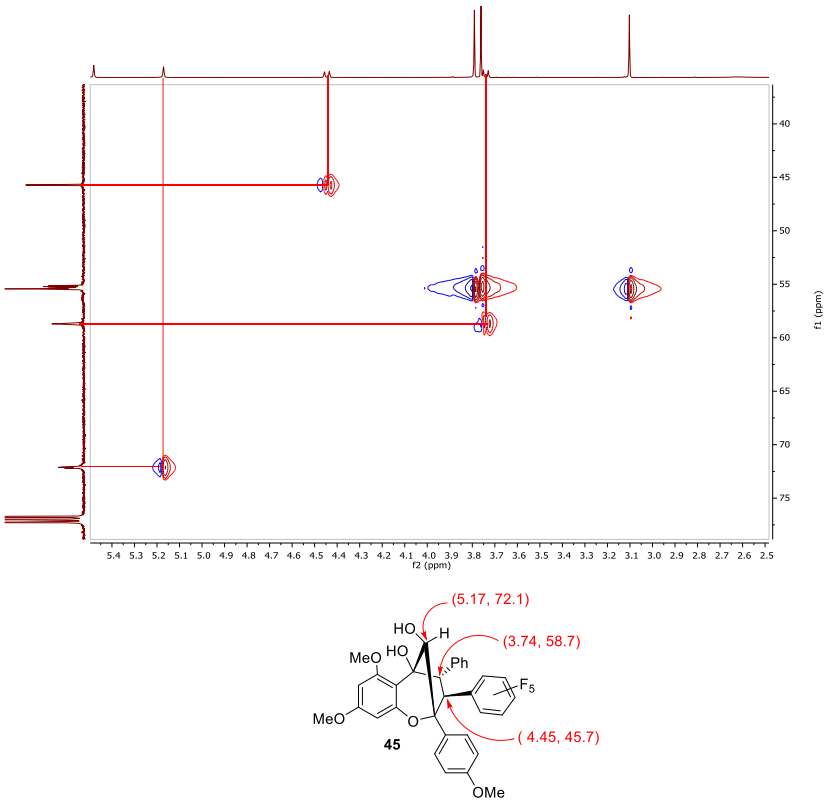

HMBC:

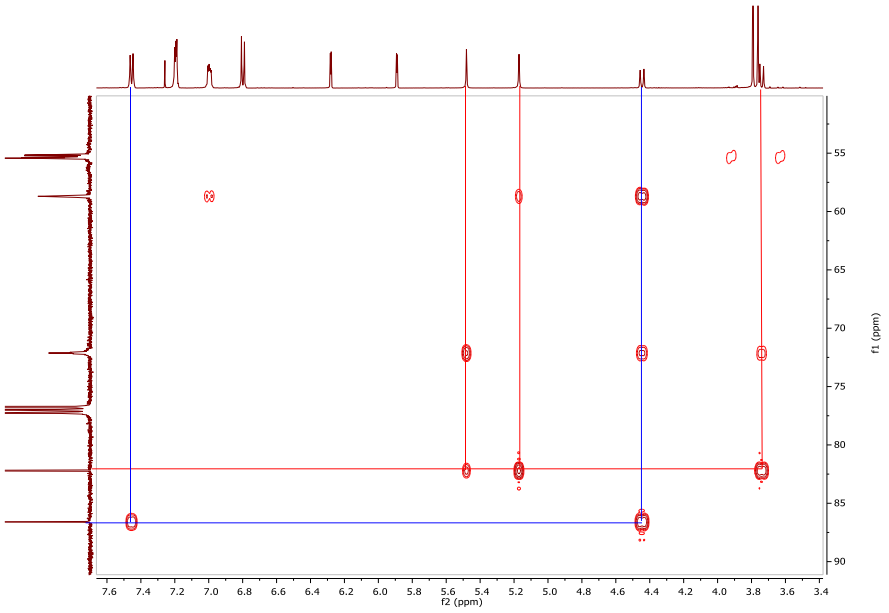

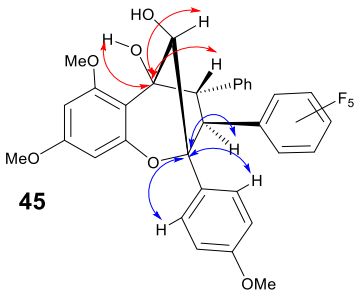

45

CHAPTER THREE

Syntheses of Aza-rocaglates *via* ESIPT Photocycloaddition

3.1 Synthetic Approaches Towards Rocaglate Analogues

As previously demonstrated, cyclopenta[*b*]benzofuran (rocaglate) scaffolds have been found to show excellent biological activities[64] by targeting the RNA helicase eukaryotic initiation factor 4A (eIF4A), an integral protein involved in the initiation of protein translation[65] (*cf.* Scetion 1.4.3). Due to the intriguing structural complexity and biological activities of the rocaglates, a number of synthetic chemists have undertaken the synthesis of natural rocaglates as well as targeted derivatives with improved[66] or novel biological properties.[67] In this chapter, we present our efforts towards synthesis of nitrogen-containing rocaglate analogs, *aza*-rocaglates, *via* ESIPT photocycloaddition of 3-hydroxylquinolinones (3-HQ's). *Aza*-rocaglates are not only synthetically challenging scaffolds but also should provide further structure activity relationship (SAR) information for rocaglate class of natural products.

Before proceeding with our synthetic studies, it is important to highlight relevant literature describing syntheses of unnatural rocaglate analogues. For example, Bruce and coworkers reported the synthesis of a carbocyclic analogue of rocaglamide (**Scheme 3.1**).[68] Starting from 2-(*p*-anisyl)-2-cyclopentenone **1**, copper-mediated Michael addition of phenylmagnesium bromide gave *anti*-biarylcyclopentanone **2** in 76% yield by epimerizing the initially formed *syn*-product during workup. Selective enolate alkylation by 3,5-dimethoxybenzyl chloride using sodium hydride provided the 2,2,3-trisubstituted cyclopentanone in good yield. Intramolecular cyclocondensation of **3** in a mixture of

polyphosphoric acid (PPA) and methanesulfonic acid produced the tricyclic core compound **4** which was further converted to ketone **6** by dihydroxylation and oxidation. Treating ketone **6** with the Stiles reagent (magnesium methyl carbonate)[69] at elevated temperature followed by acidic hydrolysis yielded carboxylic acid **7**. Amide coupling followed by hydroxyl-directed reduction furnished the carbocyclic rocaglate analogues **9** and **10**. The biological properties of the carbocyclic analogues were not reported.

Scheme 3.1 Synthesis of Carbocyclic Analogues of Rocaglamide

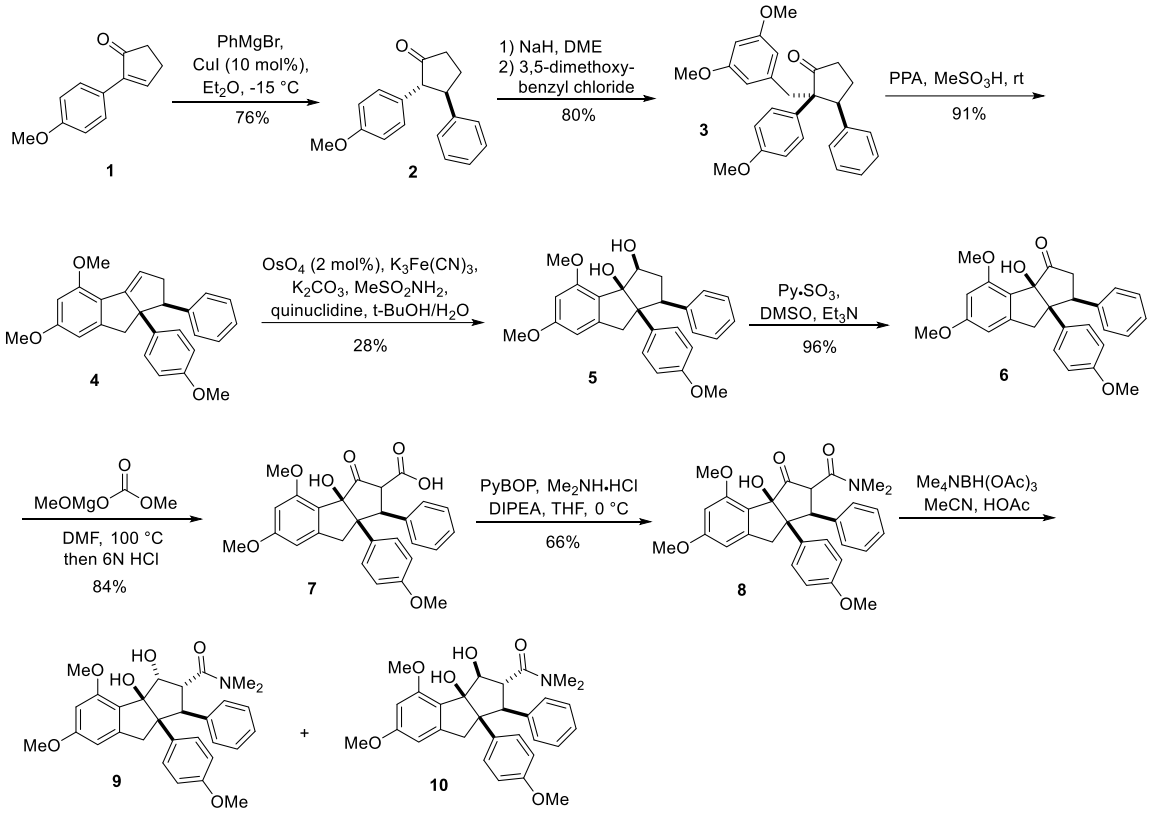

Additionally, Désaubry and coworkers reported a bioisosteric modification of flavagline scaffolds to synthesize amino-rocaglaol derivatives.[70] Treatment of rocaglaol derivative **11** with thionyl chloride afforded a cyclic sulfite **12** in quantitative yield. S_N2 displacement of **12** using sodium azide yielded compound **13** which was subsequently

reduced to amino-rocaglaol compound **14**. Additionally, compound **14** was converted to formide **15** and mesylamide **16**. After this modification was achieved, the cytotoxicity of compound **15** and **16** were tested on human cancer cell lines by the MTS assay after a 72 h treatment. However, both compounds did not show any significant cytotoxicity in Hep3B and HuH7 cancer cell lines.

Scheme 3.2 Bioisosteric Modification of Flavagline Scaffold

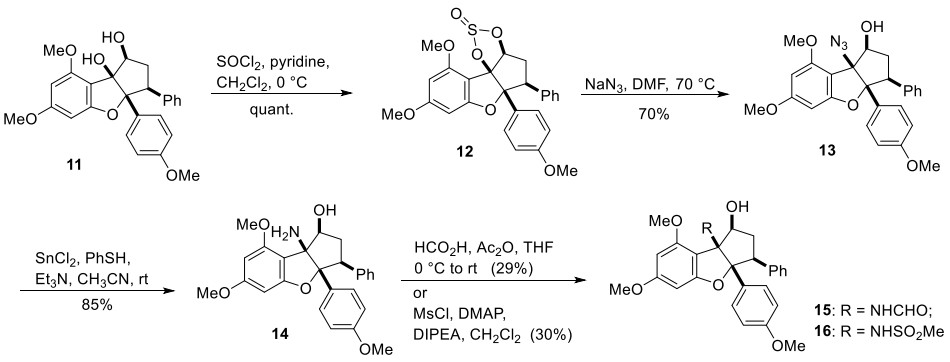

Another modification which incorporated hetereocycles into rocaglate scaffold was reported by Ishibashi and coworkers.[71] An array of 2-hetereocycle-3-hydroxyflavones (**17** to **20**) was synthesized and subjected to ESIPT photocycloaddition conditions to produce (3+2) photocycloadducts, which were subjected to NaOMe-mediated α-ketol rearrangement and diastereoselective reduction to yield various hetereocycle-containing rocaglate derivatives **21** to **24**. The corresponding rocaglaic acid **25** to **28** were also synthesized be saponification using lithium hydroxide. Subsequently, **21**, **22**, **23**, and **27** were tested to showed potent Wnt signal inhibitory activities. The Wnt signal plays crucial roles in the differentiation and proliferation of many types of cells, and inactivation of this system due to mutation would cause aberrant activation of the Wnt signal associated with

many cancers and diseases. Therefore, inhibitors of this signal pathway could be used as drug candidates or useful biological tools.

Scheme 3.3 Hetereocycle-Containing Rocaglate Analogues

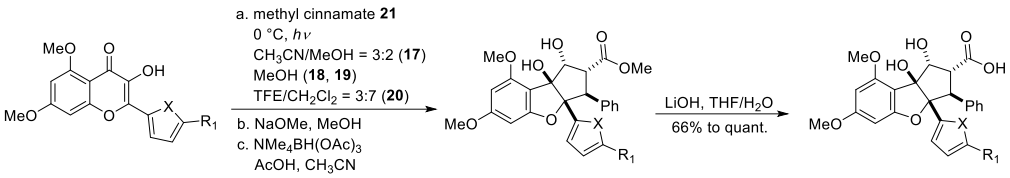

17: X = S, R_1 = H;
18: X = O, R_1 = H;
19: X = S, R_1 = Br;
20: X = O, R_1 = Br;

21: X = S, R_1 = H, 43% yield;
22: X = O, R_1 = H, 13% yield;
23: X = S, R_1 = Br, 55% yield;
24: X = O, R_1 = Br; 32% yield.

25: X = S, R_1 = H;
26: X = O, R_1 = H;
27: X = S, R_1 = Br;
28: X = O, R_1 = Br;

Porco and coworkers reported their investigations of a nitrogen analogue of 3-hydroxyflavone, 1-methyl-2-methyl-3-hydroxyquinolinone **29** (DMQ) and its utility in ESIPT photocycloadditions.[72] Upon photoexcitation, Porco and coworkers hypothesized that excited state intramolecular proton transfer (ESIPT) of DMQ could occur to generate 3-oxidoquinolinium intermediate **29*** which could be quenched with various dipolarophiles to afford photocycloadducts. Accordingly, a parallel screening approach was performed to discover suitable dipolarophiles for ESIPT photocycloaddition with DMQ **29**. As the ESIPT process for DMQ could be observed by fluorescence spectroscopy (**Figure 3.1**), quenching of the fluorescence signal of transient intermediate **29*** in the presence of a collection of dipolarophiles should provide an indication of photocycloaddition reactivity.

Figure 3.1 Absorption and Fluorescence Spectra of DMQ 29

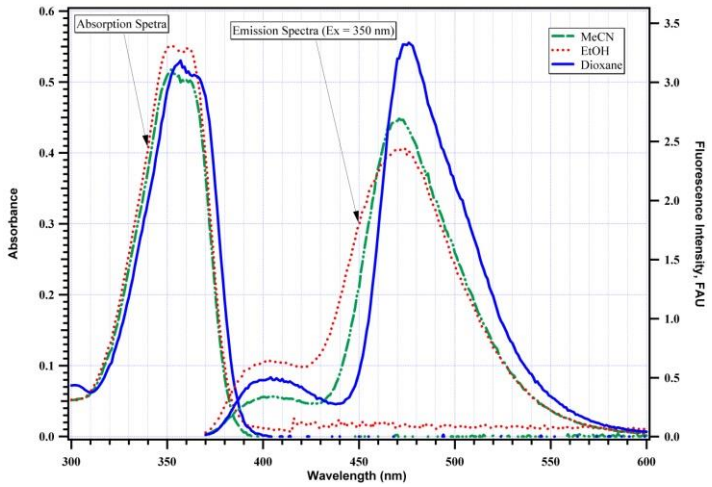

When subjected to irradiation in 1,4-dioxane, dipolarophiles **30** and **21** showed photoreactivity with DMQ **29** (**Scheme 3.4**) to afford moderate yields of photocycloadducts **31** and **32**. The structure of **31** was further confirmed by X-ray crystallographic analysis of *bis*-*p*-bromobenzoate **33**. Using methyl butynoate **34** as dipolarophile, the presumed photocycloadduct **35** was not detected but the isomeric ketol **36** was instead isolated, presumably because the doubly-conjugated enone of **36** provides a strong, thermodynamic driving force for α-ketol rearrangement. Under similar photochemical reaction conditions, two major products were isolated from the photocycloaddition of **29** with electron-rich or electron-neutral dipolarophiles including indene **37**, 2,3-dimethylbutadiene **40**, and cyclohexadiene **43**, all using 1,4-dioxane as solvent.

Scheme 3.4 ESIPT Photocycloaddition of DMQ 29 with Dipolarophiles

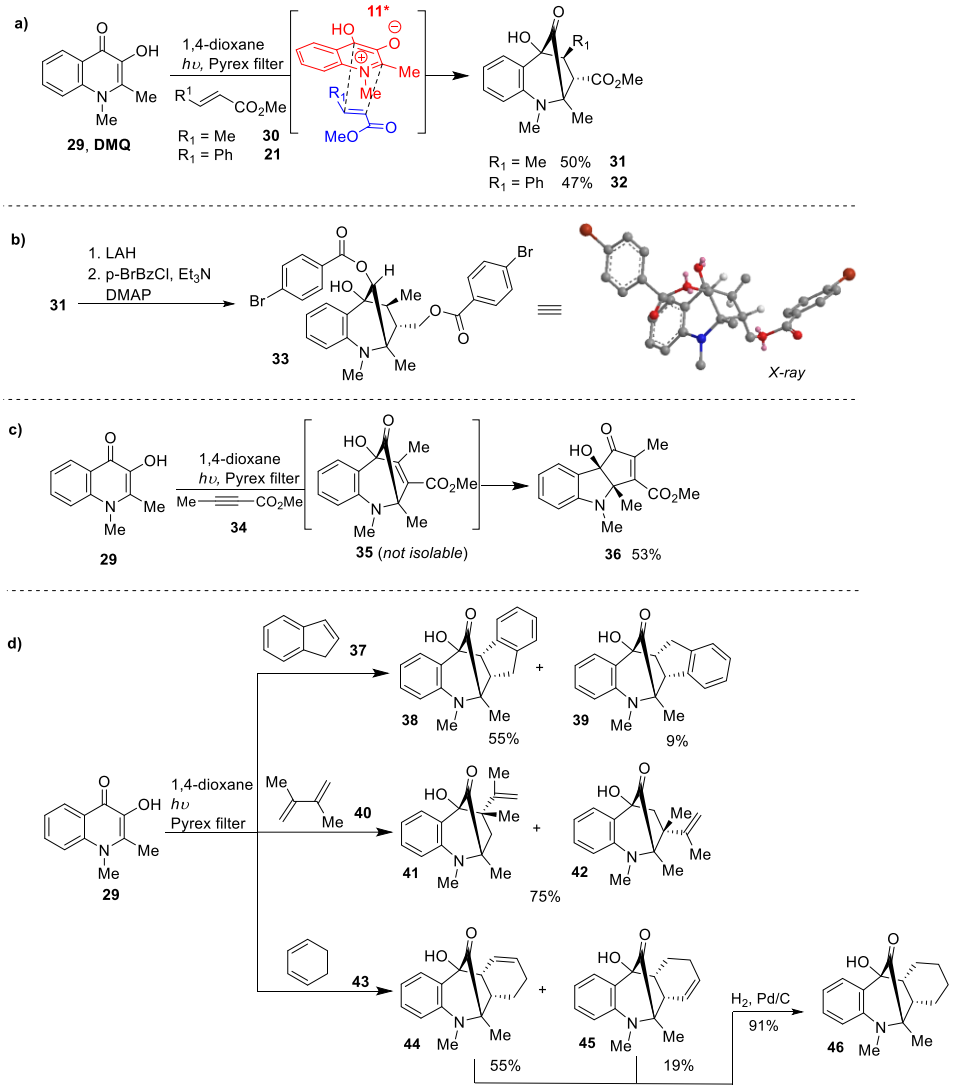

Scheme 3.5 Proposed Synthesis of *Aza*-rocaglate

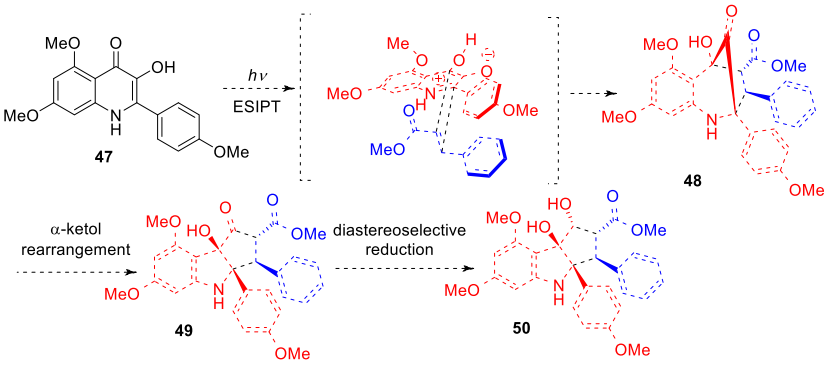

Taken together, Porco and coworkers demonstrated the feasibility for use of 3-hydroxyquinolinones in ESIPT photocycloadditions. Although ESIPT photocycloaddition of DMQ **29** with methyl cinnamate **21** showed the opposite regioselectivity in comparison to reaction with 3-hydroxyflavone, we hypothesized that by using 2-aryl-3-hydroxyquinolinone **47** instead of **29**, π-π stacking interaction between the 2-aryl substituent and methyl cinnamate may orient the regioselectivity of the presumed ESIPT photocycloaddition to furnish photocycloadduct **48**. α-Ketol rearrangement of **48** followed by diastereoselective reduction should afford the hexahydrocyclopenta[*b*]-indole scaffold of *aza*-rocaglate **50** (**Scheme 3.5**).

3.2 ESIPT Photocycloaddition of 3-HQ's with Methyl Cinnamate

Based on our synthetic proposal, a series of 2-aryl-3-hydroxyquinolinones were synthesized from phenacyl anthranilates using previously reported procedures.[72,73] Upon photoirradiation of 3-hydroxyquinolinones (*N*-H-3-HQ's **47**, **51**-**52**) in presence of methyl cinnamate, no detectable formation of photocycloadducts was found (**Scheme 3.6a**). As the previous studies were performed using an *N*-methyl-3-HQ substrate, 1-methyl-2-aryl-3-hydroxyquinolinone (*N*-Me-3-HQ, **56**)[73] was chosen as a modified substrate for ESIPT photocycloaddition (**Scheme 3.6b**).

Scheme 3.6 ESIPT Photocycloaddition of 3-HQ's with Methyl Cinnamate.

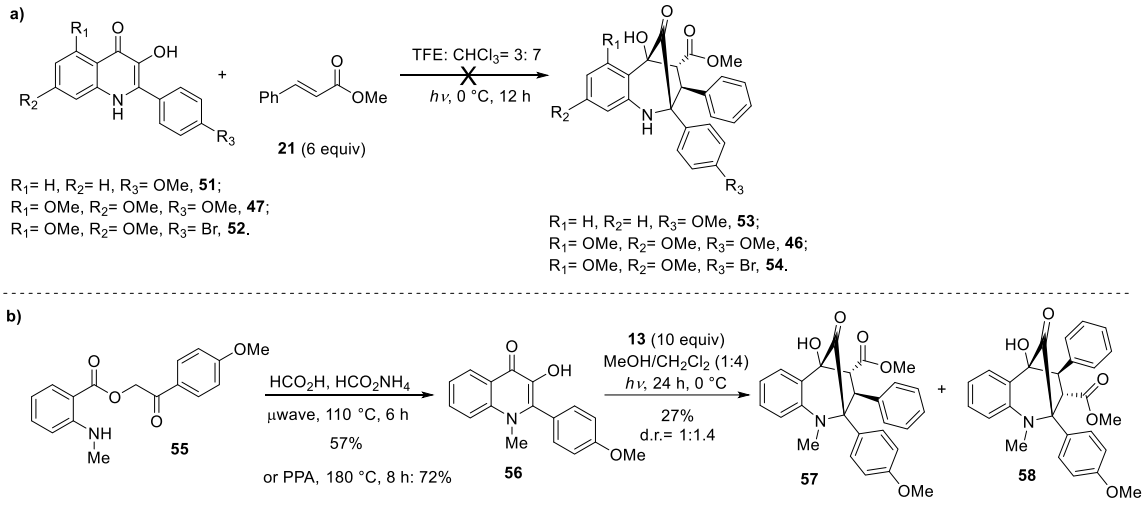

Using the reported literature procedure, treatment of phenacyl anthranilate **55** with formic acid and ammonium formate under microwave irradiation, or iteratively heating **55** in neat polyphosphoric acid (PPA) provided *N*-Me-3-HQ **56**. After subjection of **56** to photoirradiation in the presence of methyl cinnamate **21**, photocycloadducts **57** and **58** were obtained. However, only limited production of photocycloadducts was observed with significant decomposition of *N*-Me-3-HQ **56** and a very long period of photo-irradiation was required.

Table 3.2 Condition Optimization of ESIPT Photocycloaddition *N*-Me-3-HQ with Methyl Cinnamate.

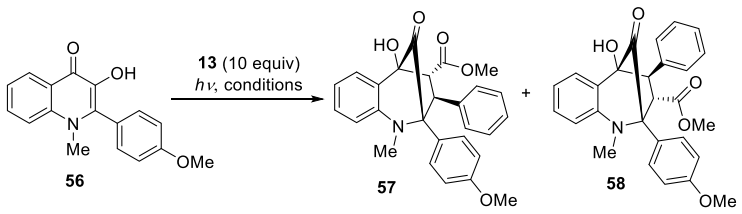

Entry	Solvent	Time (h) temp. (°C)	Photo-reactor	Ratio (**57:58**)[a]	Yield (%)[b]
1	CH_2Cl_2/MeOH (1 : 1, 0.02 M)	24, 0	Rayonet	1 : 1.4	27
2	$CHCl_3$/TFE (4 : 1, 0.02 M)	24, 0	Rayonet	3 : 1	39
3	$CHCl_3$ (0.02 M)	24, 0	Rayonet	2 : 1	31
4	$PhCF_3$/TFE (7 : 3, 0.035 M)	48, 0	Rayonet	5 : 1	40
5	$PhCF_3$/TFE (7 : 3, 0.06 M)	14, 5	Hanovia	N/A	Decomp.
6	$PhCF_3$/TFE (7 : 3, 0.04 M)	14, -20	Hanovia (Pyrex)	3 : 1	19%
7	$PhCF_3$/TFE (7 : 3, 0.06 M)	14, 0	Rayonet photoflow	4 : 1	43%
8	$PhCF_3$/TFE (7 : 3, 0.04 M)	14, -20	Rayonet photoflow	4.5 : 1	44%
9	$CHCl_3$/TFE (7 : 3, 0.035 M)	10, 0	Rayonet photoflow	4 : 1	43%
10	$PhCF_3$/TFE (4 : 1, 0.035 M)	9, 0	Rayonet photoflow	5 : 1	43%
11	$PhCF_3$: TFE = 7 : 3 (0.05 M)	9, 0	Rayonet photoflow	5 : 1	46%

[a] Diastereoselectivity was determined by 1H NMR integration; [b] Isolated yield of purified **57**.

Optimization of reaction conditions was conducted to improve the ESIPT photocycloaddition (**Table 3.1**). A Rayonet photobox (350 nm) was found to be the optimal light source, as increased decomposition of **56** was observed using a Hanovia light (entry 5). Using a 7:3 mixtures of trifluorotoluene and trifluoroethanol provided photocycloadducts **57**:**58** in 40% yield and 5:1 selectivity, however 48 h of irradiation was required for complete ESIPT photocycloaddition (entry 4). Accordingly, the aforementioned Rayonet continuous photoflow reactor[74] was introduced to further improve the photocycloaddition. In general, we were able to achieve improvement of yield in a much shorter reaction period along with significantly less decomposition in comparison to batch reactions (46% yield, **57**:**58** = 5:1).

Scheme 3.7 ESIPT Photocycloaddition in Flow and Prototype Synthesis of *Aza*-rocaglate 44

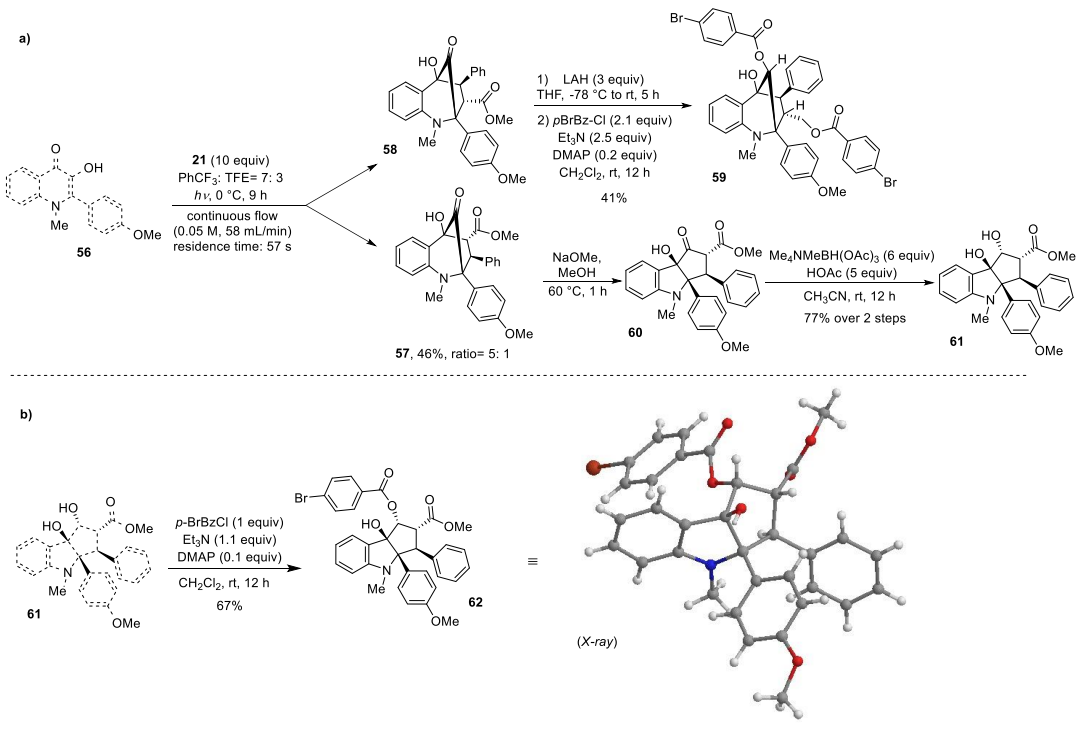

With larger amounts of **57** and **58** in hand, the minor isomer **58** was reduced with lithium aluminum hydride to afford an unstable diol derivative which was directly acylated to afford the *bis*-*para*-bromobenzoate **60**. The structure and relative stereochemistry of **60** was confirmed using HMBC and NOESY experiments. Using the major isomer **57**, sodium methoxide-mediated α-ketol rearrangement followed by a hydroxyl-directed diastereoselective reduction yielded *aza*-rocaglate **51** in 77% yield (**Scheme 3.7a**). The structure of **51** was unambiguously confirmed by X-ray crystal structure analysis of the derived bromobenzoate **62** (**Scheme 3.7b**). Interestingly, inspection of the X-ray structure reveals that the *N*-methyl moiety is coplanar to the adjacent aryl group indicating a non-pyramidalized nitrogen.[75] This is likely due to steric interaction of *N*-methyl moiety with the two nearby aryl substituents which appears to prevent nitrogen pyramidalization.

In order to provide a plausible explanation for the differential reactivity of 3-hydroxyquinolinones **51** and **56**, we measured their UV-Vis absorption spectra. We found that in CH_2Cl_2:MeOH (2:1), both substrates possess an absorption band at approximately 370 nm which can be attributed to $n \rightarrow \pi^*$ photo excitation.[76] More interestingly, we observed an additional absorption peak at 310 nm for substrate **51** (**Figure 3.2**) which indicates that *N*-H-3-HQ substrate **51** may exhibit a tautomerization in solution.[77] Therefore, we hypothesized that in solution, **51** may also be represented by an aromatic, dihydroxyquinoline tautomeric form **64** which in principle may diminish its photoreactivity. In order to support this assertion, we found that treatment of **51** with TMS diazomethane resulted in formation of 3,4-dimethoxyquinoline **63**.[78] Furthermore, by evaluation of the UV- absorption properties of **63**, an absorption shoulder at 320 nm was

also observed for compound **63** which provides supportive information on the existence of tautomeric form **64** in solution.

Figure 3.2 UV Absorption Spectra of 3-Hydroxyquinolinones 51 and 56 in Comparison to Dimethoxyquinoline 63

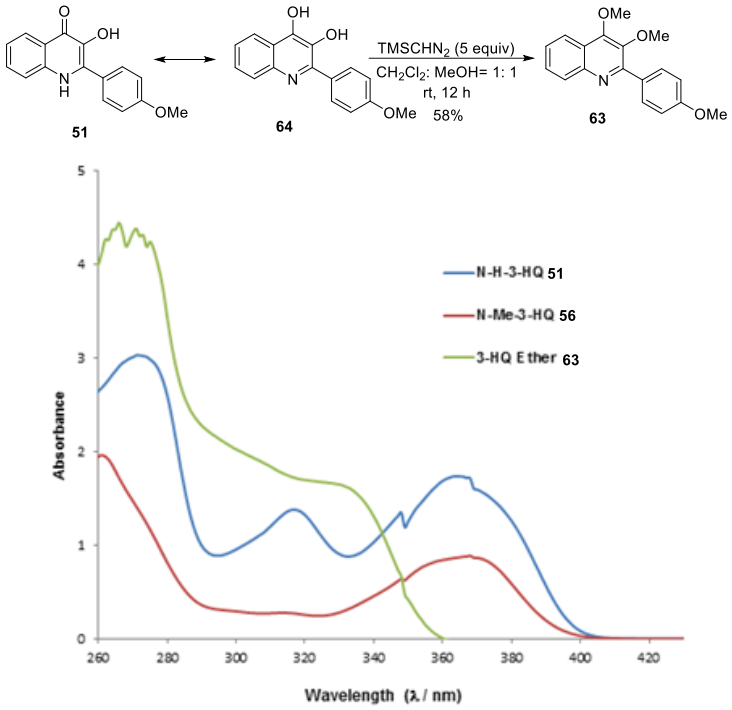

3.3 Synthesis of *N*-Methyl-3-hydroxyquinolinones Using Basic Conditions

In order to synthesize more highly functionalized *aza*-rocaglate scaffolds, we next turned our attention to prepare *N*-methyl-3-hydroxyquinolinones with increased substitution. Although various methods were reported to synthesize 3-hydroxyquinolinones, these methods were all very similar and most reports only focused on *N*-H substrates. Namely, by heating the corresponding phenacyl anthranilate precursors in the presence of acid (*cf.* **Scheme 3.6**), *N*-H-3-HQs may be obtained. A series of simple *N*-Me-3-HQs were also synthesized using this protocol. Accordingly, we planned to synthesize *N*-methyl phenacyl anthranilates with an array of functional groups to test this

methodology (**Scheme 3.8**). Dimethoxy anthranilic acid **65**[79] was first converted to isatoic anhydride **66** by treatment with triphosgene which was directly deprotonated by sodium hydride and methylated with methyl iodide. Subsequent hydrolysis by aqueous hydrochloric acid then yielded mono-methylated dimethoxy anthranilic acid **67**. We subsequently treated **67** with potassium carbonate to form the corresponding potassium salt followed by addition of 2,4'-dibromo-acetophenone to achieve an S_N2 reaction which efficiently provided access to phenacyl anthranilate **68**. However, after evaluation of all reported conditions for conversion of **68** to *N*-Me-3-HQ **69**, the best condition identified involved thermolysis of **68** to 180 °C in the presence of polyphosphoric acid (PPA) for 24 h which led to the production of only a 5% isolated yield of **69**.[80] All other reported conditions failed to provide access to *N*-Me-3-HQ **69**. After a thorough condition screening, we were able to identify that treatment of **68** with sodium hydride and heating led to the formation of*N*-Me-3-HQ **69** in 78% yield. A previously demonstrated substrate **55** was also reacted under similar conditions and afforded an 83% isolated yield of **56**.

After further investigation, we also learned that sodium hydride could provide access to *N*-Me-3-HQs. Other bases, including LDA, *t*BuOK, MeONa, and LiHMDS all failed to provide the desired product, which led us to believe that the initiation of this reaction did not involvet enolate formation upon reaction with base. Therefore, a proposed mechanism (**Scheme 3.8c**) may proceed through formation of hemiaminal **70** followed by rearrangement to alkoxide **71**.[81] 3,1-Benzoxazin-4-ones related to **71** have previously been reported from treatment of phenacyl anthranilates with acetic acid.[82] Additionally, carbamate and sulfonamide-protected phenacyl anthranilates were also synthesized and

failed to yield any corresponding 3-HQ compounds under our reaction conditions which is consistent with our mechanistic proposal, as electron withdrawing groups on nitrogen could decrease the nucleophilicity of the nitrogen and introduce steric hindrance for the hemiaminal formation.[83] Further conversion of **71** to iminium **72** followed by isomerization may generate the intramolecular hydrogen bond-stabilized enolate **73** (**Scheme 3.8c**).[84] Cyclization of **73** to benzoxazepine **74** followed by rearrangement to zwitterion **75**, elimination, and acidic workup provides 3-hydroxyquinolinone **56**. Similar benzoxazepine structures have also been synthesized previously in the literature by treatment of phenacyl anthranilates with phosphoryl chloride.[85]

Scheme 3.8 Synthesis of *N*-Methyl-3-hydroxyquinolinones Using Sodium Hydride and the Proposed Mechanism

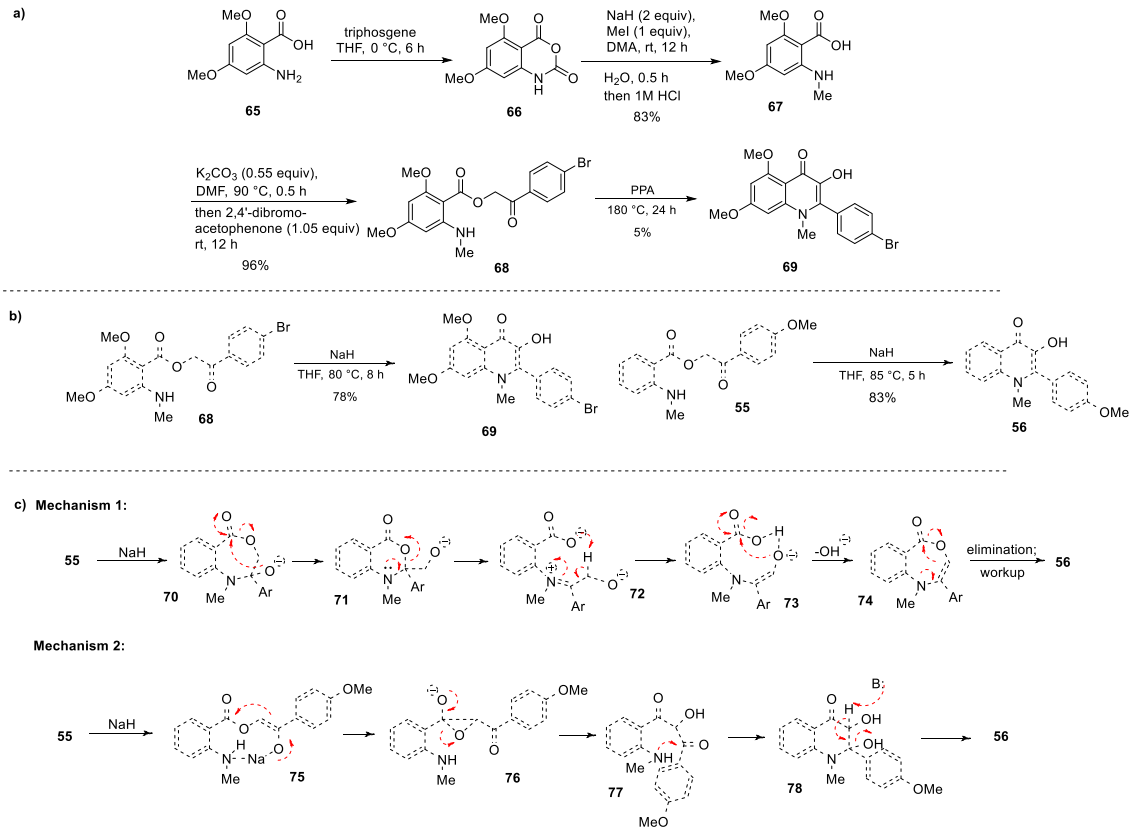

Alternatively, sodium hydride could directly deprotonate **55** to afford sodium enolate **75**, which may undergo *3-exo-trig* cyclization[86] to generate an unstable hydroxyepoxide intermediate **76**. Further rearrangement of **76** to diketone **77**. Hemiaminal formation and subsequent dehydration afforded product **56**.

Scheme 3.9 Substrate Scope for Sodium Hydride-mediated *N*-Alkyl-3-HQ Synthesis

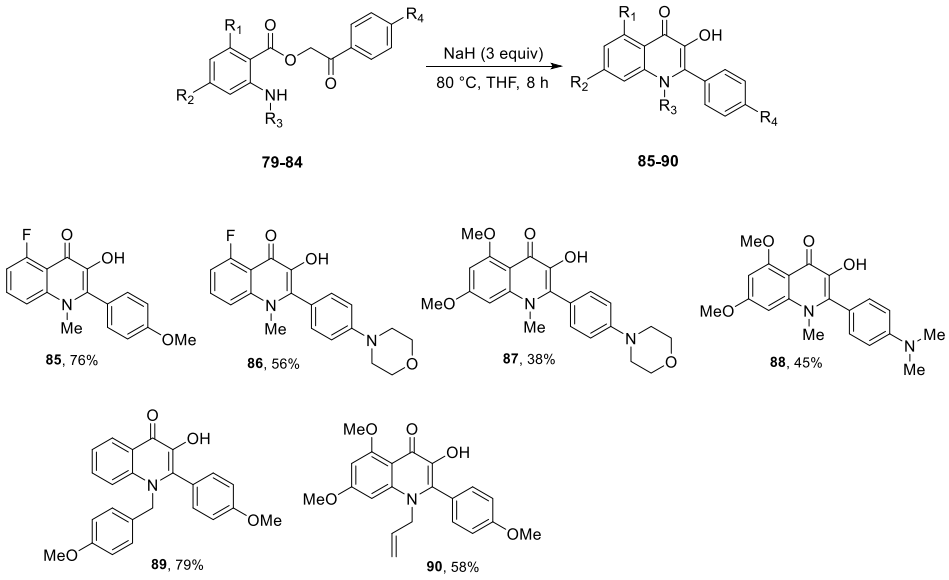

Taking advantage of this methodology, we were also able to synthesize several *N*-alkyl-3-hydroxyquinolinones from the corresponding phenacyl anthranilates (**Scheme 3.9**). From this study, we were able to see that fluorinated phenacyl anthranilate and heterocycle-containing phenacyl anthranilates could be used to synthesize *N*-Me-3-HQ **85**-**87**, as well as the dimethylamino-substrate **88**. More importantly, we also demonstrated that other *N*-alkyl substituted 3-hydroxyquinolinones may by prepared using this novel method, such as *para*-methoxybezyl substituted compound **89**, and *N*-allyl-3-HQ **90.**

3.4 Synthesis of Highly Functionalized *Aza*-rocaglates

With various *N*-alkyl-3-HQs in hand, we subsequently subjected these compounds to ESIPT photocycloadditions for the syntheses of more highly functionalized *aza*-rocaglates. Using the previously optimized photoflow conditions *N*-Me-3-HQ **69** was photo-irradiated with methyl cinnamate **21** in 7:3 trifluorotoluene : trifluoroethanol for 12 hours. Photocycloadduct **91** was produced in high diastereoselectivity which was subjected to sodium methoxide-mediated α-ketol rearrangement and subsequent hydroxyl-directed diastereoselective reduction to afford *aza*-rocaglate **93** (**Scheme 3.10a**). Saponification using lithium hydroxide followed by amide coupling yielded the corresponding hydroxamate **94**, the nitrogen-containing analogue of the corresponding synthetic cyclopenta[*b*]benzofuran compound which was found to be a highly potent protein translatioinhibitor (*vide infra*).[87]

In order to synthesize our original synthetic target, *N*-H-*aza*-rocaglate **50**, we chose to use *N*-allyl-3-HQ **90** as our ESIPT photocycloaddition reactant in which the allyl moiety could serve as a removable protecting group. The previously described photoflow condition was applied to perform the ESIPT photocycloaddition first, but significant decomposition of **90** was observed. We reasoned that use of the mildly acidic solvent trifluoroethanol may lead to photo-decomposition in which case the aprotic solvent toluene was chosen for the photocycloaddition. Gratifyingly, we could observe formation of the photocycloadduct **95** in 43% yield and in 10:1 diastereoselectivity (**Scheme 3.10b**). *N*-allyl-*aza*-rocaglate **97** was next accomplished *via* α-ketol rearrangement and diastereoselective reduction. After a thorough evaluation of allyl deprotection conditions,

we found that using Pd (0) /1,4-*bis*(diphenylphosphino)-butane complex with Meldrum's acid as nucleophile and proton source,[88,89] *N*-H-*aza*-rocaglate **50** could be obtained in 45% yield. Other *N*-deallylation conditions such as thio radical promoted-tautomerization[90] and oxidative condition[91] reported in the literature all failed to provide the desired product. Furthermore, we also demonstrated the possibility for further functionalization of the *N*-allyl moiety by introducing an olefin *via* a cross metathesis reaction on of **97** with methyl acrylate to produce *aza*-rocaglate **98**.[92]

Scheme 3.10 Synthesis of High Functionalized *Aza*-rocaglates

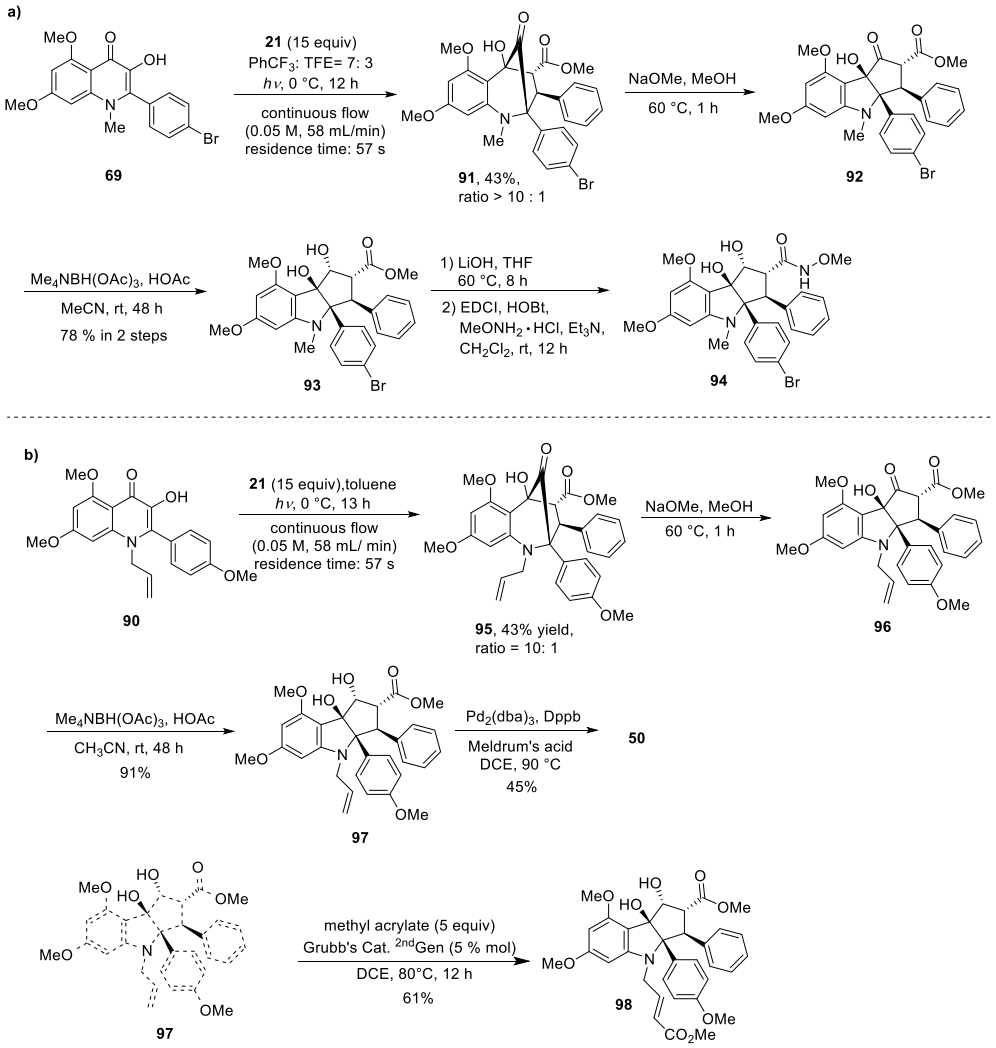

3.5 Biological Activity Studies of *Aza*-rocaglates

Rocaglates have been shown to behave as potent inhibitors of translation by interfering with the activity of eukaryotic initiation factor (eIF) 4A,[87] an RNA helicase necessary for cap-dependent protein synthesis. We therefore assessed the biological activities of compounds **50**, **93**, **94**, **97**, and **98** *in vitro* in a translation assay programmed with the bicistronic mRNA, FF/HCV/Ren (**Figure 3.3a**). In this system firefly luciferase (FF) production is eIF4A-dependent whereas Renilla luciferase (Ren) is not. Silvestrol (**101**) and rocaglates CR-1-31B **100** and (-)-SDS-1-021 **99** potently inhibited FF production (5-10 fold) at 5 μM. The only *aza*-rocaglate to affect FF production was the *N*-methyl derivative **77**, showing a ~30% reduction in FF production at 20 μM (**Figure 3.3a**). To assess activity towards cellular protein synthesis, HeLa cells were incubated with silvestrol (**101**), CR-1-31B **100**, or **93** for 1 h and metabolic protein synthesis quantitated (**Figure 3.3b**). Whereas 100 nM silvestrol (**101**) or CR-1-31B **100** completely blocked protein synthesis, compound **100** showed modest activity only at 50 μM (~20% inhibition).

Figure 3.3 a. Effect of *Aza*-rocaglates on *in vitro* Translation of FF/HCV/Ren. b. Assessing Translation Inhibition Activity of 77 on HeLa cells.

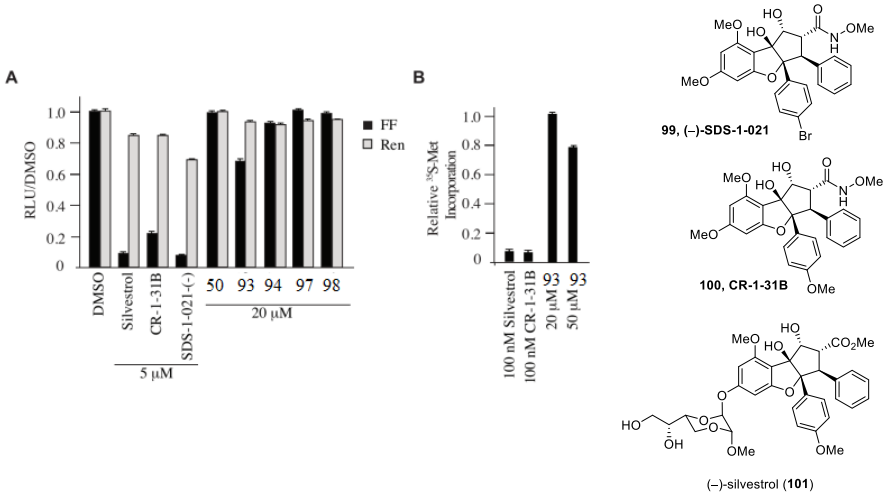

Consistent with these findings, we also found no evidence for translation inhibition over a 24 h period at concentrations up to 10 μM using a whole cell assay based on constitutive expression of the rapidly turned-over reporter protein firefly luciferase (**Figure 3.4a**). Likewise, the compounds had minimal cytotoxic activity in a standard 3-day growth assay over the same concentration range (**Figure 3.4b**). Together, these results indicate that *aza*-rocaglates do not possess the same inhibitory potency towards protein synthesis in comparison to related rocaglates such as RHT **102**.

Figure 3.4 a. Translation Inhibition (10 μM) in Whole Cells Based on Constitutive Expression of Firefly Luciferase. b. 3-Day Growth Assay (Human 293T cancer cells) Over the Same Concentration.

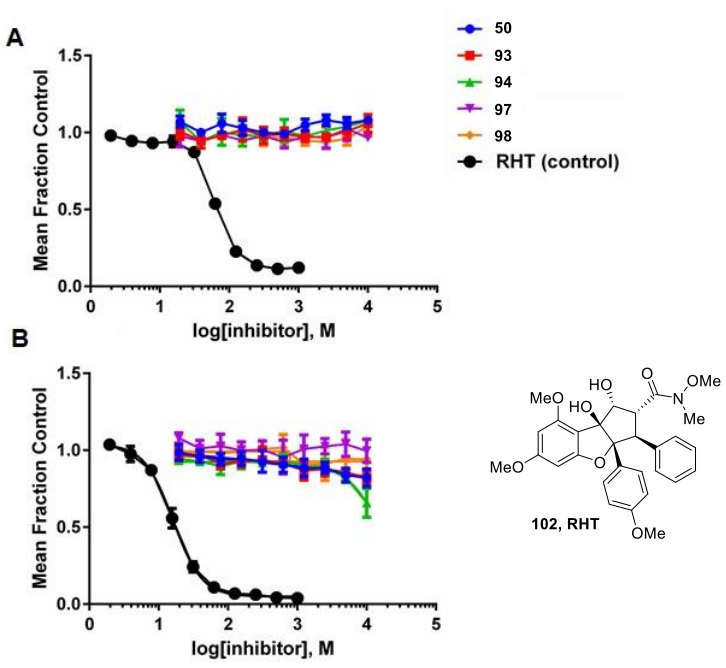

3.6 Summary

To summarize, in this chapter we have employed ESIPT photocycloaddition methodology to synthesize *aza*-rocaglates. Our studies have uncovered differential photocycloaddition reactivities between *N*-H- and *N*-Me-substituted 2-aryl-3-

hydroxyquinolinone substrates. A novel method to access 1-alkyl-2-aryl-3-hydroxyquinolinones using sodium hydride was also developed for (3+2) photocycloaddition. Use of a continuous photoflow reactor facilitated synthesis of *aza*-rocaglates with both *N*-alkyl and *N*-H substitution. Initial protein synthesis and translation inhibition data indicated that *aza*-rocaglates did not possess activity in comparison to related rocaglates which provided further information on the SAR of the natural product scaffold.

3.7 Experimental Section

General Information: ^{1}H NMR spectra were recorded at 500 MHz at ambient temperature with $CDCl_3$ (Cambridge Isotope Laboratories, Inc.) as solvent. Data for ^{1}H NMR are reported as follows: chemical shift, integration, multiplicity (brs = broad singlet, s = singlet, d = doublet, t = triplet, q = quartet, m = multiplet) and coupling constants in Hz. ^{13}C NMR spectra were recorded at 125 MHz at ambient temperature with the same solvents unless otherwise stated. Chemical shifts are reported in parts per million relative to deuterated solvents. All ^{13}C NMR spectra were recorded with complete proton decoupling. Infrared spectra were recorded on a Nicolet Nexus 670 FT-IR spectrophotometer. High-resolution mass spectra were obtained in the Boston University Chemical Instrumentation Center using a Waters Q-TOF API-US mass spectrometer. Melting points were recorded on a Mel-Temp apparatus (Laboratory Devices). Analytical LC-MS was performed on a Waters Acquity UPLC (Ultra Performance Liquid Chromatography (Waters MassLynx Version 4.1) with a Binary solvent manager, SQ mass spectrometer, Water 2996 PDA (PhotoDiode Array) detector, and ELSD (Evaporative Light Scattering Detector). An Acquity UPLC

BEH C_{18} 1.7 μm column was used for analytical UPLC-MS. The Scilligence ELN electronic laboratory notebook was used for experimental procedure planning.

Analytical thin layer chromatography was performed using 0.25 mm silica gel 60-F plates. Flash chromatography was performed using 200-400 mesh silica gel (Scientific Absorbents, Inc.). Yields refer to chromatographically and spectroscopically pure materials, unless otherwise stated. HPLC grade tetrahydrofuran, methylene chloride, diethyl ether, toluene, acetonitrile, and benzene were purchased from Fisher and VWR and were purified and dried by passing through a PURE SOLV® solvent purification system (Innovative Technology, Inc.). Other ACS grade solvents for chromatography were purchased from Clean Harbors.

Photochemistry experiments were performed using a Rayonet RPR-100 photochemical reator equipped with RPR-3500Å irradiation lamps ($\lambda > 330$ nm, $\lambda_{max} = 350$ nm). For the Hanovia photoflow reactor, a 450 medium pressure mercury lamp housed in quartz immersion well with a Pyrex absorption sleeve ($\lambda > 290$ nm) was used. An A-40 Refrigerated & Heating Circulator was used for Immersion well cooling (Anova Industries Inc.). For the Rayonet photoflow reactor, a Rayonet RPR-100 photobox was used as light source and a Thermo Scientific™ Neslab CC65 Immersion Cooler was using as a cooling system. A benchtop pump with 114DV flip top single channel pumphead (model: 120S) was chosen as the peristaltic pump for the continuous photoflow reactor (Waston Marlow Fluid Technology Group). Microwave experiments were performed using a CEM Discover microwave. All other reactions were carried out in oven-dried glassware under an argon atmosphere unless otherwise noted.

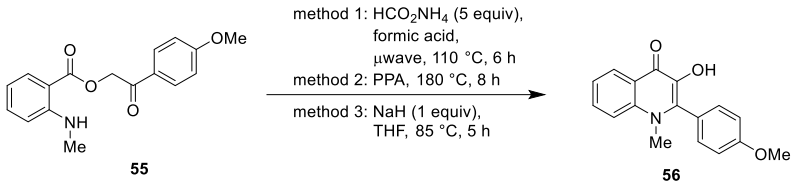

***N*-Me-3-HQ 56:** Method 1: A 20 mL microwave reaction tube was charged with anthranilate **55** (3.0 g, 10 mmol, 1 equiv) and ammonium formate (3.16 g, 50 mmol, 5 equiv). Subsequently, 10 mL formic acid was added and the resulting mixture was stirred until all the solid was completely dissolved. The tube was then plugged into the microwave reactor and irradiated for 6 hours at 110 °C. The reaction mixture was next cooled to room temperature and poured into ice water for 10 min. The solid was collected by filtration which is the crude product. After recrystallization in acetone, *N*-Me-3-HQ **56** was obtained as a white solid (1.6 g, 57% yield).

Method 2: A 100 mL Erlenmeyer flask was charged with 30 g polyphoric acid (PPA). Subsequently, the PPA was heated up to 180 °C and the stickiness of PPA was reduced after the temperature was reached. Anthranilate **55** (3.0 g, 10 mmol, 1 equiv) and a magnetic stir bar was added. After 10 min all the solid was completely dissolved. The reaction mixture was kept heated at 180 °C for 8 hours before 80 mL ice water was added. The mixture was put on sonication for 2 hours until all the gummy oil was fully dissolved by water. The dark green solid was then filtered and collected. After recrystallization in acetone, *N*-Me-3-HQ **56** was obtained as a white solid (2.1 g, 72% yield).

Method 3: A 250 mL flame-dried, round bottom flask was charged with anthranilate **55** (3.0 g, 10 mmol, 1 equiv) and 130 mL anhydrous THF and the reaction was purged with argon. After NaH (60% dispersion in mineral oil) (0.4 g, 10 mmol, 1 equiv) was added, a

water condenser was installed and the solution was heated to 85 °C for 5 h before being cooled to room temperature and immersed in an ice bath. Saturated aqueous ammonium chloride solution was added to work up the reaction until pH < 7 was achieved (250 mL was added). Then CH_2Cl_2 80 mL × 5 was used for extraction, and the combined organic layers were washed with saturated aqusous NaCl solution and dried with anhydrous Na_2SO_4. After concentrated *in vacuo*, 20 mL of cold acetone was added. The white precipitate was filtered and washed with cold acetone. Product **56** was obtained as a white solid (2.35 g, 83% yield).

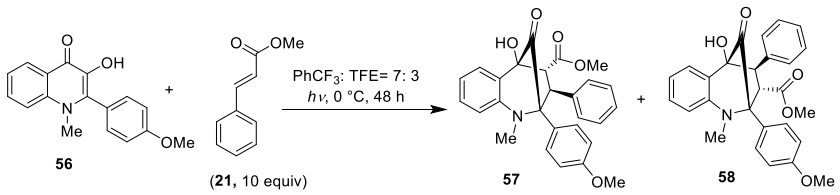

Batch photoreaction: To a Pyrex reaction tube was added *N*-Me-3-HQ **56** (500 mg, 1.78 mmol, 1 equiv), methyl cinnamate **21** (2.88 g, 17.8 mmol, 10 equiv), α,α,α-trifluorotoluene (35 mL), and 2,2,2-trifluoroethanol (15 mL). The resulting mixture was first sonicated and then sparged with argon while sonicating for 10 min. The tube was then sealed and chilled to 0 °C. The resulting solution was irradiated using a Rayonet RPR-100 photochemical reactor for 48 h at 0 °C using ice bath. In order to maintain the reaction temperature at 0 °C, every 2 hours the ice bath needed to be refilled. The reaction mixture was then concentrated and purified *via* column chromatography (EtOAc/hexanes = 1:10 to first remove methyl cinnamate then EtOAc/hexanes = 1:6 to EtOAc/hexanes = 1:4) to elute products. Compound **57** (633 mg, 40%) was obtained as a white solid and compound **58** (127 mg, 8%) was isolated as a colorless oil.

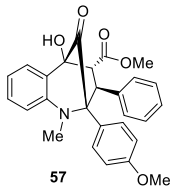

57

57: R_f = 0.19 (EtOAc / hexanes = 1 : 4); mp 103 - 105°C (CH_2Cl_2); IR (thin film): ν_{max} 3438, 2950, 1708, 1612, 1500, 1209, 1151, 1078, 1010, 815.73, 736 cm^{-1}; ^1H NMR (500 MHz, CDCl3) δ 7.29 (d, J = 7.5 Hz, 1H), 7.21 (m, 3H), 7.06 (m, 3H), 6.90 (m, 3H), 6,79 (d, J = 8.5 Hz, 1H), 6.65 (d, J = 7 Hz, 2H), 4.63 (d, J = 7 Hz, 1H), 3.70 (s, 3H), 3.54 (s, 1H), 3.50 (s, 3H), 3.35 (d, J = 7 Hz, 1H), 2.60 (s, 3H); ^{13}C NMR (125 MHz, CDCl3) δ 210.2, 170.5, 158.6, 145.6, 141.5, 131.5, 130.8, 129.8, 128.8, 128.4, 126.7, 126.6, 124.3, 120.7, 117.7, 113.0, 80.4, 72.9, 59.9, 55.1, 51.1, 38.8, 29.7; HRMS-ESI (m/z): $[M+H]^+$ calculated for $C_{27}H_{25}NO_5$ 444.1811, found 444.1809.

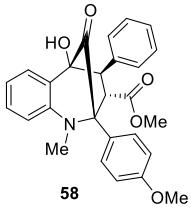

58

58: R_f = 0.27 (EtOAc / hexanes = 1 : 4); IR (thin film): ν_{max} 3507, 3065, 2950, 1738, 1601, 1487, 1255, 1181, 1088, 737, 702 cm^{-1}; ^1H NMR (500 MHz, $CDCl_3$) δ 7.57 (m, 2H), 7.42 (d, J = 10 Hz, 1H), 7.30 (m, 3H), 7.22 (m, 1H), 7.03 (d, J = 11.5 Hz, 2H), 6.98 (d, J = 11.5 Hz, 2H), 6.82 (t, J = 10 Hz, 1H), 6.52 (d, J = 10 Hz, 1H), 4.55 (d, J = 7.5 Hz, 1H), 4.10 (d, J = 7.5 Hz, 1H), 3.88 (s, 3H), 3.67 (s, 3H), 2.60 (s, 1H, OH), 2.53 (s, 3H); ^{13}C NMR (125 MHz, $CDCl_3$) δ 210.1, 171.4, 159.7, 144.3, 139.5, 129.5, 129.2, 128.9, 128.5, 127.7, 125.8, 122.8, 118.5, 113.8, 111.2, 79.1, 77.2, 73.9, 55.3, 53.8, 53.4, 52.5, 35.7; HRMS-ESI (m/z): $[M+H]^+$ calculated for $C_{27}H_{25}NO_5$ 444.1811, found 444.1811.

Continuous Photoflow Reactor:

In a 200 mL flame dried flask, *N*-Me-3-HQ **56** (1 g, 3.56 mmol, 1 equiv), methyl cinnamate **21** (8.64 g, 53.25 mmol, 15 equiv), 50 mL α,α,α-trifluorotoluene, and 21 mL 2,2,2-trifluoroethanol were added. After degassing with argon for 10 min in a sonicator, the

reaction flask was connected to the continuous photoflow reactor. After the solvent pump started, nitrogen gas was bubbled into the reaction mixture for another 10 min to further purge the remaining air out of the reaction system. The reaction mixture cooled to 0 °C and was kept circulating and irradiated (Rayonet, $\lambda > 330$ nm) at 0 °C for 9 h. After being concentrated *in vacuo*, the reaction mixture was purified by silica gel column chromatography (gradient of EtOAc/hexane 1:10 to remove the methyl cinnamate first, then EtOAc/hexane from 1:6 to 1:4 to obtain the product). Compound **57** (483.5 mg, 46%) was obtained as a white solid. and compound **58** (97 mg, 9%) was isolated as a colorless oil.

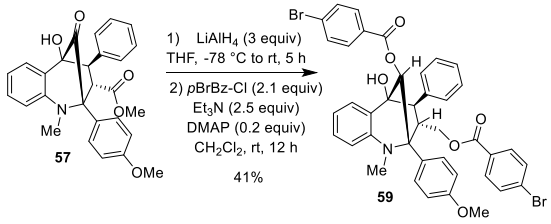

***Bis-p*-bromobenzoate 59:** A 50 mL flask was charged with compound **57** (50 mg, 0.11 mmol, 1 equiv) and a stir bar in 20 mL of dry THF. The solution was cooled to -78 °C before $LiAlH_4$ (19.1 mg, 0.56 mmol, 5 equiv) was added. The reaction mixture was warmed to room temperature and stirred overnight before saturated NH_4Cl (20 mL) and potassium sodium tartrate tetrahydrate (20 mL) aqueous solution were added to quench the reaction. 20 mL × 3 CH_2Cl_2 was used for extraction and the organic layers were combined. After drying the organic layers with anhydrous Na_2SO_4, filtration, and concentration *in vacuo*, the resulting brown oil was used in the next step without further purification. The brown oil was dissolved in 50 mL of dry CH_2Cl_2 and was cooled to 0 °C before 4-bromobenzoyl chloride (52 mg, 0.24 mmol, 2.1 equiv) was added. The reaction mixture was stirred at

room temperature for 3 h. Saturated aqueous Na_2CO_3 (20 mL) solution was added to quench the reaction. CH_2Cl_2 (3×20 mL) was used for extraction and the combined organic layers were washed with saturated aqueous NaCl and dried with anhydrous sodium sulfate. After filtration, and concentration *in vacuo*, the crude product was purified *via* SiO_2 gel column chromatography (1:10 EtOAc/hexanes to 1:5 EtOAc/hexanes) to afford compound **59** (36 mg, 41% yield) as a white solid.

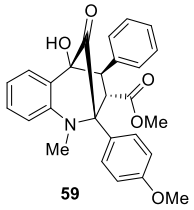

59

59: R_f = 0.63 (EtOAc / hexanes = 3 : 7); mp 151-152 °C (CH_2Cl_2); IR (thin film): ν_{max} 3062, 2927, 1719, 1590, 1513, 1265, 1102, 1012, 752 cm^{-1}; ^1H NMR (500 MHz, CDCl3) δ 7.49 (m, 6H), 7.32 (m, 11H), 6.85 (d, J = 8.5 Hz, 2H), 6.76 (t, J = 7.5 Hz, 1H), 6.73 (d, J = 8 Hz, 1H), 5.70 (s, 1H), 4.78 (dd, J_1 = 6 Hz, J_2 = 11 Hz), 4.33 (dd, J_1 = 8.5 Hz, J_2 = 11 Hz), 4.02 (ddd, J_1 = 6 Hz, J_2 = 8 Hz, J_3 = 8.5 Hz), 3.79 (s, 3H), 3.53 (d, J = 8 Hz), 2,79 (s, 3H), 2.16 (s, 1H); ^{13}C NMR (125 MHz, CDCl3) δ 165.6, 165.3, 159.3, 144.5, 139.3, 131.7, 131.4, 131.2, 131.0, 130.1, 130.0, 129.8, 129.3, 129.2, 128.5, 128.4, 128.3, 128.1, 127.7, 122.1, 116.8, 114.1, 109.8, 78.7, 77.4, 69.0, 65.9, 59.1, 55.3, 50.9, 36.9; HRMS-ESI (m/z): $[M+H]^+$ calculated for $C_{40}H_{33}Br_2NO_6$ 782.0953, found 782.0771.

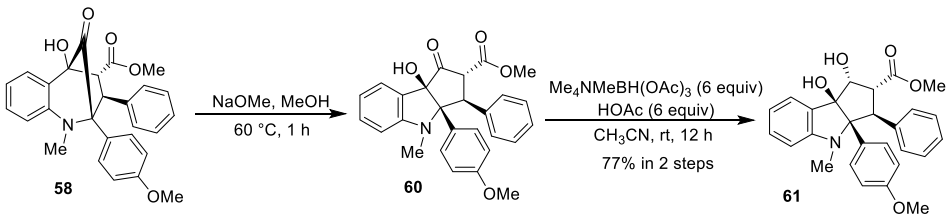

A 100 mL flame dried flask was charged with compound **58** (100 mg, 0.225 mmol, 1 equiv) and a stir bar. Then 20 mL of dry methanol were added to form a pale yellow solution. A sodium methoxide solution prepared from sodium metal (52 mg, 2.25 mmol, 10 equiv) and

10 mL of dry methanol was added to the solution of compound **58** and the resulting mixture was heated to 60 °C for 20 min before being quenched with saturated NH_4Cl aqueous (20 mL). The reaction was diluted and extracted with EtOAc (3 x 10 mL), then washed with saturated aqueous NaCl (20 mL), dried with anhydrous sodium sulfate, filtered, and concentrated *in vacuo*. Crude ^1H NMR analysis of the crude product **60** ($CDCl_3$, ratio = 2 : 1)showed a mixture of keto and enol tautomers in solution. To a 25 mL flame dried flask was added, crude product **60** (85 mg), tetramethylammonium triacetoxyborohydride (356 mg, 1.35 mmol, 6 equiv), acetic acid (65 μL, 1.13 mmol, 6 equiv) and 10 mL of dry acetonitrile. The resulting yellow solution was stirred for 14 h at room temperature before being quenched with sat. NH_4Cl solution (10 mL) and saturated aqueous potassium sodium tartrate tetrahydrate (Rochelle salt) (10 mL) to remove boron compounds by complexation. The mixture was then extracted with CH_2Cl_2 (3 x 5 mL) and the combined organic layers were washed with sat. $NaHCO_3$ (20 mL), dried over Na_2SO_4, filtered, and concentrated *in vacuo*. The crude product was purified by flash chromatography (gradient of EtOAc/hexane from 1:4 to 1:2) to afford pure *N*-Me-*aza*-rocaglate **61** (77 mg, 77% over 2 steps) as a white solid.

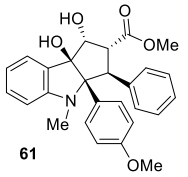

61

61: R_f = 0.12 (EtOAc / hexanes = 1 : 4); mp 85 - 86°C (CH_2Cl_2); IR (thin film): ν_{max} 3401, 2927, 1711, 1628, 1514, 1254, 1185, 1112, 1036, 773 cm^{-1}; ^1H NMR (500 MHz, $CDCl_3$) δ 7.47 (d, J = 7.5 Hz, 2H), 7.37 (d, J = 7.5 Hz, 1H), 7.22 (m, 4H), 6.83 (d, J = 9 Hz, 2H), 6.80 (d, J = 7.5 Hz, 1H), 6.60 (d, J = 9 Hz, 2H), 6.31 (d, J = 8 Hz, 1H), 4.77 (dd, J_1 = 9 Hz, J_2 = 10.5 Hz, 1H), 4.51 (d, J = 3 Hz, 1H), 3.89 (d, J = 10.5 Hz, 1H), 3.67 (s, 3H), 3.57 (s, 3H), 3.20

(dd, J_1 = 3 Hz, J_2 = 9 Hz, 1H), 2.61 (bs, 1H), 2.40 (s, 3H); ^{13}C NMR (125 MHz, $CDCl_3$) δ 172.4, 158.7, 151.2, 140.9, 130.3, 129.6, 129.4, 129.3, 128.2, 127.6, 126.4, 125.1, 117.7, 113.3, 106.0, 90.6, 85.9, 79.6, 55.0, 52.7, 52.6, 51.6, 29.6; HRMS-ESI (m/z): $[M+Na]^+$ calculated for $C_{27}H_{27}NO_5Na$ 468.1787, found 468.1779.

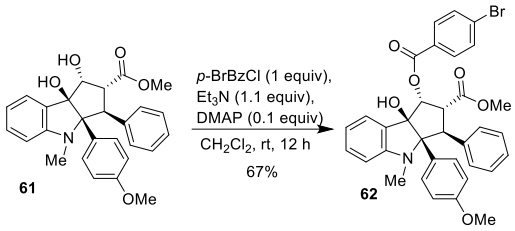

***Para*-Bromo benzoate 62**: A 25 mL flame dried flask was charged with compound **61** (52 mg, 0.12 mmol, 1 equiv), 4-bromobenzoyl chloride (27 mg, 0.12 mmol, 1 equiv), triethylamine (18 μL, 0.13 mmol, 1.1 equiv), and CH_2Cl_2 (10 mL). The resulting mixture was stirred at room temperature for 12 h before being quenched with sat. Na_2CO_3 solution. The mixture was then extracted with CH_2Cl_2 (3 x 5 mL) and the combined organic layers were washed with sat. NaCl (20 mL), dried over Na_2SO_4, filtered, and concentrated *in vacuo*. The crude material was purified by flash chromatography (gradient of EtOAc/hexane from 1:6 to 1:4) to afford compound **62** (48 mg, 67%) as a white solid.

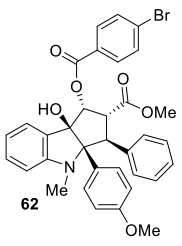

62: R_f = 0.41 (EtOAc / hexanes = 3 : 7); mp 218 - 219 °C (CH_2Cl_2); IR (thin film): ν_{max} 3491, 2952, 2837, 1733, 1161, 1511, 1269, 1121, 1038, 741 cm^{-1}; ^{1}H NMR (500 MHz, $CDCl_3$) δ 7.52 (d, J = 9 Hz, 2H), 7.45 (d, J = 9 Hz, 2H), 7.28 (d, J = 8 Hz, 2H), 7.21 (t, J = 9 Hz, 2H), 7.12 (m, 3H), 6.79 (d, J = 9 Hz, 2H), 6.62 (d, J = 9 Hz, 2H), 6,53 (t, J = 7.5 Hz, 1H), 6.41 (d, J = 7.5 Hz, 1H), 5.95 (d, J = 5.5 Hz, 1H), 4.72 (d, J = 10.5 Hz, 1H), 4.22 (dd, J_1 = 5.5 Hz, J_2 = 10.5

Hz, 1H), 3.67 (s, 3H), 3.55 (s, 3H), 3.12 (s, 3H), 1.85 (bs, 1H); ^{13}C NMR (125 MHz, $CDCl_3$) δ 170.5, 164.8, 158.6, 150.9, 138.5, 131.5, 131.0, 130.6, 130.4, 129.0, 128.5, 128.2, 128.1, 126.5, 126.2, 125.8, 125.0, 116.7, 113.1, 104.3, 93.0, 85.8, 80.6, 55.0, 54.4, 52.1, 52.0, 30.9; HRMS-ESI (m/z): $[M+H]^+$ calculated for $C_{34}H_{31}BrNO_6$ 628.1335, found 628.1348.

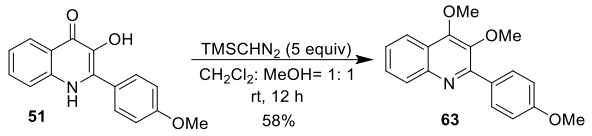

3,4-Dimethoxyquinoline 63: A flame dried test tube was charged with compound **51** (50 mg, 0.19 mmol, 1 equiv). Anhydrous CH_2Cl_2/ MeOH = 1:1 (5 mL) was added to afford a heterogeneous solution. Then, $TMSCHN_2$ (0.95 mL, 2M ether solution, 5 equiv) was added which led to slow dissolution of compound **51**. The resulting mixture was stirred at room temperature for 12 h before 10 mL of 10% aqueous AcOH solution was added dropwise to quench the reaction. The mixture was then extracted with CH_2Cl_2 (3 x 5 mL) and the combined organic layers were washed with sat. NaCl (20 mL), dried over Na_2SO_4, filtered, and concentrated *in vacuo*. Purification by silica gel column chromatography (gradient of EtOAc/hexane from 1:4 to 1:2) afforded compound **63** (32 mg, 58%) as a colorless oil.

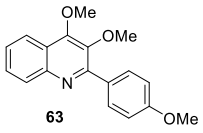

63: R_f = 0.44 (EtOAc / hexanes = 1 : 4); IR (thin film): ν_{max} 2936, 2837, 1607, 1515, 1378, 1252, 1177, 1107, 1045, 838 cm^{-1}; ^{1}H NMR (500 MHz, $CDCl_3$) δ 8.11 (d, J = 10.5 Hz, 1H), 8.06 (d, J = 10.5 Hz, 1H), 7.99 (d, J = 11 Hz, 2H), 7.62 (t, J = 10.5 Hz, 1H), 7.48 (t, J = 10.5 Hz, 1H), 7.02 (d, J = 11Hz, 2H), 4.24 (s, 3H), 3.88 (s, 3H), 3.67 (s, 3H); ^{13}C NMR (125 MHz, $CDCl_3$) δ 155.8,

154.1, 145.9, 142.4, 130.8, 130.6, 129.1, 128.5, 125.7, 123.9, 121.6, 113.6, 61.1, 60.8, 55.3; HRMS-ESI (m/z): $[M+H]^+$ calculated for $C_{18}H_{17}NO_3$ 296.1287, found 296.1287.

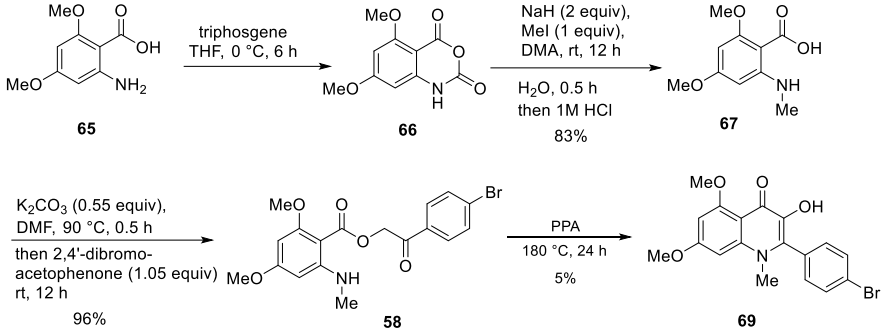

***N*-methyl-anthranilic acid 67**: To a flame dried 250 mL flask, dimethoxyanthranilic acid **65** (5.5 g, 27.9 mmol, 1 equiv) and 150 mL of anhydrous THF was added. After the resulting solution was cooled to 0 °C in an ice bath, triphosgene (2.81 g, 9.5 mmol, 0.34 equiv) was added and a precipitate formed immediately. The reaction mixture was warmed to room temperature and stirred overnight before being concentrated *in vacuo*. Then CH_2Cl_2 was added and the remaining solid was separated by filtration. The solid obtained (dimethoxy isatoic anhydride **66**) was washed with cold CH_2Cl_2, dried, and was then redissolved in 150 mL of dry DMA in a 250 mL flask. Then NaH (60 % dispersion in mineral oil) (2.23g, 55.8 mmol, 2 equiv) was added. The mixture was stirred for 10 min at room temperature before MeI (1.74 mL, 27.9 mmol, 1 equiv) was added. The reaction was stirred at room temperature for 10 h before 15 mL of H_2O was added to quench the reaction which was stirred at room temperature for 0.5 h to facilitate hydrolysis of the *N*-methyl isatoic anhydride to N-methyl anthranilic acid **67**. Then 1M aqueous HCl was added dropwise to acidify the reaction to pH 6 - 7. The mixture was extracted with 150 mL × 3 CH_2Cl_2, and the combined organic layers were washed with 150 mL × 3 H_2O to remove

the remaining DMA and was then washed with sat. NaCl (200 mL), dried over Na_2SO_4, filtered, and concentrated *in vacuo*. Purification by silica gel column chromatography (gradient of EtOAc/hexane from 1:4 to 1:2) afforded *N*-methyl dimethoxyanthranilic acid **67** (4.91 g 83%) as a white solid.

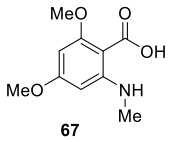

67

67: R_f = 0.32 (EtOAc / hexanes = 3 : 7); mp 131 - 133 °C (CH_2Cl_2); IR (thin film): ν_{max} 3322, 3202, 2948, 1686, 1620, 1414, 1223, 1154, 1049, 803 cm^{-1}; ^1H NMR (500 MHz, $CDCl_3$) δ 11.11 (s, 1H, OH), 8.88 (d, J = 5Hz, 1H, NH), 5.78 (s, 2H), 3.97 (s, 3H), 3.84 (s, 3H), 2.88 (d, J = 5 Hz, 3H); ^{13}C NMR (125 MHz, $CDCl_3$) δ 168.6, 164.6, 161.4, 155.9, 92.5, 88.1, 86.8, 56.6, 55.2, 29.8; HRMS-ESI (m/z): $[M+H]^+$ calculated for $C_{10}H_{13}NO_4$ 211.0845, found 211.0842.

***N*-Methyl dimethoxyanthranilate 68:** A 250 mL flame dried flask was charged with N-methyl dimethoxyanthranilic acid **67** (4.5 g, 31.3 mmol, 1 equiv), K_2CO_3 (1.62 g, 11.7 mmol, 0.55 equiv), 135 mL dry DMF and a stir bar. The reaction mixture was heated to 90 °C for 0.5 h before being cooled to room temperature. Then 2,4′-dibromoacetophenone (5.92 g, 21.3 mmol, 1 equiv) was added and the reaction mixture was stirred at room temperature overnight and added to ice water. After 5 min, compound **68** precipitated from the solution. The solid was filtered and dried. (If no precipitate was formed, extraction with CH_2Cl_2 can be used to obtain the crude product.) Purification by silica gel column chromatography (gradient of EtOAc/hexane from 1:4 to 1:1) afforded *N*-methyl dimethoxyanthranilate **68** (8.33g, 96%) as a white solid. Product recrystallization from MeOH was also found to be effective for purification of **68**: 150 mL MeOH was added to the crude solid product which was followed by heating

to 80 °C for 20 min before being cooled to 0 °C. Filtration and drying of the solid product afforded **68** 7.5 g (87% yield) product as a white solid.

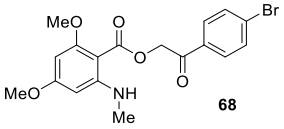

68

68: R_f = 0.36 (EtOAc / hexanes = 3 : 7); mp 126 - 127 °C (CH_2Cl_2); IR (thin film): ν_{max} 3396, 2937, 1698, 1587, 1416, 1261, 1159, 1104, 1009, 807 cm^{-1}; ^1H NMR (500 MHz, $CDCl_3$) δ 7.85 (d, J = 9 Hz, 2H), 7.54 (d, J = 9 Hz, 2H), 7.40 (d, J = 4 Hz, 1H, NH), 5.80 (d, J = 2 Hz, 1H), 5.76 (d, J = 2 Hz, 1H), 5.43 (s, 2H), 3.83 (s, 3H), 3.80 (s, 3H), 2.88 (d, J = 4 Hz, 3H); ^{13}C NMR (125 MHz, $CDCl_3$) δ 192.8, 167.3, 164.6, 163.0, 154.0, 133.1, 132.1, 129.5, 129.0, 95.4, 87.6, 87.4, 65.9, 56.0, 55.1, 30.1; HRMS-ESI (m/z): $[M+H]^+$ calculated for $C_{18}H_{19}BrNO_5$ 408.0447, found 408.0445.

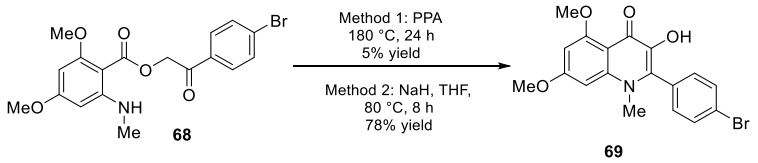

68 **69**

1-Methyl-2-(4-bromophenyl)-3-hydroxydimethoxyquinolinone 69:

Method 1: A 25 mL glass tube was charged with 10 g polyphoric acid (PPA). Subsequently, the PPA was heated up to 180 °C and the stickiness of PPA was reduced after the temperature was reached. Anthranilate **68** (0.2 g, 0.49 mmol, 1 equiv) and a magnetic stir bar was added. After 10 min all the solid was completely dissolved. The reaction mixture was kept heated at 180 °C for 24 hours before 80 mL ice water was added. The mixture was put on sonication for 2 hours until all the gummy oil was fully dissolved by water. The dark green solid was then filtered and collected. Purification by silica gel column chromatography (gradient of EtOAc/hexane from 1:2 to 1:1 to remove byproducts, then

acetone/CH_2Cl_2 from 1:2 to 1:1 to elute products) afforded *N*-Me-3-HQ **69** as a light yellow solid (9.3 mg, 5% yield).

Method 2: A 500 mL flame dried flask was charged with *N*-methyl dimethoxyanthranilate **68** (2 g, 4.9 mmol, 1 equiv), 250 mL dry THF and a stir bar. Then NaH (60 % dispersion in mineral oil) (0.17 g, 5.9 mmol, 1.2 equiv) was added to the solution at room temperature. The reaction mixture was heated to 80 °C for 8 h and was then cooled to 0 °C using an ice bath. Subsequently, the cold reaction mixture was added slowly at 0 °C to 400 mL of a sat. solution of NH_4Cl solution. Then 1 M aqueous HCl solution was added to acidify the mixture to pH = 6. The mixture was extracted 3 × 200 mL with CH_2Cl_2, the combined organic layers were washed with Sat. NaCl (20 mL), dried over Na_2SO_4, filtered, and concentrated *in vacuo*. Purification by silica gel column chromatography (gradient of EtOAc/hexane from 1:2 to 1:1 to remove byproducts, then acetone/CH_2Cl_2 from 1:2 to 1:1 to elute products) afforded compound **69** (1.5 g, 78%) as a light yellow solid.

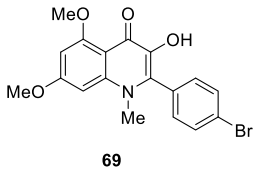

69

69: R_f = 0.41 (CH_2Cl_2 / acetone = 2 : 1); mp 192 - 193 °C (CH_2Cl_2); IR (thin film): ν_{max} 3401, 3268, 2939, 1617, 1581, 1489, 1458, 1301, 1265, 1166, 1092, 1013 cm^{-1}; ^1H NMR (500 MHz, $CDCl_3$) δ 7.66 (d, J = 8.5 Hz, 2H), 7.32 (d, J = 8.5 Hz, 2H), 6.35 (s, 2H), 3.99 (s, 3H), 3.92 (s, 3H), 3.48 (s, 3H); ^{13}C NMR (125 MHz, $CDCl_3$) δ 169.4, 162.9, 162.0, 143.5, 139.7, 132.2, 131.5, 130.8, 130.7, 123.7, 108.8, 93.7, 89.5, 56.3, 55.4, 38.1; HRMS-ESI (m/z): $[M+H]^+$ calculated for $C_{18}H_{17}BrNO_4$ 390.0341, found 390.0333.

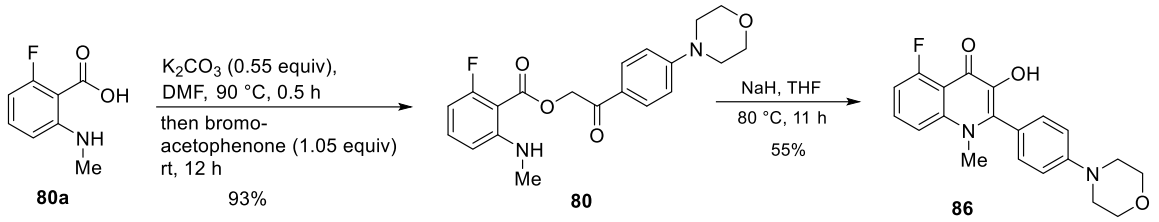

General Method for Preparation of Phenacyl Anthranilate: A 250 mL flame dried flask was charged with *N*-methyl anthranilic acid **80a** (1.0 g, 5.9 mmol, 1 equiv), K_2CO_3 (0.45 g, 3.25 mmol, 0.55 equiv), 65 mL dry DMF and a stir bar. The reaction mixture was heated to 90 °C for 0.5 h before being cooled to room temperature. Then bromoacetophenone (1.76 g, 6.2 mmol, 1.05 equiv) was added and the reaction mixture was stirred at room temperature overnight and added to ice water. After 5 min, compound **80** precipitated from the solution. The solid was filtered and dried. (If no precipitate was formed, extraction with CH_2Cl_2 can be used to obtain the crude product.) Purification by silica gel column chromatography (gradient of EtOAc/hexane from 1:4 to 1:1) afforded *N*-methyl phenacyl anthranilate **80** (2.04 g, 93%) as a white solid.

General Method for Preparation of 3-Hydroxyquinolinones: A 250 mL flame dried flask was charged with anthranilate **80** (2 g, 5.4 mmol, 1 equiv), 130 mL dry THF and a stir bar. Then NaH (60 % dispersion in mineral oil) (0.65 g, 16.1 mmol, 3 equiv) was added to the solution at room temperature. The reaction mixture was heated to 80 °C for 11 h and was then cooled to 0 °C using an ice bath. Subsequently, the cold reaction mixture was added slowly at 0 °C to 200 mL of a sat. solution of NH_4Cl solution. Then 1 M aqueous HCl solution was added to acidify the mixture to pH = 6. The mixture was extracted 3 × 200 mL with CH_2Cl_2, the combined organic layers were washed with Sat. NaCl (20 mL), dried over Na_2SO_4, filtered, and concentrated *in vacuo*. Purification by silica gel column

chromatography (gradient of EtOAc/hexane from 1:2 to 1:1 to remove byproducts, then acetone/CH_2Cl_2 from 1:2 to 1:1 to elute products) afforded compound **86** (1.04 g, 55%) as a light yellow solid.

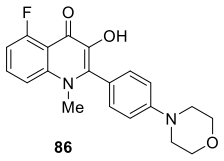

86

86: R_f = 0.32 (EtOAc / hexanes = 2 : 1); mp 230 °C decomposed (CH_2Cl_2); IR (thin film): ν_{max} 3510, 3032, 2951, 1736, 1609, 1457, 1291, 1209, 1071, 816, 737 cm^{-1}; ^1H NMR (500 MHz, $CDCl_3$) δ 1H NMR (500 MHz,) δ 8.01 (s, OH, 1H), 7.62 (m, 1H), 7.54 (d, J = 9.1 Hz, 1H), 7.29 (d, J = 8.3 Hz, 2H), 7.07 (d, J = 8.3 Hz, 2H), 7.03 (m, 1H), 3.75 (m, 4H), 3.52 (s, 3H), 3.21 (m, 4H); ^{13}C NMR (125 MHz, DMSO) δ 168.3, 162.1, 160.1, 151.6, 141.4, 140.5, 136.1, 131.7, 131.2, 122.2, 114.8, 113.5, 108.2, 66.5, 48.2, 38.5; HRMS-ESI (m/z): $[M+H]^+$ calculated for $C_{20}H_{20}FN_2O_3$ 354.1380, found 354.1377.

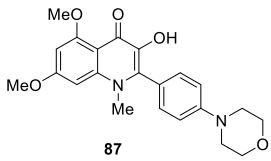

87

87: R_f = 0.26 (EtOAc / hexanes = 2 : 1); mp 210 °C decomposed (CH_2Cl_2); IR (thin film): ν_{max} 3502, 2966, 1690, 1628, 1480, 1310, 1250, 1060, 885, 726 cm^{-1}; ^1H NMR (500 MHz, $CDCl_3$) δ ^1H NMR (400 MHz,) δ 7.33 (d, J = 8.0 Hz, 2H), 7.02 (d, J = 8.0 Hz, 2H), 6.36 (d, J = 4.0 Hz, 2H), 3.99 (s, 3H), 3.91 (s, 3H), 3.88 (m, 4H), 3.52 (s, 3H), 3.25 (m, 4H); ^{13}C NMR (100 MHz, $CDCl_3$) δ 169.29, 162.53, 161.86, 151.50, 143.31, 139.94, 132.31, 130.84, 122.51, 115.05, 108.79, 93.50, 89.58, 66.80, 56.24, 55.41, 48.46, 38.09; HRMS-ESI (m/z): $[M+H]^+$ calculated for $C_{22}H_{25}N_2O_5$ 397.1763, found 397.1765.

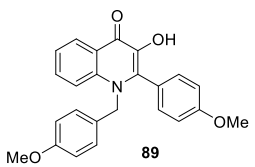

89

89: R_f = 0.28 (EtOAc / hexanes = 2 : 1); mp 216 °C decomposed (CH_2Cl_2); IR (thin film): ν_{max} 3518, 3092, 2968, 1625, 1576, 1444, 1419, 1310, 1243, 1157, 1088, 1007 cm^{-1}; ^1H NMR (400 MHz,

$CDCl_3$) δ 8.54 (d, J = 8.2 Hz, 1H), 7.51 (m, 1H), 7.38 (d, J = 8.2 Hz, 1H), 7.34 (t, J = 8.2 Hz, 1H), 7.27 (s, 1H), 6.96 (d, J = 8.2 Hz, 2H), 6.84 (d, J = 12.9 Hz, 2H), 6.79 (d, J = 12.9, 2H), 5.26 (s, 2H), 3.83 (s, 3H), 3.76 (s, 3H); ^{13}C NMR (100 MHz,) δ 170.10, 160.41, 158.87, 139.35, 138.80, 135.79, 131.59, 130.61, 128.29, 126.59, 126.23, 123.29, 123.10, 122.67, 117.15, 114.30, 55.30, 55.25, 51.38; HRMS-ESI (m/z): $[M+H]^+$ calculated for $C_{24}H_{22}NO_4$ 388.1549, found 388.1552.

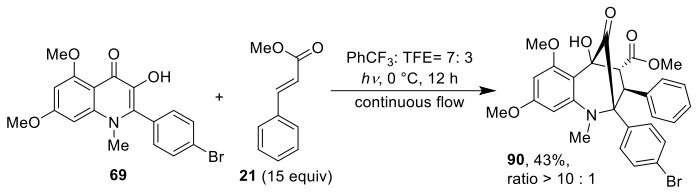

N-Methyl aglain ketone 90: The general procedure for (3+2) photocycloaddition using continuous photoflow system was used. Compound **69** (800 mg, 2.05 mmol, 1 equiv), methyl cinnamate **21** (4.99 g, 30.8 mmol, 15 equiv), 35 mL α,α,α-trifluorotoluene and 15 mL 2,2,2-trifluoroethanol were used for the reaction. The reaction mixture was purified by silica gel column chromatography (gradient of EtOAc/hexane 1:10 to first remove methyl cinnamate, then EtOAc/hexane from 1:4 to 1:2 to elute the product). Additional impurities were also removed by recrystallization from diethyl ether. Compound **90** (484 mg, 43%) was obtained as a white solid.

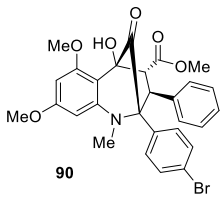

90: R_f = 0.29 (EtOAc / hexanes = 3 : 7); mp 172 - 173 °C (CH_2Cl_2); IR (thin film): ν_{max} 3510, 3032, 2951, 1736, 1609, 1457, 1291, 1209, 1071, 816, 737 cm^{-1}; ^1H NMR (500 MHz, $CDCl_3$) δ 7.21 (d, J = 8.5 Hz, 2H), 7.18 (d, J = 8.5 Hz, 2H), 6.98 (m, 3H), 6.81 (m, 3H), 6.15 (d, J = 2.5 Hz, 1H), 6.12 (d, J = 2.5 Hz, 1H), 5.62 (s, 1H, OH), 4.33 (d, J = 9.5 Hz, 1H),

3.82 (s, 3H), 3.78 (s, 3H), 3.56 (s, 3H), 3.36 (d, J = 9.5 Hz, 1H), 2.53 (s, 3H); ^{13}C NMR (125 MHz, $CDCl_3$) δ 206.6, 170.7, 161.4, 158.0, 148.4, 139.5, 134.0, 131.4, 130.7, 129.5, 128.1, 126.8, 121.4, 111.8, 99.4, 93.7, 82.1, 71.2, 56.0, 55.3, 52.6, 52.0, 41.4; HRMS-ESI (m/z): $[M+H]^+$ calculated for $C_{28}H_{27}BrNO_6$ 552.1022, found 552.1005.

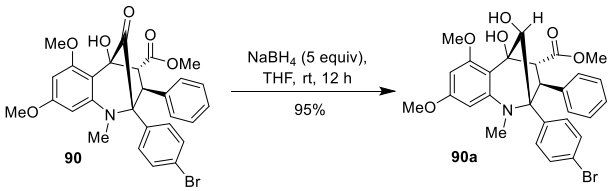

***N*-Me-*aza*-aglain 90a**: A flame-dried test tube was charged with *aza*-aglain ketone **90** (40 mg, 0.072mmol, 1.0 equiv) and 2.5 mL dry THF. Then $NaBH_4$ (13.7 mg, 0.36 mmol, 5.0 equiv) was added. The resulting mixture was stirred at room temperature for 12 h before 5 mL of a sat. NH_4Cl aqueous solution was added. The reaction mixture was extracted with 3 × 2 mL CH_2Cl_2, and the combined organic layers were washed with sat. NaCl (10 mL), dried over anhydrous Na_2SO_4, filtered, and concentrated *in vacuo*. Purification by silica gel column chromatography (gradient of EtOAc/hexane from 1:5 to 1:2) afforded compound **90a** (38 mg, 95%) as a white solid.

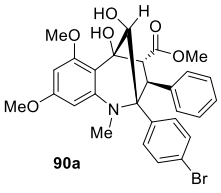

90a: R_f = 0.4 (EtOAc / hexanes = 1 : 1); mp 235-236 °C (CH_2Cl_2); IR (thin film): ν_{max} 3496, 2949, 1735, 1610, 1583, 1456, 1343, 1244, 1207, 1072, 1010, 734 cm^{-1}; ^{1}H NMR (500 MHz, $CDCl_3$) 7.19 (d, J = 9 Hz, 2H), 7.12 (d, J = 9 Hz, 2H), 6.98 (m, 3H), 6.73 (m, 2H), 6.15 (d, J = 2.5 Hz, 1H), 6.02 (d, J = 2.5 Hz, 1H), 6.015 (s, 1H, OH), 4.67 (d, J = 5 Hz, 1H), 4.00 (d, J = 9.75 Hz, 1H), 3.85 (s, 3H), 3.81 (s, 3H), 3.56 (s, 3H), 3.06 (d, J = 9.75 Hz, 1H), 2.72 (s, 3H), 2.61 (d, J = 5 Hz, 1H); ^{13}C NMR (125 MHz, $CDCl_3$) δ 166.5, 155.9, 154.6,

144.9, 136.8, 132.9, 127.2, 125.8, 123.3, 121.4, 116.3, 99.0, 91.3, 85.6, 75.9, 72.5, 70.2, 66.0, 58.9, 51.8, 50.9, 50.4, 46.9, 36.7; HRMS-ESI (m/z): $[M+H]^+$ calculated for $C_{28}H_{29}BrNO_6$ 554.1178, found 554.1163.

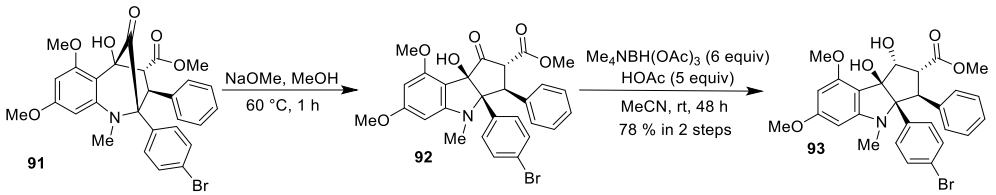

***N*-Me-Br-*aza*-rocaglate 93**: A 100 mL flame dried flask was charged with compound **91** (200 mg, 0.362 mmol, 1 equiv) and a stir bar. Then 20 mL of dry methanol were added to form a pale yellow solution. A sodium methoxide solution prepared from sodium metal (84 mg, 3.6 mmol, 10 equiv) and 10 mL of dry methanol was added to the solution of compound **91** and the resulting mixture was heated to 60 °C for 20 min before being quenched with saturated NH_4Cl aqueous (20 mL). The reaction was diluted and extracted with EtOAc (3 x 10 mL), then washed with saturated aqueous NaCl (20 mL), dried with anhydrous sodium sulfate, filtered, and concentrated *in vacuo*. Crude ^1H NMR analysis of the crude product **92** ($CDCl_3$, ratio = 2 : 1) showed a mixture of keto and enol tautomers in solution. To a 25 mL flame dried flask was added, crude product **92** (197 mg), tetramethylammonium triacetoxyborohydride (571 mg, 2.2 mmol, 6 equiv), acetic acid (125 μL, 2.17 mmol, 6 equiv) and 15 mL of dry acetonitrile. The resulting yellow solution was stirred for 14 h at room temperature before being quenched with sat. NH_4Cl solution (10 mL) and saturated aqueous potassium sodium tartrate tetrahydrate (Rochelle salt) (10 mL) to remove boron compounds by complexation. The mixture was then extracted with CH_2Cl_2 (3 x 5 mL) and the combined organic layers were washed with sat. $NaHCO_3$ (20

mL), dried over Na_2SO_4, filtered, and concentrated *in vacuo*. The crude product was purified by flash chromatography (gradient of EtOAc/hexane from 1:5 to 1:2) to afford pure *N*-Me-*aza*-rocaglate **93** (157 mg, 78% from **91**) as a white solid.

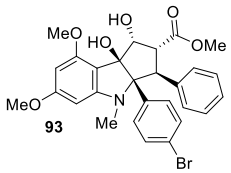

93

93: R_f =0.36 (EtOAc / hexanes = 1 : 1); mp 217 - 219 °C (CH_2Cl_2); IR (thin film): ν_{max} 3534, 2950, 1712, 1618, 1500, 1252, 1210, 1150, 1079, 736 cm^{-1}; ^1H NMR (500 MHz, $CDCl_3$) δ 7.40 (d, J = 13.5 Hz, 2H), 7.19 (m, 5H), 6.92 (d, J = 9 Hz, 2H), 5.94 (d, J = 2 Hz, 1H), 5.61 (d, J = 2 Hz, 1H), 4.78 (dd, J_1 = 7 Hz, J_2 = 9 Hz, 1H), 4.46 (d, J = 5 Hz, 1H), 3.92 (d, J = 9 Hz, 1H) 3.88 (s, 3H), 3.80 (s, 3H), 3.67 (s, 1H, OH), 3.63 (s, 3H), 3.33 (dd, J_1 = 5 Hz, J_2 = 7 Hz, 1H), 2.44 (s, 3H); ^{13}C NMR (125 MHz, $CDCl_3$) δ 172.3, 163.7, 157.4, 152.9, 140.1, 134.5, 130.7, 130.3, 129.6, 128.2, 126.5, 121.4, 106.1, 91.5, 88.3, 87.0, 86.2, 81.2, 55.7, 55.4, 52.9, 52.7, 51.7, 30.0; HRMS-ESI (m/z): $[M+H]^+$ calculated for $C_{28}H_{29}BrNO_6$ 554.1178, found 554.1188.

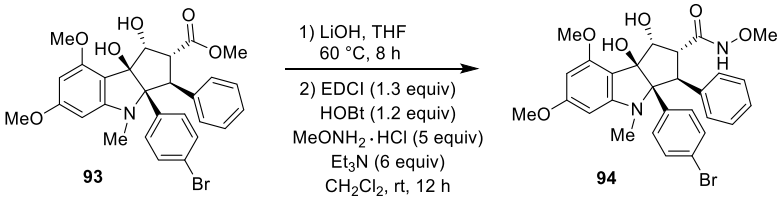

Hydroxamate 94: To a flame-dried test tube was added *N*-Me-Br-*aza*-rocaglate **93** (30.0 mg, 0.05 mmol, 1.0 equiv), LiOH (6.4 mg, 0.27 mmol, 5 equiv), and 2.5 mL of anhydrous THF. The mixture was heated to 65 °C for 12 h. Subsequently, after the reaction was cooled to room temperature, 1 M HCl (5 mL) was added to acidify the solution (pH = 6). After extraction with 3 × 2 mL CH_2Cl_2, the combined organic layers were washed with sat. NaCl (10 mL), dried over Na_2SO_4, filtered, and concentrated *in vacuo*. The resulting *aza*-

rocaglaic acid was subjected to the next step without further purification. To a flame-dried test tube was added the acid and 2.5 mL of dry CH_2Cl_2, methoxyamine hydrochloride (22.6 mg, 0.27 mmol, 5 equiv), Et_3N (45 μL, 0.32 mmol, 6 equiv), HOBt (8.8 mg, 0.065 mmol, 1.2 equiv), and EDCI (13.5 mg, 0.07 mmol, 1.3 equiv). The resulting mixture was sonicated for 3 min to dissolve the methoxyamine hydrochloride before being stirred at room temperature for 12 h. The 1 mL 1M HCl and 5 mL sat. NaCl was added to quench the reaction. After being extracted with 3 × 2 mL CH_2Cl_2, the combined organic layers were washed with sat. NaCl (10 mL), dried over anhydrous Na_2SO_4, filtered, and concentrated *in vacuo*. Purification by preparative thin layer chromatography (EtOAc/ CH_2Cl_2 = 1 : 2 with 5% MeOH) afforded hydoxamate **94** (15.8 mg, 51% over 2 steps) as a white solid.

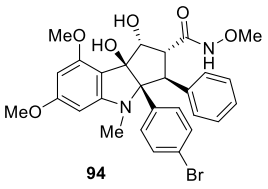

94

94: R_f = 0.27 (EtOAc / CH_2Cl_2 = 1 : 1); mp 238 - 239 °C (CH_2Cl_2); IR (thin film): ν_{max} 3372, 2933, 1615, 1500, 1254, 1149, 1076, 707 cm^{-1}; ^1H NMR (500 MHz, $CDCl_3$) δ 9.50 (s, 1H, NH), 7.41 (d, J = 7.5 Hz, 2H), 7.20 (d, J = 8.5 Hz, 2H), 7.19 (m, 3H), 6.89 (d, J = 8.5 Hz, 2H), 5.91 (d, J = 1.5 Hz, 1H), 5.60 (d, J = 1.5 Hz, 1H), 4.97 (d, J = 7 Hz, 1H), 4.68 (d, J = 2.5 Hz, 1H), 3.91 (s, 3H), 3.78 (s, 3H), 3.51 (s, 1H, OH), 3.44 (s, 3H), 3.15 (s, 1H, OH), 3.06 (dd, J_1 = 7 Hz, J_2 = 2.5 Hz, 1H), 2.41 (s, 3H); ^{13}C NMR (125 MHz, $CDCl_3$) δ 167.6, 164.1, 156.5, 153.2, 141.3, 135.3, 130.5, 130.4, 129.7, 128.2, 126.4, 121.4, 105.3, 91.2, 87.6, 86.8, 85.3, 80.9, 64.1, 55.54, 55.49, 52.7, 51.0, 29.4; HRMS-ESI (m/z): $[M+H]^+$ calculated for $C_{28}H_{30}BrN_2O_6$ 569.1278, found 569.1275.

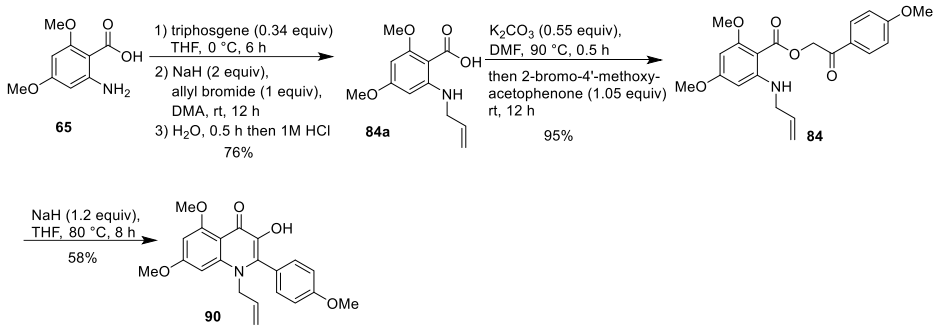

***N*-allyl-dimethoxyanthranilic acid 84a:** To a flame dried 250 mL flask, dimethoxyanthranilic acid **65** (5.5 g, 27.9 mmol, 1 equiv) and 150 mL of anhydrous THF was added. After the resulting solution was cooled to 0 °C in an ice bath, triphosgene (2.81 g, 9.5 mmol, 0.34 equiv) was added and a precipitate formed immediately. The reaction mixture was warmed to room temperature and stirred overnight before being concentrated *in vacuo*. Then CH_2Cl_2 was added and the remaining solid was separated by filtration. The solid obtained (dimethoxy isatoic anhydride) was washed with cold CH_2Cl_2, dried, and was then redissolved in 150 mL of dry DMA in a 250 mL flask. Then NaH (60 % dispersion in mineral oil) (2.23g, 55.8 mmol, 2 equiv) was added. The mixture was stirred for 10 min at room temperature before MeI (1.74 mL, 27.9 mmol, 1 equiv) was added. The reaction was stirred at room temperature for 10 h before 15 mL of H_2O was added to quench the reaction which was stirred at room temperature for 0.5 h to facilitate hydrolysis of the *N*-methyl isatoic anhydride to *N*-allyl anthranilic acid sodium salt. Then 1M aqueous HCl was added dropwise to acidify the reaction to pH 6 – 7 at 0 °C (high pH would cause decomposition of the product by decarboxylation to afford the *N*-allyl aniline). The mixture was extracted with 150 mL × 3 CH_2Cl_2, and the combined organic layers were washed with 150 mL × 3 H_2O to remove the remaining DMA and was then washed with sat. NaCl (200 mL), dried

over Na_2SO_4, filtered, and concentrated *in vacuo*. Purification by silica gel column chromatography (gradient of EtOAc/hexane from 1:6 to 1:4) afforded *N*-allyl dimethoxyanthranilic acid **84a** (5.0 g, 76 % yield) as a pale yellow oil.

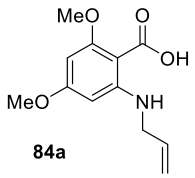

84a

84a: R_f = 0.39 (EtOAc / hexanes = 3 : 7); IR (thin film): ν_{max} 3303, 2947, 2844, 1681, 1614, 1455, 1354, 1220, 1146, 923, 807 cm^{-1}; ^1H NMR (500 MHz, $CDCl_3$) δ 11.52 (s, 1H, OH), 9.08 (s, 1H, NH), 5.88 (ddt, J_1 = 17 Hz, J_2 = 10.5 Hz, J_3 = 5.5 Hz, 1H), 5.76 (s, 1H), 5.75 (s, 1H), 5.24 (d, J = 17 Hz, 1H), 5.14 (d, J = 10.5 Hz, 1H), 3.93 (s, 3H), 3.81 (t, J = 5.5 Hz, 2H), 3.76 (s, 3H); ^{13}C NMR (125 MHz, $CDCl_3$) δ 168.6, 164.5, 161.3, 154.8, 134.2, 116.1, 92.6, 89.1, 87.0, 56.6, 55.2, 45.5; HRMS-ESI (m/z): $[M+H]^+$ calculated for $C_{12}H_{15}NO_4$ 237.1001, found 237.997.

***N*-Allyl dimethoxyanthranilate 84:** A 250 mL flame dried flask was charged with *N*-allyl dimethoxyanthranilic acid **84a** (5.0 g, 21 mmol, 1 equiv), K_2CO_3 (1.6 g, 11.6 mmol, 0.55 equiv), 135 mL dry DMF and a stir bar. The reaction mixture was heated to 90 °C for 0.5 h before being cooled to room temperature. Then 2-bromo-4′-methoxyacetophenone (5.1 g, 22.13 mmol, 1.05 equiv) was added and the reaction mixture was stirred at room temperature overnight and added to ice water. After 5 min, compound **84** precipitated from the solution. The solid was filtered and dried. (If no precipitate was formed, extraction with CH_2Cl_2 can be used to obtain the crude product.) Purification by silica gel column chromatography (gradient of EtOAc/hexane from 1:6 to 1:2) afforded *N*-allyl dimethoxyanthranilate **84** (7.76 g, 96%) as a white solid.

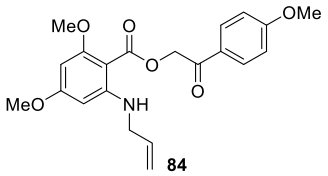

84

84: R_f = 0.35 (EtOAc / hexanes = 1 : 2); mp 95-96 °C (CH_2Cl_2); IR (thin film): ν_{max} 3370, 2937, 1683, 1602, 1459, 1233, 1155, 1106, 1021, 806 cm^{-1}; ^1H NMR (500 MHz, $CDCl_3$) δ 7.96 (d, J = 9 Hz, 2H), 7.54 (t, J = 5 Hz, 1H, NH), 6.96 (d, J = 9 Hz, 2H), 5.95 (m, 1H), 5.81 (d, J = 2 Hz, 1H), 5.79 (d, J = 2 Hz, 1H), 5.48 (s, 2H), 5.30 (ddd, J_1 = 1.5 Hz, J_2 = 3 Hz, J_3 = 17 Hz, 1H), 5.17 (ddd, J_1 = 1.5 Hz, J_2 = 3 Hz, J_3 = 10.5 Hz, 1H), 3.87 (s, 3H), 3.86 (tdd, J_1 = 5 Hz, J_2 = J_3 = 1.5 Hz, 2H), 3.80 (s, 3H), 3.79 (s, 3H); ^{13}C NMR (125 MHz, $CDCl_3$) δ 191.8, 167.1, 164.2, 164.0, 162.7, 152.4, 134.9, 130.3, 127.4, 116.0, 114.0, 96.5, 88.7, 87.6, 65.8, 56.0, 55.0, 46.0; HRMS-ESI (m/z): $[M+H]^+$ calculated for $C_{21}H_{24}NO_6$ 386.1604, found 386.1595.

***N*-Allyl-3-HQ 90:** A 500 mL flame dried flask was charged with *N*-allyl dimethoxyanthranilate **84** (2.4 g, 6.2 mmol, 1 equiv), 200 mL dry THF and a stir bar. Then NaH (60 % dispersion in mineral oil) (0.747 g, 18.7 mmol, 3 equiv) was added to the solution at room temperature. The reaction mixture was heated to 80 °C for 8 h and was then cooled to 0 °C using an ice bath. Subsequently, the cold reaction mixture was added slowly at 0 °C to 400 mL of a sat. solution of NH_4Cl solution. Then 1 M aqueous HCl solution was added to acidify the mixture to pH = 6. The mixture was extracted 3 × 200 mL with CH_2Cl_2, the combined organic layers were washed with Sat. NaCl (20 mL), dried over Na_2SO_4, filtered, and concentrated *in vacuo*. Purification by silica gel column chromatography (gradient of EtOAc/hexane from 1:2 to 1:1 to remove byproducts, then acetone/CH_2Cl_2 from 1:5 to 1:3 to elute products) afforded compound **90** (1.32 g, 58%) as a light yellow solid.

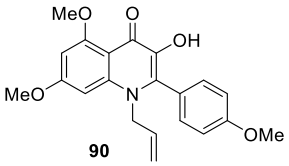

90

90: R_f = 0.33 (CH_2Cl_2 / acetone = 2 : 1); mp 159-161 °C (CH_2Cl_2); IR (thin film): ν_{max} 3268, 2936, 2839, 1579, 1508, 1239, 1205, 1165, 1033, 731 cm^{-1}; ^1H NMR (500 MHz, $CDCl_3$) δ 7.34 (d, J = 8.5 Hz, 2H), 7.01 (d, J = 8.5 Hz, 2H), 6.37 (d, J = 2 Hz, 1H), 6.33 (d, J = 2 Hz, 1H), 5.82 (m, 1H), 5.26 (d, J = 10.5 Hz, 1H), 4.98 (d, J = 17 Hz, 1H), 4.54 (s, 2H), 3.99 (s, 3H), 3.85 (s, 6H); ^{13}C NMR (125 MHz, $CDCl_3$) δ 169.5, 162.5, 161.9, 160.3, 142.6, 139.9, 132.2, 132.0, 130.8, 123.8, 117.6, 114.2, 109.0, 93.7, 90.6, 56.3, 55.34, 55.29, 51.5; HRMS-ESI (m/z): $[M+H]^+$ calculated for $C_{21}H_{22}NO_5$ 368.1498, found 368.1491.

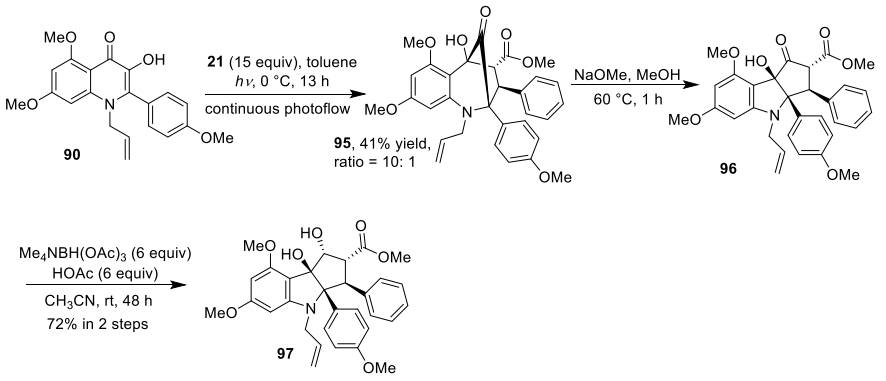

***N*-Me-Br-*aza*-rocaglate 97**: In a 200 mL flame dried flask, *N*-allyl-3-HQ **90** (500 mg, 1.36 mmol, 1 equiv), methyl cinnamate **21** (3.31 g, 20.4 mmol, 15 equiv), 40 mL toluene, were added. After degassing with argon for 10 min in a sonicator, the reaction flask was connected to the continuous photoflow reactor. After the solvent pump started, nitrogen gas was bubbled into the reaction mixture for another 10 min to further purge the remaining air out of the reaction system. The reaction mixture cooled to 0 °C and was kept circulating and irradiated (Rayonet, λ > 330 nm) at 0 °C for 13 h. We also found that compound **95** could undergo the ketol rearrangement itself, so purification by flash silica gel column

chromatography (gradient of EtOAc / hexane 1:10 to remove methyl cinnamate first, then EtOAc / hexane 1 : 5 to 1 : 4) afforded crude compound **95** (296 mg, 41% combined with **96**) which was subjected to the next step directly.

A 100 mL flame dried flask was charged with crude compound **95** (296 mg, 0.56 mmol, 1 equiv) and a stir bar. Then 20 mL of dry methanol were added to form a pale yellow solution. A sodium methoxide solution prepared from sodium metal (129 mg, 6.6 mmol, 10 equiv) and 10 mL of dry methanol was added to the solution of compound **95** and the resulting mixture was heated to 50 °C for 20 min before being quenched with saturated NH_4Cl aqueous (20 mL). The reaction was diluted and extracted with EtOAc (3 x 10 mL), then washed with saturated aqueous NaCl (20 mL), dried with anhydrous sodium sulfate, filtered, and concentrated *in vacuo*, which was subjected to next step without any further purification. To a 25 mL flame dried flask was added, crude product **96** (120 mg), tetramethylammonium triacetoxyborohydride (882 mg, 3.4 mmol, 6 equiv), acetic acid (192 μL, 3.4 mmol, 6 equiv) and 15 mL of dry acetonitrile. The resulting yellow solution was stirred for 14 h at room temperature before being quenched with sat. NH_4Cl solution (10 mL) and saturated aqueous potassium sodium tartrate tetrahydrate (Rochelle salt) (10 mL) to remove boron compounds by complexation. The mixture was then extracted with CH_2Cl_2 (3 x 5 mL) and the combined organic layers were washed with sat. $NaHCO_3$ (20 mL), dried over Na_2SO_4, filtered, and concentrated *in vacuo*. The crude product was purified by flash chromatography (gradient of EtOAc/hexane from 1:5 to 1:2) to afford pure *N*-allyl-*aza*-rocaglate **97** (213 mg, 72% from **79**) as a white solid.

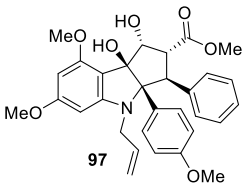

97: R_f = 0.33 (EtOAc / hexanes = 1 : 1); mp 86 - 88 °C (CH_2Cl_2); IR (thin film): ν_{max} 3525, 2951, 1744, 1610, 1512, 1463, 1249, 1151, 1039, 736 cm^{-1}; ^1H NMR (500 MHz, $CDCl_3$) δ 7.43 (d, J = 7.5 Hz, 2H), 7.19 (t, J = 7.5 Hz, 2H), 7.12 (m, 1H), 6.95 (d, J = 9 Hz, 2H), 6.61 (d, J = 9 Hz, 2H), 5.90 (d, J = 1.75 Hz, 1H), 5.72 (d, J = 1.75, 1H), 5.64 (m, 1H), 5.31 (dd, J_1 = 17.25 Hz, J_2 = 1.25 Hz, 1H), 5.15 (dd, J_1 = 10.25 Hz, J_2 = 1.25 Hz, 1H), 4.77 (m, 1H), 4.60 (d, J = 8.5 Hz, 1H), 3.84 (s, 3H), 3.79 (s, 3H), 3.76 (m, 2H), 3.69 (dd, J_1 = 8.5 Hz, J_2 = 5.5 Hz, 1H), 3.68 (s, 3H), 3.65 (s, 3H), 3.23 (d, J = 4 Hz, 1H, OH), 2.98 (s, 1H, OH); ^{13}C NMR (125 MHz, $CDCl_3$) δ 172.4, 163.5, 158.5, 157.5, 153.1, 139.8, 134.4, 130.5, 129.4, 128.03, 127.98, 126.4, 116.8, 112.6, 104.6, 92.5, 87.7, 87.1, 87.0, 80.2, 55.5, 55.3, 55.0, 54.6, 53.0, 51.8, 48.8. HRMS-ESI (m/z): $[M+H]^+$ calculated for $C_{31}H_{34}NO_7$ 532.2342, found 532.2347.

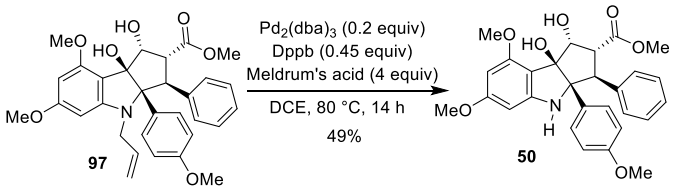

***N*-H-*aza*-rocaglate 50:** In a flame-dried test tube, *N*-allyl-*aza*-rocaglate **97** (20 mg, 0.038 mmol, 1 equiv) and Meldrum's acid (21.7 mg, 0.15 mmol, 4 equiv) was dissolved in DCE (1 mL). To another flame-dried test tube was added $Pd_2(dba)_3$ (6.89 mg, 7.52 μmol, 0.2 equiv) and 1,4- *bis*(diphenyl-phosphino)butane (dppb, 7.22 mg, 0.017 mmol, 0.45 equiv) in DCE (2 mL). The test tube was then evacuated and backfilled with argon for three times and stirred for 0.5 h at room temperature. The two solutions were combined into one test tube by cannulation then sparged with argon for 10 min with sonication. The reaction was

heated to 80 °C. After 14 h, the reaction was cooled to room temperature and quenched with saturated Na_2CO_3 aqueous solution (3 mL). Then 5 × 2 mL CH_2Cl_2 was used for extraction, and the combined organic layer was washed with sat. NaCl (20 mL), dried over Na_2SO_4, filtered, and concentrated *in vacuo*. Purification by silica gel column chromatography (gradient of EtOAc / hexane from 1 : 4 to 1 : 1 to elute the product) afforded *N*-H-*aza*-rocaglate **50** (9.1 mg, 49%) as a colorless oil.

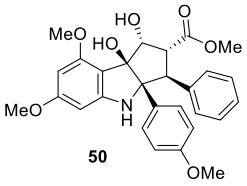

50

50: R_f = 0.27 (EtOAc / hexanes = 1 : 1); IR (thin film): ν_{max} 3466, 2927, 2849, 1743, 1614, 1515, 1456, 1218, 1202, 1151, 1034 cm^{-1}; ^1H NMR (500 MHz, $CDCl_3$) δ 7.08 (m, 3H), 6.96 (d, J = 18.5 Hz, 2H), 6.71 (d, J = 18.5 Hz, 2H), 6.69 (m, 2H), 6.09 (d, J = 1.5 Hz, 1H), 6.01 (d, J = 1.5 Hz, 1H), 5.11 (d, J = 7.5 Hz, 1H), 4.72 (bs, 1H, OH), 4.16 (bs, 1H, OH), 4.01 (d, J = 14 Hz, 1H), 3.88 (s, 3H), 3.85 (dd, J_1 = 14 Hz, J_2 = 7.5 Hz, 1H), 3.81 (s, 3H), 3.75 (s, 3H), 3.61 (s, 3H); ^{13}C NMR (125 MHz, $CDCl_3$) δ 170.7, 163.8, 158.4, 157.2, 150.9, 137.4, 129.7, 128.1, 127.89, 127.87, 126.8, 112.8, 108.5, 94.4, 90.9, 89.6, 80.9, 80.7, 56.4, 55.6, 55.5, 55.2, 51.7, 51.3. HRMS-ESI (m/z): $[M+H]^+$ calculated for $C_{28}H_{29}NO_7$ 492.2022, found 492.2029.

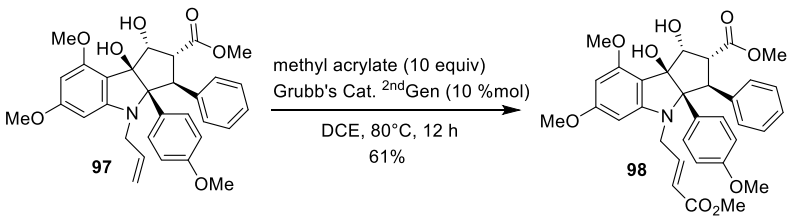

***Aza*-rocaglate 98:** To a flame-dried test tube was added *N*-allyl-*aza*-rocaglate **97** (35 mg, 0.066 mmol, 1 equiv) and methyl acrylate (60 μL, 0.66 mmol, 10 equiv) in dry DCE (2 mL). The test tube was then evacuated and backfilled with argon for three times.

Then, in a glove box, 2nd Generation Grubb's Catalyst (5.6 mg, 6.6 μmol, 0.1 equiv) was added to another flame-dried test tube and the former reaction solution was cannulated into the test tube. Then an additional 1 mL of dry DCE was used to wash the residue and the solution was combined together by cannulation. The reaction mixture was heated to 80 °C in darkness for 12 h before being cooled down to room temperature. Subsequently, 5 mL of brine was added to quench the reaction. After extraction with 3 × 2 mL CH_2Cl_2, the combined organic layers were washed with sat. NaCl solution (5 mL), dried over Na_2SO_4, filtered, and concentrated *in vacuo*. Purification by silica gel column chromatography (EtOAc / hexanes 3 : 2) afforded compound **98** (23.6 mg, 61%) as a colorless oil.

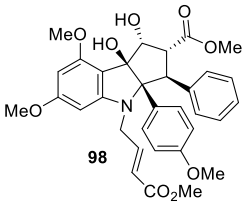

98

98: R_f = 0.25 (EtOAc / hexanes = 1 : 1); IR (thin film): ν_{max} 3525, 2951, 1718, 1610, 1513, 1462,1351, 1251, 1152, 1040 cm^{-1}; ^1H NMR (500 MHz, $CDCl_3$) δ 7.34 (d, J = 7.5 Hz, 2H), 7.20 (t, J = 7.5 Hz, 2H), 7.14 (m, 1H), 6.94 (d, J = 9 Hz, 2H), 6.69 (m, 1H), 6.60 (d, J = 9 Hz, 2H), 4.80 (dd, $J_1 = J_2 = 7$ Hz, 1H), 4.51 (d, J = 7 Hz, 1H), 3.865 (s, 3H), 3.864 (m, 1H), 3.78 (s, 3H), 3.73 (m, 1H), 3.672 (s, 3H), 3.665 (s, 3H), 3.65 (s, 3H), 3.57 (d, J = 7 Hz, 1H, OH), 3.55 (dd, $J_1 = J_2 = 7$ Hz, 1H), 3.25 (s, 1H, OH); ^{13}C NMR (125 MHz, $CDCl_3$) δ 172.5, 166.4, 163.5, 158.7, 157.6, 152.3, 144.3, 139.9, 130.4, 129.4, 128.2, 128.0, 126.5, 121.7, 112.8, 105.5, 91.9, 88.3, 87.3, 86.9, 80.5, 55.6, 55.4, 54.9, 54.3, 52.8, 51.9, 51.4, 46.8. HRMS-ESI (m/z): $[M+Na]^+$ calculated for $C_{33}H_{35}NO_9Na$ 612.2210, found 612.2214.

X-ray Crystallographic Data for Compound **62:**

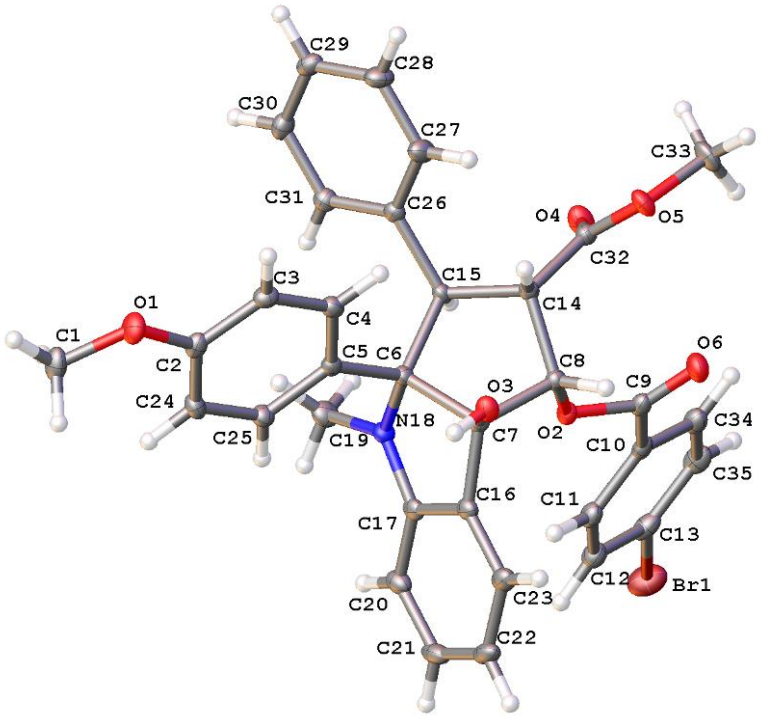

Crystals of compound **62** suitable for X-ray analysis were obtained by slow evaporation from hexanes/CH_2Cl_2. Crystallographic data have been deposited with the Cambridge Cystallograhic Data Centre (CCDC# 1457719). Copies of the data can be obtained free of charge on application to the CCDC, 12 Union Road, Cambridge CB21EZ, UK (fax: (+44)-1223-336-033; e-mail: deposit@ccdc.cam.ac.uk).

Computing details: Data collection: *APEX2* (Bruker, 2006); cell refinement: *SAINT* (Bruker, 2006); data reduction: *SAINT* (Bruker, 2006); program(s) used to solve structure: SHELXT (Sheldrick, 2015); program(s) used to refine structure: *SHELXL2014*/7 (Sheldrick, 2014); molecular graphics: Olex2 (Dolomanov *et al.*, 2009); software used to prepare material for publication: Olex2 (Dolomanov *et al.*, 2009).

Crystal Data:

$C_{34}H_{30}BrNO_6$	$Z = 2$
$M_r = 628.50$	$F(000) = 648$
Triclinic, $P\bar{1}$	$D_x = 1.484$ Mg m^{-3}
$a = 9.979$ (4) Å	Cu $K\alpha$ radiation, $\lambda = 1.54178$ Å
$b = 11.195$ (4) Å	Cell parameters from 9870 reflections
$c = 13.087$ (5) Å	$\theta = 4.1–74.4°$
$\alpha = 77.795$ (15)°	$\mu = 2.40$ mm^{-1}
$\beta = 81.273$ (19)°	$T = 100$ K
$\gamma = 83.202$ (16)°	Block, colorless
$V = 1406.8$ (10) Å^3	0.2 × 0.1 × 0.08 mm

Data collection:

Bruker D8 Quest diffractometer	5750 independent reflections
Radiation source: Microfocus sealed tube	5262 reflections with $I > 2\sigma(I)$
Bruker MX	$R_{int} = 0.032$
ω and phi scans	$\theta_{max} = 74.8°$, $\theta_{min} = 3.5°$
Absorption correction: multi-scan *SADABS* (Bruker, 2006)	$h = -12 \square 12$
$T_{min} = 0.658$, $T_{max} = 0.754$	$k = -13 \square 13$
41363 measured reflections	$l = -16 \square 16$

Refinement:

Refinement on F^2	0 restraints

Least-squares matrix: full	Hydrogen site location: mixed
$R[F^2 > 2\sigma(F^2)] = 0.031$	H atoms treated by a mixture of independent and constrained refinement
$wR(F^2) = 0.074$	$w = 1/[\sigma^2(F_o^2) + (0.0298P)^2 + 1.3237P]$ where $P = (F_o^2 + 2F_c^2)/3$
$S = 1.04$	$(\Delta/\sigma)_{max} = 0.001$
5750 reflections	$\Delta\rangle_{max} = 0.62$ e Å^{-3}
373 parameters	$\Delta\rangle_{min} = -0.65$ e Å^{-3}

Special details

Geometry: All esds (except the esd in the dihedral angle between two l.s. planes) are estimated using the full covariance matrix. The cell esds are taken into account individually in the estimation of esds in distances, angles and torsion angles; correlations between esds in cell parameters are only used when they are defined by crystal symmetry. An approximate (isotropic) treatment of cell esds is used for estimating esds involving l.s. planes.

Refinement: CheckCIF Alert and Discussion:

Alert level B PLAT420_ALERT_2_B D—H Without Acceptor O3 – H3. Please Check Discussion: While H3 does not have a strong H-bond acceptor due to packing constraints, there is a close OH-pi inter-action with C22 with the H3 – C22 distance at 2.590 Angstroms.

Fractional atomic coordinates and isotropic or equivalent isotropic displacement parameters (Å²)

	x	*y*	*z*	U_{iso}*/U_{eq}
Br1	0.54030 (2)	0.85482 (2)	0.98152 (2)	0.03175 (7)
O1	1.48134 (12)	-0.08455 (11)	0.63504 (10)	0.0216 (3)

O2	0.72363 (11)	0.33194 (10)	0.79972 (9)	0.0146 (2)
O3	0.88737 (12)	0.03125 (10)	0.80277 (9)	0.0161 (2)
H3	0.946 (2)	-0.005 (2)	0.8285 (18)	0.024*
O4	0.68413 (12)	0.42167 (11)	0.55496 (10)	0.0219 (3)
O5	0.59996 (12)	0.24241 (10)	0.56141 (9)	0.0181 (2)
O6	0.50480 (12)	0.34615 (12)	0.76999 (10)	0.0226 (3)
C1	1.60845 (17)	-0.06256 (16)	0.66123 (15)	0.0234 (4)
H1A	1.6822	-0.1112	0.6258	0.035*
H1B	1.6086	-0.0862	0.7377	0.035*
H1C	1.6221	0.0248	0.6382	0.035*
C2	1.37016 (16)	-0.00940 (15)	0.66373 (13)	0.0162 (3)
C3	1.25421 (17)	-0.01664 (15)	0.61884 (13)	0.0168 (3)
H3A	1.2559	-0.0730	0.5736	0.020*
C4	1.13694 (17)	0.05761 (15)	0.63969 (12)	0.0154 (3)
H4	1.0585	0.0512	0.6089	0.018*
C5	1.13142 (16)	0.14238 (14)	0.70552 (12)	0.0136 (3)
C6	1.00307 (16)	0.22660 (14)	0.72642 (12)	0.0125 (3)
C7	0.88783 (16)	0.15613 (14)	0.80678 (12)	0.0135 (3)
C8	0.75351 (16)	0.21607 (14)	0.76594 (12)	0.0134 (3)
H8	0.6775	0.1620	0.7913	0.016*
C9	0.59516 (16)	0.38517 (15)	0.80092 (12)	0.0163 (3)

C10	0.58266 (16)	0.49863 (15)	0.84552 (12)	0.0164 (3)
C11	0.66764 (17)	0.51086 (16)	0.91717 (13)	0.0184 (3)
H11	0.7358	0.4470	0.9373	0.022*
C12	0.65263 (18)	0.61627 (16)	0.95913 (14)	0.0203 (3)
H12	0.7083	0.6243	1.0096	0.024*
C13	0.55536 (18)	0.70941 (16)	0.92630 (14)	0.0212 (3)
C14	0.79292 (16)	0.23437 (14)	0.64626 (12)	0.0131 (3)
H14	0.8080	0.1519	0.6264	0.016*
C15	0.93037 (15)	0.29001 (14)	0.62642 (12)	0.0126 (3)
H15	0.9088	0.3782	0.6317	0.015*
C16	0.90733 (16)	0.18310 (15)	0.91093 (13)	0.0156 (3)
C17	0.98491 (16)	0.28404 (15)	0.89096 (13)	0.0155 (3)
N18	1.02820 (14)	0.31863 (12)	0.78541 (10)	0.0145 (3)
C19	1.11368 (18)	0.41758 (16)	0.74101 (14)	0.0203 (3)
H19A	1.1917	0.3882	0.6948	0.031*
H19B	1.1462	0.4459	0.7980	0.031*
H19C	1.0610	0.4856	0.7001	0.031*
C20	1.00652 (17)	0.33636 (16)	0.97423 (13)	0.0197 (3)
H20	1.0559	0.4067	0.9620	0.024*
C21	0.95320 (18)	0.28207 (18)	1.07615 (14)	0.0236 (4)
H21	0.9673	0.3164	1.1337	0.028*
C22	0.88037 (18)	0.17978 (18)	1.09600 (13)	0.0234 (4)

H22	0.8474	0.1436	1.1664	0.028*
C23	0.85548 (17)	0.12981 (16)	1.01162 (13)	0.0194 (3)
H23	0.8040	0.0608	1.0237	0.023*
C24	1.36557 (17)	0.06954 (15)	0.73282 (13)	0.0177 (3)
H24	1.4429	0.0730	0.7661	0.021*
C25	1.24611 (17)	0.14407 (15)	0.75315 (13)	0.0157 (3)
H25	1.2433	0.1976	0.8011	0.019*
C26	1.00617 (10)	0.29006 (10)	0.51484 (6)	0.0137 (3)
C27	0.96738 (10)	0.22014 (10)	0.45010 (8)	0.0210 (3)
H27	0.8951	0.1691	0.4754	0.025*
C28	1.03440 (11)	0.22496 (10)	0.34832 (7)	0.0215 (4)
H28	1.0079	0.1772	0.3041	0.026*
C29	1.14019 (11)	0.29971 (10)	0.31129 (6)	0.0185 (3)
H29	1.1860	0.3030	0.2417	0.022*
C30	1.17898 (9)	0.36963 (9)	0.37603 (8)	0.0186 (3)
H30	1.2513	0.4207	0.3507	0.022*
C31	1.11197 (10)	0.36481 (9)	0.47781 (7)	0.0160 (3)
H31	1.1385	0.4126	0.5221	0.019*
C32	0.68787 (16)	0.31204 (15)	0.58250 (12)	0.0143 (3)
C33	0.48553 (18)	0.30850 (17)	0.51147 (15)	0.0238 (4)
H33A	0.5189	0.3585	0.4435	0.036*
H33B	0.4339	0.3618	0.5570	0.036*
H33C	0.4264	0.2498	0.5002	0.036*

C34	0.48351 (17)	0.59226 (16)	0.81540 (13)	0.0205 (3)
H34	0.4246	0.5829	0.7676	0.025*
C35	0.47017 (19)	0.69944 (16)	0.85492 (14)	0.0229 (4)
H35	0.4040	0.7645	0.8334	0.028*

Selected NMR Spectra:

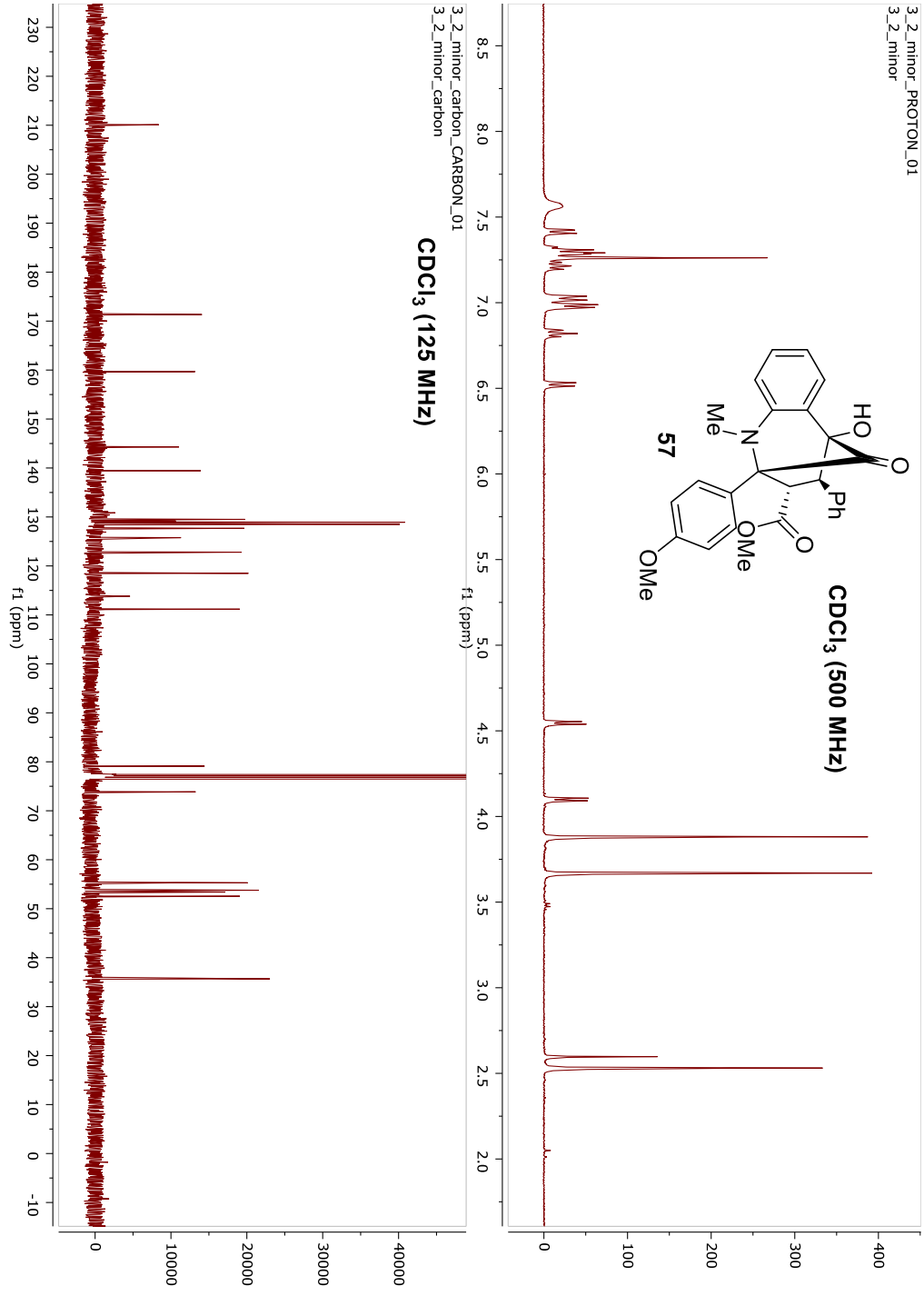

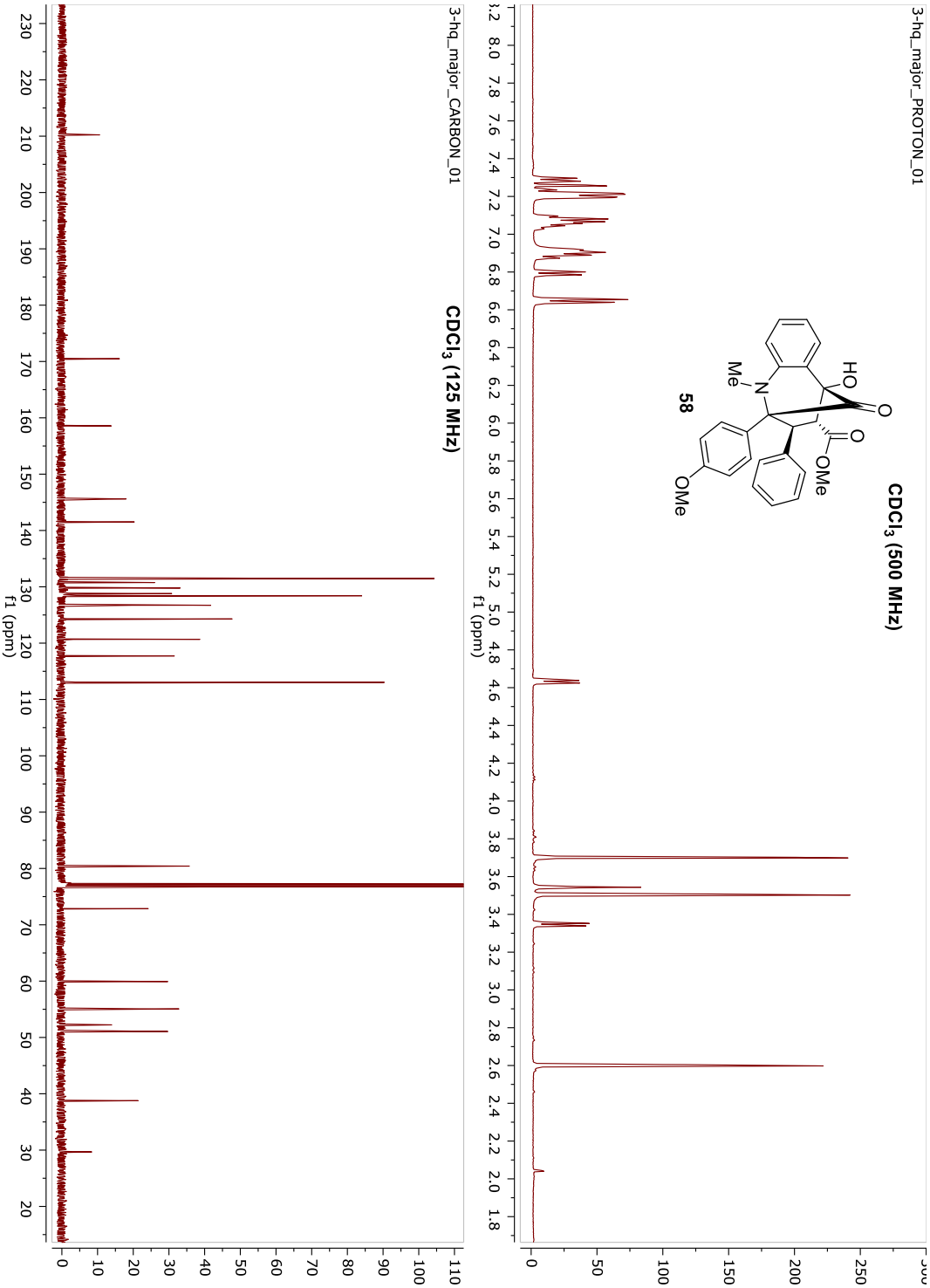
3-hq_major_PROTON_01
CDCl3 (500 MHz)
HO
O
O
OMe
Me
N
58
OMe
f1 (ppm)
3-hq_major_CARBON_01
CDCl3 (125 MHz)
f1 (ppm)

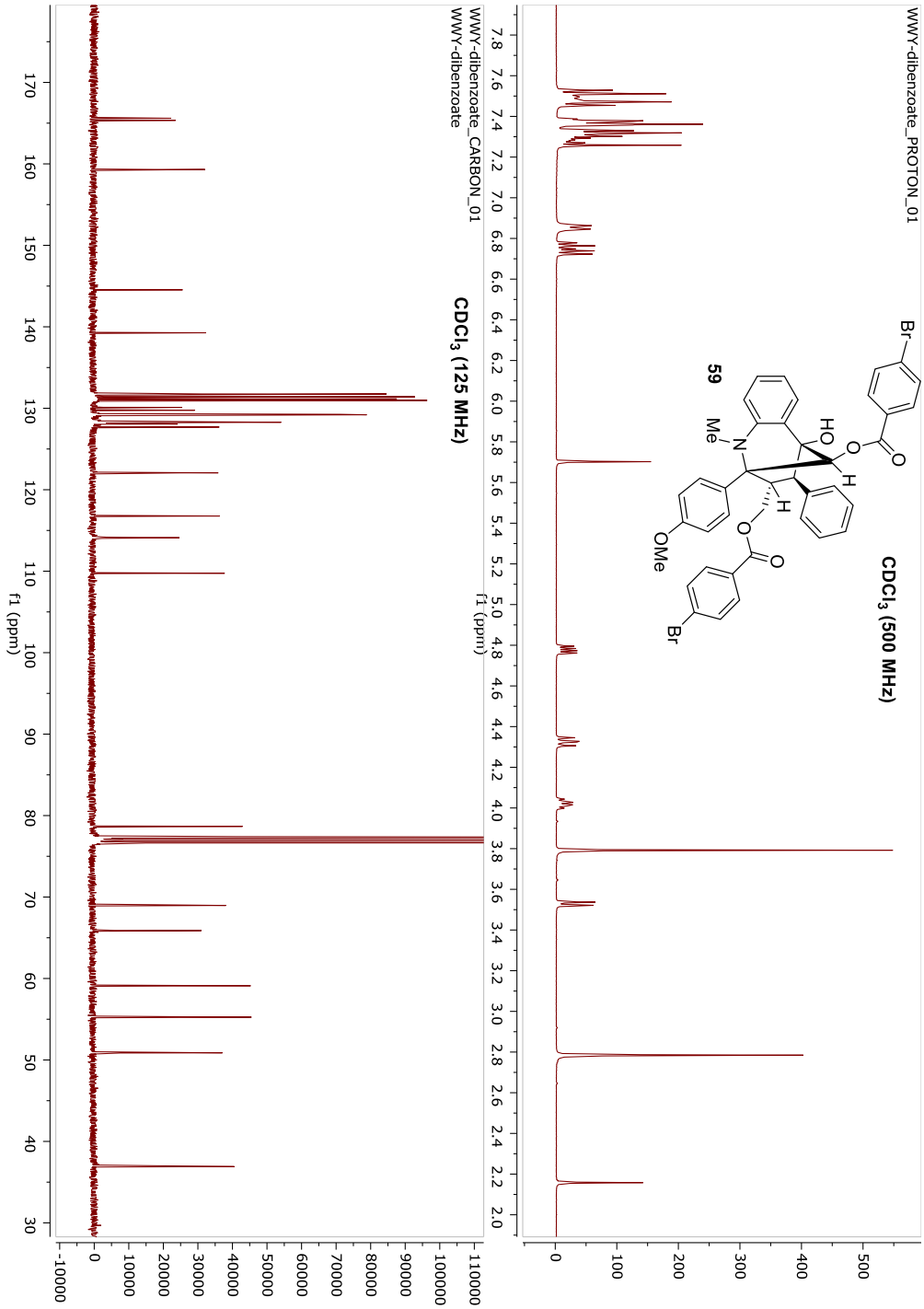
WWY-dibenzoate_PROTON_01
CDCl3 (500 MHz)
59
Br
HO
O
H
N
Me
H
O
OMe
O
Br
WWY-dibenzoate_CARBON_01
WWY-dibenzoate
CDCl3 (125 MHz)
f1 (ppm)

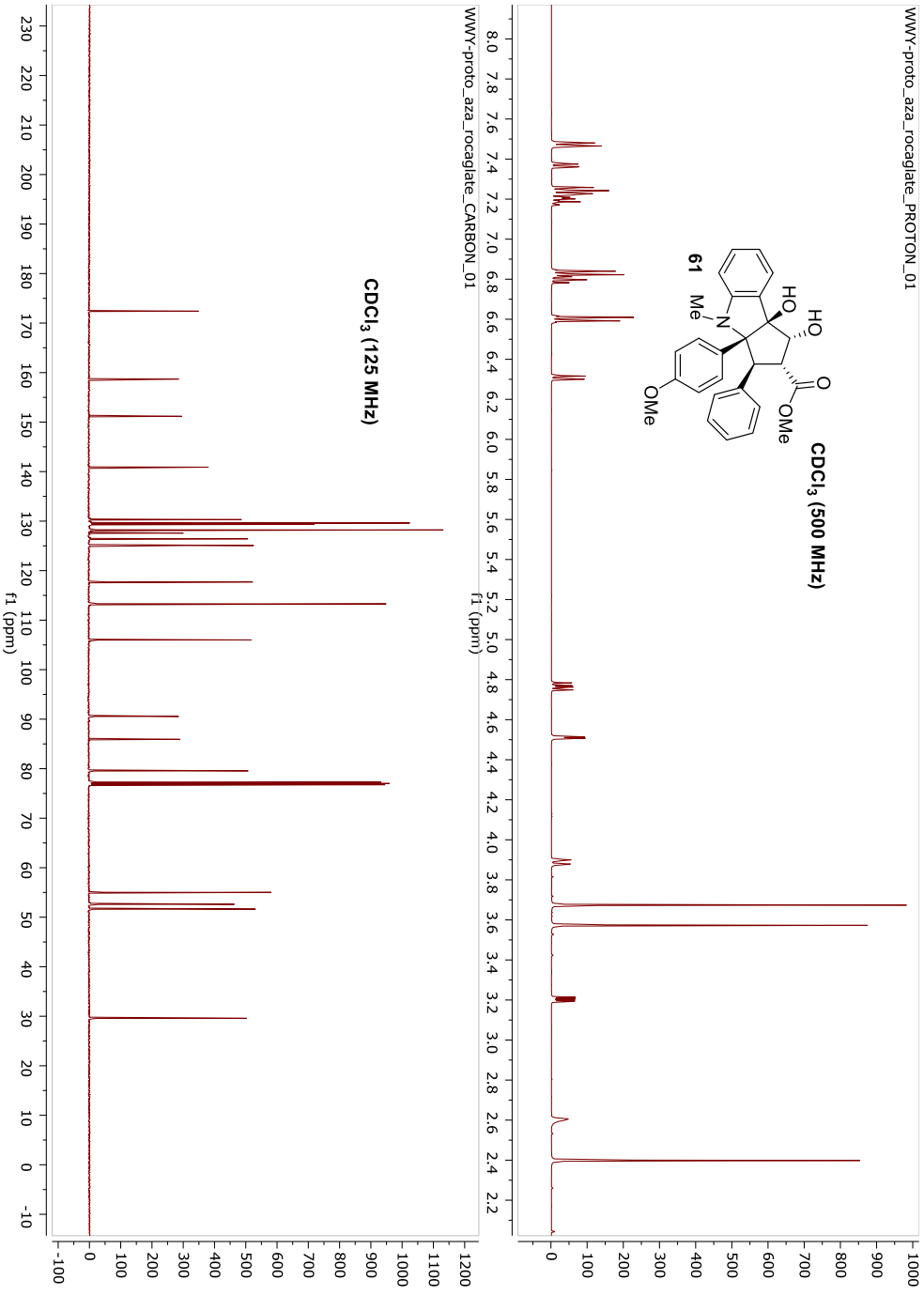
WWY-proto_aza_rocaglate_PROTON_01
CDCl3 (500 MHz)
61
Me
N
HO
HO
O
OMe
OMe
WWY-proto_aza_rocaglate_CARBON_01
CDCl3 (125 MHz)
f1 (ppm)

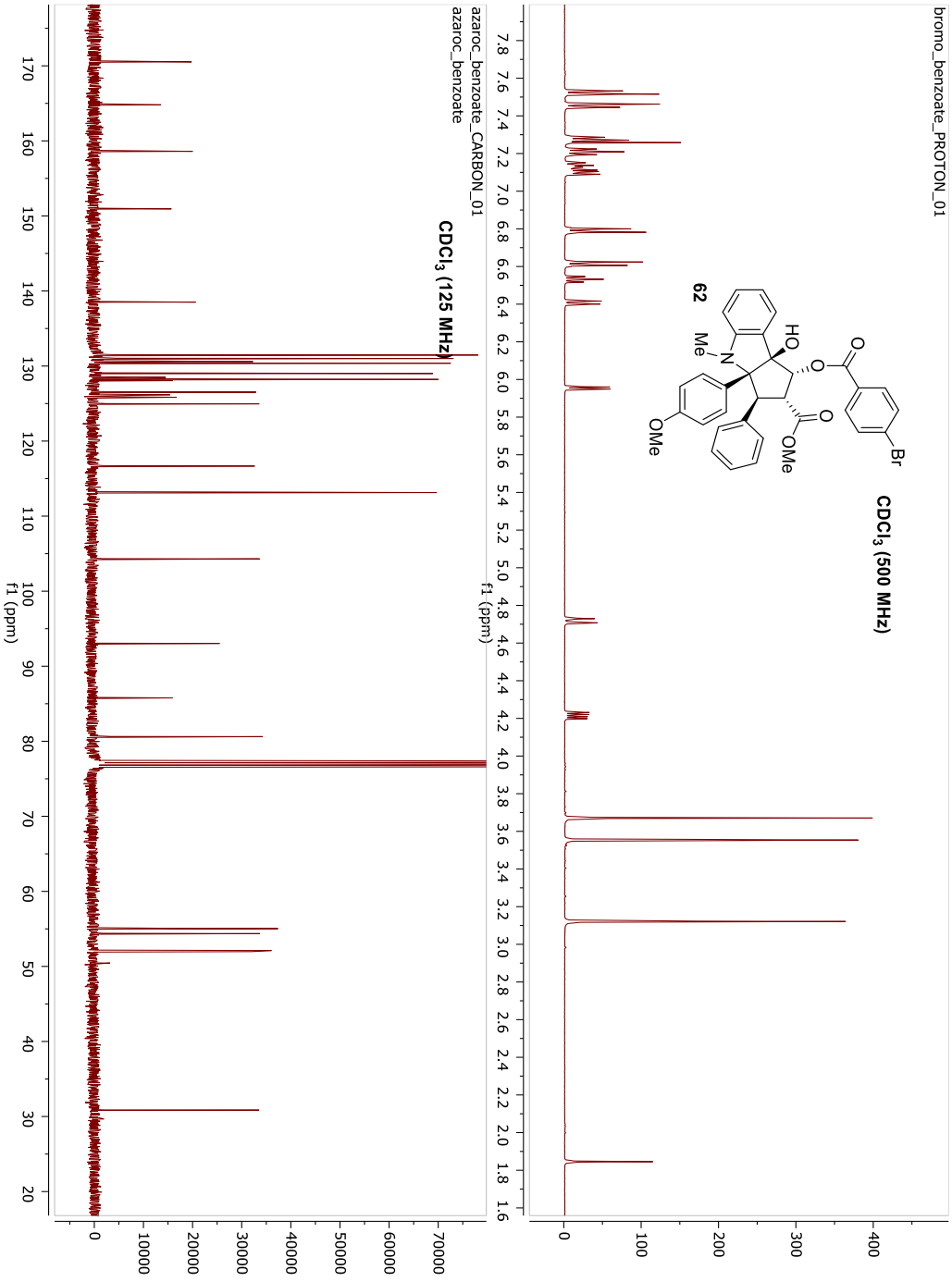
bromo_benzoate_PROTON_01
CDCl3 (500 MHz)
62
azaroc_benzoate_CARBON_01
azaroc_benzoate
CDCl3 (125 MHz)
f1 (ppm)

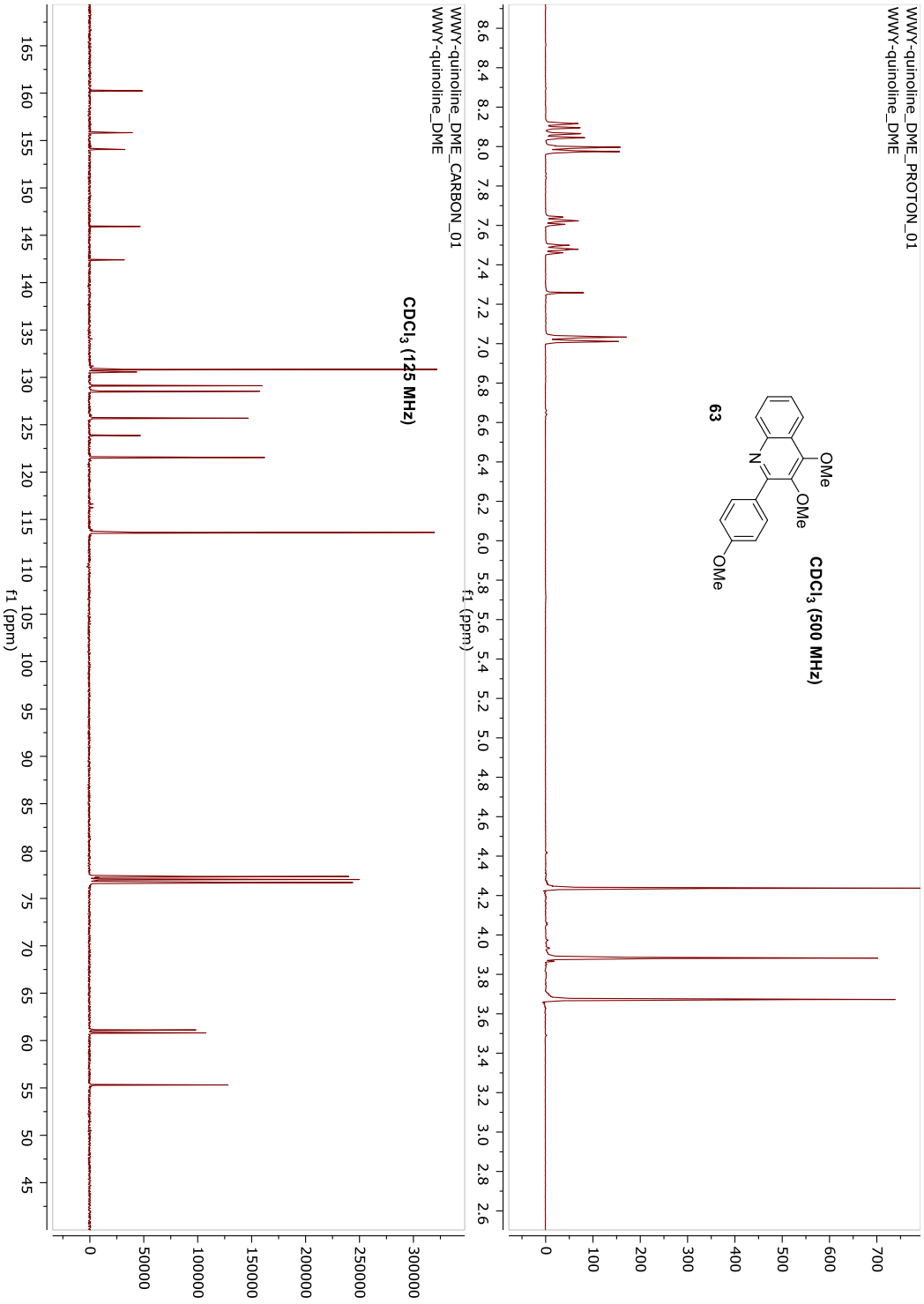
WWY-quinoline_DME_PROTON_01
WWY-quinoline_DME
63
OMe
OMe
OMe
N
CDCl3 (500 MHz)
f1 (ppm)
WWY-quinoline_DME_CARBON_01
WWY-quinoline_DME
CDCl3 (125 MHz)
f1 (ppm)

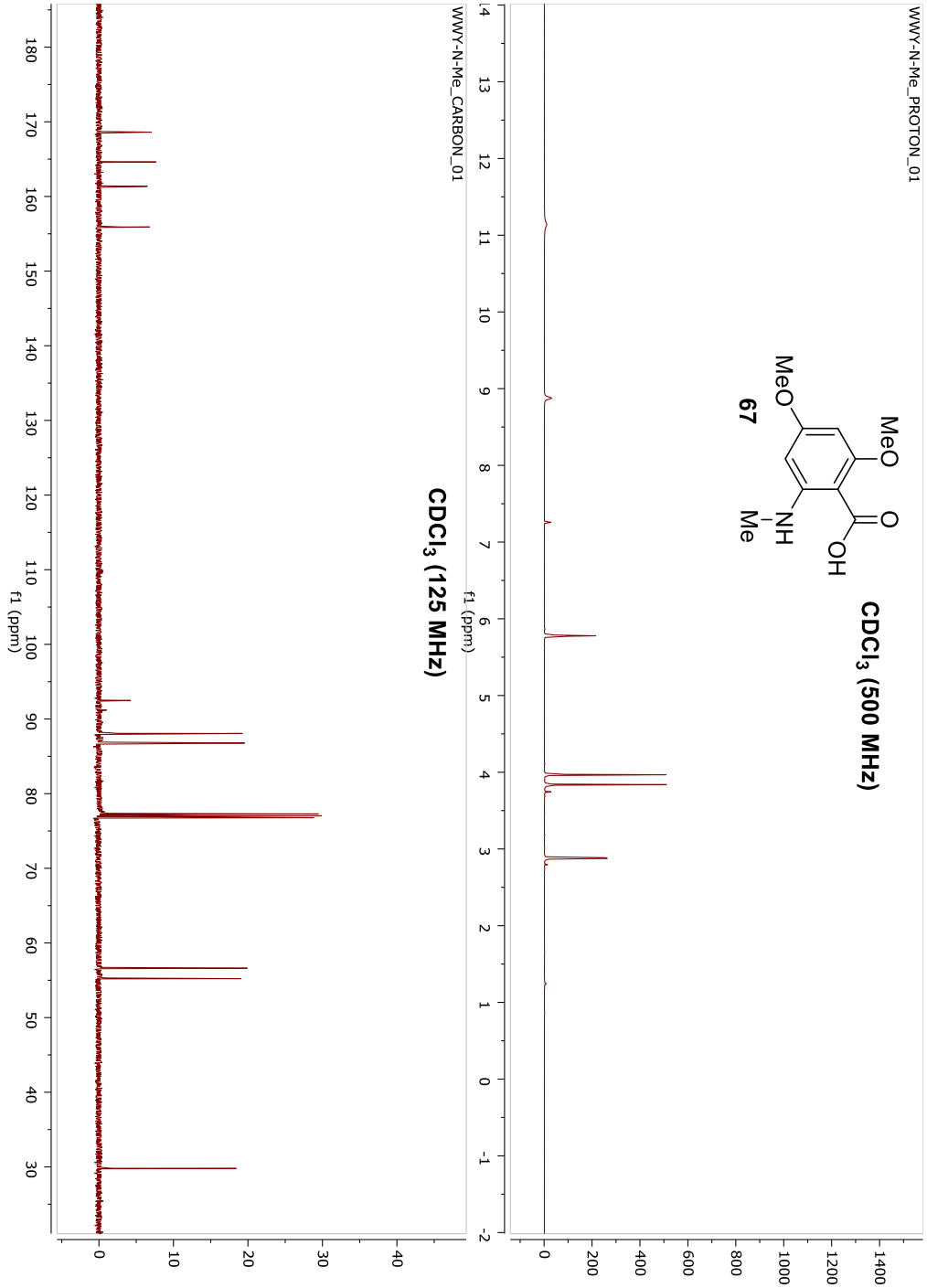
WWY-N-Me_PROTON_01
MeO
O
OH
MeO
NH
Me
67
CDCl3 (500 MHz)
f1 (ppm)
WWY-N-Me_CARBON_01
CDCl3 (125 MHz)
f1 (ppm)

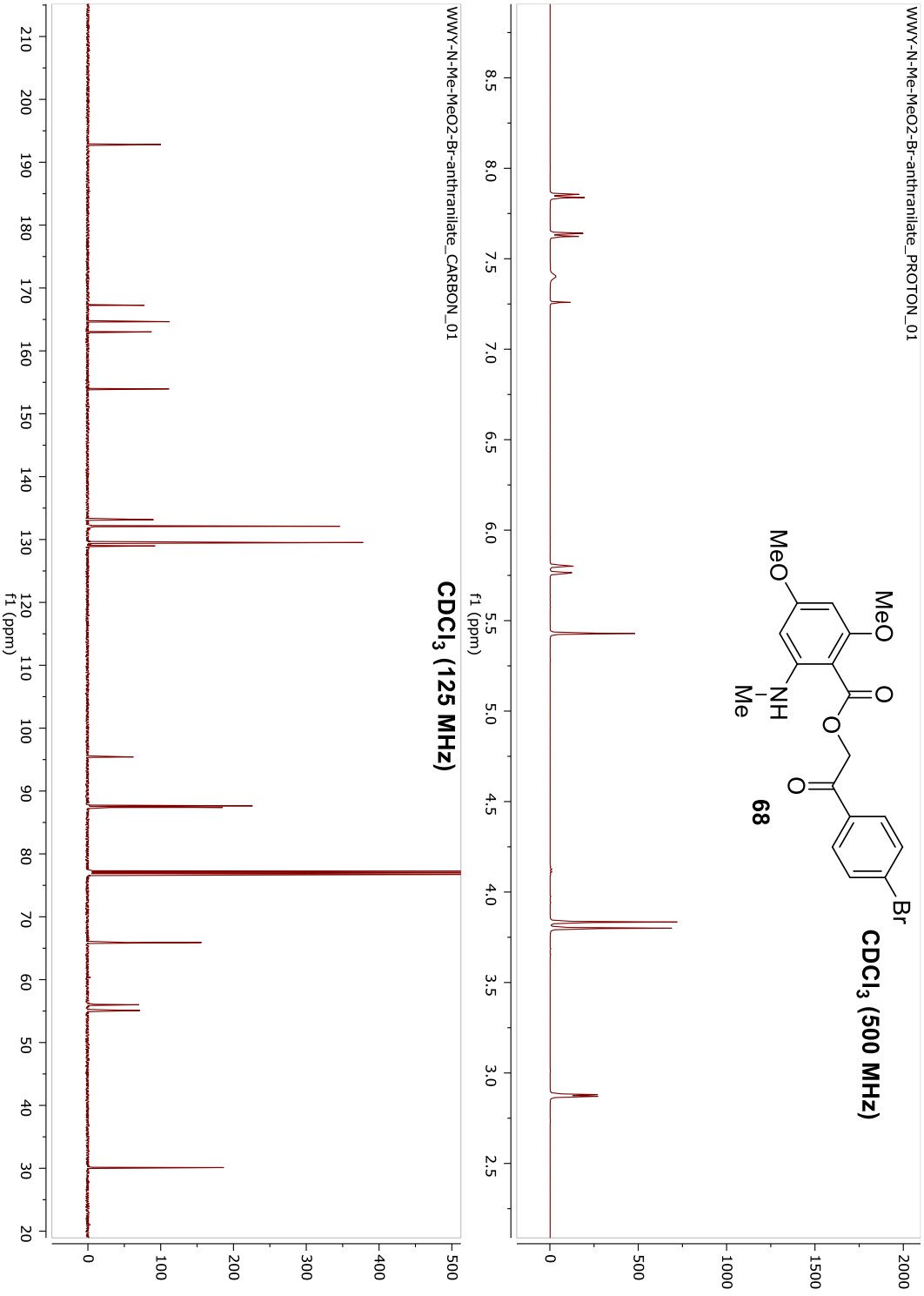
WWY-N-Me-MeO2-Br-anthranilate_PROTON_01
MeO
O
O
O
NH
Me
MeO
Br
68
CDCl3 (500 MHz)
f1 (ppm)
WWY-N-Me-MeO2-Br-anthranilate_CARBON_01
CDCl3 (125 MHz)
f1 (ppm)

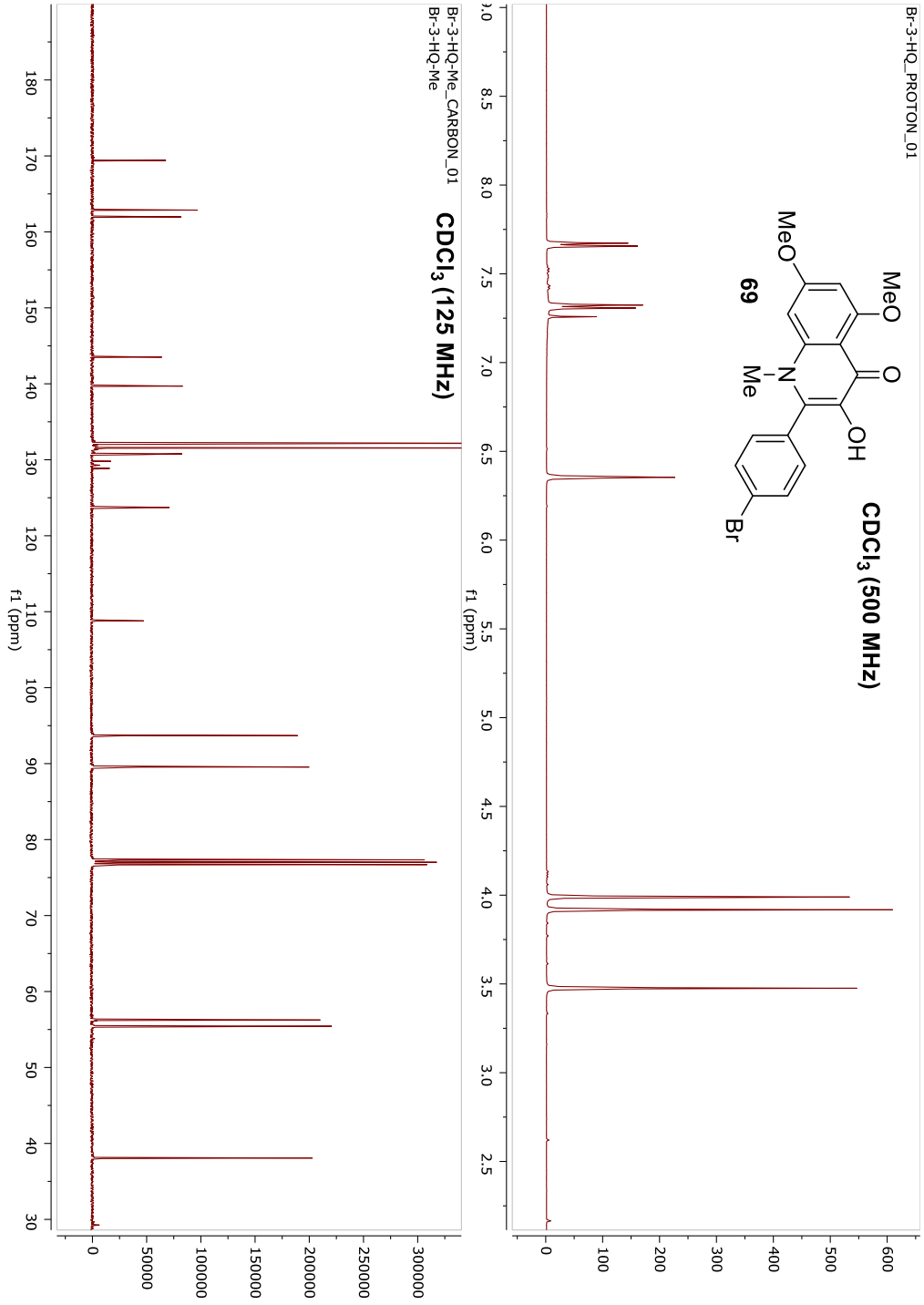
Br-3-HQ_PROTON_01
MeO
O
OH
MeO
N
Me
Br
69
CDCl3 (500 MHz)
f1 (ppm)
Br-3-HQ-Me_CARBON_01
Br-3-HQ-Me
CDCl3 (125 MHz)
f1 (ppm)

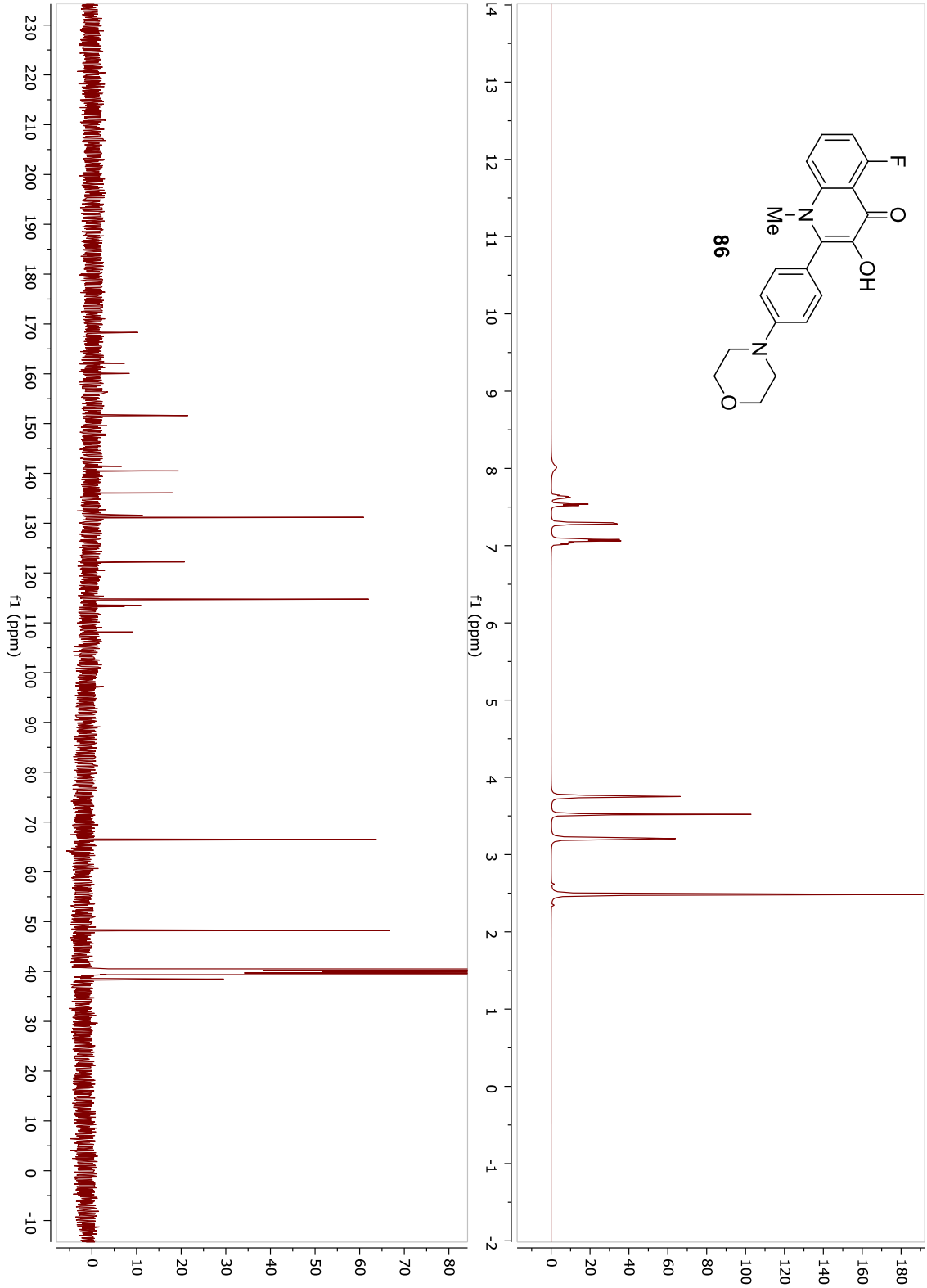
F
O
N
Me
OH
N
O
86
f1 (ppm)
f1 (ppm)

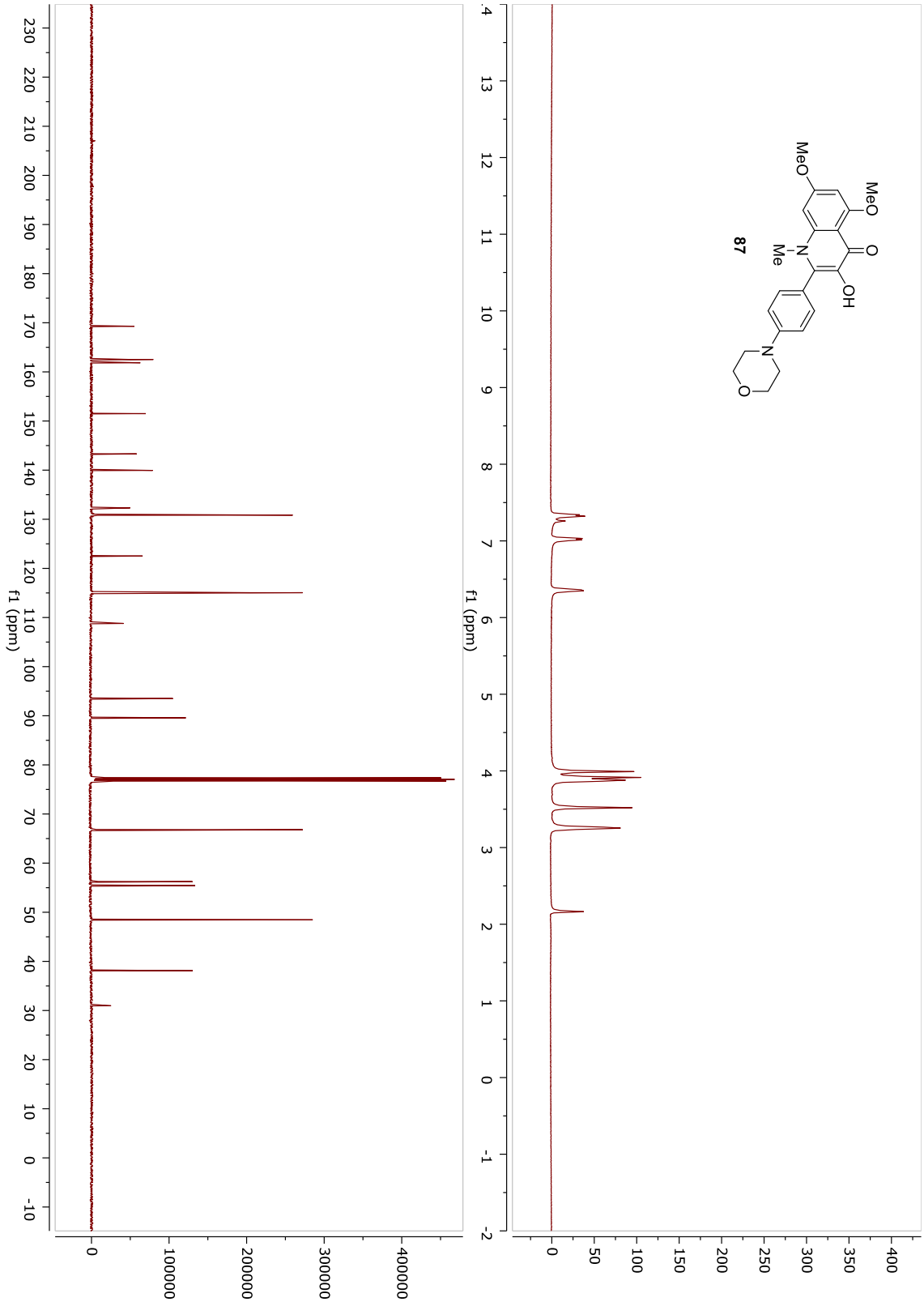
MeO
MeO
O
N
Me
OH
N
O
87
f1 (ppm)
f1 (ppm)

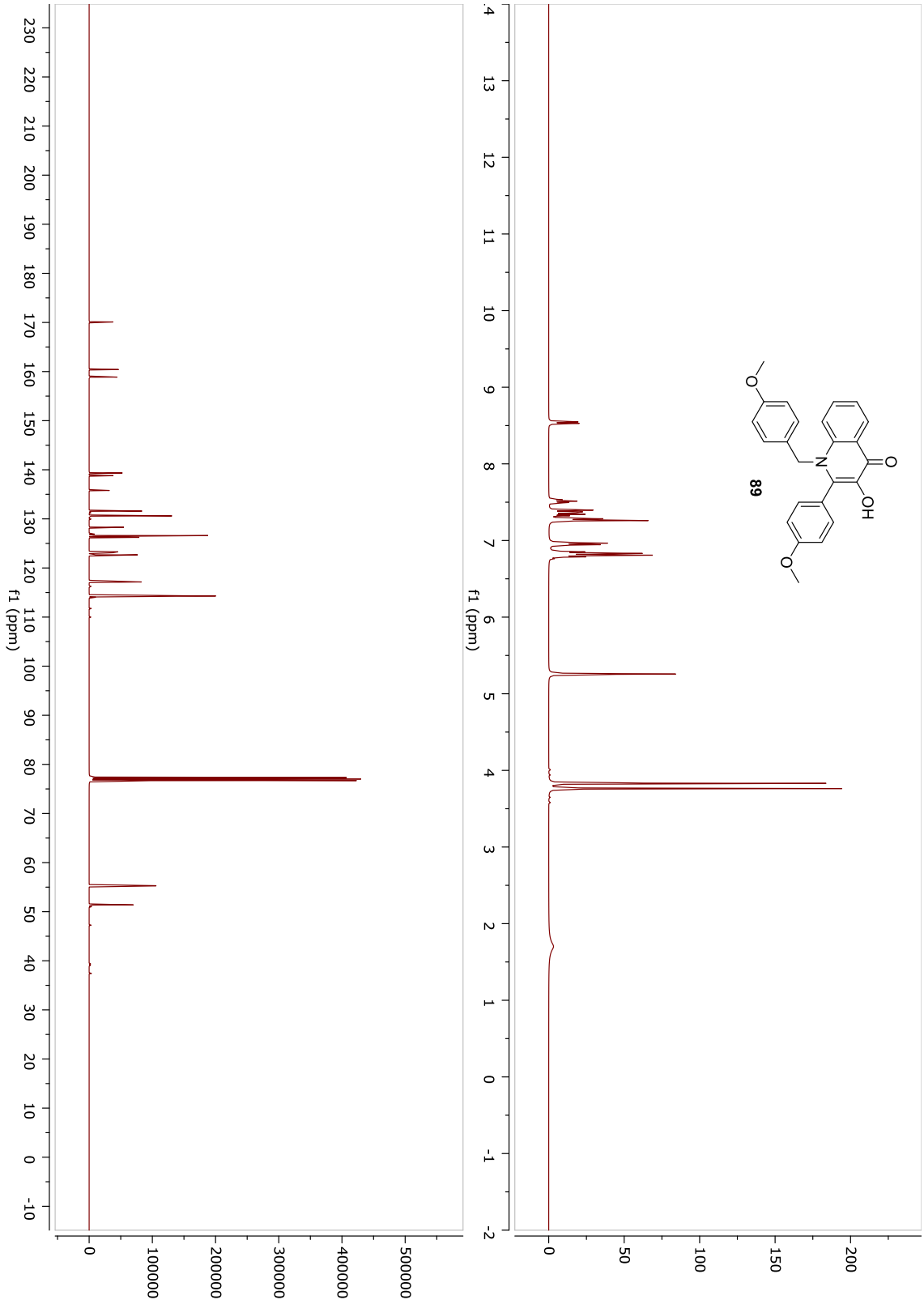
89
f1 (ppm)
f1 (ppm)

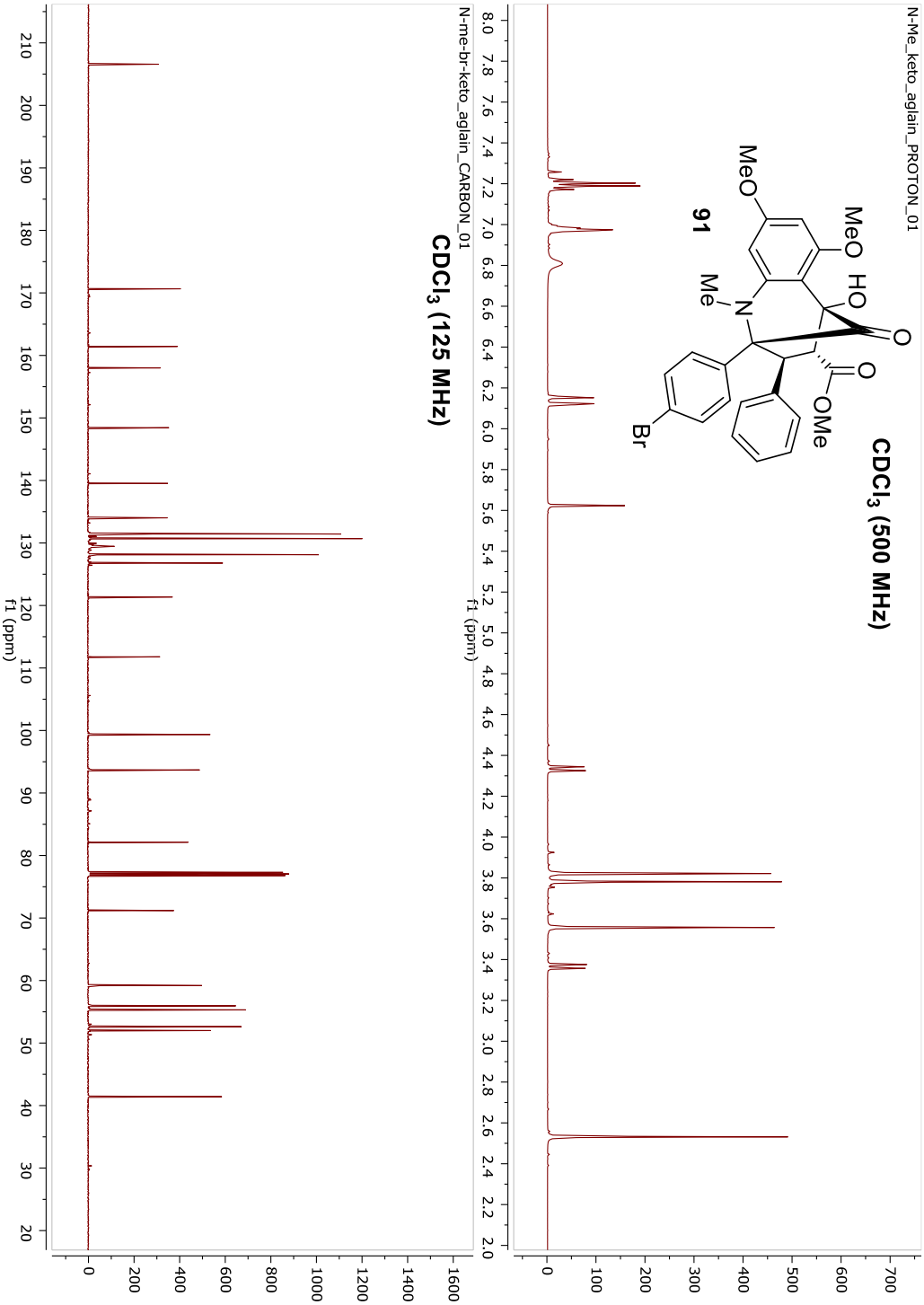
N-Me_keto_aglain_PROTON_01
CDCl3 (500 MHz)
MeO
HO
O
O
OMe
MeO
91
Me
N
Br
N-me-br-keto_aglain_CARBON_01
CDCl3 (125 MHz)
f1 (ppm)

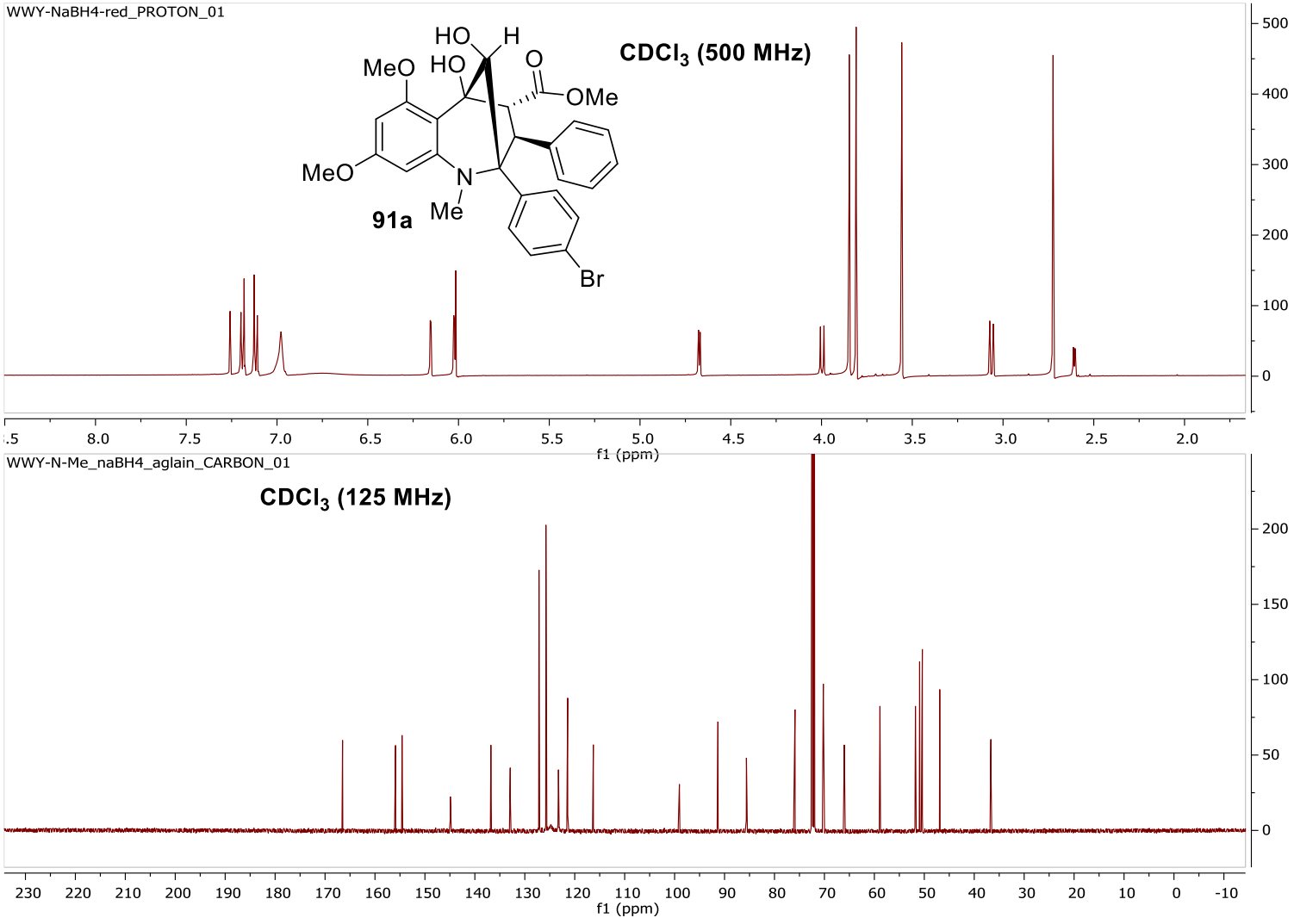
WWY-NaBH4-red_PROTON_01
HO
H
MeO
HO
O
OMe
MeO
N
Me
91a
Br
CDCl3 (500 MHz)
f1 (ppm)
WWY-N-Me_naBH4_aglain_CARBON_01
CDCl3 (125 MHz)
f1 (ppm)

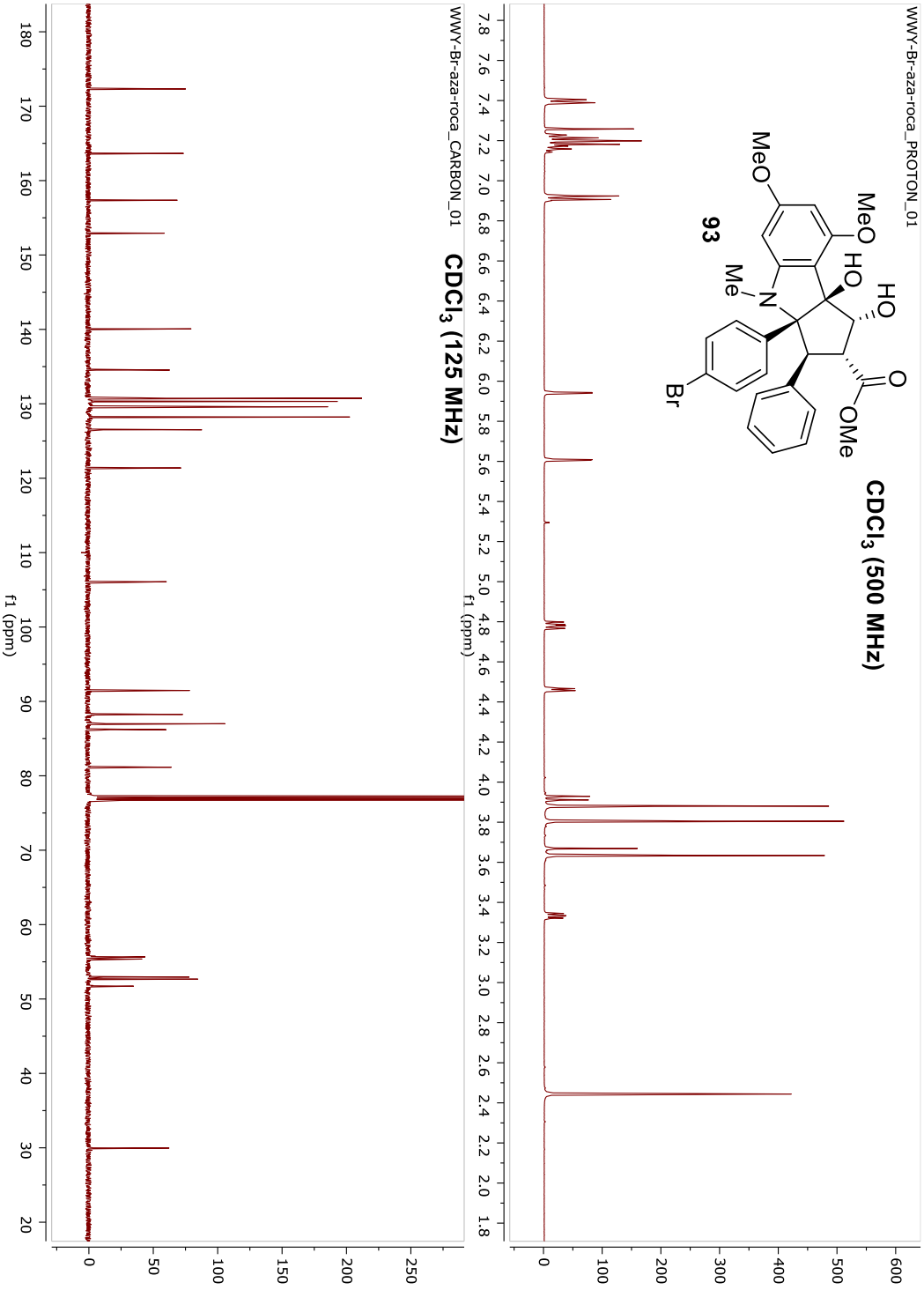
WWY-Br-aza-roca_PROTON_01
CDCl3 (500 MHz)
93
MeO
MeO
HO
HO
Me
N
O
OMe
Br
f1 (ppm)
WWY-Br-aza-roca_CARBON_01
CDCl3 (125 MHz)
f1 (ppm)

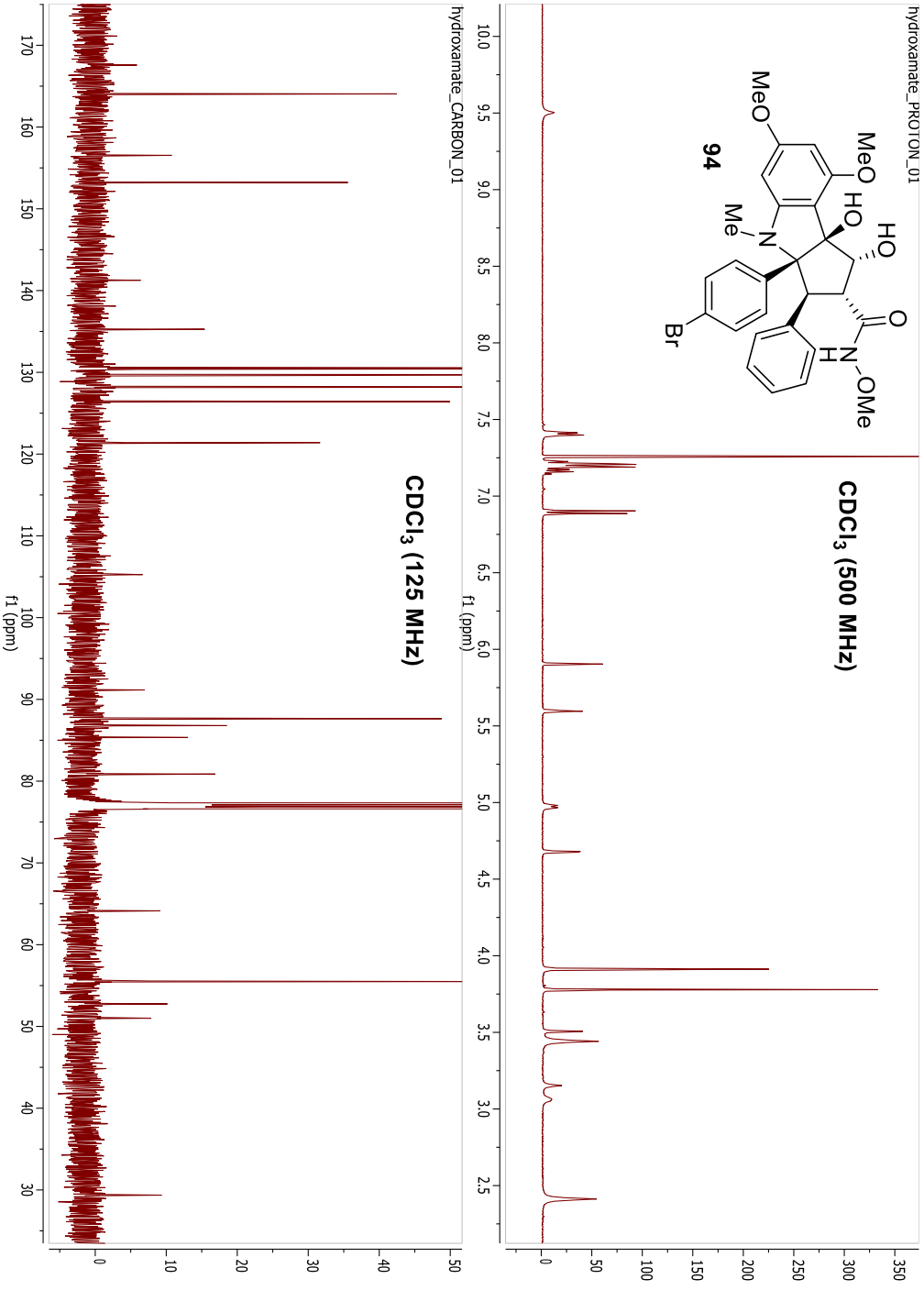
hydroxamate_PROTON_01
CDCl3 (500 MHz)
94
MeO
HO
HO
Me
N
Br
O
N
H
OMe
f1 (ppm)
hydroxamate_CARBON_01
CDCl3 (125 MHz)
f1 (ppm)

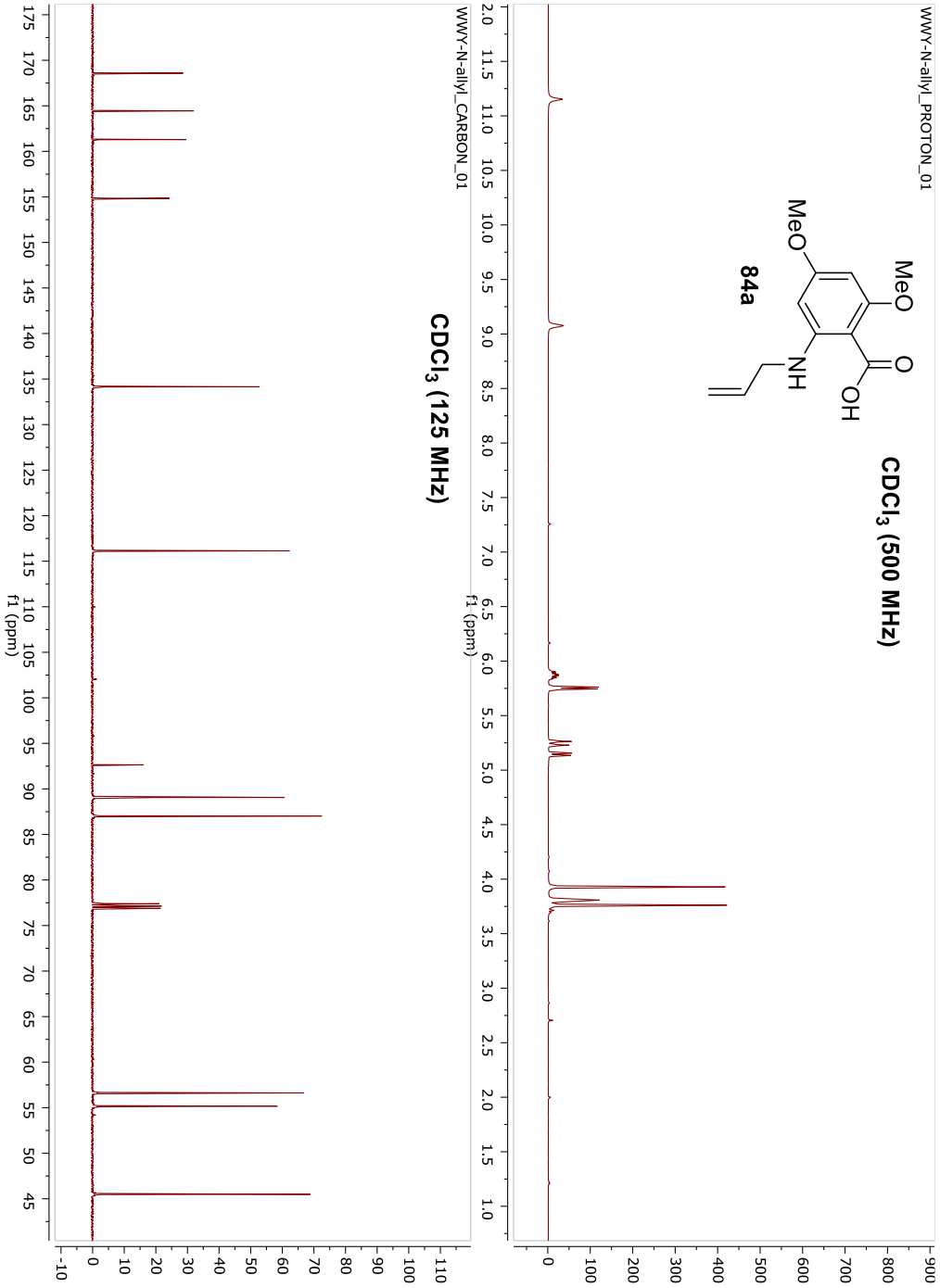
WWY-N-allyl_PROTON_01
MeO
O
OH
MeO
NH
84a
CDCl3 (500 MHz)
f1 (ppm)
WWY-N-allyl_CARBON_01
CDCl3 (125 MHz)
f1 (ppm)

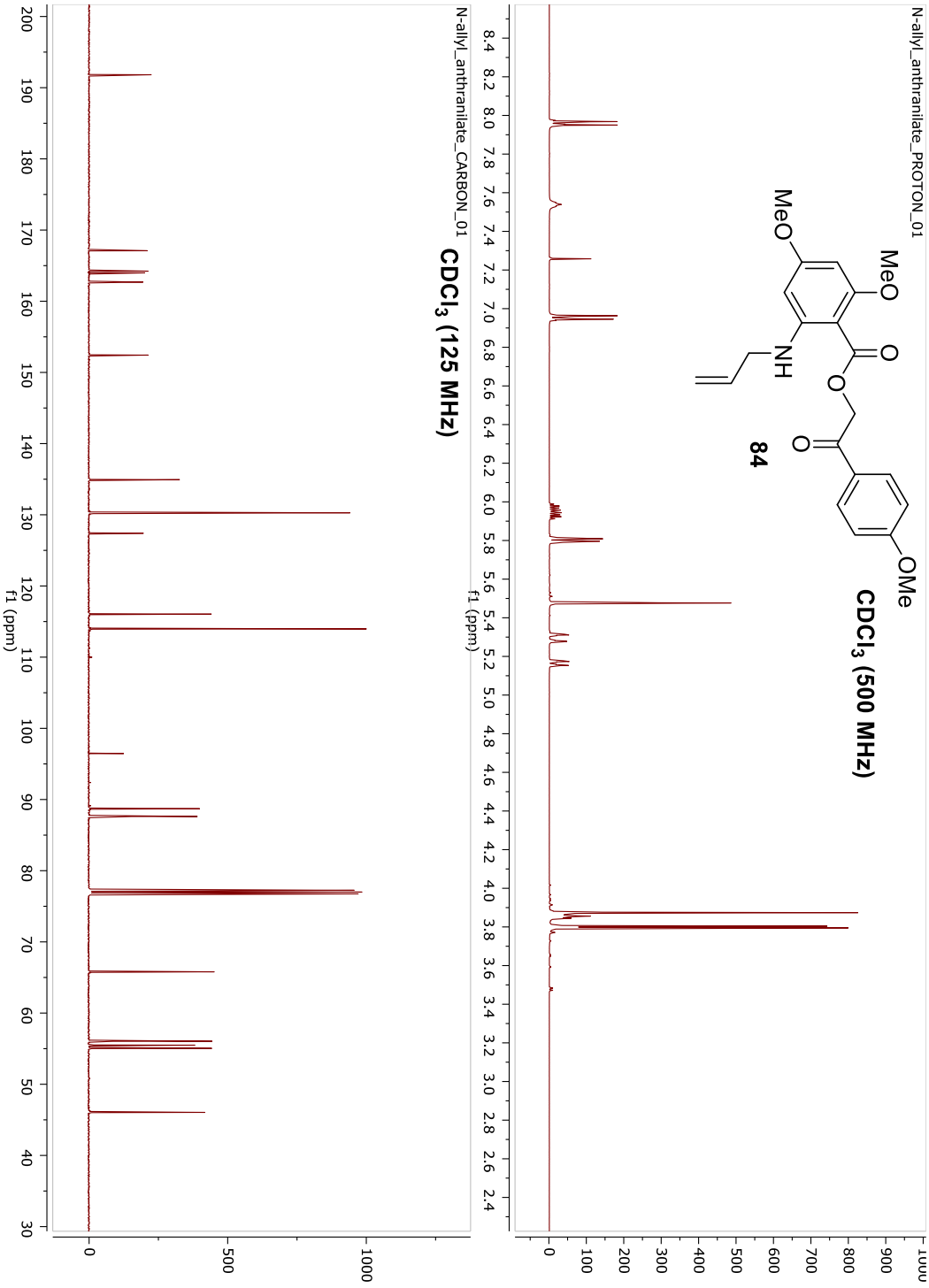
N-allyl_anthranilate_PROTON_01
MeO
O
O
O
MeO
NH
OMe
84
CDCl3 (500 MHz)
N-allyl_anthranilate_CARBON_01
CDCl3 (125 MHz)
f1 (ppm)

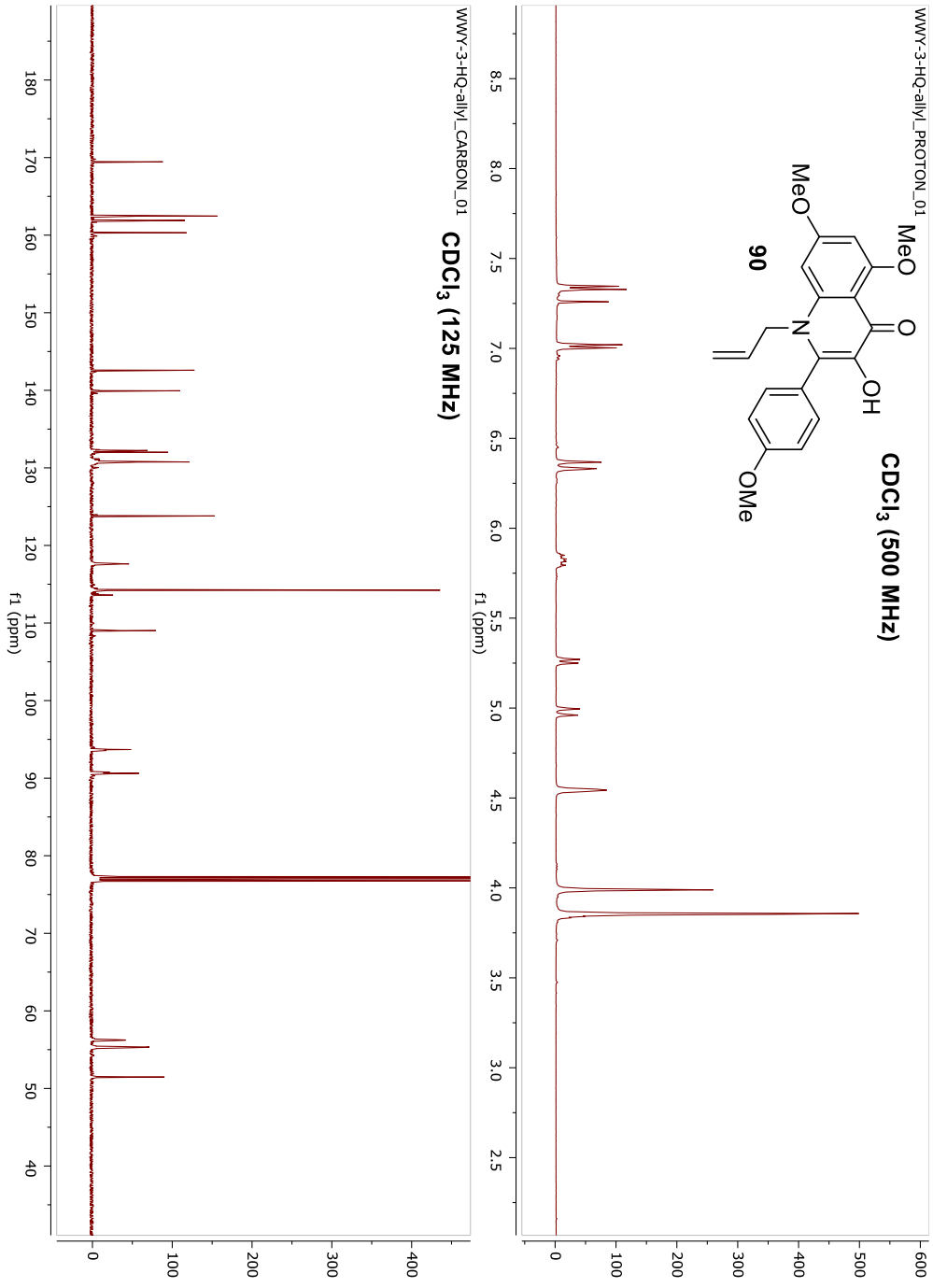
WWY-3-HQ-allyl_PROTON_01
MeO
O
OH
N
MeO
OMe
90
CDCl3 (500 MHz)
f1 (ppm)
WWY-3-HQ-allyl_CARBON_01
CDCl3 (125 MHz)
f1 (ppm)

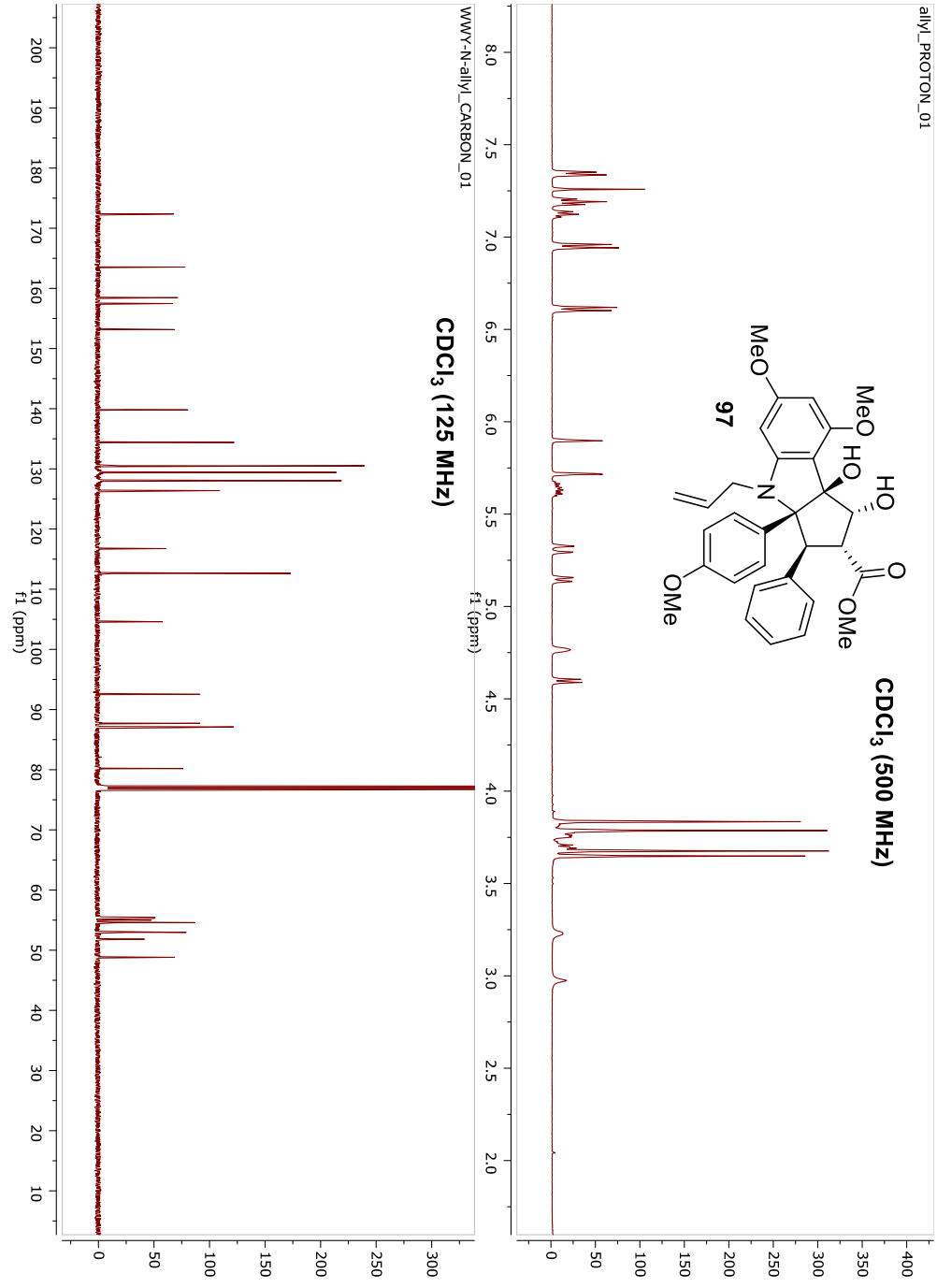
allyl_PROTON_01
CDCl3 (500 MHz)
MeO
HO
HO
O
OMe
MeO
97
N
OMe
f1 (ppm)
WWY-N-allyl_CARBON_01
CDCl3 (125 MHz)
f1 (ppm)

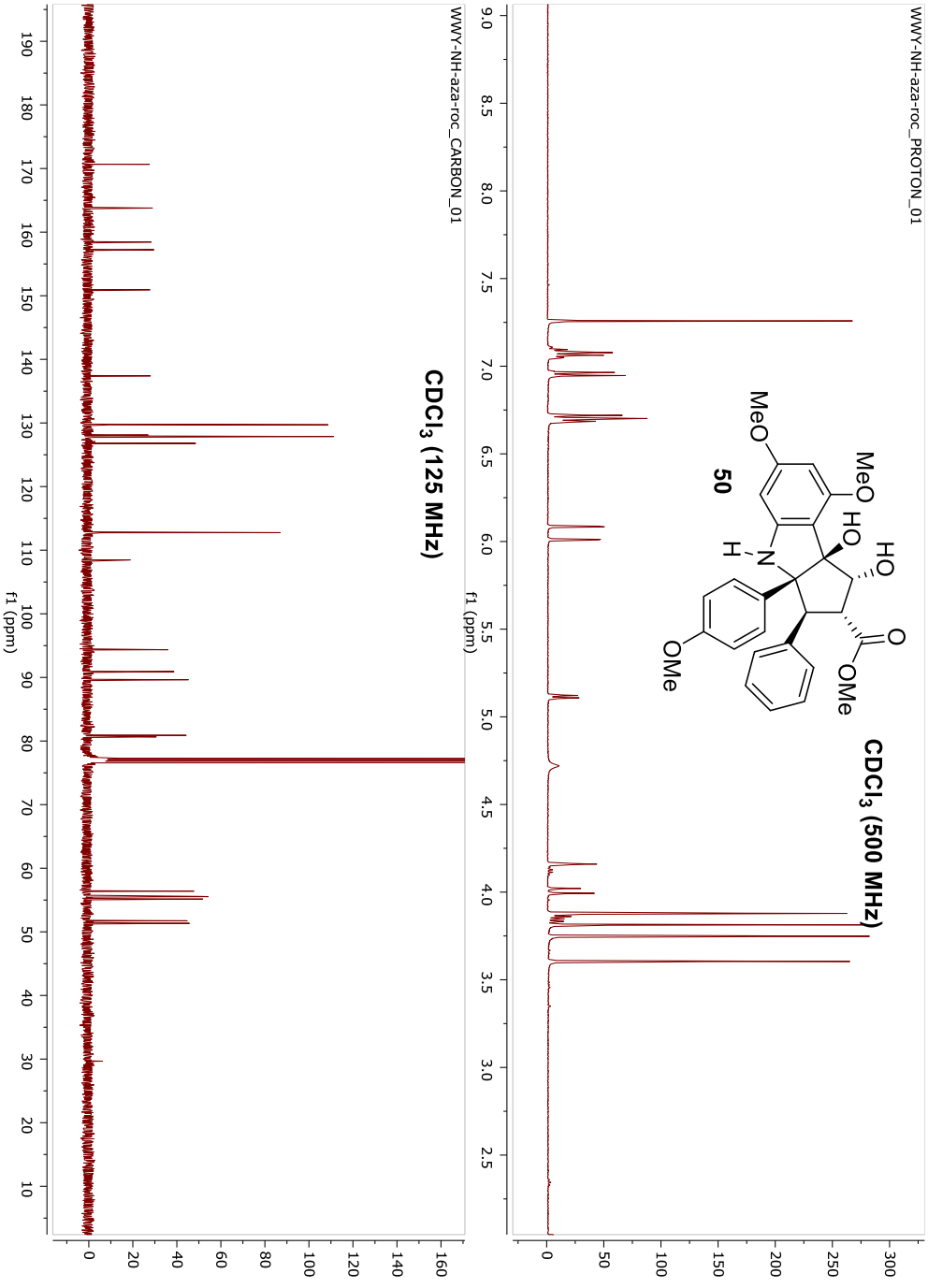
WWY-NH-aza-roc_PROTON_01
CDCl3 (500 MHz)
50
MeO
HO
MeO
HO
H
N
O
OMe
OMe
f1 (ppm)
WWY-NH-aza-roc_CARBON_01
CDCl3 (125 MHz)
f1 (ppm)

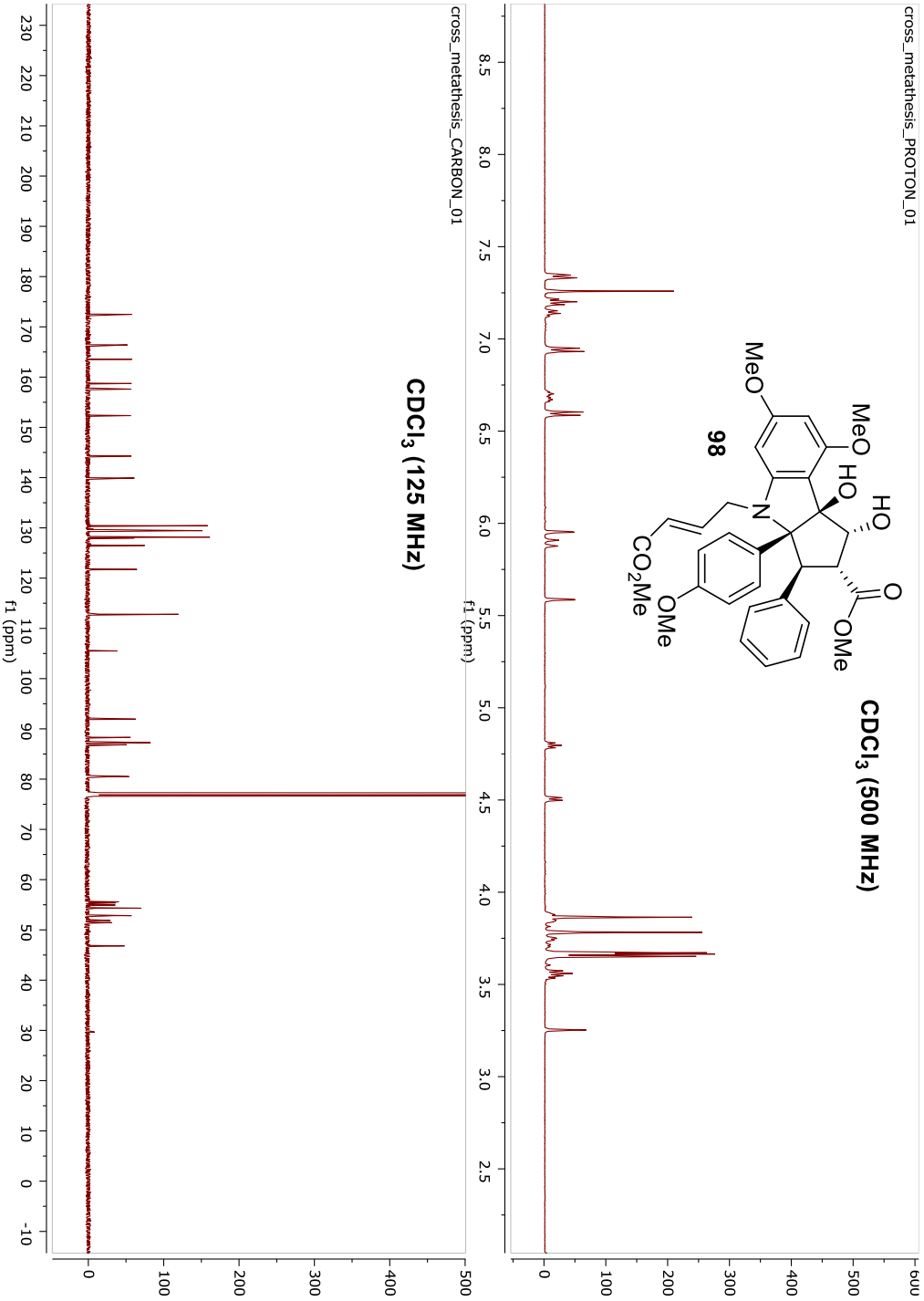
cross_metathesis_PROTON_01
CDCl3 (500 MHz)
98
cross_metathesis_CARBON_01
CDCl3 (125 MHz)
f1 (ppm)

HSQC, HMBC, and NOESY Studies for Compound **42**

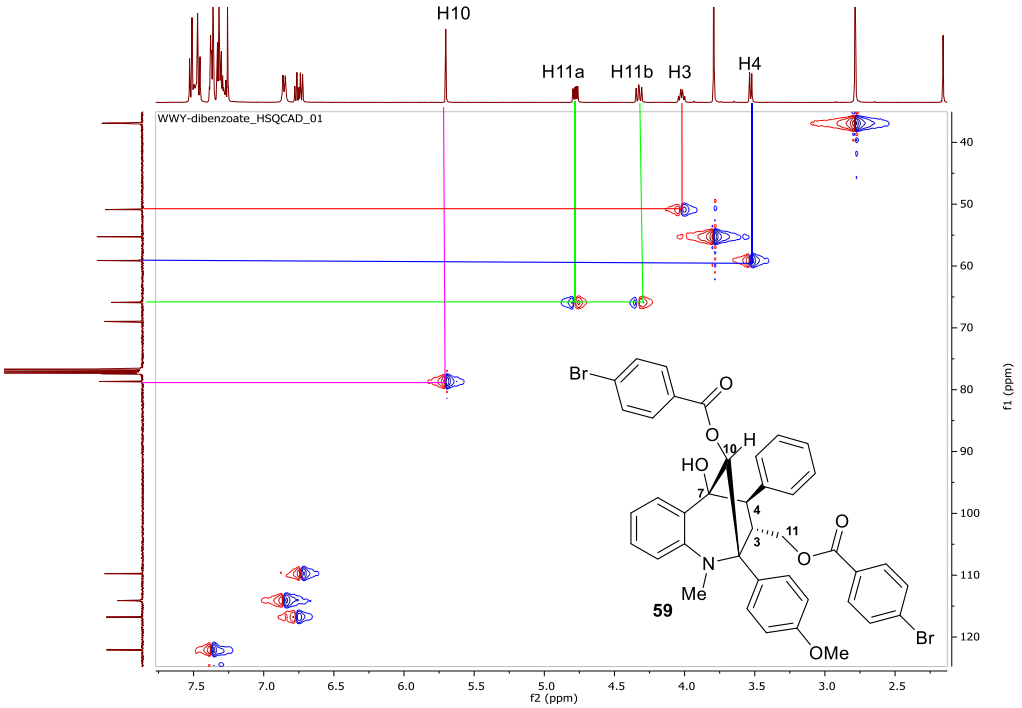

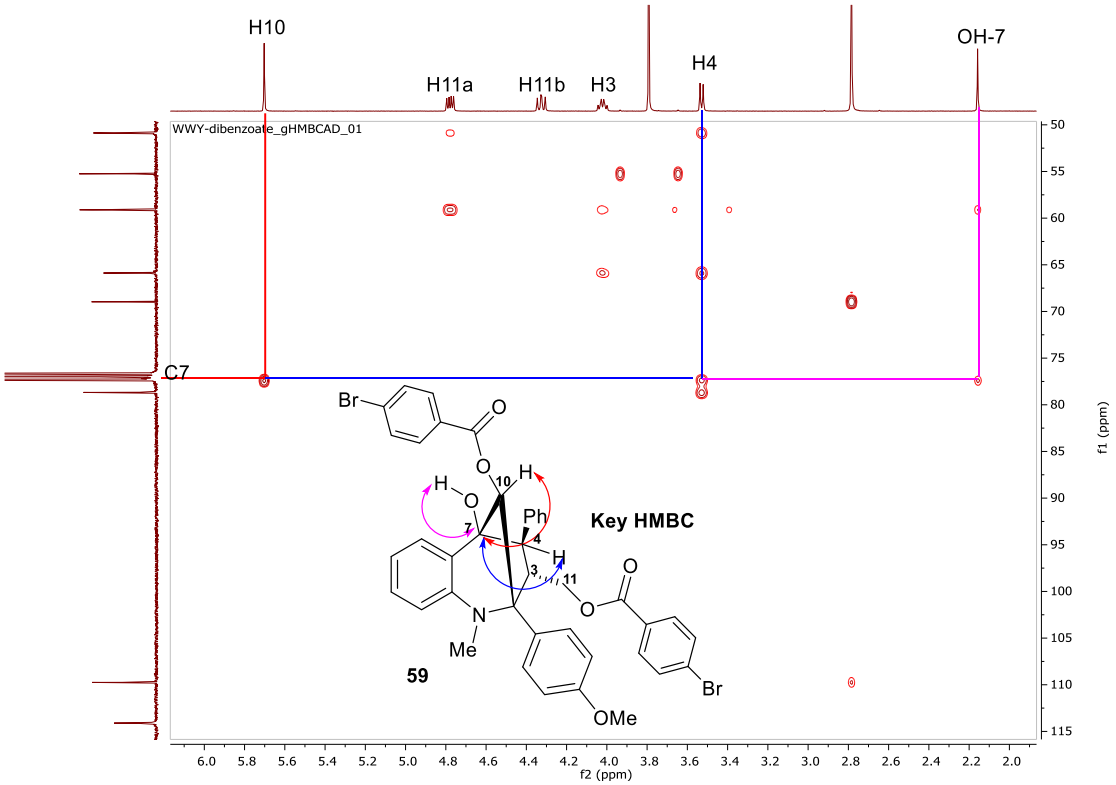

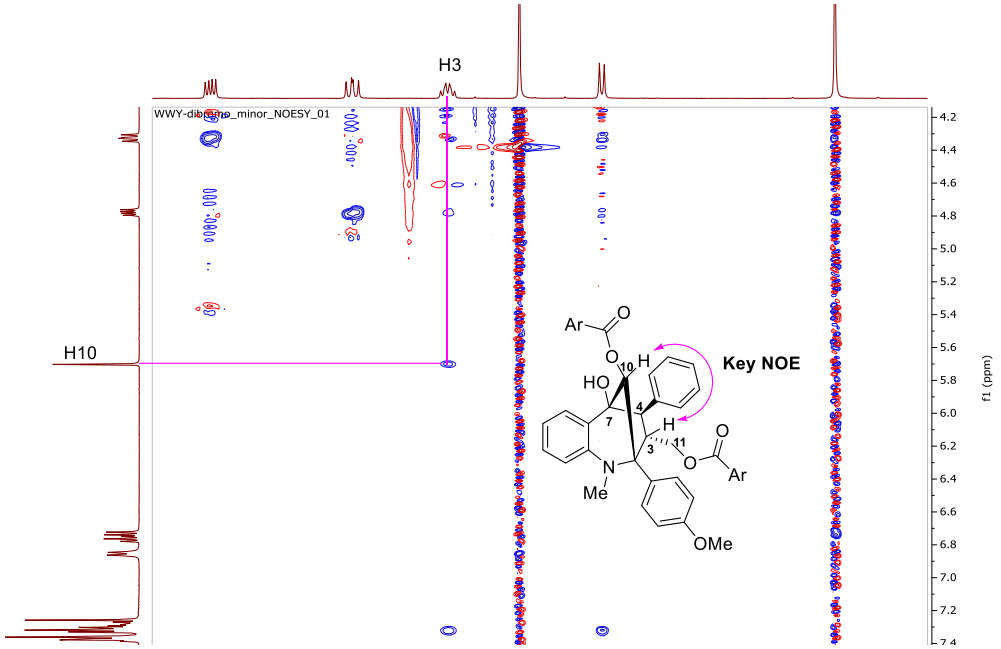

NOESY Spectrum for Compound **91a**:

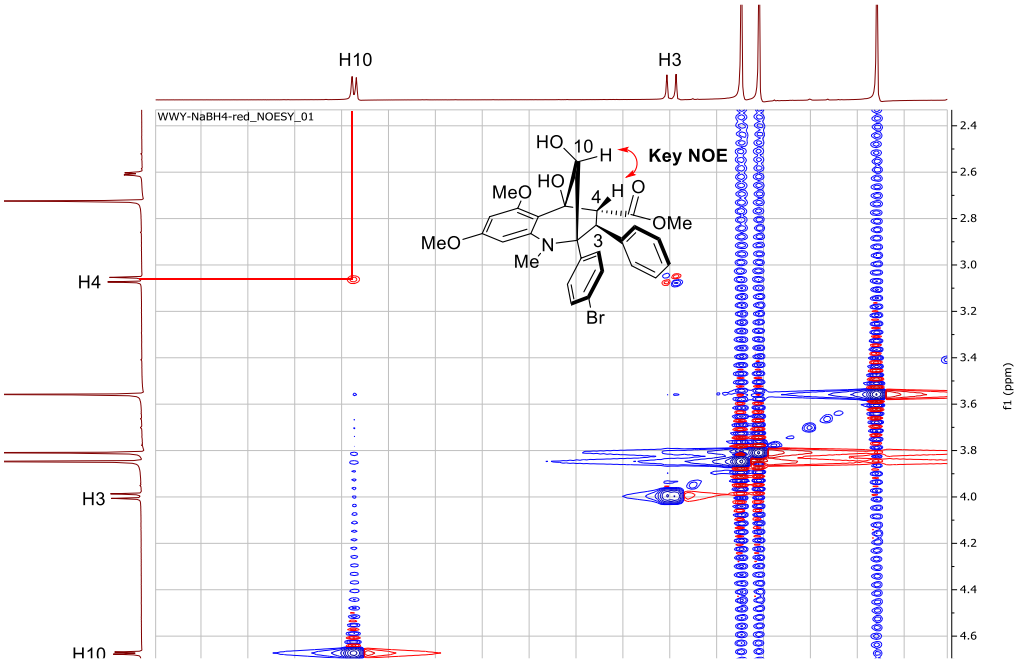

NOESY Spectrum for Compound **97**:

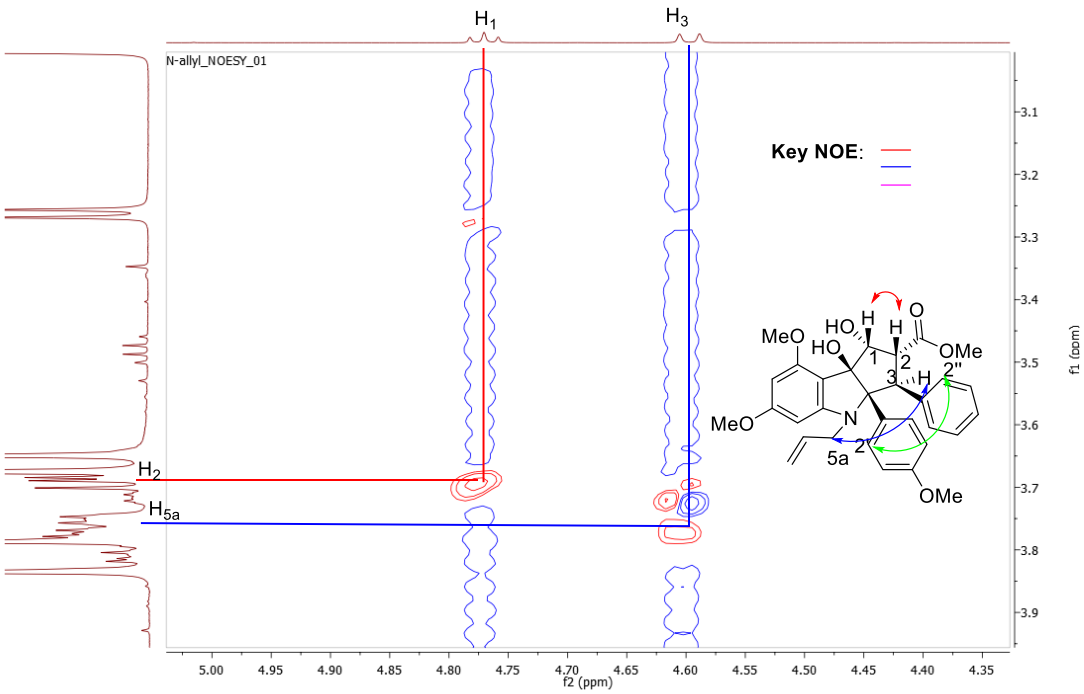

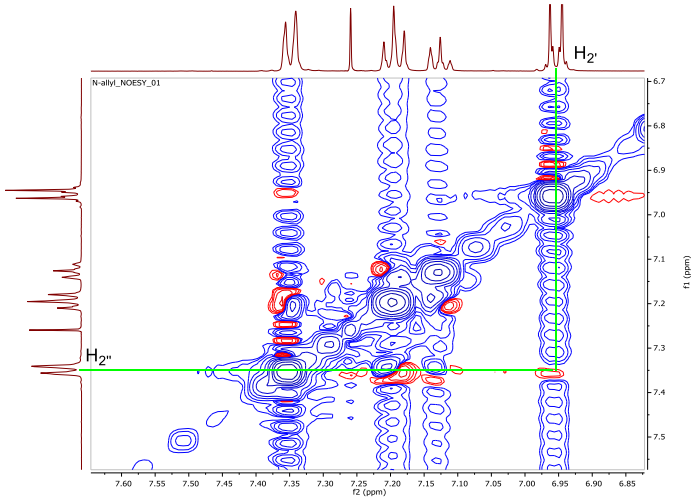

CHAPTER FOUR

Computational Studies of TADDOL-Mediated Enantioselective ESIPT Photocycloadditions

As described in section 1.3.2, 3-hydroxyflavone (3-HF, **1**) and methyl cinnamate **2** undergo enantioselective ESIPT photocycloaddition in the presence of *tetrakis*-1-pyrenyl TADDOL **3** or *tetrakis*-9-phenanthrenyl TADDOL **5** as chiral hydrogen bonding additives (**Scheme 4.1**). Although this methodology was an elegant enantioselective photocycloaddition strategy to access rocaglate natural products, the mechanism by which TADDOL imparts enantioselectivity in the reaction was still poorly understood, providing motivation for detailed inquiry. Furthermore, such mechanistic studies may provide additional insight for future development of a catalytic variant of this asymmetric ESIPT photocycloaddition. In this section, we will present our collaborative work with Prof. David Coker and coworkers (Boston University) to elucidate the enantio-determining transition state for the asymmetric ESIPT photocycloaddition employing Metadynamics calculations.

Scheme 4.1 TADDOL-Mediated Enantioselective ESIPT Photocycloaddition

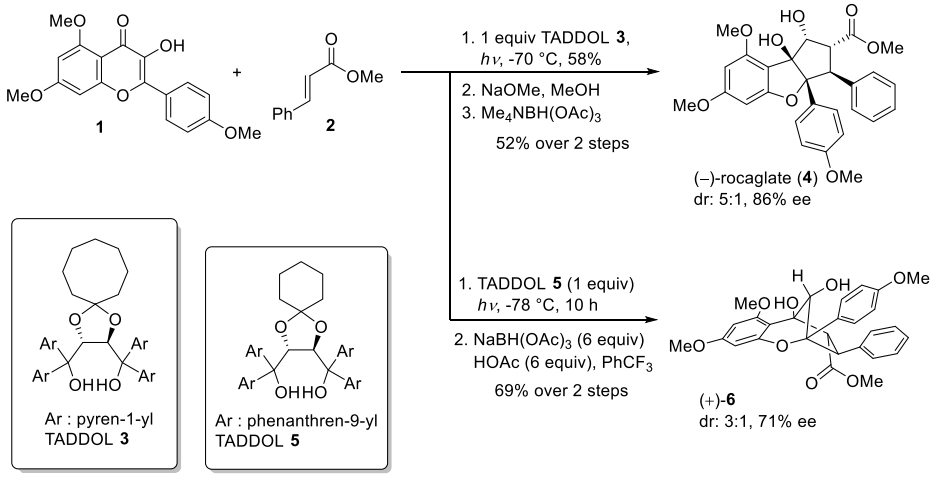

4.1 Catalytic, Enantioselective Photochemical Reactions

Before proceeding with our computational studies, it is important to highlight relevant literature describing the advancement of catalytic, enantioselective photochemical reactions.[93] In 2005, Bach and coworkers presented the first catalytic, enantioselective photochemical cyclization using chiral benzophenone catalyst **9** which may form two hydrogen bonds with substrate **7** (**Scheme 4.2a**).[94] Upon photoirradiation, the benzophenone moiety may trigger photoinduced electron transfer (PET) to generate radical intermediate **8**. Subsequently, asymmetric cyclization affords the chiral spirocyclic pyrrolizidine product **10** in 38% ee They proposed a model wherein the bottom face of the substrate was blocked, thus leading to stereochemical induction. More recently, Bach and coworkers reported the utilization of a chiral xanthone catalyst **12**[95] which was selectively excited using a 366 nm light source followed by triplet energy transfer ($E_T \approx 310$ kJ/mol) to lactam **12** ($\lambda_{max} = 315$ nm, $E_T \approx 280$ kJ/mol, with no absorbance at 366 nm) (**Scheme 4.2b**). This efficient process was also assisted by a double hydrogen bonding interaction between catalyst **12** and lactam **11.** Rapid intramolecular [2+2]-cycloaddition inside the chiral environment yielded regioisomers **13** and **14**, each in 94% ee.

Scheme 4.2 Catalytic, Enantioselective Photoreaction Using Double Hydrogen Bonding Catalysts

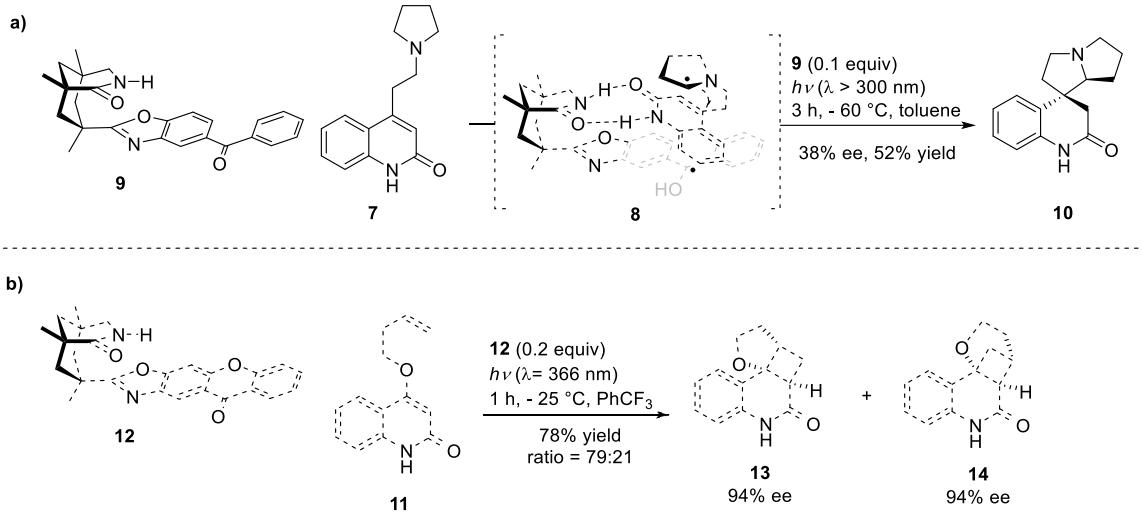

Bathochromic shifts of the absorbance of a reactant's chromophore to eliminate background photoreactions was also employed in catalytic, enantioselective photochemistry development. In 2013, Bach and coworkers applied this strategy to intramolecular [2+2]-cylcoaddition of the homoallylic alkene-tethered lactam **15** (**Scheme 4.3**).[96] Chiral Lewis acid **16** could sufficiently bind substrate **15** and lead to a bathochromic shift of the maximum absorption wavelength of **15** from 290 nm to 343 nm so that photoexcitation at 366 nm promoted the [2+2]-cycloaddition, leading to the formation of **17** in 84% yield and 88% ee

Scheme 4.3 Bathochromic Shift Strategy in Catalytic Enantioselective Photocycloaddition

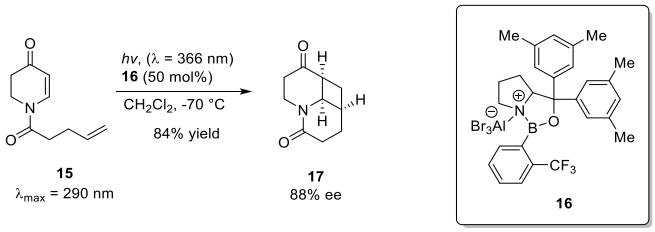

Additionally, Sivaguru and coworkers have reported a catalytic, enantioselective [2+2]-photocycloaddition of alkenyl coumarins to afford photocycloadducts in 96% ee with 10 mol% catalyst loading (**Scheme 4.4**).[97] In this report, the authors proposed that thiourea catalyst **19** was donating neither its triplet nor its singlet energy to the ground state of coumarin **18** which is supported by fluorescence data (singlet energy) and phosphorescence (triplet energy) measurements. Because both the singlet and triplet energies of coumarin **18** were higher than that of catalyst **19**, direct energy transfer from catalyst **19** to substrate **18** to introduce asymmetric photocycloaddition was ruled out. On the other hand, since the fluorescence signal of thiourea **19** was quenched by addition of coumarin substrate **18**, exciplex formation between photoexcited **19*** and **18** was proposed to be responsible for the observed catalysis. They also propose that the reaction most likely proceeded in the triplet state, as oxygen in the solvent could act as a triplet quencher resulting in lower conversions.

Scheme 4.4 Catalytic, Enantioselective [2+2] Photocycloaddition *via* Exciplex Formation

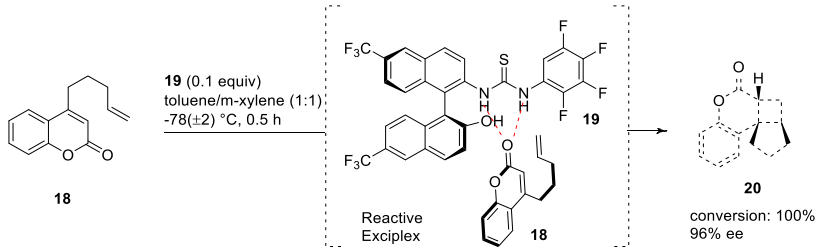

Melchiorre and coworkers reported a catalytic asymmetric quaternary carbon center formation *via* iminium ion trapping of photoinduced electron transfer-generated radicals.[98] Upon photoirradiation, tetrabutylammonium decatungstate (TBADT) could generate a nucleophilic carbon-centered radical by homolytically cleaving the methylene C–H bond in **22** *via* a hydrogen atom transfer (HAT) mechanism (**Scheme 4.5**). Subsequent

radical addition to iminium intermediate **25** generate from condensation between cyclohexenone **21** and amine catalyst **23** to afford intermediate **26**. Carbazole functionality was found to be an optimal moiety in the catalyst design because of its excellent electron-donating capability and the high stability of the long-lived carbazole radical cation which should lead to formation of radical cation **27**. After tautomerization, back electron transfer (BET) and hydrolysis, product **24** was produced in 69% yield and 97% ee.

Scheme 4.5 Catalytic Asymmetric Iminium Ion Trapping of Radicals *via* Photoredox/Organocatalysis Combination

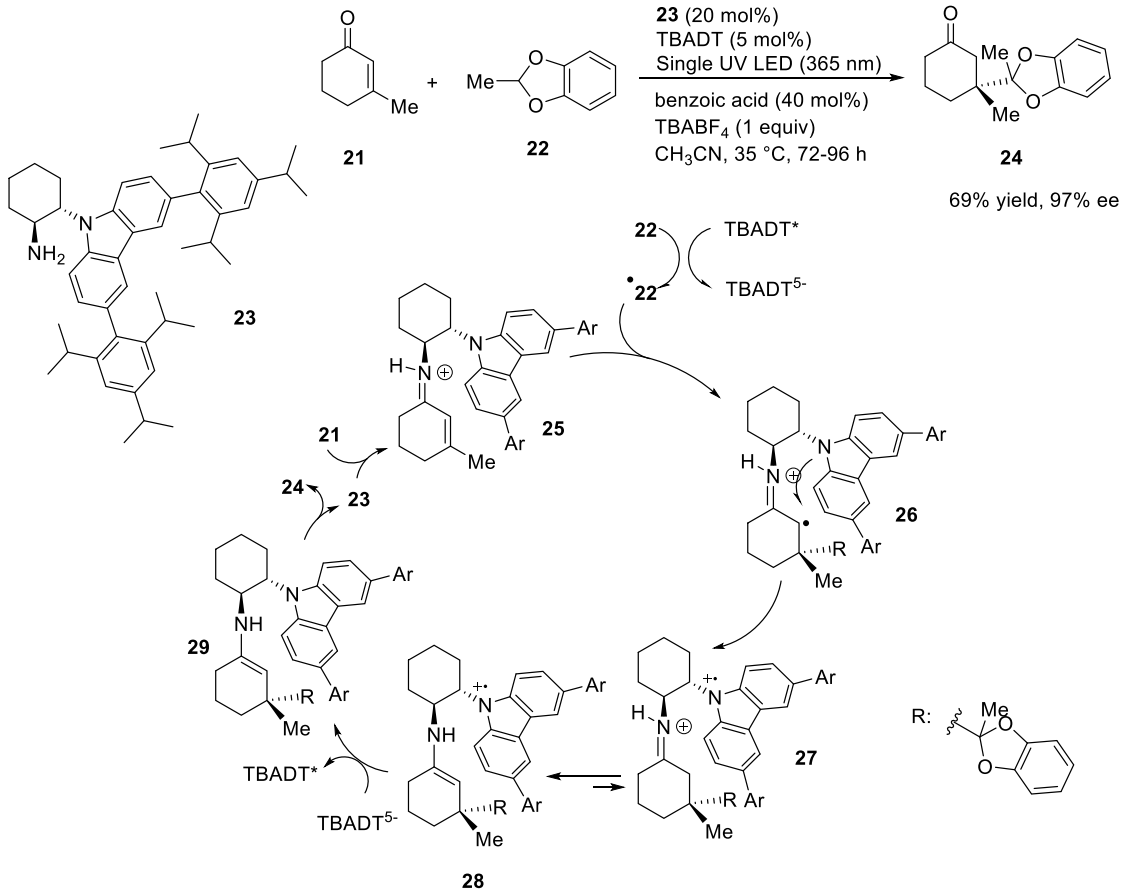

Lastly, Yoon and coworkers disclosed a chiral Lewis acid complex catalyzed asymmetric [2 + 2] photocycloadditions of 2′-hydroxychalcones *via* triplet energy transfer

from an electronically excited photosensitizer (**Scheme 4.6**).[99] In their reaction design, the triplet energy of 2′-hydroxychalcone **30** was determined to be 54 kcal/mol which is higher than the photocatalyst **32** (46 kcal/mol) indicating that electronically excited photocatalyst **32** could not transfer its triplet energy to 2′-hydroxychalcone **30** to achieve photocycloaddition. By this means, the racemic background reaction can be minimized. However, when the reaction was conducted with various oxophilic Lewis acids, formation of [2+2] cycloadduct **33** was observed because chelation with Lewis acid could induce a dramatic decrease in the triplet energy of substrate **30** (33 kcal/mol) enabling the triplet energy transfer. Based on this discovery, use of a chiral Lewis acid complex should induce a highly enantioselective reaction. After condition optimization, using 10 mol% of a scandium/*t*-BuPyBox complex as catalyst, [2+2] photocycloadduct **33** was obtained in 84% yield and 93% ee.

Scheme 4.6 Catalytic Asymmetric [2+2] Photocycloaddition *via* Lewis Acid-Catalyzed Triplet Energy Transfer

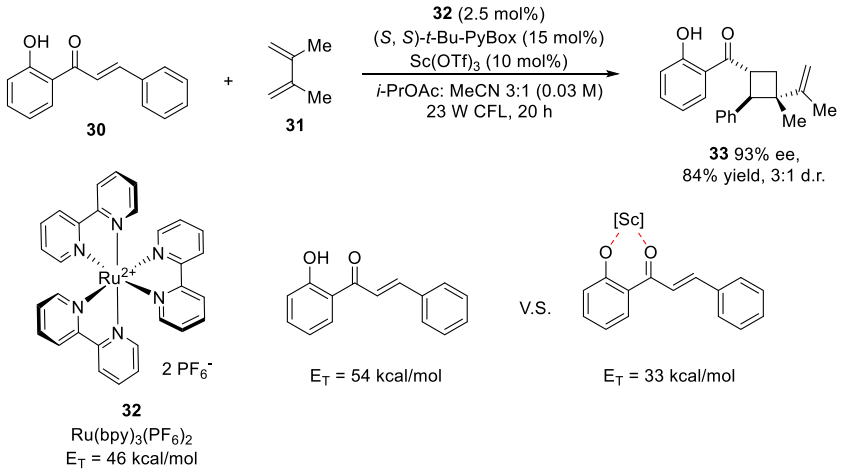

4.2 Computational Studies of TADDOL-Mediated Enantioselective ESIPT Photocycloadditions

It is likely that TADDOL **5** is inducing enantioselectivity by forming a hydrogen bond complex with the substrate, and we hoped to more accurately elucidate in the natural of the complex and the mechanism of stereochemical induction for the ESIPT photocycloadditions. Prior to our computational studies, it is also important to highlight pioneering computational study by Houk and coworkers on 1-naphthyl-TADDOL[100]-catalyzed hetero-Diels-Alder (HDA) reaction.[101] Using a combination of molecular mechanics and ONIOM(B3LYP/6-31G(d):AM1) as calculation method, Houk and coworkers elucidated that 1-naphthyl-TADDOL promotes the reaction by coordination of the carbonyl oxygen through a cooperative hydrogen bonding motif and orientation of the aldehyde by CH-π interaction (**Scheme 4.7**). Herein, in collaboration with Professor David Coker, Mr. Thomas Heavey, and Dr. Juan Ortiz-Sanchez (Boston University), we considered whether 9-phenanthrenyl TADDOL **5** was inducing enantioselectivity by first binding to 3-HF **1** in the ground state (**Figure 4.1**). To elucidate the hydrogen bonding mechanism of TADDOL in the enantioselective ESIPT photocycloaddition, we introduced a biased sampling approach using well-tempered metadynamics,[102] an approach to calculating free energies in systems that exhibit rare events by choosing a set of collective variables as a function of coordinates in which free energy could be sampled. We employed metadynamics calculations[103] under the assumption that a ground state equilibrium exists prior to photoexcitation, and that these ground state catalytic complexes ultimately take part in the subsequent photocycloaddition event.

Scheme 4.7 Houk's Computational Modeling of TADDOL-catalyzed HDA Reaction

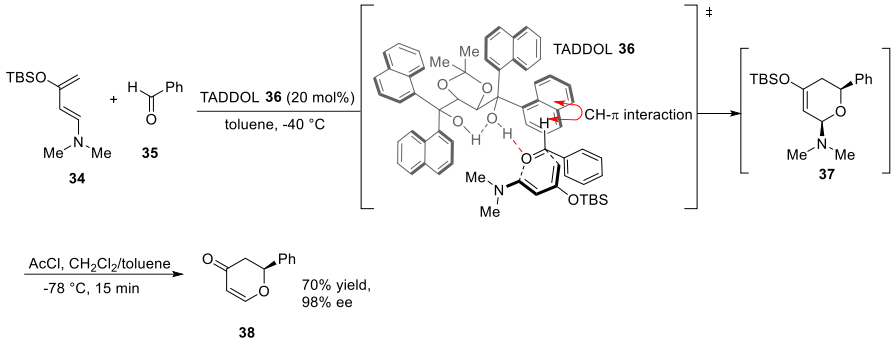

In order to exhaustively explore configurations in the ground state, we chose to use metadynamics simulations, which would allow us to sample molecular conformations that are not accessible by regular molecular dynamics simulation time-scales, and to map out the underlying free energy surface (FES) associated with the sampled configurations of 3-HF **1** / methyl cinnamate **2** docking to the TADDOL **5** additive in solution. In addition, we chose a set of collective variables as a function of coordinates to sample the free energy. The collective variables (CVs) used in the metadynamics simulations consisted of the hydrogen bond distances between the carbonyl oxygen of 3-HF **1**, one of alcohol proton of TADDOL **5** (CV1), and between the alcohol proton of 3-HF **1** and the second alcohol oxygen of TADDOL **5** (CV2) (**Figure 4.1**). To measure the enantioselectivity of the hydrogen bonding interaction in the ground state, we set up reactants in four distinct orientations. These experimentally relevant conformations are *re-si-endo*, *si-re-endo*, *re-si-exo* and *si-re-exo* (**Figure 4.2**) which model the facial selectivity and diastereoselectivity of the ESIPT photocycloaddition.

Figure 4.1 Collective Variables Used in Metadynamics Trajectories

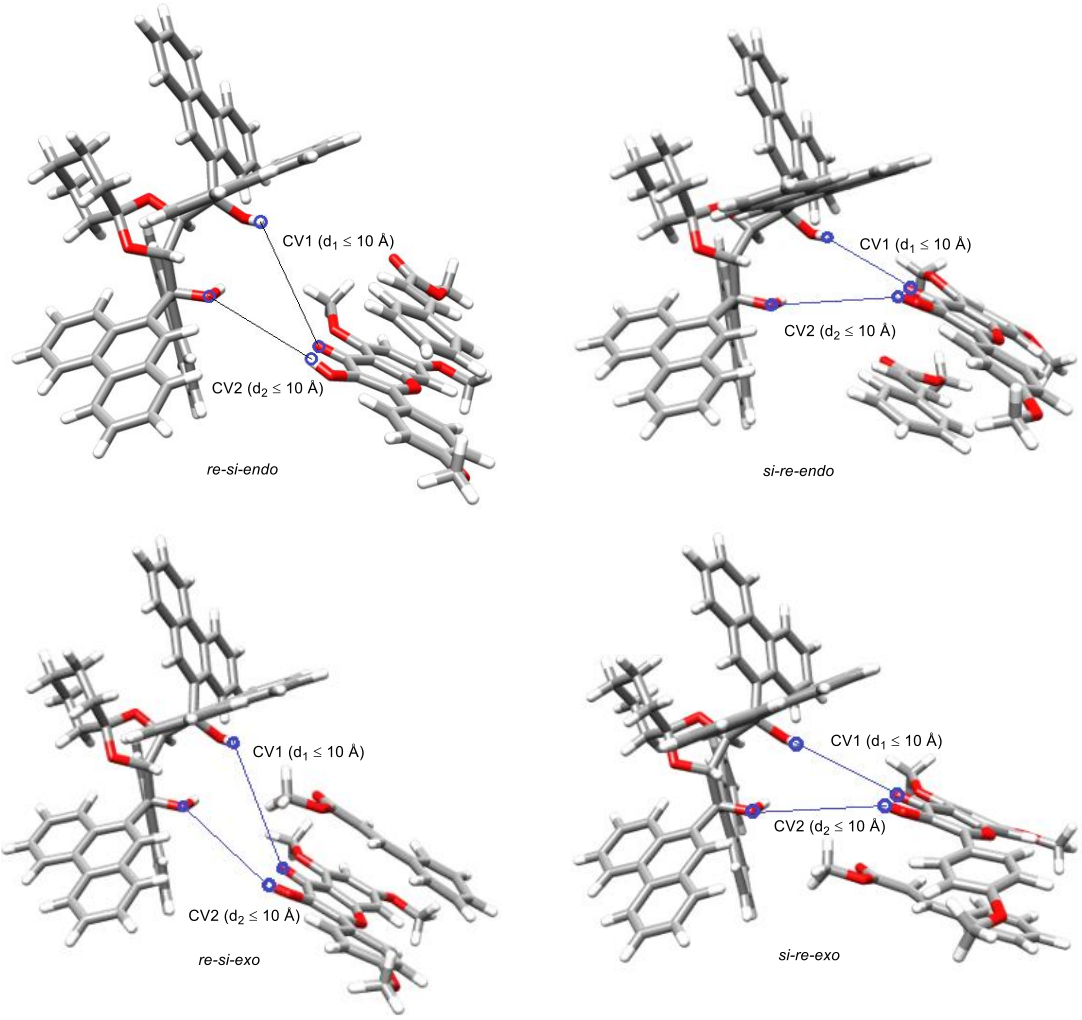

Each studied system was set up following a standard molecular dynamics geometry optimization and equilibration procedure before full metadynamics production. The Gromacs 5.0.2 package[104] and the all-atom Generalized Amber Force Field (GAFF)[105] were employed. The Antechamber software[106] was used to generate the topologies from the coordinate files. The geometries of TADDOL **5**, 3-HF **1**, and methyl cinnamate **2** were optimized in the gas phase and atomic partial charges were computed at the Hartree-Fock/6-31G* basis set level of theory using the Gaussian 09 package. Furthermore, the

atomic partial charges were constructed using the RESP (Restrained Electro Static Potential)[107,108] scheme and constrained during the fit in accordance to the GAFF protocol, as implemented in Antechamber.

We next examined our computation based on our definition of CVs (**Figure 4.1**) the formation of pre-reactant complexes (PRCs) between TADDOL **5** and 3-HF **1** at short distance values of CV1 and CV2 corresponding to the hydrogen-bonding interactions. The obtained FESs from the four considered systems revealed a set of FES topologies, such as **Figure 4.2** for *re-si-endo* which would lead to formation of the major product based on our experimental observations.

Figure 4.2 Free Energy Surfaces (FES) with TADDOL/3-HF/methyl cinnamate in *re-si-endo*

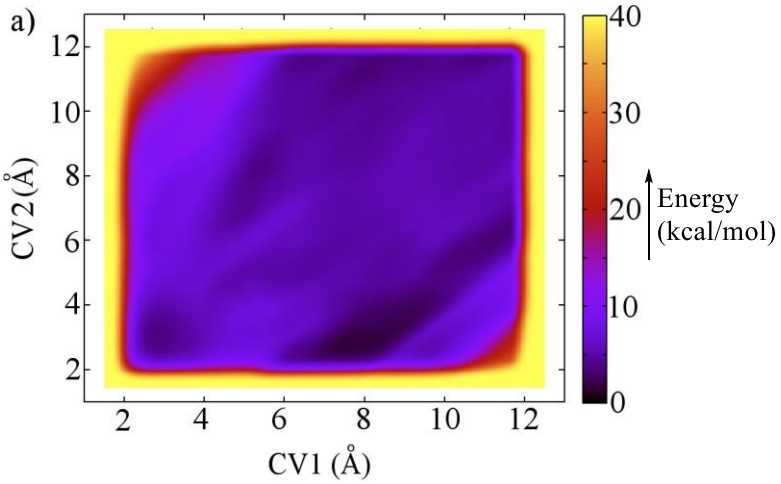

A deeper analysis of the geometries sampled in the energy minima outlined in **Figure 4.2** revealed a common trend across the four studied systems. At short CV distances (either CV1 or CV1 and CV2), 3-HF establishes one or two hydrogen-bonding interactions with TADDOL across the defined CVs or between atoms not defined in our set of CVs, for example between the carbonyl oxygen of 3-HF and the alcohol hydrogen of TADDOL not

included in the corresponding CV definition. Simultaneously, these hydrogen-bonding interactions are reinforced by a π-π stacking interaction between one phenanthren-9-yl group of TADDOL and the phloroglucinol moiety of 3-HF **1**. This particular interaction also blocked one face of 3-HF leaving the other open to enantioselective approch.

As shown in **Figure 4.2**, the most relevant energy minima associated to TADDOL trajectories for our definition of CVs correspond to a combination of short distances CV1/CV2. In **Figure 4.3** we highlight these minima by plotting the free energy profiles of the TADDOL 3-HF/methyl cinnamate system over CV1 along the cuts CV2 = 3 Å. The *re-si-endo* profiles clearly showed the deeper energy minima and the shape and depth of the energy minima for the *re-si-endo* and *si-re-endo* systems do not drastically change.

Figure 4.3 Free Energy Profiles Across CV2 = 3 Å with TADDOL/3-HF/methyl cinnamate in a) *re-si-endo*, b) *si-re-endo*, c) *re-si-exo* and d) *si-re-exo* Orientations

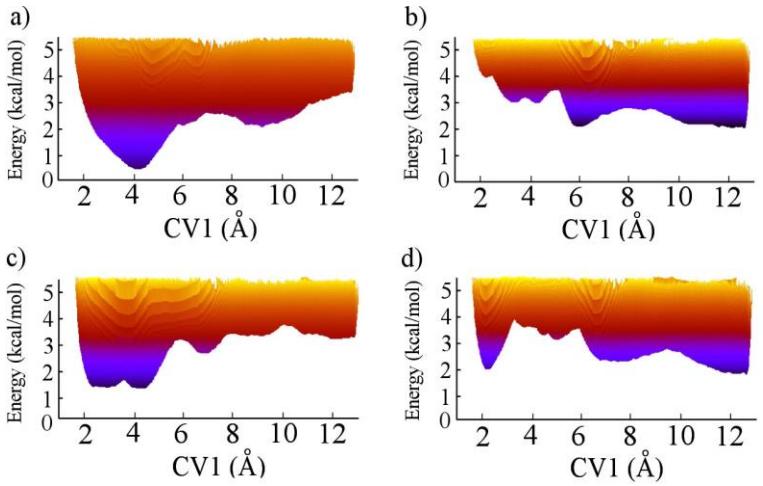

In order to identify chemically relevant PRCs, we have processed every sampled geometry contained in each energy minima and extracted those complexes that simultaneously exhibit hydrogen-bonding and π-π stacking interaction between TADDOL and 3-HF. These two conditions are defined as the distance between any hydrogen bond

donor and acceptor pairs between TADDOL **5** and 3-HF **1** with a maximum of 2.5 Å, and the distance between the center of 3-HF and any phenanthren-9-yl group of TADDOL up to a maximum of 3.5 Å. **Table 4.1** shows the percentages over the total of sampled geometries that fulfill these two conditions for each system.

Table 4.1 Percentages of Sampled TADDOL/3-HTMF/methyl cinnamate Pre-reactant Complexes that Simultaneously Contain Hydrogen-bonding Interaction and a π- π Stacking Interaction Between TADDOL and 3-HF.

Endo		*Exo*	
re-si	*si-re*	*re-si*	*si-re*
98.6	74.3	90.3	89.5

As is evident, at least 70% of the total sampled geometries in the most predominant energy minima for each system fulfill the specified conditions, indicating that hydrogen-bonding and π-π stacking interactions significantly contribute to the stability of the PRCs. It is important to note that not all of these hydrogen-bonding or π-π stacking interactions were included in our definition of CVs. As it has been shown in previous studies, the sampling performed with metadynamics under a specific set of CVs can also provide useful insight on other relevant coordinates and interactions in the system under study. Nonetheless, we cannot ignore the involvement of excited electronic states in this reaction. The Coker group is currently investigating the energy barriers in both uncatalyzed and catalyzed reactions in both the ground and excited states as well as the involvement of excited triplet state of 3-HF **1** to further improve our calculation.

4.3 Experimental Validations

Using metadynamics calculations, we determined the hydrogen bonding complex between TADDOLs and 3-hydroxyflavone to be the enantio-determining assembly for the

ESIPT photocycloaddition. In order to test this hypothesis, we have conducted an array of enantioselective ESIPT photocycloadditions using methyl cinnamate **2** and stilbene **34**[44] as dipolarophiles with stoichiometric quantities of TADDOL **5**. In collaboration with Dr. Neil Lajkiewicz, **Table 4.2** was constructed to show photocycloadditions with varying equivalencies of the dipolarophile methyl cinnamate **2** (or stilbene **34**) and stoichiometric amounts of 3-HF **5**. Interestingly, by reducing the equivalents of **2**, the enantiomeric excess of the observed photocycloadducts (+)-**6** and (+)-**35** was found to decrease. These results indicate that by decreasing the equivalents of methyl cinnamate, lower enantioselectivities were observed, which supports the idea that formation of a hydrogen bonding complex between TADDOL **5** and 3-HF **1** is crucial for the enantioselectivity in the ESIPT photocycloaddition. Presumably, this may be due to the excited tautomeric intermediate of 3-hydroxyflavone **1** dissociating from TADDOL **5** before photocycloaddition with methyl cinnamate **2**. Therefore, lowering the equivalents of methyl cinnamate **2** when employing a stoichiometric amount of host complex should have this effect according to studies and proposals outlined by Bach and coworkers.[95]

Figure 4.4 Possible Host-Guest Complex of TADDOL 5 with 3-HF 1 in Comparison with TADDOL 5 with Methyl Cinnamate 2.

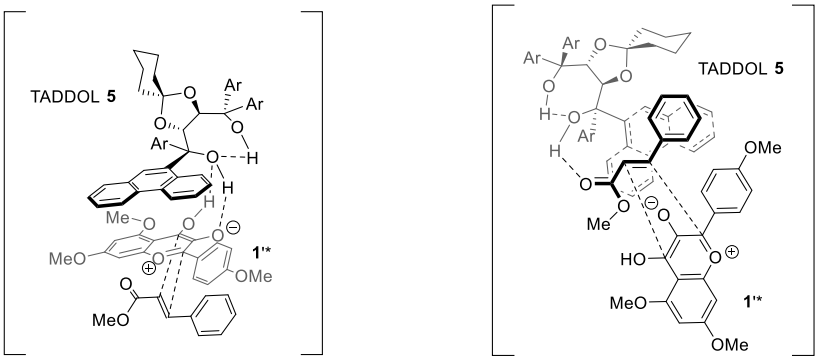

methyl cinnamate approaches from the bottom face of tautomer **1'***.

tautomer **1'*** approaches from the top face of methyl cinnamate.

Additionally, the relevance of a hydrogen-bonded complex was supported by use of *trans*-stilbene **39** as dipolarophile because the hydrogen bonding acceptor, the methyl ester moiety on methyl cinnamate **2** (**Figure 4.4**), is now substituted by a phenyl group. Despite the lack of hydrogen bonding acceptor on *trans*-stilbene **39**, the photocycloaddition still afforded high enantioselectivity in the photocycloaddition and suggested a trend that higher equivalents of TADDOL relative to methyl cinnamate **2** leads to greater enantiomeric excess. In a previous study, we have determined the absolute conformation of (+)-**6** using X-ray crystallography.

Table 4.2 Effects of Dipolarophile and Equivalence on Enantioselectivity of ESIPT Photocycloaddition.

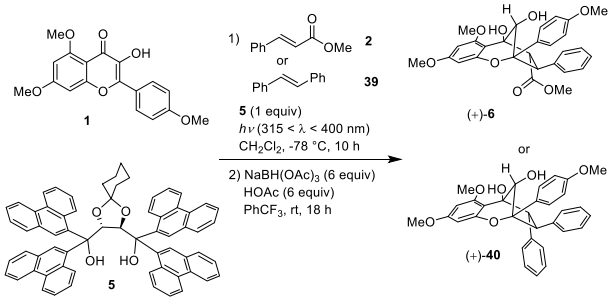

Entry	Equiv of **1**	Dipolarophile (equiv)	Product (yield)	ee (%)
1	1	**2** (5 equiv)	**6** (34%)	78
2	1	**2** (2 equiv)	**6** (15%)	66
3	1	**2** (1 equiv)	**6** (6%)	48
4	2	**2** (1 equiv)	**6** (3%)	60
5	1	**39** (5 equiv)	**40** (27%)	82
6	1	**39** (2 equiv)	**40** (15%)	67
7	1	**39** (1 equiv)	**40** (9%)	48
8	2	**39** (1 equiv)	**40** (6%)	41

In order to study and compare hydrogen bonding complexation for both reactions, it was important to obtain the absolution configuration of the corresponding aglain derivative (+)-**39**. We first attempted to obtain an enantioenriched crystal of (+)-**39** or its *para*-bromobenzoate derivative. However, we were only able to obtain racemic material after recrystallization due to centrosymmetric crystallization. Previously, we have reported a method to employ kinetic resolution of aglain ketones using asymmetric transfer hydrogenation.[10] We anticipated that using this methodology on the racemic stilbene photocycloadduct (±)-**40**, we could obtain an enantioenriched crystal of (+)-**39** to compare with products obtained using enantioselective photocycloaddition (**Table 4.2**). Gratifyingly, we found that asymmetric transfer hydrogenation of aglain ketone (±)-**41** *via* Rh-(III) catalysis afforded the enantioenriched aglain (±)-**40** in 98% ee and 45% yield (**Scheme 4.8**). Using isopropanol with diethyl ether as a solvent mixture for recrystallization, compound **40** was obtained in enantioenriched form which was unambiguously confirmed by X-ray crystallography. The major enantiomer of **40** produced by photocycloaddition (**Table 4.2**) was found to be in agreement with the antipode shown in **Scheme 4.8**. With this data in hand, we can conclude that TADDOL-mediated enantioselective photocycloaddition proceeded *via* a hydrogen bonded complex of TADDOL and 3-hydroxyflavone being the enantio-determining assembly.

Scheme 4.8 Asymmetric Transfer Hydrogenation of Aglain Ketone (±)-41

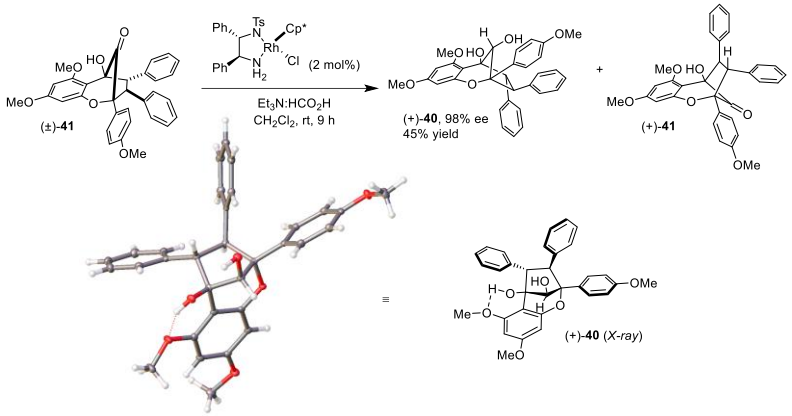

4.4 Progress Towards Catalytic Asymmetric ESIPT Photocycloaddition

Having established that hydrogen-bonding in combination with π-π stacking interactions could play an important role in enantioselective ESIPT photocycloadditions using metadynamics calculations, we next planned to take advantage of this discovery to design a catalytic asymmetric ESIPT photocycloaddition. Previously, Dr. Neil Lajkiewicz in the Porco laboratory had evaluated a substantial number of catalysts including thioureas, TADDOLs, and chiral trifluoroethanols in an attempt to identify ESIPT photocycloaddition catalysts. Namely, under UV irradiation (λ_{max} = 350 nm) , 3-HF **1** was reacted with 1 equivalent of methyl cinnamate **2** in -78 °C using 20 mol% catalyst (**Scheme 4.9**). However, 40% enantiomeric excess of the product **6** was the best result achieved in the presence of **44** due to undesired racemic background reaction.

Scheme 4.8 Previous Attempts Towards Catalytic Asymmetric ESIPT Photocycloaddition

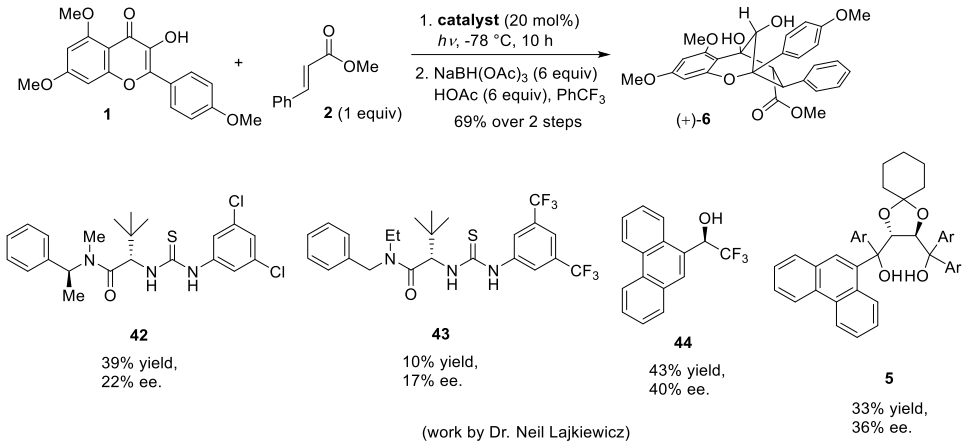

From metadynamics-sampled geometries between TADDOL **5** and 3-HF **1**, there is substantial population which contains a short distance between one phenanthren-9-yl group of TADDOL and the phloroglucinol moiety of 3-HF **1**. This observation also leads us to consider the possibility of the formation of an exciplex between TADDOL **5** and 3-HF **1** *via* π-π stacking. In order to test our hypothesis, a fluorescence quenching study was performed (**Figure 4.5b**), which clearly showed quenching of the fluorescence signal of TADDOL **5** upon addition of 3-HF **1** (*cf.* **Scheme 4.4**). This study indicates that formation of an exciplex between TADDOL **5** and 3-HF **1** is highly possible in solution.

Figure 4.5 UV-Vis Absorption of TADDOL 5 and Fluorescence Quenching Study.

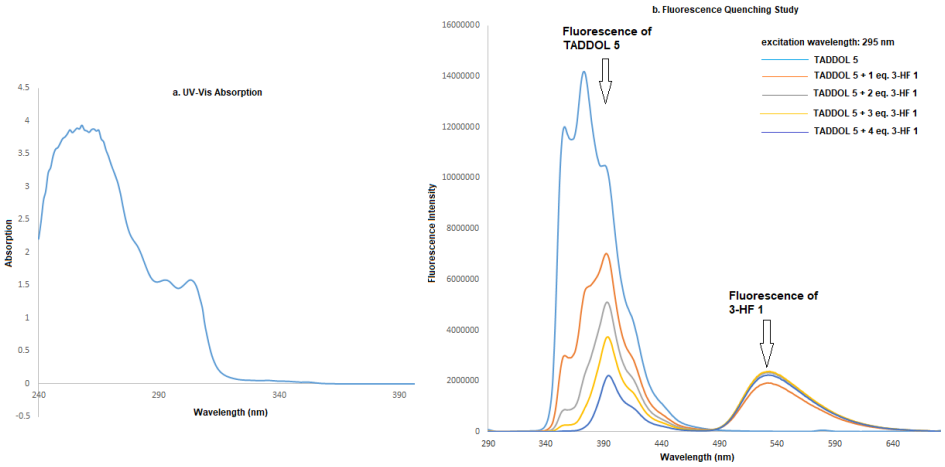

In order to achieve catalytic asymmetric ESIPT photocycloaddition, we need to minimize or eliminate the racemic background reaction. Accordingly, use of a red-shifted light source in comparison to the previously used UV-lamp (λ_{max} = 350 nm) may be helpful for elimination of the background reaction (3-HF **1**, $\lambda_{ab,max}$ = 365 nm). Towards this end, two visible light sources, namely Kessil® purple LED's (370 nm < λ < 405 nm, λ_{max} = 390 nm) and Kessil® blue LED's (400 nm < λ < 450 nm, λ_{max} = 427 nm) were used.[109] In order to compare with our previous stoichiometric results, we chose TADDOL **5** as catalyst. Gratifyingly, we did observe some improvement by using visible light sources for the ESIPT photocycloaddition. First, using a Kessil® purple LED (390 nm) as light source, a 49% ee of product (+)-**6** was observed after 36 h of irradiation. When Kessil® blue LEDs (427 nm) were used, the enantiomeric excess of the product was increased to 60% (**Scheme 4.10**).

Scheme 4.10 Catalytic Asymmetric ESIPT Photocycloaddition using Visible Light

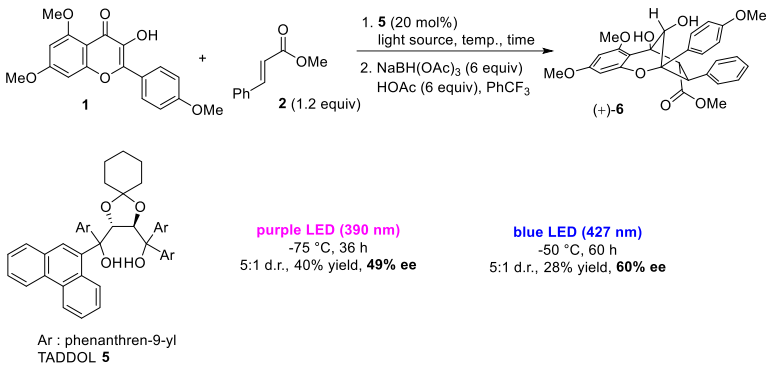

These preliminary results are quite encouraging; however, further photophysical studies will be required to decipher the mechanism of the visible light-mediated, catalytic asymmetric ESIPT photocycloaddition. More importantly, we will screen additional hydrogen bonding catalysts bearing polyaromatic substitution such as phenanthrenyl or anthracenyl which may potentially have π-π stacking interactions with 3-HF **1**. Furthermore, the impact of reaction solvent and temperature should also be studied as well to identify optimal conditions for the catalytic asymmetric ESIPT photocycloadditions.

4.5 Summary

In summary, we have utilized computation to decipher the enantio-determining hydrogen bonding complex for the TADDOL-mediated enantioselective ESIPT photocycloadditions. Using metadynamic simulations under the assumption that ground state pre-reactant complexes (PRCs) exists prior to photoexcitation, free energy surfaces (FESs) were obtained based on two defined collective variables. Evaluation of these FESs also showed good agreement with our experimental data that *re-si-endo* orientation would lead to formation of the major enantiomer as well as diastereomer. From the sampled geometries in the energy minimum of the FES, we also discovered that in addition to

hydrogen-bonding interactions, π-π stacking interactions between TADDOL and 3-HF may also contribute to the stability of the PRCs.

To further validate our computational data, we conducted a series of TADDOL-mediated enantioselective ESIPT photocycloadditions which unambiguously confirmed that the hydrogen-bonding complex between 3-HF and TADDOL is the enantio-determining assembly for the enantioselective ESIPT photocycloaddition. Furthermore, metadynamics calculations have also provide further insight to aid development of catalytic, asymmetric ESIPT photocycloadditions.

4.6 Experimental Section

Instrumentation and Methods: ^{1}H NMR spectra were recorded at 400 or 500 MHz at ambient temperature with $CDCl_3$(Cambridge Isotope Laboratories, Inc.) as solvent. Data for ^{1}H NMR are reported as follows: chemical shift, integration, multiplicity (brs = broad singlet, s = singlet, d = doublet, t = triplet, q = quartet, m = multiplet) and coupling constants in Hz. ^{13}C NMR spectra were recorded at 100.0 or 125 MHz at ambient temperature with the same solvents unless otherwise stated. Chemical shifts are reported in parts per million relative to the deuterated solvents. All ^{13}C NMR spectra were recorded with complete proton decoupling. Infrared spectra were recorded on a Nicolet Nexus 670 FT-IR spectrophotometer. High-resolution mass spectra were obtained in the Boston University Chemical Instrumentation Center using a Waters Q-TOF API-US mass spectrometer. Melting points were recorded on a Mel-Temp apparatus (Laboratory Devices). Optical rotations were recorded on an AUTOPOL III digital polarimeter at 589 nm, and specific rotations are given $[\alpha]^{D}_{20}$ (concentration in grams/100 mL solvent). Chiral HPLC analysis of enantioenriched compounds was performed using a Waters 1525 Binary HPLC Pump with a Waters 2487 diode array detector. Analytical thin layer chromatography (TLC) was performed using 0.25

mm silica gel 60-F plates (Silicycle, Inc.) Analytical thin layer chromatography was performed using 0.25mm silica gel 60-F plates. Flash chromatography was performed using 200-400 mesh silica gel (Scientific Absorbents, Inc.). Yields refer to chromatographically and spectroscopically pure materials, unless otherwise stated. HPLC grade tetrahydrofuran, methylene chloride, diethyl ether, toluene, acetonitrile, and benzene were purchased from Fisher and VWR and were purified and dried by passing through a PURE SOLV® solvent purification system (Innovative Technology, Inc.). Other ACS grade solvents for chromatography were purchased from Clean Harbors.

General Procedure and Synthesis:

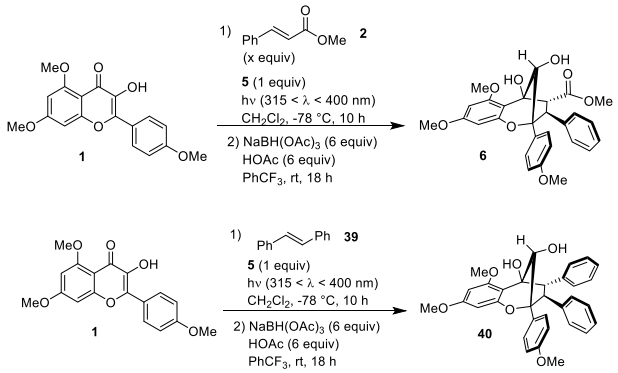

General Procedure to Perform Low Temperature, Asymmetric Photocycloaddition with TADDOL 5:

A flame-dried Pyrex photoreaction tube was charged with 3-hydroxyflavone **1** (20 mg, 0.061 mmol, 1 equiv), methyl cinnamate **2** (Reaction 1 in **Table 4.2**, 49.4 mg, 0.305 mmol, 5 equiv), TADDOL **5** (55.1 mg, 0.061 mmol, 1 equiv) and 2 mL dry CH_2Cl_2 (0.03 M). After degassing with argon for 10 min, the mixture was irradiated at -78 °C in the Rayonet RPR-3100 reactor ($300 < \lambda < 400$ nm) for 10 h. The solution was concentrated *in vacuo* to afford a brown-yellow oil. Purification *via* flash

chromatography using a gradient of hexanes/EtOAc (80:20 to 30:70) afforded cyclopenta[*bc*]benzopyran aglain ketone compound, a light yellow foam, as a mixture of isomers (e.g. Reaction 1 in **Table 4.2** 13 mg). This mixture of isomers was used without further purification and was transformed into the desired reduced aglain **6** using sodium triacethoxyborohydride. A dry test tube was charged with a stir bar, reducing agent (0.166 mmol, 6 equiv.), acetic acid (9 µL, 0.166 mmol, 6 equiv.), and trifluorotoluene (1.5 mL) at rt under argon. The mixture was then sonicated briefly and stirred at rt for 10 min. The crude aglain from the previous reaction (13 mg) was then added at rt in one portion under argon. The resulting mixture was then stirred for 24 h and was quenched with saturated ammonium chloride, extracted with CH_2Cl_2, washed with saturated sodium bicarbonate, and dried over sodium sulfate. The filtrate was concentrated *in vacuo*. Column chromatography using 5:95 EtOAc/CH_2Cl_2 afforded compound **5** as a white solid (10.2 mg, 0.021 mmol, 34%). Reaction 1 - 8 in **Table 4.2** were all conducted using this general procedure.

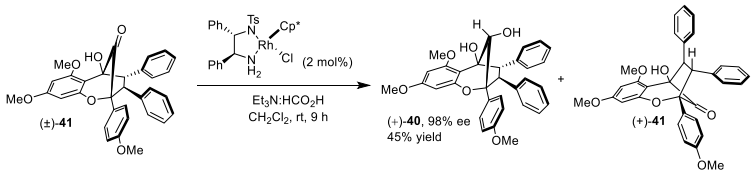

Kinetic Resolution of Aglain (±)-41:

A dry flask was charged with a stir bar, (±)-**41** (100 mg, 0.19 mmol, 1 equiv) and CH_2Cl_2 (5 mL). In a separate dry test tube, $[RhCl_2(Cp^*)]_2$ (1.17 mg, 0.0019 mmol, 1 mol%), (*S*,*S*)-*N*-Tosyl diphenylethylenediamine (1.39 mg, 0.0038 mmol, 2 mol%), formic acid (14.33 µL, 0.38 mmol, 2.0 equiv), triethylamine 52.7 mL, 0.38 mmol, 2.0 equiv), and CH_2Cl_2 (2 mL) were combined and stirred for 30 min. At this time, the entire contents of the separate flask were added to the reaction mixture and the reaction was allowed to stir at room temp. for 12 h. After this time, a saturated sodium bicarbonate solution was added (5 mL), the reaction was diluted and extracted with CH_2Cl_2

(3 × 10 mL), and finally dried with anhydrous sodium sulfate, filtered, and concentrated *in vacuo*. The crude product was purified *via* silica gel column chromatography (1:3 EtOAc/hexanes to 2:3 EtOAc/hexanes) to afford compound **40** in 45% yield (46 mg, 0.0946 mmol) as a white solid. The enantiopurity of (+)-**40** was determined using analytical chiral HPLC (98% ee). $[\alpha]_D^{20}$ = + 53.1° (*c* = 0.1, CH_2Cl_2). R_f = 0.43 (EtOAc: hexanes = 1 : 1); m.p. = 108 - 110 °C (CH_2Cl_2). IR ν_{max} (film): 3482, 2941, 2839, 1618, 1518, 1252, 1148, 1090, 829, 701 cm^{-1}; ^1H NMR (500 MHz, $CDCl_3$) δ 7.48 (d, J = 9 Hz, 2H), 7.15 (m, 5H), 6.97 (m, 5H), 6.70 (d, J = 9 Hz, 2H), 6.17 (d, J = 2.25 Hz, 1H), 5.85 (d, J = 2.25, 1H), 5.35 (s, 1H), 4.92 (s, 1H), 4.23 (d, J = 10 Hz, 1H), 4.12 (d, J = 10 Hz, 1H), 3.76 (s, 3H), 3.72 (s, 3H), 3.48 (bs, 1H), 3.10 (s, 3H); ^{13}C NMR (125 MHz, $CDCl_3$) δ 160.9, 158.8, 158.7, 153.4, 141.9, 137.2, 130.30, 130.25, 129.9, 128.9, 128.7, 127.5, 126.7, 125.8, 112.9, 106.2, 94.1, 92.4, 89.4, 82.1, 79.0, 66.1, 59.3, 55.6, 55.4, 55.1; HRMS-ESI (m/z): $[M+H]^+$ calcd for $C_{32}H_{30}O_6$, 511.2121; found 511.2121.

Chiral HPLC Analysis:

Chiral HPLC analysis of aglain compound 6.

The following chiral HPLC conditions were used for the separation of enantiomers of **6**: ChiralPak AD 150 × 4.6 mm column, 20% isopropanol in hexane. Flow rate: 1.0 mL/min. UV detector: 214 nm. Retention times: 13.5 min and 21.7 min.

Reaction 1 in **Table 4.2**: ESIPT photocycloaddition of 3-hydroxyflavone **1** with 5.0 equiv of methyl cinnamate **2** in the presence of 1.0 equiv of TADDOL **5**.

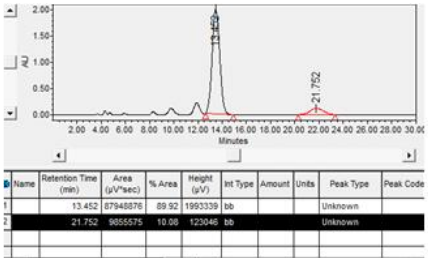

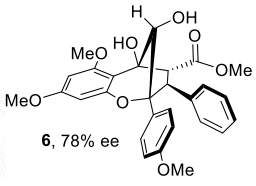

6, 78% ee

Reaction 2 in **Table 4.2**: ESIPT photocycloaddition of 3-hydroxyflavone **1** with 2.0 equiv of methyl cinnamate **2** in the presence of 1.0 equiv of TADDOL **5**.

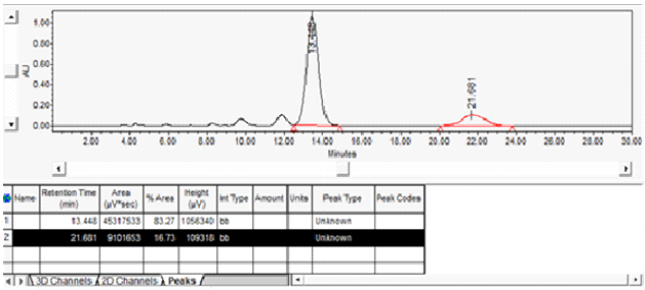

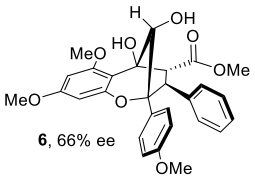

6, 66% ee

Reaction 3 in **Table 4.2**: ESIPT photocycloaddition of 3-hydroxyflavone **1** with 1.0 equiv of methyl cinnamate **2** in the presence of 1.0 equiv of TADDOL **5**.

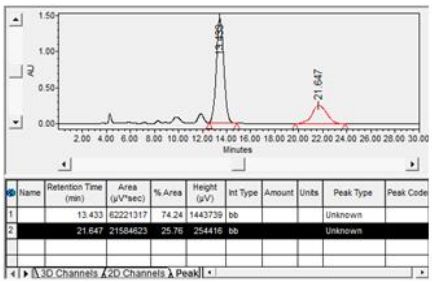

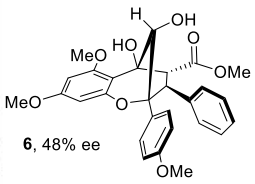

6, 48% ee

Reaction 3 in **Table 4.2**: ESIPT photocycloaddition of 3-hydroxyflavone **1** with 0.5 equiv of methyl cinnamate **2** in the presence of 1.0 equiv of TADDOL **5**.

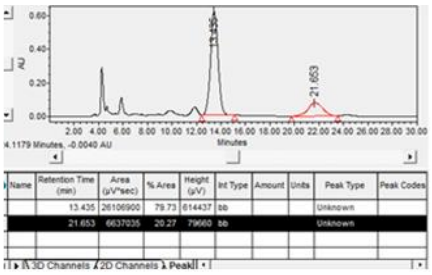

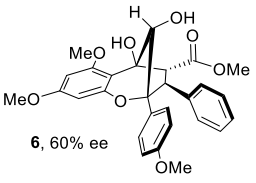

6, 60% ee

Chiral HPLC analysis of aglain 40.

The following chiral HPLC conditions were used for the separation of enantiomers of **40**: ChiralPak AD 150 × 4.6 mm column, 20% isopropanol in hexane. Flow rate: 1.0 mL/min. UV detector: 214 nm. Retention times: 8.6 min and 15.2 min.

Reaction 5 in **Table 4.2**: ESIPT photocycloaddition of 3-hydroxyflavone **1** with 5.0 equiv of *trans*-stilbene **39** in the presence of 1.0 equiv of TADDOL **5**.

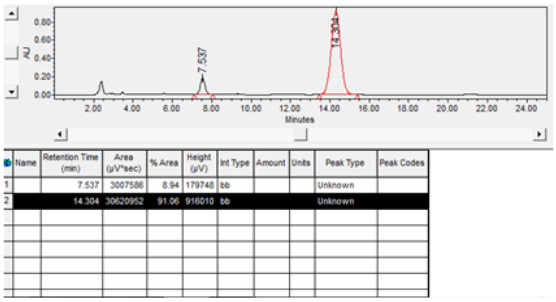

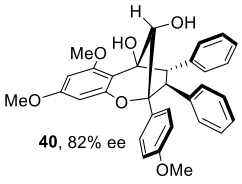

40, 82% ee

Reaction 6 in **Table 4.2**: ESIPT photocycloaddition of 3-hydroxyflavone **1** with 2.0 equiv of *trans*-stilbene **39** in the presence of 1.0 equiv of TADDOL **5**.

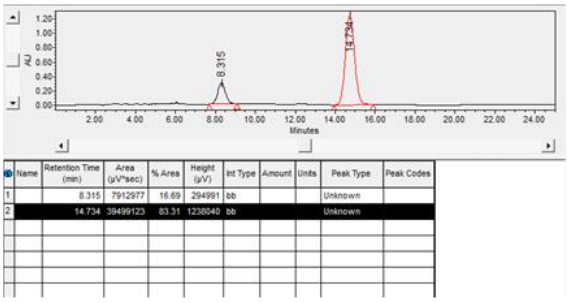

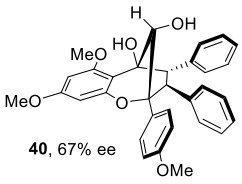

40, 67% ee

Reaction 7 in **Table 4.2**: ESIPT photocycloaddition of 3-hydroxyflavone **1** with 1.0 equiv of *trans*-stilbene **39** in the presence of 1.0 equiv of TADDOL **5**.

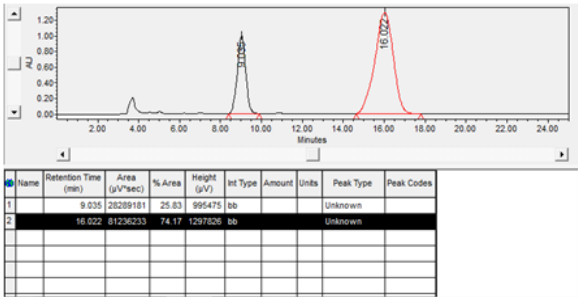

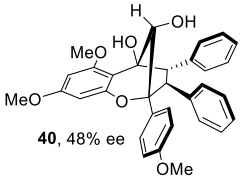

40, 48% ee

Reaction 5 in **Table 4.2**: ESIPT photocycloaddition of 3-hydroxyflavone **1** with 0.5 equiv of *trans*-stilbene **39** in the presence of 1.0 equiv of TADDOL **5**.

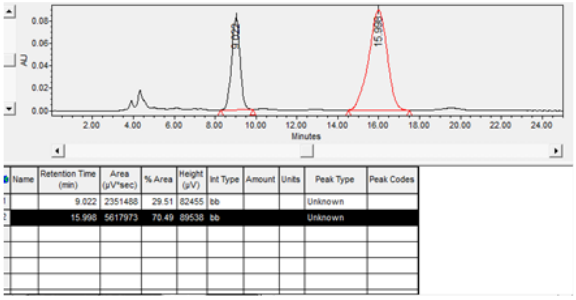

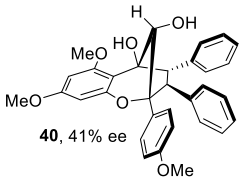

Kinetic resolution of agalin ketone compound (±)-**41** using asymmetric transfer hydrogenation.

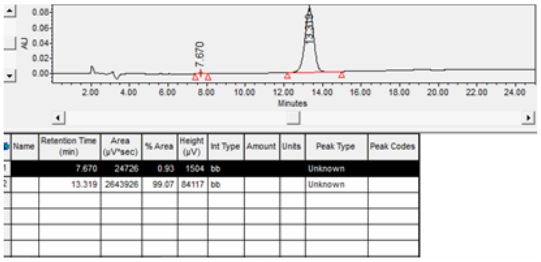

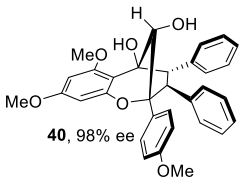

Visible Light-mediated Catalytic Asymmetric ESIPT Photocycloaddition.

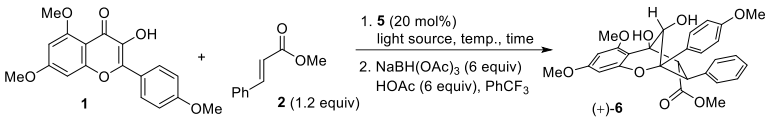

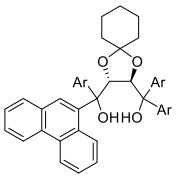

Ar : phenanthren-9-yl
TADDOL **5**

purple LED (390 nm)
-75 °C, 36 h
5:1 d.r., 40% yield, 49% ee

blue LED (427 nm)
-50 °C, 60 h
5:1 d.r., 28% yield, 60% ee

To a flame-dried test tube was charged with 3-HF **1** (30 mg, 0.091 mmol, 1 equiv), TADDOL **5** (16.6 mg, 0.018 mmol, 0.2 equiv), methyl cinnamate **2** (18 mg, 0.111 mmol, 1.2 equiv), and 9 mL dry CH_2Cl_2 (0.01 M). The resulting mixture was degassed for 15 min using sonication in combination with simultaneously bubbled argon into the solution. The test tube was then carefully sealed and put into a dewar. The low temperature was kept using a cooling finger which was also monitored by a thermometer. After certain time of

irradiation, the reaction mixture was concentrated *in vacuo* and redissolved in 3 mL trifluorotoluene. Subsequently, sodium triacetoxyborohydride (116 mg, 0.55 mmol, 6 equiv) and acetic acid (0.031 mL, 0.55 mmol, 6 equiv) were added. The resulting mixture was stirred at room temperature for 10 hours before quenched with 10 mL Sat. NH_4Cl (aq.). After extraction with CH_2Cl_2, the solution was dried over anhydrous Na_2SO_4. The reaction mixture was concentrated *in vacuo* and purified *via* column chromatograph (eluent: hexanes/EtOAc = 15:1 to remove TADDOL and remaining methyl cinnamate, then hexanes/EtOAc = 2:1) to yield the desired product (+)-**6**. ^{1}H NMR of obtained (+)-**6** was found in good agreement with previous characterized spectrum.

Chiral HPLC analysis of aglain compound 6.

The following chiral HPLC conditions were used for the separation of enantiomers of **6**: ChiralPak AD 150 × 4.6 mm column, 20% isopropanol in hexane. Flow rate: 1.0 mL/min. UV detector: 214 nm.

ESIPT photocycloaddition of 3-hydroxyflavone **1** with 1.2 equiv of methyl cinnamate **2** in the presence of 0.2 equiv of TADDOL **5** using purple LED as light source:

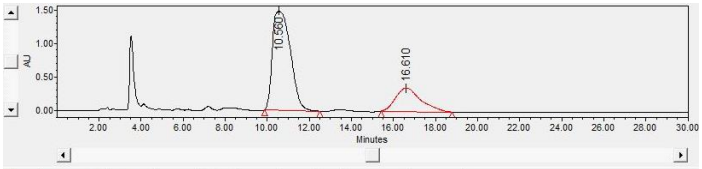

	Name	Retention Time (min)	Area (μV*sec)	% Area	Height (μV)	Int Type	Amount	Units	Peak Type	Peak Codes
1		10.560	88327090	75.34	1479092	bb			Unknown	
2		16.610	28915735	24.66	350783	bb			Unknown	

3D Channels / 2D Channels \ Peaks /

ESIPT photocycloaddition of 3-hydroxyflavone **1** with 1.2 equiv of methyl cinnamate **2** in the presence of 0.2 equiv of TADDOL **5** using blue LED as light source:

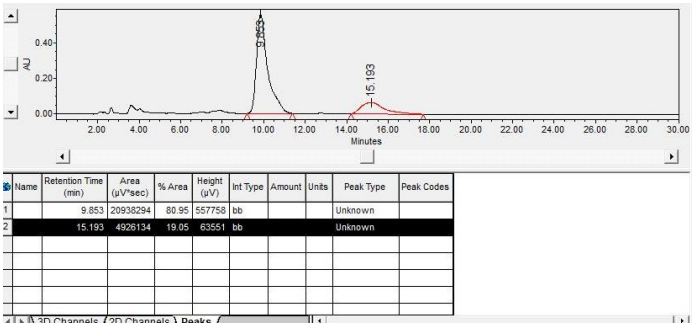

X-Ray Crystallographic Data for Compound (+)-40:

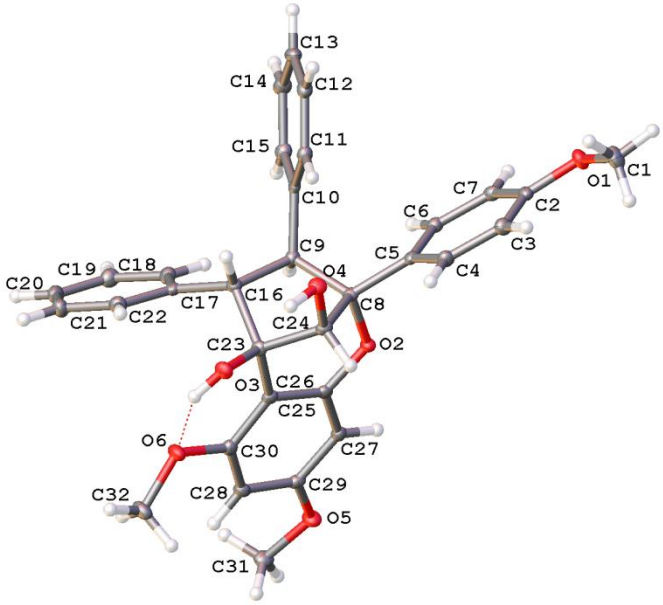

Crystals of compound **40** suitable for X-ray analysis were obtained by slow evaporation from Et_2O / isopropanol = 1 : 1.

Crystal Data:

$C_{32}H_{30}O_6$	D_x = 1.389 Mg m^{-3}
M_r = 510.56	Cu $K\alpha$ radiation, λ = 1.54178 Å
Orthorhombic, $P2_12_12_1$	Cell parameters from 9448 reflections

a = 6.4886 (3) Å	θ = 3.8–66.6°
b = 12.6920 (5) Å	μ = 0.77 mm^{-1}
c = 29.6551 (12) Å	T = 100 K
V = 2442.20 (18) $Å^3$	Block, colorless
Z = 4	0.44 × 0.32 × 0.30 mm
F(000) = 1080	

Data collection:

Bruker Proteum-R diffractometer	4264 independent reflections
Radiation source: rotating anode	4263 reflections with $I > 2\sigma(I)$
Montel	R_{int} = 0.039
ω and ϕ scans	θ_{max} = 66.7°, θ_{min} = 3.8°
Absorption correction: multi-scan *SADABS* (Bruker, 2006)	h = -7→7
T_{min} = 0.699, T_{max} = 0.753	k = -15→15
75526 measured reflections	l = -35→35

Refinement:

Refinement on F^2	Hydrogen site location: difference Fourier map
Least-squares matrix: full	H atoms treated by a mixture of independent and constrained refinement
$R[F^2 > 2\sigma(F^2)]$ = 0.022	$w = 1/[\sigma^2(F_o^2) + (0.020P)^2 + 0.695P]$ where $P = (F_o^2 + 2F_c^2)/3$
$wR(F^2)$ = 0.054	$(\Delta/\sigma)_{max} < 0.001$
S = 1.05	$\Delta\rangle_{max}$ = 0.21 e $Å^{-3}$
4264 reflections	$\Delta\rangle_{min}$ = -0.15 e $Å^{-3}$
352 parameters	Absolute structure: Flack x determined using 1791 quotients [(I+)-(I-)]/[(I+)+(I-)] (Parsons, Flack and Wagner, Acta Cryst. B69 (2013) 249-259).
0 restraints	Flack parameter: 0.038 (11)

Special details

Geometry. All esds (except the esd in the dihedral angle between two l.s. planes) are estimated using the full covariance matrix. The cell esds are taken into account individually in the estimation of esds in distances, angles and torsion angles; correlations between esds in cell parameters are only used when they are defined by crystal symmetry. An approximate (isotropic) treatment of cell esds is used for estimating esds involving l.s. planes.

Refinement. CheckCIF Alert and Discussion:

PLAT089_ALERT_3_C Poor Data / Parameter Ratio (Zmax < 18). 7.12 Note Discussion: The detector on the Proteum-R has a large face which imposes geometric constraints on the collection of data at high angle. Though the data set is reasonably complete to 0.84 Angstroms, there is almost no data to resolution < 0.84 Angstroms, and this tends to yield data sets with a low data to parameter ratio for noncentrosymmetric space groups.

Fractional atomic coordinates and isotropic or equivalent isotropic displacement parameters (Å^2)

	x	*y*	*z*	U_{iso}*/U_{eq}
O2	0.35157 (17)	0.55401 (8)	0.32504 (3)	0.0122 (2)
O3	0.71480 (17)	0.29006 (8)	0.34882 (4)	0.0146 (2)
H3	0.652 (3)	0.2306 (17)	0.3424 (6)	0.022*
O4	0.85687 (17)	0.48478 (8)	0.37095 (3)	0.0141 (2)
H4	0.921 (3)	0.4248 (16)	0.3658 (6)	0.021*
O5	-0.13385 (17)	0.37294 (8)	0.23871 (4)	0.0165 (2)
O1	0.69180 (17)	0.99123 (8)	0.37181 (4)	0.0181 (2)
O6	0.40646 (18)	0.17914 (8)	0.31553 (4)	0.0171 (2)
C10	0.4531 (2)	0.55661 (11)	0.44887 (5)	0.0118 (3)
C2	0.6604 (3)	0.88500 (11)	0.36752 (5)	0.0144 (3)
C9	0.4133 (2)	0.50250 (11)	0.40407 (5)	0.0112 (3)
H9	0.2607	0.4996	0.3996	0.013*
C29	0.1346 (2)	0.26957 (12)	0.27521 (5)	0.0141 (3)
H29	0.0837	0.2052	0.2632	0.017*
C26	0.2870 (2)	0.45739 (12)	0.30956 (5)	0.0117 (3)
C15	0.2885 (3)	0.57899 (12)	0.47744 (5)	0.0146 (3)
H15	0.1520	0.5626	0.4681	0.018*
C28	0.0401 (2)	0.36501 (12)	0.26468 (5)	0.0135 (3)

C6	0.4240 (2)	0.74178 (12)	0.37979 (5)	0.0133 (3)
H6	0.2930	0.7173	0.3896	0.016*
C5	0.5698 (2)	0.66922 (12)	0.36392 (5)	0.0119 (3)
C13	0.5193 (3)	0.65025 (12)	0.53301 (5)	0.0168 (3)
H13	0.5420	0.6819	0.5616	0.020*
C17	0.3562 (3)	0.30213 (12)	0.42292 (5)	0.0132 (3)
C7	0.4675 (2)	0.84833 (12)	0.38146 (5)	0.0144 (3)
H7	0.3666	0.8965	0.3921	0.017*
C16	0.4953 (2)	0.38706 (11)	0.40371 (5)	0.0117 (3)
H16	0.6232	0.3868	0.4225	0.014*
C11	0.6521 (3)	0.58186 (11)	0.46312 (5)	0.0139 (3)
H11	0.7664	0.5666	0.4442	0.017*
C23	0.5663 (2)	0.37135 (12)	0.35399 (5)	0.0118 (3)
C30	0.3051 (2)	0.27043 (12)	0.30362 (5)	0.0133 (3)
C27	0.1181 (2)	0.45931 (12)	0.28071 (5)	0.0130 (3)
H27	0.0572	0.5244	0.2721	0.016*
C25	0.3843 (2)	0.36374 (12)	0.32205 (5)	0.0123 (3)
C18	0.1535 (3)	0.31974 (12)	0.43649 (5)	0.0153 (3)
H18	0.0949	0.3878	0.4329	0.018*
C8	0.5104 (2)	0.55441 (12)	0.36060 (5)	0.0112 (3)
C22	0.4376 (3)	0.20087 (12)	0.42895 (5)	0.0163 (3)
H22	0.5762	0.1872	0.4204	0.020*
C14	0.3212 (3)	0.62491 (13)	0.51935 (5)	0.0173 (3)
H14	0.2077	0.6389	0.5387	0.021*
C24	0.6747 (2)	0.47640 (11)	0.34465 (5)	0.0124 (3)
H24	0.7047	0.4853	0.3118	0.015*
C19	0.0354 (3)	0.23923 (13)	0.45521 (5)	0.0184 (3)
H19	-0.1022	0.2530	0.4644	0.022*
C12	0.6844 (2)	0.62904 (12)	0.50465 (5)	0.0158 (3)
H12	0.8202	0.6470	0.5138	0.019*
C3	0.8058 (2)	0.81452 (12)	0.35122 (5)	0.0157 (3)
H3A	0.9365	0.8390	0.3413	0.019*
C4	0.7585 (2)	0.70718 (12)	0.34950 (5)	0.0148 (3)
H4A	0.8582	0.6592	0.3382	0.018*
C21	0.3199 (3)	0.12042 (13)	0.44708 (5)	0.0197 (3)

H21	0.3774	0.0520	0.4504	0.024*
C20	0.1176 (3)	0.13918 (13)	0.46048 (5)	0.0188 (3)
H20	0.0368	0.0841	0.4731	0.023*
C31	-0.2458 (2)	0.27785 (12)	0.22959 (5)	0.0177 (3)
H31A	-0.1674	0.2342	0.2084	0.027*
H31B	-0.3799	0.2954	0.2164	0.027*
H31C	-0.2667	0.2389	0.2578	0.027*
C32	0.3694 (3)	0.08586 (12)	0.28974 (6)	0.0208 (4)
H32A	0.3893	0.1012	0.2576	0.031*
H32B	0.2277	0.0619	0.2948	0.031*
H32C	0.4659	0.0306	0.2991	0.031*
C1	0.8883 (3)	1.03058 (13)	0.35839 (6)	0.0224 (4)
H1A	0.9090	1.0171	0.3262	0.034*
H1B	0.9966	0.9951	0.3757	0.034*
H1C	0.8945	1.1066	0.3641	0.034*

BIBLIOGRAPHY

(1) Pan, L.; Woodard, J. L.; Lucas, D. M.; Fuchs, J. R.; Kinghorn, A. D. *Nat. Prod. Rep.* **2014**, *31* (7), 924–939.

(2) King, M. L.; Chaing, C.-C.; Ling, H.-C.; Fujita, E.; Ochiai, M.; McPhail, A. T. *J. Chem. Soc. Chem. Commun.* **1982**, *260*, 1150–1151.

(3) Ko, F. N.; Wu, T. S.; Liou, M. J.; Huang, T. F.; Teng, C. M. *Eur. J. Pharmacol.* **1992**, *218*, 129–135.

(4) Ishibashi, F.; Satasook, C.; Isman, M. B.; Towers, G. H. N. *Phytochemistry* **1993**, *32*, 307–310.

(5) Wang, S. K.; Cheng, Y. J.; Duh, C. Y. *J. Nat. Prod.* **2001**, *64*, 92–94.

(6) Ohse, T.; Ohba, S.; Yamamoto, T.; Koyano, T.; Umezawa, K. *J. Nat. Prod.* **1996**, *59*, 650–652.

(7) Hwang, B. Y.; Su, B.; Chai, H.; Mi, Q.; Kardono, L. B. S.; Afriastini, J. J.; Riswan, S.; Santarsiero, B. D.; Mesecar, A. D.; Wild, R.; Fairchild, C. R.; Vite, G. D.; Rose, W. C.; Farnsworth, N. R.; Cordell, G. A.; Pezzuto, J. M.; Swanson, S. M.; Kinghorn, A. D. *J. Org. Chem.* **2004**, *69*, 3350–3358.

(8) Trost, B. M.; Greenspan, P. D.; Yang, B. V.; Saulnier, M. G. *J. Am. Chem. Soc.* **1990**, *112*, 9022–9024.

(9) Gerard, B.; Sangji, S.; O'Leary, D. J.; Porco, J. A., Jr. *J. Am. Chem. Soc.* **2006**, *128*, 7754–7755.

(10) Stone, S. D.; Lajkiewicz, N. J.; Whitesell, L.; Hilmy, A.; Porco, J. A., Jr. *J. Am. Chem. Soc.* **2015**, *137*, 525–530.

(11) Salim, A. A.; Pawlus, A. D.; Chai, H. B.; Farnsworth, N. R.; Douglas Kinghorn, A.; Carcache-Blanco, E. J. *Bioorganic Med. Chem. Lett.* **2007**, *17*, 109–112.

(12) Lajkiewicz, N. J.; Roche, P.; Gerard, B.; Porco, J. A., Jr. *J. Am. Chem. Soc.* **2012**, *134*, 13108–13113.

(13) Salim, A. A.; Chai, H. B.; Rachman, I.; Riswan, S.; Kardono, L. B. S.; Farnsworth, N. R.; Carcache-Blanco, E. J.; Kinghorn, A. D. *Tetrahedron* **2007**, *63*, 7926–7934.

(14) Pan, L.; Acuña, U. M.; Li, J.; Jena, N.; Ninh, T. N.; Pannell, C. M.; Chai, H.; Fuchs, J. R.; Carcache De Blanco, E. J.; Soejarto, D. D.; Kinghorn, A. D. *J. Nat.*

Prod. **2013**, *76*, 394–404.

(15) Dumontet, V.; Thoison, O.; Omobuwajo, O. R.; Martin, M.; Perromat, G.; Chiaroni, A.; Riche, C.; Païs, M.; Sévenet, T.; Chimie, I. De; Cedex, G.; Hadi, A. H. A. *Tetrahedron* **1996**, *52*, 6931–6942.

(16) Nugroho, B. W.; Edrada, R. A.; Wray, V.; Witte, L.; Bringmann, G.; Gehling, M.; Proksch, P. *Phytochemistry* **1999**, *51*, 367–376.

(17) Hailes, H. C.; Raphael, R. A.; Staunton, J. *Tetrahedron Lett.* **1993**, *34*, 5313–5316.

(18) Davey, A. E.; Taylor, R. J. K. *J. Chem. Soc. Chem. Commun.* **1987**, *1*, 25–27.

(19) Kraus, G. A.; Sy, J. O. *J. Org. Chem.* **1989**, *54*, 77–83.

(20) Gerard, B.; Jones, G.; Porco, J. A., Jr. *J. Am. Chem. Soc.* **2004**, *126*, 13620–13621.

(21) Woolfe, G. J.; Thistlethwaite, P. J. *J. Am. Chem. Soc.* **1981**, *103*, 6916–6923.

(22) Seebach, D.; Beck, A. K.; Heckel, A. *Angew. Chem. Int. Ed.* **2001**, *40*, 92–138.

(23) Müller, C.; Bach, T. *Aust. J. Chem.* **2008**, *61*, 557–564.

(24) Gerard, B.; Cencic, R.; Pelletier, J.; Porco, J. A., Jr. *Angew. Chem. Int. Ed.* **2007**, *46*, 7831–7834.

(25) El Sous, M.; Khoo, M. L.; Holloway, G.; Owen, D.; Scammells, P. J.; Rizzacasa, M. A. *Angew. Chem. Int. Ed.* **2007**, *46*, 7835–7838.

(26) Murata, K.; Ikariya, T.; Noyori, R. *J. Org. Chem.* **1999**, *64*, 2186–2187.

(27) Malona, J. A.; Cariou, K.; Frontier, A. J. *J. Am. Chem. Soc.* **2009**, *131*, 7560–7561.

(28) Magnus, P.; Freund, W. A.; Moorhead, E. J.; Rainey, T. *J. Am. Chem. Soc.* **2012**, *134*, 6140–6142.

(29) Zhou, Z.; Tius, M. A. *Angew. Chem. Int. Ed.* **2015**, *54*, 6037–6040.

(30) WELLER, A. H. *Z. Ekectrochem.* **1956**, *60*, 1144–1147.

(31) Paterson, M. J.; Robb, M. A.; Blancafort, L.; DeBellis, A. D. *J. Phys. Chem. A* **2005**, *109* (33), 7527–7537.

(32) Han, D. Y.; Kim, J. M.; Kim, J.; Jung, H. S.; Lee, Y. H.; Zhang, J. F.; Kim, J. S. *Tetrahedron Lett.* **2010**, *51*, 1947–1951.

(33) Pla-Dalmau, A. *J. Org. Chem.* **1995**, *60*, 5468–5473.

(34) Chen, D. Y.; Chen, C. L.; Cheng, Y. M.; Lai, C. H.; Yu, J. Y.; Chen, B. S.; Hsieh, C. C.; Chen, H. C.; Chen, L. Y.; Wei, C. Y.; Wu, C. C.; Chou, P. T. *ACS Appl. Mater. Interfaces* **2010**, *2*, 1621–1629.

(35) Isaks, M.; Yates, K.; Kalanderopoulos, P. *J. Am. Chem. Soc.* **1984**, *106*, 2728–2730.

(36) Doria, F.; Percivalle, C.; Freccero, M. *J. Org. Chem.* **2012**, *77*, 3615–3619.

(37) Lukeman, M.; Wan, P.; Shibahara, F. *J. Am. Chem. Soc.* **2002**, *124*, 9458–9464.

(38) Lukeman, M.; Wan, P. *J. Am. Chem. Soc.* **2003**, *125*, 1164–1165.

(39) Mukhina, O. A.; Bhuvan Kumar, N. N.; Arisco, T. M.; Valiulin, R. A.; Metzel, G. A.; Kutateladze, A. G. *Angew. Chem. Int. Ed.* **2011**, *50*, 9423–9428.

(40) Mukhina, O. A.; Kuznetsov, D. M.; Cowger, T. M.; Kutateladze, A. G. *Angew. Chem. Int. Ed.* **2015**, *54*, 11516–11520.

(41) Mukhina, O. A.; Kutateladze, A. G. *J. Am. Chem. Soc.* **2016**, *138*, 2110–2113.

(42) Kuznetsov, D. M.; Mukhina, O. A.; Kutateladze, A. G. *Angew. Chem. Int. Ed.* **2016**, *55*, 6988–6991.

(43) Mukhina, O. A.; Cronk, W. C.; Kumar, N. N. B.; Sekhar, M. C.; Samanta, A.; Kutateladze, A. G. *J. Phys. Chem. A* **2014**, *118*, 10487–10496.

(44) Roche, S. P.; Cencic, R.; Pelletier, J.; Porco, J. A., Jr. *Angew. Chem. Int. Ed.* **2010**, *49*, 6533–6538.

(45) Santagata, S.; Mendillo, M. L.; Tang, Y.; Subramanian, A.; Perley, C. C.; Roche, S. P.; Wong, B.; Narayan, R.; Kwon, H.; Koeva, M.; Amon, A.; Golub, T. R.; Porco, J. A.; Whitesell, L.; Lindquist, S. *Science.* **2013**, *341*, 242–243.

(46) Matsuura, T.; Takemoto, T.; Nakashima, R. *Tetrahedron* **1973**, *29*, 3337–3340.

(47) McQuade, D. T.; Seeberger, P. H. *J. Org. Chem.* **2013**, *78*, 6384–6389.

(48) Goh, K. S.; Tan, C.-H. *RSC Adv.* **2012**, *2*, 5536–5538.

(49) Wang, W.; Clay, A.; Krishnan, R.; Lajkiewicz, N. J.; Brown, L. E.; Sivaguru, J.; Porco, J. A., Jr. *Angew. Chemie - Int. Ed.* **2017**, DOI: 10.1002/anie.201707539.

(50) Pirkle, W. H.; Sikkenga, D. L.; Pavlin, M. S. *J. Org. Chem.* **1977**, *42*, 384–387.

(51) Brewer, W. E.; Studer, S. L.; Standiford, M.; Chou, P. T. *J. Phys. Chem.* **1989**, *93*, 6088–6094.

(52) Cao, G.; Sofic, E.; Prior, R. L. *Free Radic. Biol. Med.* **1997**, *22*, 749–760.

(53) Liu, J.; Boarman, K. J.; Wendt, N. L.; Cardenas, L. M. *Tetrahedron Lett.* **2005**, *46*, 4953–4956.

(54) Rehm, D.; Weller, A. *Isr. J. Chem.* **1970**, *8*, 259–271.

(55) Berthiol, F.; Doucet, H.; Santelli, M. *Synlett* **2003**, 841–844.

(56) Zhu, S.; Xing, C.; Pang, W.; Zhu, S. *Tetrahedron Lett.* **2006**, *47*, 5897–5900.

(57) Singh, A. K.; Darshi, M.; Kanvah, S. *J. Phys. Chem. A* **2000**, *104*, 464–471.

(58) Verma, S. K.; Acharya, B. N.; Kaushik, M. P. *Org. Lett.* **2010**, *12*, 4232–4235.

(59) Denmark, S. E.; Regens, C. S.; Kobayashi, T. *J. Am. Chem. Soc.* **2007**, *129*, 2774–2776.

(60) Bochevarov, A. D.; Harder, E.; Hughes, T. F.; Greenwood, J. R.; Braden, D. A.; Philipp, D. M.; Rinaldo, D.; Halls, M. D.; Zhang, J.; Friesner, R. A. *Int. J. Quantum Chem.* **2013**, *113*, 2110–2142.

(61) Kuppens, T.; Bultinck, P.; Langenaeker, W. *Drug Discov. Today Technol.* **2004**, *1*, 269–275.

(62) Shen, Y.; Wang, T. *J. Fluor. Chem.* **1994**, *67*, 33–35.

(63) Lemhadri, M.; Battace, A.; Berthiol, F.; Zair, T.; Doucet, H.; Santelli, M. *Synthesis.* **2008**, No. 7, 1142–1152.

(64) Chu, J.; Cencic, R.; Wang, W.; Porco, J. A., Jr.; Pelletier, J. *Mol. Cancer Ther.* **2016**, *15*, 136–141.

(65) Cencic, R.; Carrier, M.; Galicia-Vázquez, G.; Bordeleau, M. E.; Sukarieh, R.; Bourdeau, A.; Brem, B.; Teodoro, J. G.; Greger, H.; Tremblay, M. L.; Porco, J. A., Jr.; Pelletier, J. *PLoS One* **2009**, No. 4, e5223.

(66) Liu, S.; Wang, W.; Brown, L. E.; Qiu, C.; Lajkiewicz, N.; Zhao, T.; Zhou, J.; Porco, J. A.; Wang, T. T. *EBioMedicine* **2015**, *2* (11), 1600–1606.

(67) Basmadjian, C.; Thuaud, F.; Ribeiro, N.; Désaubry, L. *Future Med. Chem.* **2013**, *5*, 2185–2197.

(68) Bruce, I.; Cooke, N. G.; Diorazio, L. J.; Hall, R. G.; Irving, E. *Tetrahedron Lett.* **1999**, *40*, 4279–4282.

(69) Stiles, M. *J. Am. Chem. Soc.* **1959**, *81*, 2598–2599.

(70) Zhao, Q.; Tijeras-Raballand, A.; De Gramont, A.; Raymond, E.; Désaubry, L. *Tetrahedron Lett.* **2016**, *57*, 2943–2944.

(71) Arai, M. A.; Kofuji, Y.; Tanaka, Y.; Yanase, N.; Yamaku, K.; Fuentes, R. G.; Karmakar, U. K.; Ishibashi, M. *Org. Biomol. Chem.* **2016**, *14*, 3061–3068.

(72) Xia, B.; Gerard, B.; Solano, D. M.; Wan, J.; Jones, G.; Porco, J. A., Jr. *Org. Lett.* **2011**, *13*, 1346–1349.

(73) Pavel, H.; Martin, G.; Jan, H.; Antonin, L. *Heterocycles* **2007**, *71*, 269–280.

(74) Cambié, D.; Bottecchia, C.; Straathof, N. J. W.; Hessel, V.; Noël, T. *Chem. Rev.* **2016**, *116*, 10276–10341.

(75) Langlois, N.; Claude, E. T. *Acta Crystallogr.* **1977**, *B33*, 3410–3414.

(76) Yushchenko, D. a.; Shvadchak, V. V.; Klymchenko, A. S.; Duportail, G.; Mély, Y.; Pivovarenko, V. G. *New J. Chem.* **2006**, *30*, 774.

(77) Yushchenko, D. A.; Shvadchak, V. V.; Klymchenko, A. S.; Duportail, G.; Pivovarenko, V. G.; Mély, Y. *J. Phys. Chem. A* **2007**, *111*, 8986–8992.

(78) Pietro, V.; Aurora, B.; Franco, P.; M.Luisa, M. *Heterocycles* **1976**, *4*, 1089–1094.

(79) Hennequin, L. F.; Allen, J.; Breed, J.; Curwen, J.; Fennell, M.; Green, T. P.; Lambert-Van Der Brempt, C.; Morgentin, R.; Norman, R. A.; Olivier, A.; Otterbein, L.; Plé, P. A.; Warin, N.; Costello, G. *J. Med. Chem.* **2006**, *49*, 6465–6488.

(80) Hradil, P.; Hlaváč, J.; Lemr, K. *Journal of Heterocyclic Chemistry*. 1999, pp 141–144.

(81) Morgenstern, A.; Schuijt, C.; Nauta, W. T. *J. Chem. Soc. C* **1971**, 3706–3712.

(82) Spence, T. W. M.; Tennant, G. *J. Chem. Soc. C* **1971**, 3712–3719.

(83) Sicker, D. *J. für Prakt. Chemie* **1990**, *332*, 336–344.

(84) Zhu, Y.; Drueckhammer, D. G. *J. Org. Chem.* **2005**, *70*, 7755–7760.

(85) Gandhi, S.; Bell, K. L.; Gibson, M. S. *Tetrahedron* **1995**, *51*, 13301–13308.

(86) Martin-Fontecha, M.; Agarrabeitia, A. R.; Ortiz, M. J.; Armesto, D. *Org. Lett.* **2010**, *12*, 4082–4085.

(87) Rodrigo, C. M.; Cencic, R.; Roche, S. P.; Pelletier, J.; Porco, J. A., Jr. *J. Med. Chem.* **2012**, *55*, 558–562.

(88) Wang, H.; Reisman, S. E. *Angew. Chem. Int. Ed.* **2014**, *53*, 6206–6210.

(89) Garro-Helion, F.; Merzouk, A.; Guibé, F. *J. Org. Chem.* **1993**, *58*, 6109–6113.

(90) Escoubet, S.; Gastaldi, S.; Timokhin, V. I.; Bertrand, M. P.; Siri, D. *J. Am. Chem. Soc.* **2004**, *126*, 12343–12352.

(91) Kitov, P. I.; Bundle, D. R. *Org. Lett.* **2001**, *3*, 2835–2838.

(92) Wang, W.; Cencic, R.; Whitesell, L.; Pelletier, J.; Porco, J. A., Jr. *Chem. - A Eur. J.* **2016**, *22*, 12006–12010.

(93) Brimioulle, R.; Lenhart, D.; Maturi, M. M.; Bach, T. *Angew. Chem. Int. Ed.* **2015**, *54*, 3872–3890.

(94) Bauer, A.; Westkämper, F.; Grimme, S.; Bach, T. *Nature* **2005**, *436*, 1139–1140.

(95) Müller, C.; Bauer, A.; Bach, T. *Angew. Chem. Int. Ed.* **2009**, *48*, 6640–6642.

(96) Brimioulle, R.; Bach, T. *Science.* **2013**, *342*, 840–843.

(97) Vallavoju, N.; Selvakumar, S.; Jockusch, S.; Sibi, M. P.; Sivaguru, J. *Angew. Chem. Int. Ed.* **2014**, *53*, 5604–5608.

(98) Murphy, J. J.; Bastida, D.; Paria, S.; Fagnoni, M.; Melchiorre, P. *Nature* **2016**, *532*, 218–222.

(99) Blum, T. R.; Miller, Z. D.; Bates, D. M.; Guzei, I. A.; Yoon, T. P. *Science.* **2016**, *354*, 1391–1395.

(100) Huang, Y.; Unni, A. K.; Thadani, A. N.; Rawal, V. H. *Nature* **2003**, *424*, 146–146.

(101) Anderson, C. D.; Dudding, T.; Gordillo, R.; Houk, K. N. *Org. Lett.* **2008**, *10*, 2749–2752.

(102) Barducci, A.; Bussi, G.; Parrinello, M. *Phys. Rev. Lett.* **2008**, *100*, 1–4.

(103) Laio, A.; Parrinello, M. *Proc. Natl. Acad. Sci.* **2002**, *99*, 12562–12566.

(104) Van Der Spoel, D.; Lindahl, E.; Hess, B.; Groenhof, G.; Mark, A. E.; Berendsen,

H. J. C. *J. Comput. Chem.* **2005**, *26*, 1701–1718.

(105) Wang, J.; Wang, W.; Kollman, P. A.; Case, D. A. *J. Mol. Graph. Model.* **2006**, *25*, 247–260.

(106) Wang, J. M.; Wolf, R. M.; Caldwell, J. W.; Kollman, P. A.; Case, D. A. *J. Comput. Chem.* **2004**, *25*, 1157–1174.

(107) Bayly, C. I.; Cieplak, P.; Cornell, W.; Kollman, P. A. *J. Phys. Chem.* **1993**, *97*, 10269–10280.

(108) Cornell, W. D.; Cieplak, P.; Bayly, C. I.; Kollman, P. A. *J. Am. Chem. Soc.* **1993**, *115*, 9620–9631.

(109) Le, C. C.; Wismer, M. K.; Shi, Z. C.; Zhang, R.; Conway, D. V.; Li, G.; Vachal, P.; Davies, I. W.; MacMillan, D. W. C. *ACS Cent. Sci.* **2017**, *3*, 647–653.

CURRICULUM VITAE